UNIVERSITY OF LIVERPOOL

國立清華大學
NATIONAL TSING HUA UNIVERSITY

MULTI-SCALE STRUCTURAL AND MECHANICAL INVESTIGATIONS ON DISEASED MINERALISED TISSUES

Thesis submitted in accordance with the requirements of the University of Liverpool and the National Tsing Hua University for the degree of Doctor in Philosophy by

Fabio Bohns

November 2023

“Here lies the RPG-part of this game.
We will miss you!”

Cipsoft – Tibia

Acknowledgements

"*If I have seen further, it is by standing on the shoulders of giants*" – Sir Isaac Newton.

Firstly, I would like to focus my gratitude to my primary supervisor Dr Riaz Akhtar and secondary supervisor Dr Po-Yu Chen for giving me the opportunity to pursue my academic objectives. I would like to show you both my immense gratitude and admiration for all the support, trust and encouragement provided across the four and a half years that I spent in your laboratories. The good memories and knowledge I acquired from you will remain within me.

I would like to thank Dr Yung-Jen Chuang, for the support with zebrafish model, and Dr Elizabeth Laird, for the support with murine models.

My appreciation to Mr David Atkinson for providing training and for the cultural bliss at every sight in George Holt building.

I would like to thank my colleagues in NTHU, especially Ashish Ghimire, Shih-Chieh Chao, Jackie Tung, Yang-Rong Shi, Yu-Min Lin, Yen-Shuo (Eric), Haw-Kai, Rishabh and Yu-Yi Lai. But also, to all the others that shared office with me at any point in time.

To my colleagues in UoL: Martin Hossack, Ahmed Kazaili, Joe Roberts, Bojin Marinov, Ben Peek, Michael Ward, Joshua Preston, Eman, Shagufta and Hong Ma.

Finally, I would like to thank my parents Tania Rocha and Paulo Bohns for being understanding of my situation in many opportunities. Thank my sisters Rafaelle Bohns and Karina Bohns, and their respective families.

A special thanks for my auntie Neuza Bohns and her family. I am where I am now because of your incredible support early in my career.

Thank all my dearest friends that supported and made me laugh in difficult moments: Thiago Beresford, Matheus Weber, Gabriel Santos, Renata Duarte, Vinicius Guerra, Lisiane Assis Brasil, Lucca Mello, Julia Brito, Giovani Ghiggi, Katarine Rosso, Matheus Serpa, Eric Quanz, Gabriel Borges, Jorge Lucas, Romel Falcão, André Willers, Fausto Velho, Filipe, Marla Cuppini, Isadora Garcia, Gabriela Balbinot, Felipe Leitzke, Angela Casaril, Michael Butlin, Ricardo Ritter, to all Kops family and all the others that would make this list longer than it is already.

Thanks to the RA team members I had in Liverpool, especially to Hrushikesh Kshirsagar, Sreeraj Rajmohan and Dr Monika Grabias-Rodriguez.

To the family Tung, especially to Yu-Shan for the immense support.

To the School of Engineering in the UoL and to the iPhD for having funded me.

Abstract

Bone is a multi-functional material that protect our organs, sustain our body weight and produce skeletal cells. Osteoporosis and osteogenesis imperfecta are chronic and genetic bone diseases, respectively, that share a phenotype of bone fragility. Bone fracture is an important subject for discussion due to the economic burden that it causes across all ages, but especially in the elderly. In order to minimise the negative consequences of bone diseases, a series of medical recommendations should be followed; they involve the intake of anti-resorptive drugs (i.e., alendronate) and maintaining an active and healthy routine. Despite the advances in the understanding of osteoporosis and osteogenesis imperfecta, some underlying mechanisms of bone fragility and its relationship with bone morphometrics (e.g., mineral density and bone volume), remain unanswered. To further the knowledge on bone diseases, animal models have been proposed.

Zebrafish are small teleost fish that the bones have shown high conservation with those of human. These fish are able to regenerate parts of their body, like caudal fin, contributing to the 3Rs (*Reduction, Replacement and Refinement*) in animal research by, for example, reducing the number of rodents in research. Because of this, zebrafish have been used for the exacerbation of clinical bone conditions such as glucocorticoid-induced osteoporosis. *Osteogenesis imperfecta murine* is a spontaneous mutation of mild-to-severe cases of osteogenesis imperfecta. These mice show deformed skeleton and brittle bones. These mice have been used to evaluate effects of collagen defects in bone properties. In this study, a series of structural and mechanical analysis were used in zebrafish and murine models to establish a relationship between poor mechanical properties caused by bone diseases and parameters used to measure bone quality.

The potential of zebrafish to regenerate their amputated caudal fins was used to explore the effects of osteoporosis and alendronate on the mineralisation of the fin bony rays. Diseased fish displayed a slower bone formation than controls; fish treated with alendronate showed increased bone formation than both groups. Similarly, the reduced elastic modulus and hardness levels were decreased in osteoporotic bones (5.60 ± 5.04 GPa and 0.12 ± 0.17 GPa, respectively), whereas alendronate recovered them to the pre-amputation condition (8.68 ± 8.74 GPa and 0.34 ± 0.47 GPa, respectively). Prednisolone and alendronate effects on zebrafish vertebrae were exacerbated by the reduction of the bone-mineral density and recuperation of hardness to controls levels. In the osteogenesis imperfecta model, the misfolding of α2 chains (homozygous) produced bones with decreased biomechanics at early age.

Zebrafish showed that osteoporosis is exacerbated by hampered mineral formation (fin bony rays), reduced hardness (fin bony rays and vertebrae) and reduction of bone-mineral density (vertebrae). In murine models, the biomechanical properties increased with age, demonstrating that low elastic modulus and hardness, and high creep rates at young ages may play key role in osteogenesis imperfecta phenotype. The techniques applied in this thesis have potential, in the future, to be applied in humans to better understand osteoporosis and osteogenesis imperfecta.

List of Publications

International Journal Articles

BOHNS, FABIO ROCHA; SHIH, YANG-RONG; CHUANG, YUNG-JEN; AKHTAR, RIAZ; CHEN, PO-YU. Influence of Prednisolone and Alendronate on the *de novo* Mineralization of Zebrafish Caudal Fin. JBMR Plus. 2020. (*Fully published*). doi.org/10.1002/jbm4.10435**.** [Chapter 4].

BOHNS, FABIO ROCHA; CHUANG, YUNG-JEN; AKHTAR, RIAZ; CHEN, PO-YU. Alendronate Improves Osteoporotic Vertebral Bone Quality in Zebrafish Model. (*Submitted).* [Chapter 5]

List of conferences

BOHNS, FABIO ROCHA; CHUANG, YUNG-JEN; AKHTAR, RIAZ; CHEN, PO-YU. Talk on Multi-scale Elemental, Structural and Mechanical Characterization of the Influence of Different Medicines on the *de novo* Mineralization of Zebrafish Caudal Fin. (*Oral*). The Minerals, Metals and Materials Society (TMS2020) – San Diego, California, United States. 2020.

BOHNS, FABIO ROCHA, LEE, KATIE JOANNA; CHEN, PO-YU, CANTY-LAIRD, ELIZABETH; AKHTAR, RIAZ. Mutated Collagen Alpha Chains Decrease the Biomechanical Properties of Bone. (*Poster*) BioMedEng – London, United Kingdom. 2022.

BOHNS, FABIO ROCHA, LEE, KATIE JOANNA; CHEN, PO-YU, CANTY-LAIRD, ELIZABETH; AKHTAR, RIAZ. Type-I Collagen Mutations Cause Increased Biomechanical Properties with Age in Osteogenesis Imperfecta Murine Model. (*Poster*) CIMA/CMAR – Birmingham, United Kingdom. 2023.

BOHNS, FABIO ROCHA; CHUANG, YUNG-JEN; AKHTAR, RIAZ; CHEN, PO-YU. Alendronate Enhances Osteoporotic Vertebral Bone by Increasing the Bone-Mineral Density in Zebrafish Model (***Oral***). BioMedEng23 – Swansea, Wales, UK. September 2023.

UoL / NTHU dual conference

BOHNS, FABIO ROCHA; AKHTAR, RIAZ; CHEN, PO-YU. Talk on Multi-Scale Structural and Mechanical Investigations on Diseased Mineralized Tissues. 10th Annual Bi-Lateral conference between National Tsing Hua University, Taiwan, and University of Liverpool, UK. Place: NTHU, Hsinchu, Taiwan. Date: January 2020.

BOHNS, FABIO ROCHA; AKHTAR, RIAZ; CHEN, PO-YU. Talk on Multi-Scale Structural and Mechanical Investigations on Diseased Mineralized Tissues. 10th Annual Bi-Lateral conference between National Tsing Hua University, Taiwan, and University of Liverpool, UK. Place: NTHU, Hsinchu, Taiwan. Date: April 2021.

BOHNS, FABIO ROCHA; CHEN, PO-YU; AKHTAR, RIAZ. Talk on Multi-Scale Structural and Mechanical Investigations on Diseased Mineralized Tissues. 10th Annual Bi-Lateral conference between National Tsing Hua University, Taiwan, and University of Liverpool, UK. Place: UoL, Liverpool, United Kingdom. Date: November 2022.

Structure of thesis

This thesis consists of eight chapters:

- **Chapter 1:** background stating the motivation for doing this research. The specific division of this thesis was stated, as well as the objectives.
- **Chapter 2:** introductory chapter with the literature review that will serve to guide this thesis. This chapter starts with the relationship between bone fractures and ageing; it finishes with the animal models used in this thesis to evaluate bone diseases.
- **Chapter 3:** methodological procedures used in this thesis. Focus was given to key equipment used through this study.
- **Chapter 4:** zebrafish caudal fin model to glucocorticoid-induced osteoporosis. This chapter focus on the regeneration of zebrafish lepidotrichia while mineralogenic compounds is administered to the fish.
- **Chapter 5:** zebrafish vertebrae model to glucocorticoid-induced osteoporosis. This chapter focus on evaluating bone mineral density of diseased fish and compares with healthy and bisphosphonate treated fish. The relationship between mineral density and mechanical properties is addressed.
- **Chapter 6:** murine models for osteogenesis imperfecta. Bone quality of mice mutations was evaluated by the means of their biomechanical properties.
- **Chapter 7:** discussion of the findings of this thesis. Comparison of the results of this work with the available literature.
- **Chapter 8:** summary and conclusions found in this study. Future work is addressed.

Contribution of authors

Authors contributing to this thesis include: Mr Fabio Rocha Bohns (FRB), Dr Riaz Akhtar (RA), Dr Elizabeth Canty-Laird (EC-L) and Dr Katie Lee (KL) in the University of Liverpool (UoL), Liverpool, UK; Dr Po-Yu Chen (P-YC), Dr Yung-Jen Chuang (Y-JC) and Mr Yang-Rong Shi (Y-RS) in the National Tsing Hua University (NTHU), Hsinchu, Taiwan.

The work in chapter 4 was conducted in NTHU in collaboration with P-YC, RA, Y-JC and Y-RS.

The work in chapter 5 was conducted in NTHU and UoL in collaboration with P-YC, RA, Y-JC and Y-RS.

The work in chapter 6 was conducted in UoL in collaboration with P-YC, RA, EC-L and KL.

List of abbreviation

UN	United Nations
OP	Osteoporosis
OI	Osteogenesis Imperfecta
oim	Osteogenesis Imperfecta Murine
GIOP	Glucocorticoid-Induced Osteoporosis
BMD	Bone-Mineral Density
μ-CT	Micro-Computed Tomography
WT	Wild Type
ECM	Extracellular Matrix
HAp	Hydroxyapatite
OCs	Osteoclasts
OBs	Osteoblasts
E'	Young's Modulus
n_{STRESS}	Stress exponent
SEM	Scanning Electron Microscopy
SAIDs	Steroidal Anti-Inflammatory Drugs
PN	Prednisolone
Het	Heterozygous
Hom	Homozygous
mg	milligram
m	metres

P-C-P	Phosphorus-Carbon-Phosphorus
OH	Hydroxyls
AR-S	Alizarin Red-S
dpf	Days Post Fertilisation
WA	Weberian Apparatus
PC	Precaudal Vertebrae
CV	Caudal Vertebrae
CFV	Caudal Fin Vertebrae
E	Elastic Modulus
H	Hardness
AFM	Atomic Force Microscopy
NI	Nanoindentation
w	Weeks
λ	Wavelength
Å	Angstrom
mm	Millimetre
EDS	Energy Dispersive Spectroscopy
υ	Poisson's Ratio
P	Load
mN	Millinewton
h	Displacement
t	Time
O-P	Oliver-Pharr

h_f	Final residual indentation depth
h_s	Amount of sink-in
ϕ	Half-included angle
S_T	Stiffness
A_U	Unloading contact area
E_R	Reduced Elastic Modulus
C_{IT}	Creep Index
h_b	Displacement in the beginning of hold period
h_{max}	Displacement in the end of hold period
TZCAS	Taiwan Zebrafish Core Facility at Academia Sinica
NTHU	National Tsing Hua University
A.U.	Arbitrary Units
V	Volts
d	days
mL	millilitres
DMSO	Dimethyl Sulfoxide
μM	Micromolar
CTRL	Control
n	Number (of samples)
dpa	Days Post Amputation
RMA	Real Mineralised Area
RAY	Mean Ray Width
REG	Total Regenerated Area

STU	Stump Width
Ca	Calcium
P	Phosphorus
nm	Nanometres
cm	Centimetres
OCT	Optimal Cutting Temperature
PBS	Phosphate-Buffered Solution
ROI	Region of Interest
ACP	Amorphous Calcium Phosphate
BV	Bone Volume
TV	Tissue Volume
B.Th	Cortical Bone Thickness
NaCl	Sodium Chloride
KH_2PO_4	Monopotassium Phosphate
Na_2HPO_4	Disodium Phosphate
KCl	Potassium Chloride
F	Female
M	Male
EtOH	Ethanol
r^2	Pearson Correlation

List of figures

List of tables

Contents

1. Chapter 1: Background

This chapter briefly explains the motivation behind the conduction of this research. The overall aim and specific objectives are listed.

1.1. Motivation

The 20th century marked the lengthening of human life span, causing the elderly to be the fastest growing share of population nowadays, totalising 19% of Europe's inhabitants (United Nations, 2017). Projections for the next three decades suggest that developing continents will close the gap with Europe in terms of people with 60 years of age or older. The older population are therefore making up a larger part of the population and living longer as elders. In this context, bone fractures pose a social and economic burden (Wu *et al.*, 2021; Xu *et al.*, 2022).

Bones are fundamental for vertebrate's life maintenance. They provide mechanical support for the body and protect organs from direct impact to list a few (Chen and McKittrick, 2011). It is widely known that human bone mass decreases as they biologically age (El-Gazzar and Högler, 2021). With this, not only the fracture risk increases, but the type and location of traumas vary from those observed in younger bodies (Bergh *et al.*, 2020; Wu *et al.*, 2021). The poor biomechanics of an aged bone is associated with higher occurrence of fractures in the pelvis and femurs (Hernlund *et al.*, 2013). In already impaired physiological systems, these lower limb traumas are life threatening and required extended hospitalization (Clynes *et al.*, 2020; Hernlund *et al.*, 2013). A significant percentage of these fractures are result of bone diseases (Bergh *et al.*, 2020), thus, understanding better the biomechanics of bone conditions may reduce fracture's burden.

Osteoporosis (OP) is an acquired skeleton disease characterized by "*porous bones*" (El-Gazzar and Högler, 2021). It affects especially (but not only) elderly women, deteriorating the bones' microarchitecture (Clynes *et al.*, 2020). OP is the most prevalent of the bone diseases, affecting 200 million women today (Salari *et al.*, 2021). Conversely, osteogenesis imperfecta (OI) is a rare inherited disorder of "*imperfect bone formation*" (Forlino and Marini, 2016). It develops

from mutations in the type I collagen fibrils, the most abundant in bones. OI is estimated to affect 1 person in every 10,000 births (El-Gazzar and Högler, 2021; Forlino and Marini, 2016). Despite differences in their onset, OP and OI share impaired bone strength, resulting in brittle bones phenotype (El-Gazzar and Högler, 2021). To date, the underlying biomechanical mechanisms of bone fragility in both disorders remains a challenge.

Small vertebrate animals have been proposed as readily available models to assess OP and OI. Among mammals, mice are preferred due to their size, and easy access to naturally occurring mutations, as in the case of the *osteogenesis imperfecta murine* (*oim*) (Gremminger *et al.,* 2021; Lee *et al.,* 2022). Zebrafish are small teleost fish with high conservation of bone physiology with humans (Barrett *et al.,* 2006; Santos *et al.,* 2023). Zebrafish model contributes to the reduction, replacement and refinement (3Rs) of animals research by, for example, reducing the number of mammals used in experimentation (Embry *et al.,* 2010).

Even though the use of rodents is predominant and relevant in biomedical research, the use of zebrafish has increased exponentially since its discovery and should be given more attention. Modelling human diseases in zebrafish allows researchers to reduce time and the use of laboratory resources, mitigating potential problems associated with animals wellbeing (Bailone *et al.,* 2020). Hence, this work aims to use material science approach to characterize OP and OI in zebrafish and mice models, respectively.

1.2. Aims and Objectives

The general aim of this study is to characterise the properties of mineralised tissues affected by osteoporosis and osteogenesis imperfecta. This aim will be achieved through the completion of the following specific objectives:

Objective I: Investigate whether glucocorticoid-induced osteoporosis (GIOP) and the treatment with bisphosphonate, influence the morphology, biomechanics and mineralisation of zebrafish lepidotrichia.

Objective II: To assess the bone-mineral density (BMD), and other morphometric parameters, with micro-computed tomography (μ-CT), as well as the biomechanical values of zebrafish vertebrae after the onset of GIOP and the treatment with bisphosphonate.

Objective III: Characterize the biomechanics of femurs of *oim* mice and compare to those of COL1A2-null (tm1b) and wild type (WT).

References

Bailone, R.L., Fukushima, H.C.S., Ventura Fernandes, B.H., De Aguiar, L.K., Corrêa, T., Janke, H., Grejo Setti, P., Roça, R.D.O., Borra, R.C., 2020. Zebrafish as an alternative animal model in human and animal vaccination research. Lab Anim Res 36, 13.

Barrett, R., Chappell, C., Quick, M., Fleming, A., 2006. A rapid, high content, in vivo model of glucocorticoid-induced osteoporosis. *Biotechnology Journal*. 1, 651–655.

Bergh, C., Wennergren, D., Möller, M., Brisby, H., 2020. Fracture incidence in adults in relation to age and gender: A study of 27,169 fractures in the Swedish Fracture Register in a well-defined catchment area. *PLoS ONE.* 15, e0244291.

Chen, P.-Y., McKittrick, J., 2011. Compressive mechanical properties of demineralized and deproteinized cancellous bone. *Journal of the Mechanical Behavior of Biomedical Materials.* 4, 961–973.

Clynes, M.A., Harvey, N.C., Curtis, E.M., Fuggle, N.R., Dennison, E.M., Cooper, C., 2020. The epidemiology of osteoporosis. *British Medical Bulletin*. 133(1), 105-117.

El-Gazzar, A., Högler, W., 2021. Mechanisms of Bone Fragility: From Osteogenesis Imperfecta to Secondary Osteoporosis. *International Journal of Molecular Sciences.* 22, 625.

Embry, M.R., Belanger, S.E., Braunbeck, T.A., Galay-Burgos, M., Halder, M., Hinton, D.E., Léonard, M.A., Lillicrap, A., Norberg-King, T., Whale, G., 2010. The fish embryo toxicity test as an animal alternative method in hazard and risk assessment and scientific research. *Aquatic Toxicology.* 97, 79–87.

Forlino, A., Marini, J.C., 2016. Osteogenesis imperfecta. *The Lancet*. 387, 1657–1671.

Gremminger, V.L., Harrelson, E.N., Crawford, T.K., Ohler, A., Schulz, L.C., Rector, R.S., Phillips, C.L., 2021. Skeletal muscle specific mitochondrial dysfunction and altered energy metabolism in a murine model (oim/oim) of severe osteogenesis imperfecta. *Molecular Genetics and Metabolism.* 132, 244–253.

Hernlund, E., Svedbom, A., Ivergård, M., Compston, J., Cooper, C., Stenmark, J., McCloskey, E.V., Jönsson, B., Kanis, J.A., 2013. Osteoporosis in the European Union: medical management, epidemiology and economic burden: A report prepared in collaboration with the International Osteoporosis Foundation (IOF) and the European Federation of Pharmaceutical Industry Associations (EFPIA). *Archives Osteoporosis*. 8, 136.

Lee K. J., Lisa Rambault, George Bou-Gharios, Peter D. Clegg, Riaz Akhtar, Gabriela Czanner, Rob van't Hof, Elizabeth G. Canty-Laird; 2022 Collagen (I) homotrimer potentiates the osteogenesis imperfecta (oim) mutant allele and reduces survival in male mice. Dis Model Mech 1 September; 15 (9): dmm049428.

Salari, N., Ghasemi, H., Mohammadi, L., Behzadi, M. Hasan, Rabieenia, E., Shohaimi, S., Mohammadi, M., 2021. The global prevalence of osteoporosis in the world: a comprehensive systematic review and meta-analysis. *Journal of Orthopaedic Surgery Research.* 16, 609.

Santos, J.M.A., Laizé, V., Gavaia, P.J., Conceição, N., Cancela, M.L., 2023. Zebrafish Models to Study Ectopic Calcification and Calcium-Associated Pathologies. *International Journal of Molecular Sciences.* 24, 3366.

United Nations, 2017. World population ageing: 2017 highlights. United Nations, New York. 1-40.

Wu, A.-M., Bisignano, C., James, S.L., Abady, G.G., Abedi, A., Abu-Gharbieh, E., Alhassan, R.K., Alipour, V., Arabloo, J., Asaad, M., Asmare, W.N., Awedew, A.F., Banach, M., Banerjee, S.K., Bijani, A., Birhanu, T.T.M., Bolla, S.R., Cámera, L.A., Chang, J.-C., Cho, D.Y., Chung, M.T., Couto, R.A.S., Dai, X., Dandona, L., Dandona, R., Farzadfar, F., Filip, I., Fischer, F., Fomenkov, A.A., Gill, T.K., Gupta, B., Haagsma, J.A., Haj-Mirzaian, A., Hamidi, S., Hay, S.I., Ilic, I.M., Ilic, M.D., Ivers, R.Q., Jürisson, M., Kalhor, R., Kanchan, T., Kavetskyy, T., Khalilov, R., Khan, E.A., Khan, M., Kneib, C.J., Krishnamoorthy, V., Kumar, G.A., Kumar, N., Lalloo, R., Lasrado, S., Lim, S.S., Liu, Z., Manafi, A., Manafi, N., Menezes, R.G., Meretoja, T.J., Miazgowski, B., Miller, T.R., Mohammad, Y., Mohammadian-Hafshejani, A., Mokdad, A.H., Murray, C.J.L., Naderi, M., Naimzada, M.D., Nayak, V.C., Nguyen, C.T., Nikbakhsh, R., Olagunju, A.T., Otstavnov, N., Otstavnov, S.S., Padubidri, J.R., Pereira, J., Pham, H.Q., Pinheiro, M., Polinder, S., Pourchamani, H., Rabiee, N., Radfar, A., Rahman, M.H.U., Rawaf, D.L., Rawaf, S., Saeb, M.R., Samy, A.M., Sanchez Riera, L., Schwebel, D.C., Shahabi, S., Shaikh, M.A., Soheili, A., Tabarés-Seisdedos, R., Tovani-Palone, M.R., Tran, B.X., Travillian, R.S., Valdez, P.R., Vasankari, T.J., Velazquez, D.Z., Venketasubramanian, N., Vu, G.T., Zhang, Z.-J., Vos, T., 2021. Global, regional, and national burden of bone fractures in 204 countries and territories, 1990–2019: a systematic analysis from the Global Burden of Disease Study 2019. *The Lancet Healthy Longevity.* 2, e580–e592.

Xu, Q., Ou, X., Li, J., 2022. The risk of falls among the aging population: A systematic review and meta-analysis. *Frontiers of Public Health.* 10, 902599.

2. Chapter 2: Literature Review

This chapter provides extensive information on the main subjects of this thesis. Starting from the section 2.1 with the burden of ageing. Section 2.2 introduce the reader to bones, its cells and bone remodelling process. Section 2.3 addresses bone biomechanics from *stress vs. strain* curves to, macro-level analysis, time-dependence and constitutive modelling. Section 2.4 bone diseases (osteoporosis and osteogenesis imperfecta), as well as the ways used to manage/treat these diseases (Section 2.5). This chapter concludes by introducing small animal models frequently used in bone disease assessment, as the cases of zebrafish and mice (Section 2.6).

2.1. Ageing

2.1.1. Ageing definition and prospects

Modern healthcare advances, especially those happening in the last century, permitted humans to live longer. One could say that the increase of human lifespan in itself, was not the primary outcome expected by those that worked to improve healthcare systems, but ensuring quality of life (Parambi *et al.*, 2020). The fact is that, as a secondary effect of improving living conditions across the different continents, the World has a higher elderly population proportionally than ever before (United Nations, 2017a). It has been demonstrated in an analysis of life expectancy from 1970 to 2010, that the substantive change in the age distribution of the population influence deeply the economic, social and political aspects of the society (Wang *et al.*, 2012). Due to this, understanding and discussing the challenges in responding to a population ageing have become fundamental for humanity's continuous development.

Defining "*ageing*" is not an easy task and has no universal definition (Ebert *et al.*, 2022). Evolutionary biologists seem to agree that ageing is an inevitable event in life that increase the mortality rate, while decrease the reproductive rate with time (Ackermann *et al.*, 2007; Rose, 1991). The terms "*biological ageing*" and "*chronological ageing*," were proposed, since ageing occur at different rates depending on the geographic location and other factors regarding the population being assessed (Colloca *et al.*, 2020). The context of ageing is based on the adaptation of the individual to its environment: their general experiences, social environment, personality, beliefs, diet, amount of exercise, and social and mental engagement with the place they live (Hughes and Touron, 2021). Colloca *et al.*, (2020) define chronological ageing as the actual age of a person (i.e., years of age) and biological age as how functional a person remains

while ageing. Thus, biological ageing has a stronger influence on the quality of life of a person than the former (Chang *et al.,* 2019).

When governmental agencies perform systematic acquisition and calculation of population information, also known as census, it is widely accepted to consider every individual with and age of over 65 years old, with an ageing phenotype (United Nations, 2017b), independent of their biological age. According to UN estimations, the year 2020 marked the first year in human documented history that the numbers of elderly (>65 years old) surpassed the number of children with less than <5 years old of age (Parambi *et al.,* 2020). This important event was possible because of the faster growth rate of older population in comparison to the number of new births globally. Currently, the European continent has the highest percentage of elderly people in the World (**Fig. 1**). Projections for the next three decades indicate that the elderly population will continue to increase (United Nations, 2017b), especially in emerging countries from Asia (**Fig. 1c**), South America (**Fig. 1d**) and Africa (**Fig. 1e**). These three continents together will represent a considerable proportion of the geriatric population, globally, by 2050 (**Fig. 1h**), which is, on itself, expected to account for 16% of the total inhabitants (double of the observed in the year 2020).

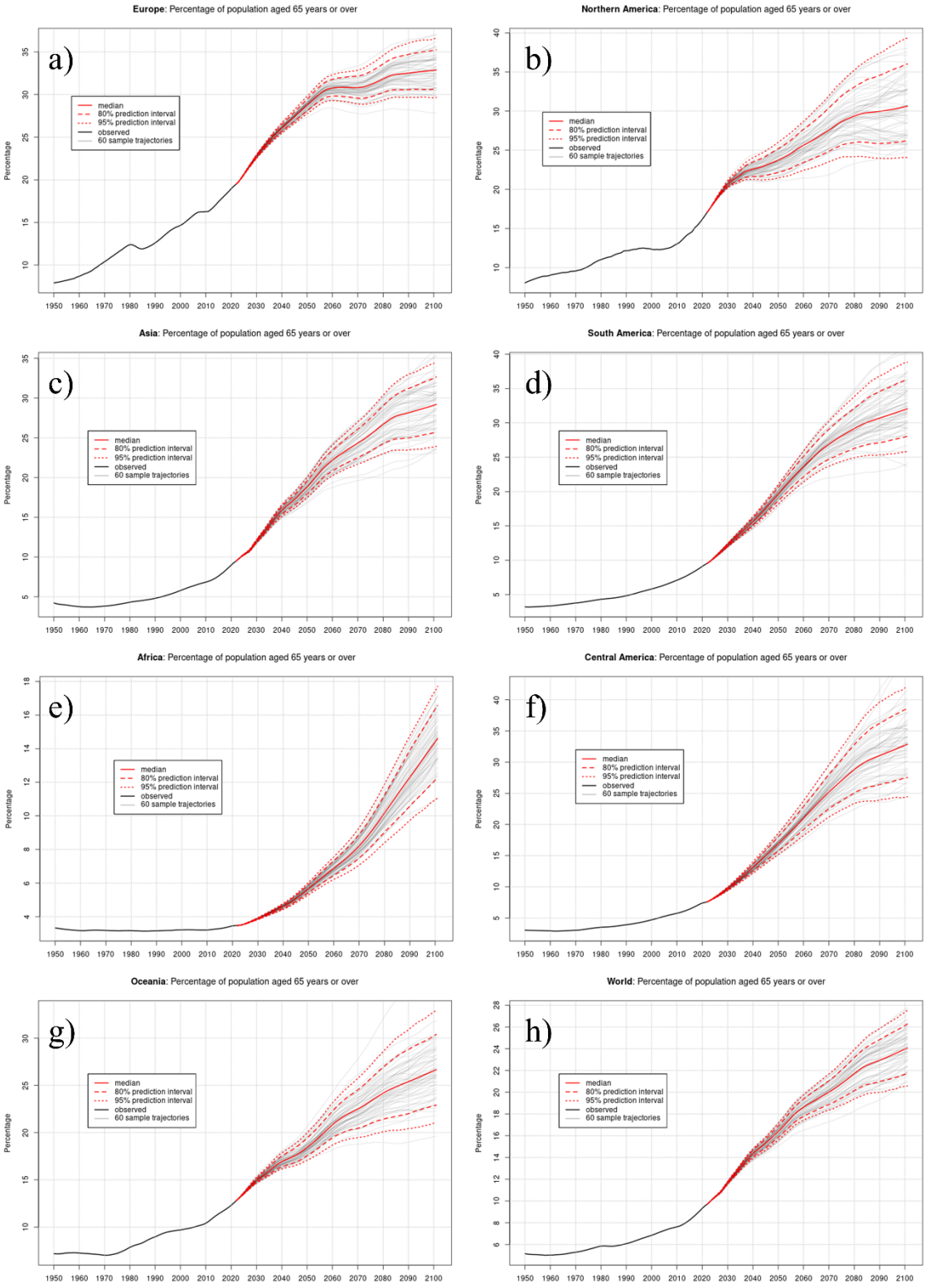

Fig. 1 Percentage of elderly population (>65 years of age) and the prediction of increase in Europe (a), North America (b), Asia (c), South America (d), Africa (e), Central America (f), Oceania (g) and the World (h). Montage by the author with data collected from United Nations (2017b).

2.1.2. Ageing burden

The constant ageing of the population, despite illustrating the success of modern healthcare systems, may pose an economic and social burden to the future generations of people. Another secondary effect to the lifespan expansion, is the prevalence of chronic diseases (i.e., persistent, or long-lasting diseases with generally slow progression), that became a more dominant factor for the health care systems than infectious diseases, as reported by the World Health Organization (WHO) (World Health Organization, 2020).

It has been reported that deaths caused as consequence of chronic diseases account for 63% of the total Global deaths (Yuan *et al.*, 2022). This expressive number may be attributed to the fact that, differently from bacterial or viral infection, chronic conditions can be controlled, but not cured (Marengoni *et al.*, 2011), reducing body's physiological reserve overtime, increasing death rate. Additionally, persistent conditions often require prolonged hospitalization and specialised treatment, rising economic burden and affecting daily routine by impairing normal physical activities and ability to work, especially in low-income countries (Chang *et al.*, 2019; Hajat and Stein, 2018; Marengoni *et al.*, 2011; Rashmi and Mohanty, 2023). Thus, people facing such illnesses need to adapt their lifestyle to their new condition, controlling the symptoms as long as possible, rather than expecting to be cured. Among the many persistent conditions affecting humans, one of the most life impairing and cause of major public health issues globally, are those that affect our musculoskeletal system (Wu *et al.*, 2021).

2.2. Musculoskeletal system

Our musculoskeletal system is composed of materials with distinctive characteristics that, together, contribute to the unique properties of the framework of our body (Fan *et al.*, 2022). Muscles, tendon, ligaments, cartilage and bone are the pieces of the mechanism that enables

humans to sustain their weight and move. It is well known that each of these parts are interconnected with one another, for example: decreased muscle strength and mass are directly correlated to low bone strength and mineral density and, consequently, to elevated risk of fragile fractures (Szulc, 2020). This thesis will focus on the role of bone in relation to musculoskeletal issues.

2.2.1. Bone

Human bone is a multi-functional heterogeneous and anisotropic (properties differ when measured in different directions) mineralized biological material (Chen and McKittrick, 2011; Fan *et al.*, 2022). Bones provide mechanical support for the body, generates motion and protects internal organs from direct impact (Tadano and Giri, 2011). They are composed by an inorganic phase (carbonated apatite) and an organic/protein phase (collagen of type I); these compounds are assembled together into a complex hierarchical structure, with dimensions ranging from nano- to the macro-scale (Chen and McKittrick, 2011). **Fig. 2** is a representation of the structure of bone, highlighting the features visible for the human eye (macro level), down to the nanostructures.

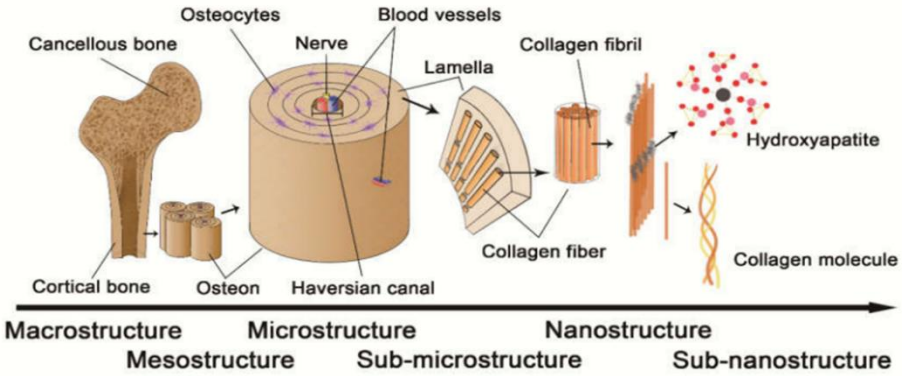

Fig. 2 Eight levels of hierarchical structure of bone. From the left to the right, different length scales are shown. The aggregation and maturation of both collagen molecules and HAp are the main building blocks of the bone as we know. This image was extracted from Fan et al., 2022.

Bones are fabricated by skeletal cells enclosed within a specialised tissue known as extracellular matrix (ECM) (Lin *et al.,* 2020; Liu *et al.,* 2016; Oftadeh *et al.,* 2015). This ECM is composed by collagenous proteins and polysaccharides; they serve as a scaffolding support so the HAp precursors can settle, aggregate, mature and grow in an organized way, such as plate- or rod-like structures (Chen and McKittrick, 2011; Lin *et al.,* 2020; Liu *et al.,* 2016). This intricate entanglement between minerals and protein forms the bones, a material with unique properties that are difficult (or impossible) to be reproduced by a composite materials approach used in engineering (Liu *et al.,* 2016).

2.2.2. Collagen

Type-I collagen is the most abundant protein in the composition of human bones (Ibrahim *et al.,* 2020; Meyers and Chen, 2014; Wang *et al.,* 2001). At the lowest level, it is arranged in heterotrimers composed of $(\alpha1)_2$ and $(\alpha2)_1$ which are derived from the *Col1a1* and *Col1a2* genes, respectively (Forlino and Marini, 2016). Collagen molecules have lengths of about 300 nm and are shifted by 67 nm from their neighbouring molecules (D-period) (Fratzl, 2008).

Collagenous fibres are considered biological materials with superior mechanical qualities especially if assessed in the fibre direction (anisotropic) (Fratzl, 2008). In composite materials, such as tendons (collagen/ECM) and bones (collagen/apatite), the mechanical characteristics of collagen fibrils are due to 1) their cross-linking with one another, 2) their orientation in comparison to the load direction (e.g., tension, bending or compression) and 3) the degree of mineralisation of the tissue they are contained (Ibrahim *et al.,* 2020; Screen *et al.,* 2015; Wang *et al.,* 2001). **Fig. 3** shows typical stress *vs.* strain curves of collagen-based tissues with different collagen orientations. It is possible to observe the increased energy that can be dissipated (post-yield deformation) by the less mineralised tendons (dark grey area below the curves) in comparison to bones. Thus, the collagenous matrix's contribution to the

biomechanics of bone is enormous, once the apatite alone cannot bear the compressive loads in which bones are exposed daily (Fratzl, 2008).

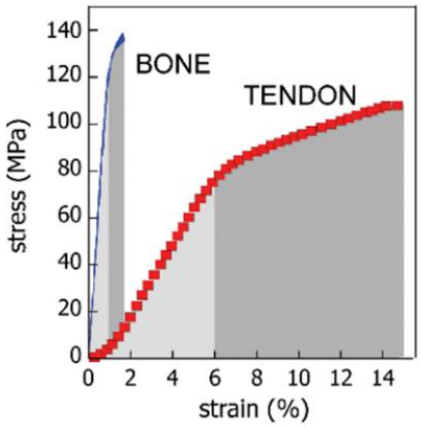

Fig. 3 Stress vs. strain curves of two collagen-based tissues: Bone (blue) and tendon (red). The area under each curves shows the effects of collagen mineralisation in the mechanical properties of the tissues. Image obtained from (Fratzl, 2008).

The synthesis of type-I collagen and its assembly into apatite minerals is a complex event and undergoes several stages. Collagen molecules are first synthesized as procollagen molecules precursor with large N- and C-terminal propeptide domains (Fratzl, 2008), and are moved to the rough endoplasmic reticulum; in this phase the pro-α1 chains and the pro-α2 assemble in a carboxyl amino direction, forming the triple helices and fold. The now stable folded triple helix is then transported from the rough endoplasmic reticulum to the ECM by the Golgi complex. In the Golgi complex the N- and C-terminal propeptide are removed, triggering the spontaneous formation of fibrils. Collagen fibrils synthesis is facilitated by both intra- and inter-crosslinking among them; crystalline HAp is then deposited within the fibres (Holmes *et al.*, 2018).

2.2.3. Types of ossification

Bones can be found in all vertebrate organisms as examples of fish, reptiles and mammals, and are divided in two subgroups depending on their ossification process: intramembranous or endochondral (Breeland *et al.,* 2021; Meyers and Chen, 2014). Both subgroups start their ossification processes with mesenchymal cell precursor. For intramembranous bones, their precursor differentiates directly into specialized cells that form the bones. Intramembranous ossification is the major form of skeletal ossification in small vertebrates, such as fish (Weigele and Franz-Odendaal, 2016). In endochondral formation, the process is more complex, being divided into three phases: 1) the precursor transforms into chondrocytes; 2) quick proliferation of cells and building of a cartilaginous intermediate mould; 3) the secondary process of ossification occurs (Breeland *et al.,* 2021). This is the main process of bone formation in human and high vertebrates bodies (Lin *et al.,* 2020).

These two ossification paths will lead to mineralised tissues with different biomechanics. While intramembranous bones are related to the formation of flat bones in human (e.g., hip and mandible), the endochondral build the so called "long bones" (e.g., vertebral column, the femur and the tibia) (Breeland *et al.,* 2021; Buck and Dumanian, 2012; Liu *et al.,* 2016).

2.2.4. Types of bones

As mentioned previously in **section 2.2.1**, bones are fundamental for the maintenance of vertebrates' life and activities. They display many vital functions to keep our body protected and functioning properly. Vertebrate's bodies evolved so bones are both biomechanically resistant and lightweight. Maximum strength with least mass configuration is only possible due to their multifaceted nature: one of them highly porous (~40% to ~90%) called trabecular and the other denser (~5% to ~15%), called cortical (Morgan *et al.*, 2018).

Trabecular bone (also called cancellous or spongy) are normally found at the ends and in the middle of long bones, and in the vertebral column (Morgan *et al.*, 2018). They are arranged in a cellular-like structure, resembling a prismatic or polyhedral cells (Chen and McKittrick, 2011; Gibson, 2003). This type of structure can resist compressive forces due to their ability to sustain large strains (~50% while holding their biomechanical integrity) and absorb energy originated from impact (Morgan *et al.*, 2018). The porous configuration of trabecular bone resembles those configurations of foam-like materials, such as wood, which is a major responsible for the large strains sustained by these materials under compressive loads (Chen and McKittrick, 2011). The failure or fracture of trabeculae causes the debris of bone to fill the interconnected pores within the trabeculae, starting a stiffening process which increases the energy that can be absorbed before its total failure (Linde *et al.*, 1989). Moreover, trabecular bone is considered the most metabolically active of the bones for various reasons: 1) increased surface-to-volume ratio; 2) increased demand of calcium and phosphorus to maintain mechanical integrity; and 3) its role in transferring loads from joints to the peripheral regions of bone (mechanobiology) (Oftadeh *et al.*, 2015). However, this is different depending on the species of the animal (Clarke, 2008).

Cortical, or compact, bone is the denser between the two (Chen and McKittrick, 2011). They are solid and surround the trabecular structure, being found in the diaphysis, metaphysis and epiphysis of bones. Cortical bone is highly mineralised and represents most of the weight of our skeletal system. It is also, metabolically speaking, less active than trabecular bone. The inner layer of the cortical bone is called endosteal layer; this is where most of the mechanical loading is absorbed; the outer layer is called periosteal and is responsible for fracture healing and bone growth (Clarke, 2008; Zimmermann *et al.*, 2015). **Fig. 4** shows a scheme of the trabecular and cortical regions of bone with their respective structural features. Generally, long

bones are formed by endochondral and membranous ossifications, while flat bones have membranous ossification (Clarke, 2008).

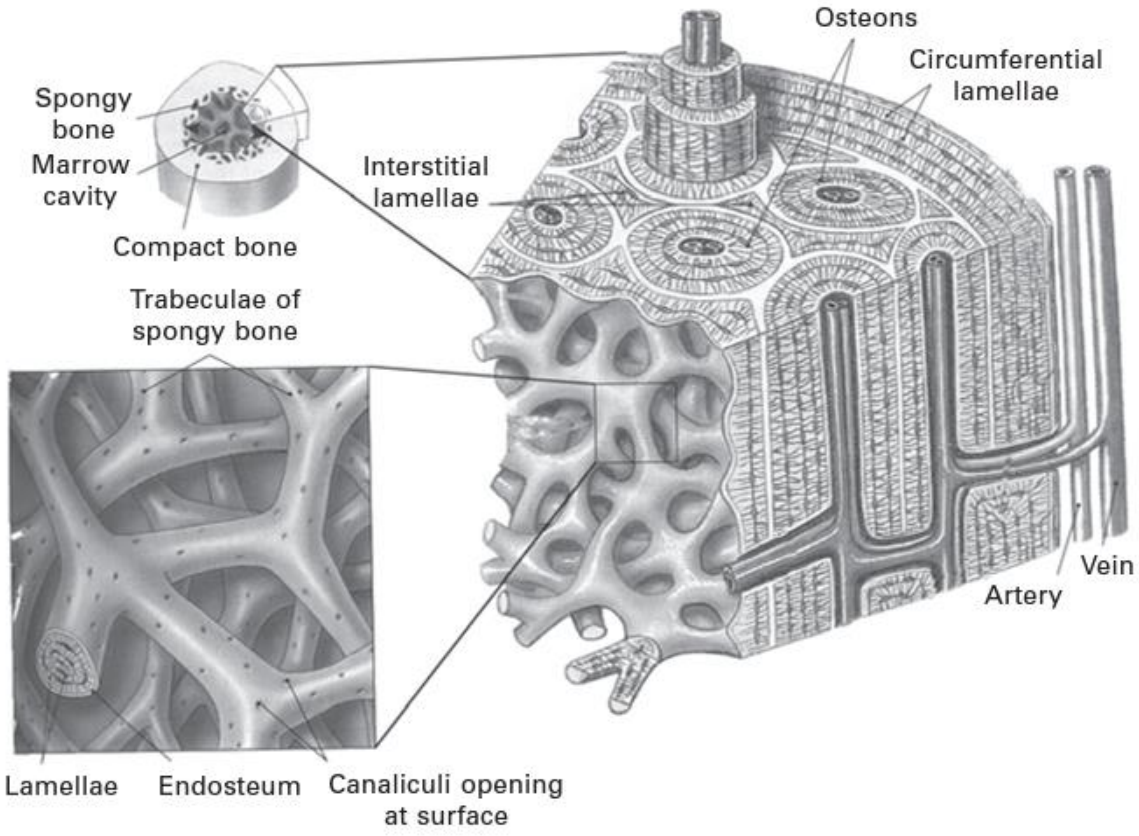

Fig. 4 Schematics of the two types of bones. A horizontal cut representation of the cortical (compact) and trabecular (spongy) bones. The cortical region has a lamellar structure with osteons (cylindrical structures), while the trabecular bone has interconnected porosity with canaliculi in its surface. Figure from Lacroix (2009).

2.2.5. Bone cells

More than supporting body weight and protecting vertebrate's internal organs, bones work as a calcium reservoir and produce skeletal cells that actively participate in its renewing process (Florencio-Silva *et al.,* 2015; Harada and Rodan, 2003). If a representative volume of bone is

analysed, it is possible to find four different skeletal cells: osteoclasts (OCs; responsible for bone resorption), osteoblasts (OBs; bone builders), lining cells, and osteocytes; the first three cells listed are found in the inner parts of the periosteum, as well as in the trabecular endosteum sites of bone, while the last is spread throughout a layer below the these surfaces (Mohamed, 2008). These cells are critical for the continuous remodelling of bone. OCs and OBs are actively involved in our organism maturation and development, and in the healing process of fractures, still maintaining the newly formed bone with its original properties (Hadjidakis and Androulakis, 2006; Harada and Rodan, 2003). For the purpose of this thesis, the change in "*the quantity of bone*" is defined by delta (Δ) and can be negative ($\Delta < 0$; trend in direction of bone removal), positive ($\Delta > 0$; trend in direction of bone building) or stable ($\Delta = 0$; homeostasis).

2.2.5.1. Osteoclasts

OCs are large, multinucleated and highly specialised cells. Their key role is to remove layers of mineralised tissue ($\Delta < 0$) from the surface of bones (phagocytosis). After they receive a signal that bone should be removed, they migrate through the bone marrow to a specific site, eroding the location and forming a shallow cavity called Howship's lacunae (Everts *et al.*, 2002; Mohamed, 2008). They contribute to the lifelong process of bone remodelling by responding to growth factors or to mechanical loadings applied to the skeleton (Mohamed, 2008).

2.2.5.2. Osteoblasts

OBs are cuboidal fibroblasts-like cells that work as new bone builders ($\Delta > 0$). However, more than only promoting mineralisation, they also synthesize the parts that constitute the ECM of bone, for example, the collagen of type-I in human bones (Mohamed, 2008). The bone forming process performed by the OBs are divided into two steps: 1) OBs secrete type-I collagen and other proteins to form an organic matrix scaffold; 2) mineralisation takes place on the site. As

OBs reach their final stage, they can either become entrapped within the mineralized matrix (osteocytes) or become lining cells; they may also undergo apoptosis (cell death) (Florencio-Silva *et al.*, 2015).

2.2.5.3. Osteocytes

Osteocytes are by far the most predominant and mature cells in the skeleton; they may live up to 25 years and are entrapped in the bone, being surrounded by mineralised tissue (Mohamed, 2008). The osteocytes found in cortical sites of the bones have elongated shape, while trabecular osteocytes are round. These cells are paramount for the bone remodelling process, being the regulators of OBs and OCs recruitment, prioritising locations for mineral deposition or removal. Osteocytes also work as mechanoreceptors, being responsible for detecting mechanical stresses on the bone and adapting the tissue for the most diverse mechanical requirements of our daily lives (Florencio-Silva *et al.*, 2015).

2.2.5.4. Lining cells

Lining cells are present in the surface of bone when no formation or removal is taking place ($\Delta = 0$). They are believed to work protecting the surface of the bone after OBs promoted new bone formation; thus, they may be fundamental for a proper coupling phenomenon (formation *vs.* resorption) (Florencio-Silva *et al.*, 2015). These cells are responsible for burying the collagen fibrils left exposed by OCs in the Howship's lacunae (Everts *et al.*, 2002).

2.2.6. Bone modelling

Adaptation that bones suffer when physiological and/or external mechanical forces induce the activity of skeletal cells. This process is not related to the coupling mechanism of OCs and OBs and is directly associated with the shape and growth of bones (Langdahl *et al.*, 2016).

2.2.7. Bone remodelling

The four types of cells defined in **section 2.2.5** have a cyclic process that involves 1) bone resorption; 2) bone signalling (or reversal phase); 3) bone formation; 4) mineralisation, and 5) resting phase (lining cells cover the surface of bone while osteocytes achieve their maturity). These steps are repeated indefinitely throughout the vertebrate's life. This process is called bone remodelling; its representation as well as each of the skeletal cells' roles on the process is shown in **Fig. 5**.

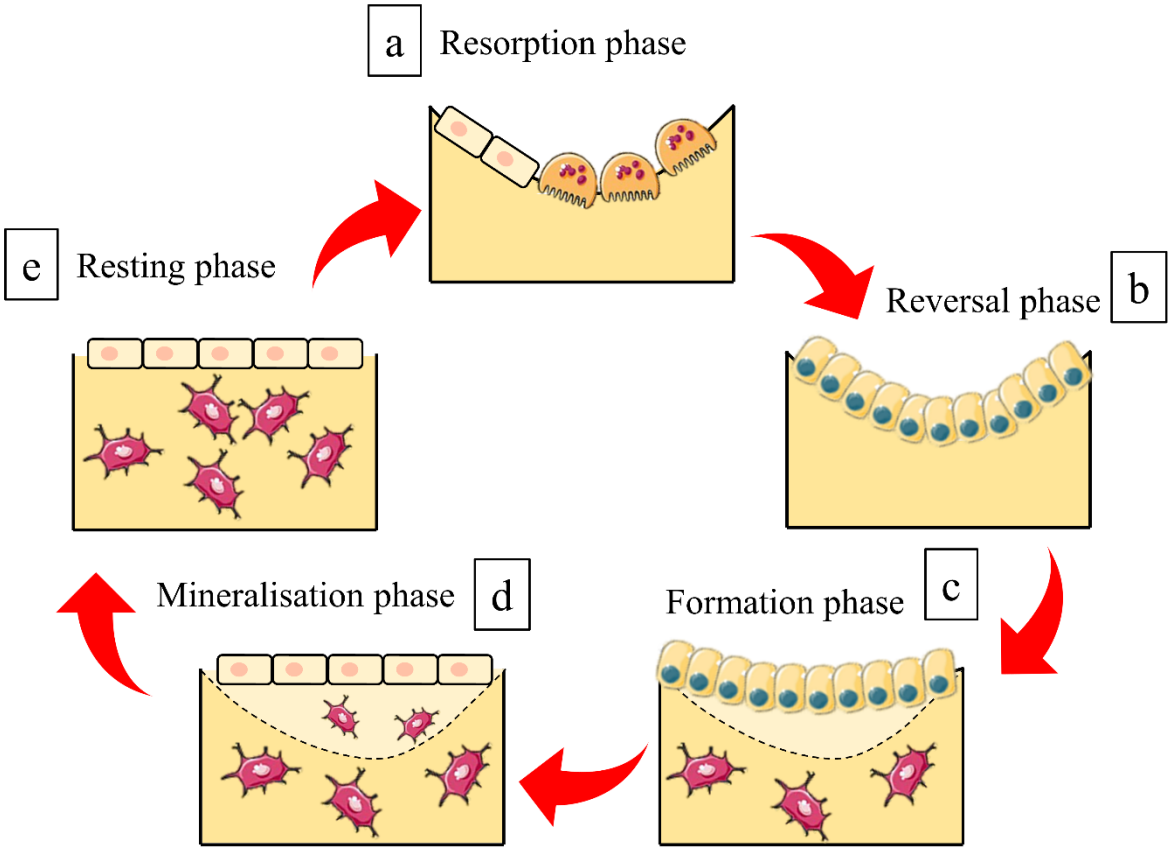

Fig. 5 Bone remodelling steps (a-e). (a-c) Sequential cycles bone resorption by OCs and bone formation by OBs. (d) Lining cells protect the newly formed bone layer from further bone resorption. (e) Well protected by the lining cells, the osteocytes have plenty of time to become matured cells, being entrapped just below the surface of bone. Figure adapted from Mohamed (2008) by the author.

Bone resorption and bone formation processes (by OCs and OBs, respectively), are a coupled phenomenon (Florencio-Silva *et al.*, 2015; Jensen *et al.*, 2021; Mohamed, 2008). In most cases, to achieve bone health and quality, this coupling mechanism must happen in a state of homeostasis ($\Delta = 0$) (Andersen *et al.*, 2013; Hadjidakis and Androulakis, 2006). This means that OCs and OBs should work as a team, removing and forming bone in the same rate to preserve skeleton function (Clarke, 2008).

2.3. Bone biomechanics

The elastic-plastic mechanism of bone is of fundamental importance for the understanding of bone fractures. Bones are at the same time tough and strong, and this is one of their most remarkable properties, as it is common for engineering materials to be strong or tough, but not both (Meyers and Chen, 2014). As mentioned previously in **section 2.2.1**, cortical and trabecular bones show, at sub tissue level, similar compositions (Chen and McKittrick, 2011). Thus, one should expect their properties are similar, which is not necessarily the case. **Fig. 6** show classic *stress vs. strain* curves obtained from compressive and tensile tests of cortical and trabecular bone.

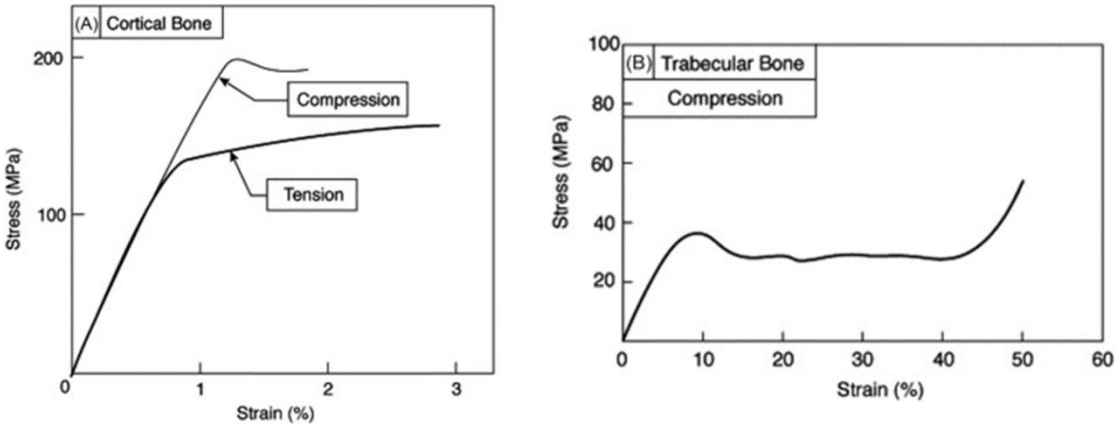

Fig. 6 Schematics of compressive and tensile stress vs. strain curves for cortical bone (left) and compressive stress vs. strain curve for trabecular bone (right). Image from Mercer et al., (2006).

The differences observed in the curves shows that their density and microarchitecture play a key role in their distinct biomechanical properties (Mercer *et al.*, 2006). At low strain rates, cortical bone shows elastic behaviour (linear *stress vs. strain* increase); if the elastic limit is surpassed, bone displays a shy plastic behaviour (nonlinear) until failure. Conversely, trabecular bone displays an extensive plastic deformation, being able to reach strain of 60% or more (Mercer *et al.*, 2006). The postelastic behaviour of bone is attributed to microcrack accumulation and diffusion of microdamage that occurs when load is applied (Ma *et al.*, 2022).

Bone is considered a time-independent tissue for research purposes; however, bone biomechanics is time-dependent. Their mechanical properties depend heavily on the loading rate (i.e., viscoelasticity) (Dall'Ara and Cheong, 2022; Xie *et al.*, 2017). Understanding bone creep behaviour is of great clinical relevance. It helps in the comprehension of many of the underlying mechanisms occurring in humans life, for example, bones ability to dissipate energy during exercise, the relationship between ageing and bone fractures, bone implants longevity and the role of mechanical deterioration in bone diseases (Pollintine *et al.*, 2009; Xie *et al.*, 2017). Pollintine *et al.*, (2009) analysed the compressive behaviour of human vertebral segments (two vertebrae with the intervening disc and ligaments) of adult and elderly human cadavers. They found that, independently of pre-existing crack-damage, creep deformation was responsible for height decrease in elderly vertebrae. Taylor *et al.*, (2002) used finite element analysis to simulate the fatigue behaviour of trabecular bone. Their model predicted the gradual failure of individual trabeculae that, after its fracture, redistribute the stresses to neighbouring trabeculae. As the stresses redistribute across nearby trabeculae, they experience higher fracture rates, creating a "s*nowball*" effect until the complete collapse of the material. The authors attributed this behaviour to the time-dependent degradation of the modulus caused by fatigue.

Finally, time, in years of age, has a negative influence in bones. Bones are prone to lose strength and stiffness with age. The mechanism behind these loses are numerous, for example loss of mineralised tissue caused by a reduction in OBs activity, lower bone remodelling response to mechanical loading and reduction in collagen production (Dall'Ara and Cheong, 2022). Moreover, ageing is related to the onset of chronic diseases and with the worsen of inherited (genetic) conditions (Bonicelli *et al.,* 2022; El-Gazzar and Högler, 2021). Thus, the access to health care and clinical follow up is essential for the maintenance of health quality and reduction of economic burden.

There are diverse ways to measure the mechanical properties of materials which are normally divided depending on the level of analysis (from macro- to nano-level). The available methods rely on the researcher's understanding of the features present in their samples, such as the size and shape, and which type of information the researcher desires to obtain. The selection of the appropriate method is of paramount importance for materials like bone due to their complex hierarchical structure and convoluted shape (Chen and McKittrick, 2011; Sharir *et al.,* 2008; Szabo and Rimnac, 2022).

2.3.1. Macro-mechanical

The mechanical assessment of bones in the macro-level (e.g., whole bone assessment) is very interesting for both researchers and clinicians. It is at this scale that most of the daily fractures are observed. On this level of analysis, commonly, two techniques are used: compressive tests (Chen and McKittrick, 2011; Loundagin *et al.,* 2020) and bending tests with three- or four-point bending machines (Cutcliffe and DeFrate, 2021; Deckard *et al.,* 2017; Diab *et al.,* 2006; Lee *et al.,* 2022; Sharir *et al.,* 2008); other techniques such as torsion and impact measurements are also performed, however, way less frequently due to the complexity of their analyses (Sharir *et al.,* 2008).

Bending tests involve placing the piece of analysis (bone) into two supports. In three-point bending, a single loading cell is pressed onto the middle of the opposite side of the sample, creating a sharp conical-shaped bending moment into the neutral axis (middle) the bone (Deckard *et al.*, 2017; Sharir *et al.*, 2008); in four-point bending, two equally distant cells are pressed onto the opposite side of the sample; this creates a trapezoidal bending moment into the neutral axis of the sample (Cutcliffe and DeFrate, 2021; Sharir *et al.*, 2008). **Fig. 7** shows a representation of these two methods.

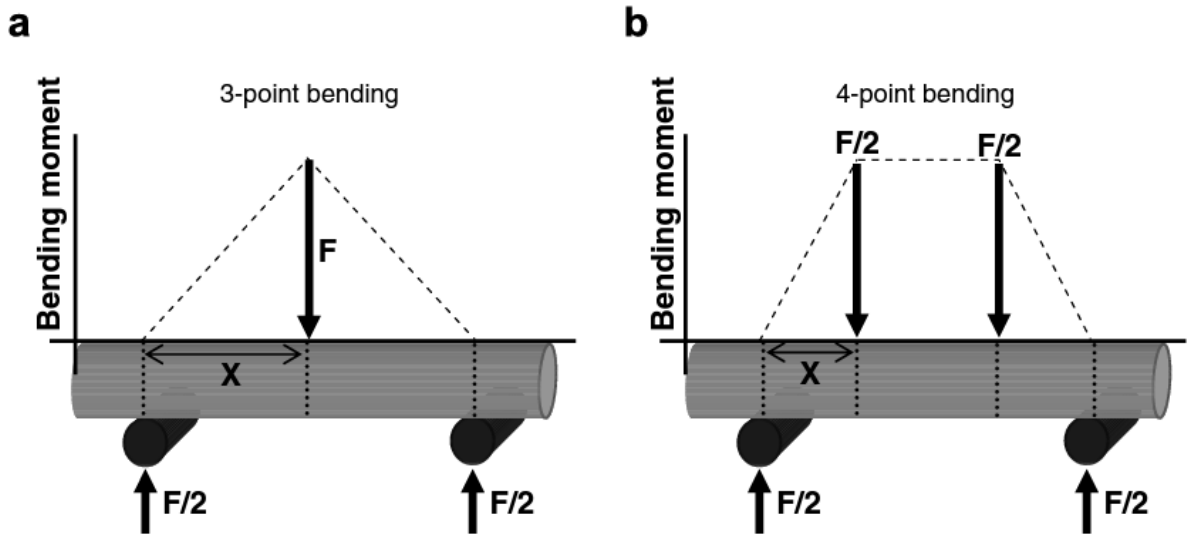

Fig. 7 Schematics showing the equipment configuration and bending moments of (a) three-point bending and (b) four-point bending. The dotted lines represent the bending moments created by the two setups. Image from Sharir et al., 2008.

Using four-point bending techniques can be advantageous compared to three-point bending, as the moment resultant from the forces applied is uniform through the length of the sample; also, by testing a larger area, the probability of incorporating a bone defect or porosity into the results is increased. Three-point bending tests are preferable as the analysis of large pieces of bone relies heavily in the geometry of the piece, and it can be troublesome to put the two loading cells into contact with an uneven surface (Sharir *et al.*, 2008). As a load is applied to the sample,

a deflection originated from this load is recorded by a software, generating a force-deflection graph (Cutcliffe and DeFrate, 2021; Deckard *et al.*, 2017). From bending tests, it is possible to obtain information about the stiffness, yield point and maximum and fracture loads of a material. The Young's modulus (here referred to as *E'* to avoid confounding with elastic modulus obtained by other mechanical tests) can be estimated by deriving the area below the elastic region of a *stress vs. strain* curve (Morgan *et al.*, 2018). For the purpose of this thesis, a simplified analysis of the Young's modulus can be given by, in a three-point bending setup:

$$M = \frac{F}{2}(L - x) = \frac{F \cdot L}{4} \quad (1)$$

Where F is the force being applied by the load cell, L is the distance between the two bottom supports and x is the middle point in the sample.

$$\epsilon = \frac{12 \cdot c}{L^2} \cdot \mathrm{h}_{vertical} \quad (2)$$

Where c is the distance from the neutral axis and *h* is the vertical displacement. Finally:

$$\mathrm{E}' = \frac{\sigma}{\epsilon} = \frac{F \cdot L^3}{48 \cdot I \cdot h_{vertical}} \quad (3)$$

Where *I* is the cross-section moment of inertia.

Szabo and Rimnac (2021) compiled, in their systematic review, a series of studies involving three-point bending tests on still developing human cortical bone. They found the *E'* of young individuals increases as their bones become more mature (up to 17 years old); the values of *E'* range from 0.45-1.98 GPa at 0~1 years of age, to approximately 16 GPa at 16~17 years of age.

Moreover, they found that the *E'* increases exponentially at birth and, after two years, the increase happens at lower rate.

2.3.2. Nano-mechanical

The quality of bones to be organised in hierarchical structures makes it necessary to investigate its biomechanical properties in the multi-scale (Meyers and Chen, 2014; Rodriguez-Florez *et al.*, 2013). Differently from macro- and micro-level analyses, at sub tissue level, the mechanical testing is not affected by the shape, size or porosity of the samples (Rodriguez-Florez *et al.*, 2013). However, the technique depends on other factors, such as sample hydration, surface finishing, probe geometry and analysis methods (Bembey *et al.*, 2006; Bushby *et al.*, 2004; Ebenstein and Pruitt, 2006; Rodriguez-Florez *et al.*, 2013). The nano-mechanical attributes of samples are usually measured by Nanoindentation (NI) or Atomic Force Microscopy (AFM) (Ebenstein and Pruitt, 2006). These sub-tissue techniques have been used to test a range of materials from mineralised tissues (Bushby *et al.*, 2004; Ge *et al.*, 2006), soft tissues (Ebenstein and Pruitt, 2006) and materials for engineering applications in general (Wang *et al.*, 2022). For the purpose of this thesis, the focus of the discussion will be centred in mineralised tissues, more specifically bone.

By investigating the small features of bones, it was possible to verify that, not only the mechanical properties are distinct in cortical and trabecular bones, but also varies in diverse directions (e.g., longitudinal *vs.* transverse) (Rho *et al.*, 1997). Zysset *et al.*, (1999) analysed cadaveric human femurs from donors with an average of 75.3 ± 11.7 years of age, as shown in **Fig. 8**. They indented the diverse features present in the diaphysis and the necks of these femoral bones; in both locations, the *E* of the interstitial lamellae showed higher values than those obtained from the osteonal regions. In the same study, Zysset and collaborators (1999) showed that the cortical shell of the neck of femoral heads have intermediate *E* to the diaphyseal

and trabecular femoral bone, attributing this behaviour to a mechanism to avoid mismatch between the structures.

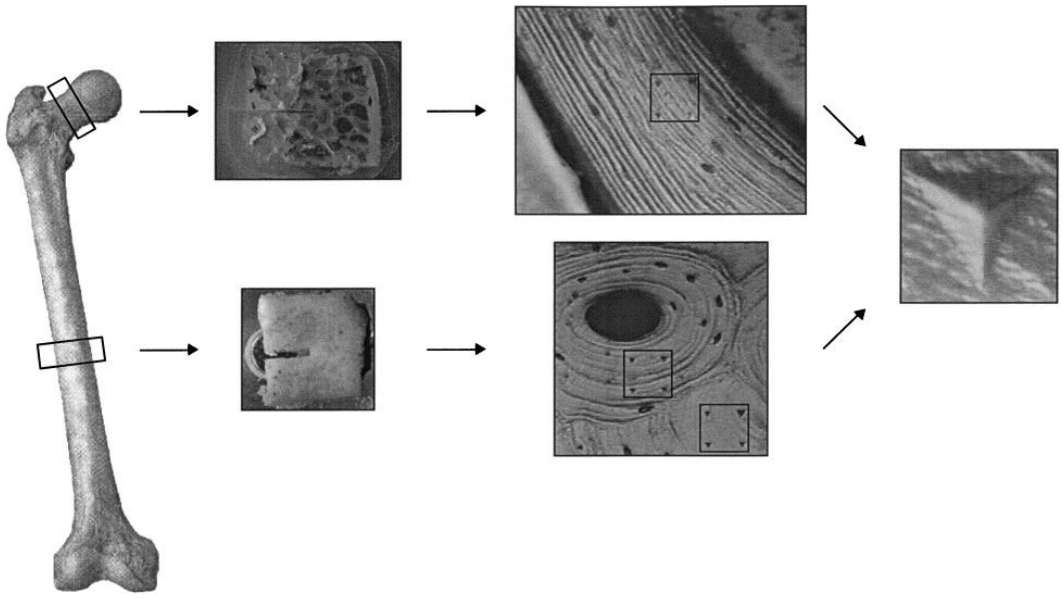

Fig. 8 Bone specimens that were retrieved from cadaveric donors. The diaphysis and the neck of the femurs were embedded into resin. Osteonal, interstitial lamellae and trabecular regions were tested. Image from Zysset et al., 1999.

Another application of NI is on the evaluation of diseased mineralised tissues and effects of genetic mutations on the biomechanics of bone (Ebenstein and Pruitt, 2006). These often involve the use of small animals such as mice and zebrafish, that help to understand the role of hierarchical structures and local tissue properties on bone diseases and bone malformation (Lee *et al.*, 2022; Zhang *et al.*, 2002). However, nanomechanical assessment has been shown useful to test effects of drugs used as medication for bone diseases (e.g., OP) in humans. In a study, bone biopsies from patients intaking bisphosphonate, for the duration of 1.1 to 20 years, were collected and analysed with a NI (Pienkowski *et al.*, 2019). They found that the treatment of OP with bisphosphonates increases *E* for six years from the start of medicine administration; afterwards, the *E* has a steady behaviour, not demonstrating any significant increase of decrease.

On the other hand, the bones *H* reached its peak in double the time but, similarly to *E* behaviour, showed no more significant increasing or decreasing afterwards.

2.3.2.1. Creep measurements

Bone creep is the deformation suffered by a material when a constant load is applied to its surface (Novitskaya *et al.,* 2014; Wang *et al.,* 2022; Wu *et al.,* 2011). The creep happening in our bones have relationship with many mechanisms, for example, the decrease in the height, that affect specially the elderly, may be attributed to the constant creep-deformations occurring in their vertebrae (Pollintine *et al.,* 2009). Another important application of creep in humans life is the failure in the interface bone/prosthetics (Novitskaya *et al.,* 2014).

Bone failure due to creep may cause burden since the load needed to fracture is lower than the ones needed to fracture healthy and intact bone; the microdamage caused by creep accumulates over the time until they develop to the point of fracture (Novitskaya *et al.,* 2014; Pollintine *et al.,* 2009). Creep behaviour is composed by three distinct stages, as described by the *stress vs. strain* curve in **Fig. 9**. In the primary region (purple), the strain increases rapidly in a short period of time. Then, a steady, but less rapid, increase in the strain can be observed as the load is constantly applied for longer times (secondary region (green); if the load is removed at any point when the material is in the secondary region, then a small elastic recovery happen, remaining a permanent plastic strain, classified as creep damage. Ultimately, the tertiary region (dark yellow) is where the accumulation of microdamage leads to the failure of the material.

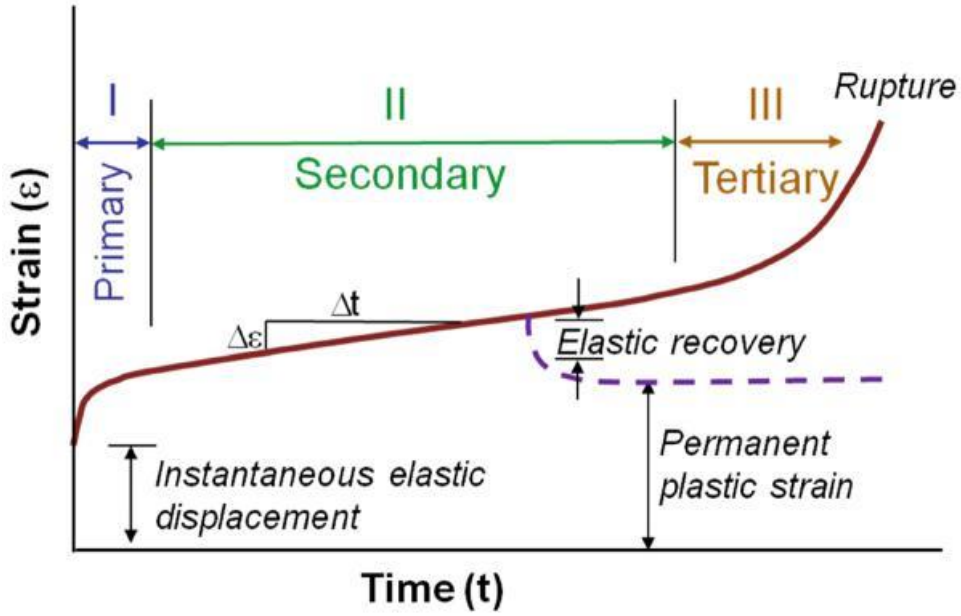

Fig. 9 Primary, secondary and tertiary behaviour of a specific material when subjected to constant load. Image from Novitskaya et al., 2014.

In order to obtain classic creep curves as the one showed in the figure above, often uniaxial tests such as compressive (Novitskaya *et al.*, 2014) or tensile (Bowman *et al.*, 1994) apparatus are used. As explained in the **section 2.3.2** of this chapter, nanoindentation possess many advantages over uniaxial testing for bone measurements; these advantages involve especially sample size and geometry, that do not jeopardise results in nano-level (Rodriguez-Florez *et al.*, 2013). Thus, methods to obtain plasticity characteristics using NI instrumentation were proposed, including the "*stress exponent*" (n_{STRESS}) (Burley *et al.*, 2020). This method involves a series of simplifications on the complex *stress vs. strain* patterns originated by the contact of an indenter tip (e.g., Berkovich) to the surface of a material via creep deformation. The derivation of this method and its application is, although, out of the scope of this thesis, but might be useful for future analysis of bone.

2.3.3. Mechanical properties and constitutive modelling

A growing field in the biomechanical evaluation of bone is computational modelling, more specifically, constitutive modelling. As described by Pahr and Reisinger (2020), constitutive models "*aims to replicate what has been observed in reality by means of a mathematical framework based on fundamental physical principles*". In other words, these models aim to investigate (and potentially solve) problems that surround the interaction between two distinct materials, for example, of prosthetics and bone (Natali *et al.*, 2008). These models are fed with input data (e.g., *E*, bone morphometrics and anisotropy) and generate trustworthy outputs (Pahr and Reisinger, 2020). **Fig. 10** represents the principle of constitutive modelling as described in this section. Further analysis on constitutive modelling is out of the scope of this thesis.

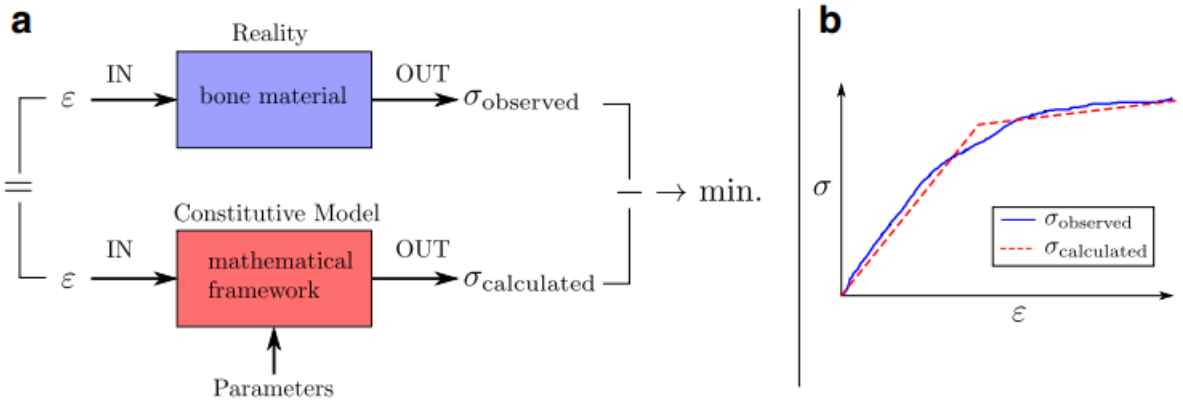

Fig. 10 (a) Schematics of constitutive modelling. Material characteristics are fed to a model (e.g., strain) and an output is received (e.g., stress). (b) A produced stress vs. strain curve from the constitutive model used in (a). Image by Pahr and Reisinger, 2020.

Further discussion on the biomechanics at nano-level will be carried further in this thesis, where topics such as the effects of hydration in *E* and *H*, as well as creep deformation will be addressed. Compressive mechanical tests on bone, despite important, are out of the scope of this thesis.

2.4. Bone diseases

Bone diseases may develop when these perfectly timed cycles lose their balance or uncouple. Uncoupling of bone removal/fabrication, may lead to bone diseases and, consequently, may impair the individual's normal activities by reducing bone strength and reshaping microarchitecture (Andersen *et al.,* 2013; Forlino and Marini, 2016). Conversely, some bone diseases are not chronic in their nature, but originate from qualitative/quantitative mutations during the formation or incorporation of type-I collagen into the bone matrix. Collagen mutations inevitably change the ratio between protein and mineral in the bone, consequently, it modifies the mechanical properties and may increase brittleness (Morgan *et al.,* 2018; Wang *et al.,* 2001).

2.4.1. Osteoporosis

The WHO (1993) introduced the modern definition of OP: a "*systemic skeletal disease characterised by low bone mass and microarchitectural deterioration of bone tissue, with an increase in bone fragility and susceptibility to fragile fractures*". These bone microarchitectural changes might occur in a situation where the skeletal cells are either forming or removing more bone than it should (uncouple), shifting bone homeostasis to positively or negatively, in this order (Mohamed, 2008). In this case, excluding a normal situation where bone remodelling is working as intended, four scenarios are possible:

I. High OBs activity with normal OCs activity ($\Delta > 0$).
II. High OBs activity with decreased OCs activity ($\Delta > 0$).
III. High OCs activity with normal OBs activity ($\Delta < 0$).
IV. High OCs activity with decreased OBs activity ($\Delta < 0$).

The scenarios I and II will lead to more bone being formed than resorbed, decreasing bone porosity, causing a condition called "osteopetrosis," which means "*stony or petrified bones"* (Whyte, 2023). Conversely, scenarios III and IV will eventually increase the porosity of bone and reduce its BMD, leading to the most prevalent of the bones diseases OP, which translates to "*porous bones*" (Chandra and Rajawat, 2021). **Fig. 11** shows a graphical representation of healthy, osteopetrosis and OP conditions.

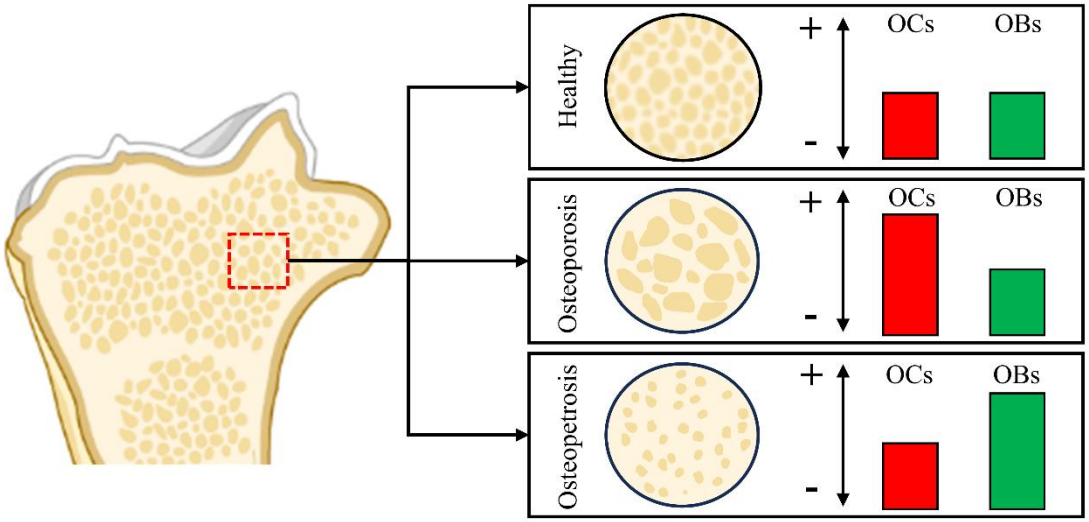

Fig. 11 Schematic representation of healthy, OP and osteopetrosis conditions of bones. Bone removal and formation should be maintained to have a healthy status. In the case of imbalance, one of the conditions may arise. Figure by the author.

Osteoporosis affects over 3 million people only in the United Kingdom (UK) and, every year, more than 500 thousand people receive some type of hospital treatment because of fractures happening as result of the disease (NHS, 2022). In South-East Asia, studies addressing OP received more attention in the 80's, later than what was seen in the West. They estimate that, by 2050, hip fracture rates will increase 3.55-, 3.53- and 2.79-fold in Malaysia, Singapore and Thailand, respectively (Cheung *et al.,* 2018). Studies suggests that, also by 2050, 4.5~6.3 million of hip fractures will occur, accounting for direct costs of 15 billion USD with hospital interventions (Cheung *et al.*, 2018; Cooper *et al.*, 1992; Gullberg *et al.*, 1997). On the long

term, the costs of treating osteoporosis will burden the World's economy (Hajat and Stein, 2018; Rachner *et al.,* 2011; World Health Organization, 2020; Wu *et al.,* 2021). Moreover, it has been shown in meta-analysis that a subsequent fracture is more likely to occur in cases of fracture history, independent if bone diseases (e.g., OP) are present (Kanis *et al.,* 2004). Another study has compiled and amplified the findings of Kanis *et al.,* (2004) and showed an increase of 23 % of fractures incidence, in the first 10 years of follow-up, in women that self-reported having no fractures in their hip or spine since the age of 50 years old (Gehlbach *et al.,* 2012). These data represent some of the economic burden of OP and bone fractures in the years to come.

Osteoporosis often affects woman in their post-menopausal stage of life, but may also affect men, younger adults and children (NHS, 2022). In a recent study, OP burden in men was considered underestimated, since the death rate associated with OP in men is higher than women for the entire lifespan cycle (Zhu *et al.,* 2023). OP can be divided in two groups: primary and secondary. Primary OP arises from natural causes or idiopathic (not known) in their nature (e.g., menopause). Secondary OP may occur as consequence of some habit or medicine intake; the prolonged use of steroidal medications (e.g., glucocorticoids), habit of smoking and/or drinking, eating disorders, ovariectomized women, lack of regular exercising and people who have family history with the disease are among the causes (NHS, 2022). Independent of the reason, OP is an impairing disease that needs to be tracked and treated properly, starting by a correct diagnosis of the cause and identification of the stage of the disease so far. The most common approaches to detect OP are by measuring the BMD of individuals with high resolution spatial tomography or histological techniques (when feasible) (Cheng *et al.,* 2018; Kelley *et al.,* 2013; Marcu *et al.,* 2011). Both techniques have been shown strengths to diagnose outcomes of primary and secondary osteoporosis and, in a scenario where the population is aging and the use of steroidal drugs like glucocorticoids is widespread, the

development of new techniques and models to characterize the disease are extremely important (Becker, 2013; Compston, 2018; Cooper, 2010).

2.4.1.1. Glucocorticoid-induced osteoporosis

As its name indicates, this type of secondary OP develops with the prolonged use or high dosage of steroidal drugs called "glucocorticoids" (Compston, 2018; Cooper, 2010; Silverman *et al.,* 2015). Glucocorticoids are a group of medicinal compounds that is used to treat a vast range of diseases, for example allergies, inflammations, asthma and autoimmune diseases, among others (Becker, 2013; Compston, 2018). These compounds are also called steroidal anti-inflammatory drugs (SAIDs), and they have stronger effect than non-SAIDs since they display both anti-inflammatory and immunosuppressive effects (Becker, 2013). The inflammatory response is common during our body's healing processes. However, the intensity and/or its duration may become harmful on some occasions, leading to a "inflammatory disease." In the cases when this adverse event happens, intervention with SAIDs is interesting due to their dual-phase inhibition mode of action (Becker, 2013).

Most glucocorticoids present similar molecular structure and clinical effects. They differ from each other by the recommended dosage, retention of salts and half-life, as we can see in **Table 1**. Despite the half-life of glucocorticoids became shorter with the development of new compounds, their effects are still considered last longing (NHS, 2022). A specific type of glucocorticoid will often be prescribed depending on their administration route; for example, to treat a condition in the mouth's mucosa, rubbing the location with a cream containing the drug is often recommended, but systemic administration is needed in other cases (Becker, 2013). Another characteristic in favour of the use of glucocorticoids is its relative low price. Prednisolone (PN) is a cheap compound and is the most used glucocorticoid globally (Becker, 2013; Compston, 2018). The prolonged use of PN has been linked with the development of

GIOP (Compston, 2018; Zinganell *et al.*, 2023), and its use is one of the commonest causes of this type of secondary OP (Adami and Saag, 2019). PN and the other compounds in the family of glucocorticoids, are related to increased OCs activity and numbers, while reducing the production of bone regulatory factors (e.g., osteoprotegerin) by OBs (Becker, 2013; Compston, 2018). With the increase OCs and reduction of OBs in the surface of the skeleton, the conditions necessary to the onset of GIOP are met.

Table 1 Commonly used SAIDS and their differences in dosage, Na^+/H_2O retention and half-life.

Drug	**Dose, mg**	**Na^+/H_2O Retention**	**Biologic Half-Life [h]**
Cortisol (Solu-Cortef)	20.00	1	8–12
Prednisone (Deltasone)	5.00	0.8	12–36
Methylprednisolone (Medrol)	4.00	0.5	12–36
Triamcinolone (Kenalog)	4.00	0	12–36
Dexamethasone (Decadron)	0.75	0	36–72
Betamethasone (Celestone)	0.75	0	36–72

Data from Becker (2013).

Osteoporotic fragile fractures due to GIOP are associated with age, gender, history of fractures through life, glucocorticoid dosage and duration (Cooper, 2010; Laurent *et al.*, 2022). It has been reported that brittle fractures due to GIOP occurs in 30- to 50% of people that intake glucocorticoids for prolonged times (Laurent *et al.*, 2022). Glucocorticoids cause a rapid increase in bone loss in the first days of administration, influencing especially the regions of the human skeleton with the highest amount of trabecular bone, such as the spinal cord and the hips; despite the continuous effect of bone loss, the rate of bone resorption decreases as the treatment continues (Laan, 1993). Given the rapid susceptibility to fractures and the potential

economic burden of GIOP, the early diagnosis, the counter medication and the promotion of an active and healthy life could relieve the pressure in healthcare.

2.4.2. Osteogenesis imperfecta

There are several diseases that affect collagen molecules and their ability to assemble properly within each other and the mineralised matrix. One of the most notable examples is OI, also known as "*brittle bone disease*" (Forlino and Marini, 2016). OI is a rare inherited disorder in the *Col1a1* and *Col1a2* that encode the α1(I) and α2(I) chains of type-I collagen (Forlino and Marini, 2016). OI was first classified into four types (I, II, III and IV), based on their clinical severity, by Sillence *et al.,* (1979); years later, other variations of the disorder were added, totalising seventeen classifications (Van Dijk and Sillence, 2014). **Table 2** shows the four original classifications of OI, as described in 1979, as well as their symptoms. People with OI type I accounts for ~71% of the total cases; the most severe (the lethal type II), accounts for 12% of the total cases (Folkestad *et al.,* 2016). In addition to bone fragility, OI patients may show blue sclerae (white of the eyes turn bluish due to the thinning of the collagen fibres), deformed bones, dentinogenesis imperfecta, hearing abnormalities among others (Sillence *et al.,* 1979).

Table 2 Classic OI nomenclature, with their respective inheritance and common features. From Sillence (1979).

Type	Inheritance	Features
I	Autosomal dominant	Mildest form, presents at preschool age (*tarda*), hearing deficit in 50% and is divided into type A and B based on tooth involvement
II	Autosomal recessive	Perinatal lethal
III	Autosomal recessive	Most severe survivable form, fractures at birth and progressively short stature
IV	Autosomal dominant	Moderate severity, bowing bones and vertebral fractures are common, normal hearing and is divided into type A and B based on tooth involvement

The prevalence of OI is 1 to 2 individuals in every 10,000 (Mc Donald *et al.*, 2023); at birth, the prevalence increases to 2 to 3 individuals in every 10,000 babies conceived (Folkestad *et al.*, 2016). One of the most documented features of OI are the frequent bone fractures occurring during a person's lifespan (Folkestad *et al.*, 2016; Forlino and Marini, 2016; Van Dijk and Sillence, 2014). The increased bone fragility is related directly to the type I collagen that is incorporated into the bone. However, the excessive number of fractures are not necessarily connected to the mortality of OI patients (Folkestad *et al.*, 2016). Since type I collagen is the most abundant of the collagens in the human body, its negative effects in other organs of the human body should not be overlooked or neglected. Studies have been linking OI mortality with lungs (Gochuico *et al.*, 2023), the major cause of deaths in OI, and heart conditions (Ashournia *et al.*, 2015). Breathing capacity is severely altered in OI; the deformations in the ribcage caused by defective collagen, impair the natural movements of the organ (Gochuico *et al.*, 2023). Collagen of type I is commonly found in various region of the heart, such as the heart valves and the interventricular septum (Ashournia *et al.*, 2015). Thus, OI, despite being of fairly rare occurrence, cause significant burden to those affected by the disease, especially

at young ages (OI type III) and advanced ages (types I and IV). It has been reported that the median survival times of males with OI is around 9 years below the reference population; for females, the median survival is 7 years below the reference population (Folkestad *et al.*, 2016). **Fig. 12** shows representations of key symptoms of people suffering from OI.

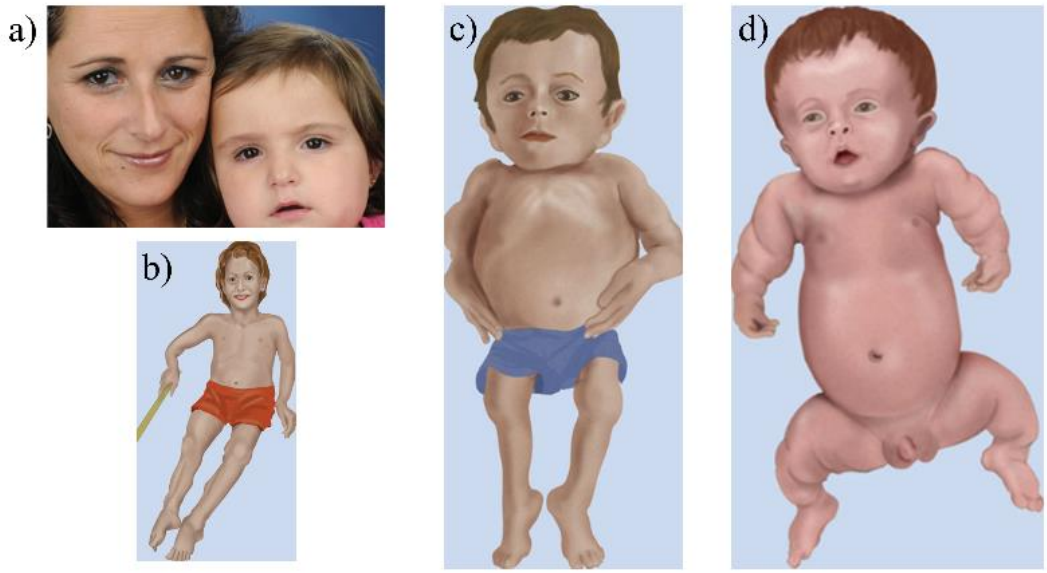

Fig. 12 Severity of OI. (a) Blue sclera in mild OI; (b) bone deformities with decreased growth velocity and height; (c) shortening of long bones in severe OI; (d) shortening of long bones, decreased ossification of the skull and crushed vertebrae. Figure adapted from Van Dijk & Sillence (2014).

Collagen mutations in the bone can be divided into quantitative and qualitative. In general, quantitative defects are related to mild forms of OI (type I). This type of mutation causes the reduction of type I collagen in the bone tissue (haploinsufficiency) and are of common occurrence in heterozygous (Het) variants of *Col1a1*. Not so common are the cases involving "*null*" *Col1a2* variants; they are related to cause Ehlers-Danlos syndrome, characterised by loose joints (Lee *et al.*, 2022; Van Dijk and Sillence, 2014). Qualitative collagen defects occur in more severe cases of OI (types II, III and IV). As its name indicates, qualitative defects originate as result of misfolding, stunned chain propagation and abnormal modifications of the protein (Forlino and Marini, 2016). Qualitative mutations have direct influence in the fibrillogenesis process of collagen. Due to this, the bone matrix is severely affected, generating

stronger phenotypes, especially in Hom mutations (Forlino and Marini, 2016; Lee *et al.*, 2022). In addition, similarly to what occurs in chronic diseases, OI phenotype has been shown increase its prevalence with age (Mc Donald *et al.*, 2023).

OI is still not as well understood as OP, given the heterogeneity of causes and phenotypes of the disease. However, it is important to highlight that, depending on the severity of mutations happening in the collagen fibrils, OI can end up with bone architectures that resemble OP bones (El-Gazzar and Högler, 2021).

2.5. Bone diseases management

Although no cure is available for both GIOP and OI, there are several clinical guidelines and recommendations on how to slow the progress of these conditions and manage their phenotypes (Laurent *et al.*, 2022; Mc Donald *et al.*, 2023). Since they are under "bone disease" category, it is expected that the treatment used to be similar in both diseases.

2.5.1. Glucocorticoid-induced osteoporosis treatment

In GIOP, the terms "prevention" and "treatment" are important and sometimes ambiguous. The first one is related to the intervention, normally made through medication, concomitant to the start of the corticoid therapy; the latter is considered the intervention starting after the third month counting from the first dose of glucocorticoid administered (Rizzoli and Biver, 2015). Prevention and treatments are divided into three categories: general measures, supplementation and anti-resorptive drugs (Devogelaer *et al.*, 2006; Rizzoli and Biver, 2015).

General measures are recommended for all patients taking SAIDS; these measures changes in different countries and should be monitored to adapt to the national guidelines (Rizzoli and Biver, 2015). These guidelines work in a conservative way, being suggested the lowest possible

doses of glucocorticoid that are able to minimize GIOP effects. In addition, a well-balanced nutrition and regular weight-bearing exercising are fundamental. Also, the use of compounds related to boost the body's defence, such as Vitamin D and calcium supplementation intake led to positive outcomes (Laurent *et al.,* 2022). Calcium and Vitamin D associated use show significant decrease in bone resorption rates in the spine; single uses of each substances show decreased medical effect, but still better results than no treatment at all (Homik *et al.,* 1998). Finally, the use of "anti-resorptive drugs" is recommended (Chavassieux *et al.,* 2019; Iba *et al.,* 2020; Laurent *et al.,* 2022). Anti-resorptive drugs comprise all synthetic compounds related to decrease bone resorption and/or to improve bone construction (Rizzoli and Biver, 2015). The bisphosphonates are the group of medicines most used as a treatment to GIOP, and they present a higher potential to reverse the effects of SAIDs in human bones (Drake *et al.,* 2008; Iba *et al.,* 2020; Russell, 2007).

2.5.2. Osteogenesis imperfecta treatment

As mentioned in the introductory part of this section, treatment for OI is never curative. But, with a multidisciplinary approach, it is possible to improve the quality of life of the patients significantly. A number of interventions have been proposed to achieve such objective, such as: 1) drug treatment with bisphosphonates; 2) surgical procedures and 3) physical rehabilitation with moderate exercising and vitamin D (Etich *et al.,* 2020; Forlino and Marini, 2016).

Bisphosphonates are considered the main treatment for OI (Astrom, 2002; Etich *et al.,* 2020). In OI patients, they can improve the BMD of bones, improving its microarchitecture and, consequently, reducing the number of fragile fractures (Forlino and Marini, 2016). In addition, bisphosphonates are often prescribed to reduce bone pain in severe cases of OI (Van Dijk and Sillence, 2014). A study assessed the effects of intravenous bisphosphonate (10~40 mg/m^2) in

28 patients under the age of 18 (Astrom, 2002). In 21 out of 28 of them, no pain was reported; in another two of these patients, pain decreased significantly. The authors attributed the clinical improvements to the increased BMD and increased mineralisation especially in the lumbar spine, which increased children's life quality.

OI is a systemic disease; thus, it affects all long bones in the body. Surgical procedures are recommended depending on the deformity/curvature and working area of the long bones (Wirth, 2019). Surgical procedures in OI involve, firstly, the analysis of the shape of bone and selection of the size of telescoping rod to be used. Osteotomies (procedures that involve cutting the bone to reshape or realign) are performed and, finally, the telescoping rod in inserted (Cho *et al.*, 2007; Fassier, 2021). **Fig. 13** shows a representation of an osteotomy of a curved bone, with the insertion of a telescoping rod. After going through surgery, it was reported an increased survival rate in OI patients (Cho *et al.*, 2007).

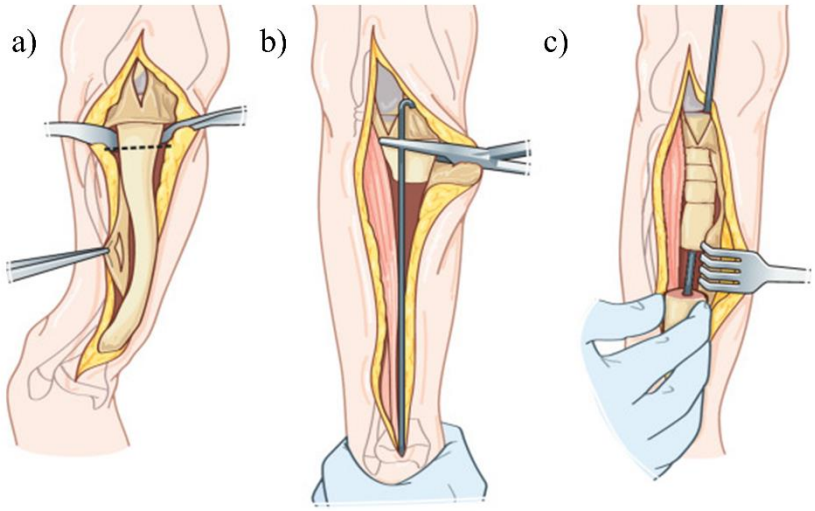

Fig. 13 Realignment procedure in a curved bone due to OI. (a) The affected limb is opened, and the bone was assessed. (b) Osteotomy is performed, and the telescoping rod is inserted. (c) The bones are put into place guided by the rod. In some cases, further material (e.g., bone scaffold) is inserted to promote bone healing. Figure obtained from Fassier (2021).

Lastly, physical therapy guided by professionals provide, among other treatments, the most effective contribution to the rehabilitation of a functional body. Conceptually, the bone structures generated by collagen defects in OI cause higher numbers of fractures, promoting periods of time which the limbs movement are restricted (or disused); as a secondary effect to movement restriction, muscles tend to become weaker (Forlino and Marini, 2016). Physiotherapy promotes muscle strength and, consequently, improves limbs' function and independence. The prescription of bisphosphonates prior to the adoption of physiotherapy has been related to improved results, as the patients feel reduced bone pain (Astrom, 2002).

2.5.3. Bisphosphonates

Bisphosphonates were first called "diphosphonates" because of their Phosphorus-Carbon-Phosphorus (P-C-P) structures (Russell, 2007). They belong to a class of compounds that have high affinity with the insoluble mineral salts encountered in the bones and were firstly used to prevent pathological calcification in Wistar rats (Fleisch *et al.,* 1970). Bisphosphonates promote OCs apoptosis in environments where there is an imbalance in favour of bone resorption (Russell, 2007). More scientific attention was given to the bisphosphonates when research showed their potential to inhibit HAp dissolution and tissue destruction in bones (Russell *et al.*, 1970). Since then, a vast range of P-C-P-based compounds were formulated, and nowadays they are divided into "simple" or "nitrogen-containing" bisphosphonates (Drake *et al.,* 2008; Russell, 2007).

Simple bisphosphonates were the first developed compounds: etidronate and clodronate. Etidronate, even in small doses (5 mg/kg/day), may cause major clinical issues, such as excessive skeleton mineralisation impairment (Siris *et al.,* 1996). Avoiding severe mineralisation impairment is important in cases where bone diseases are in advanced stage and in children that are still developing their skeleton. Nitrogen-containing bisphosphonates are a

bigger and newer family that includes the compounds we use nowadays to treat diverse bone conditions. Important examples of this family of bisphosphonates are alendronate, ibandronate, risedronate, zoledronate and pamidronate (Russell, 2007). **Fig. 14** shows a scheme with the family members of simple and nitrogen-containing bisphosphonates.

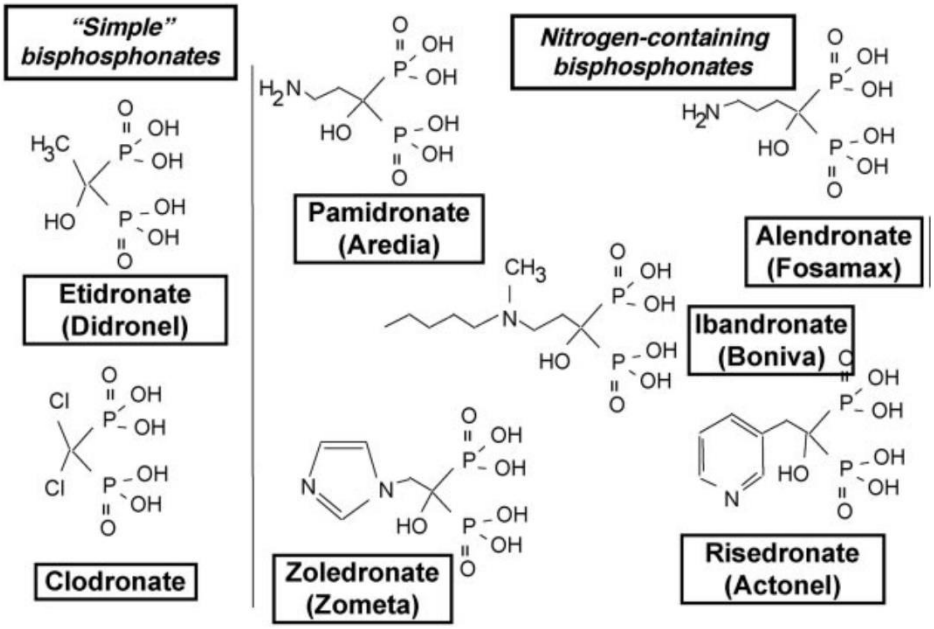

Fig. 14 Structure of the most commonly used bisphosphonates. Nitrogen-containing compounds binds to the bone with the hydroxyls (-OH) termination and inhibit OCs with their nitrogen-containing ends by steric hinderance. Figure obtained from Russell (2007).

Bisphosphonates are both dose- and time-dependent compounds. They remain active in the person's system for prolonged times, with continuing effects recorded for months after the treatment is terminated (Chavassieux *et al.,* 2019; Russell, 2007). A study suggests that bisphosphonates may have a half-life that ranges from 1 to 10 years, depending on the patient rate of bone turnover (Papapoulos and Cremers, 2007). However, this value might be misleading (Cremers *et al.,* 2019).

Nitrogen-containing bisphosphonates display better efficiency in treating bone conditions than simple bisphosphonates due to the bulky nitrogen contained in the R_2 side of their molecules. The reactive -OH ends in the R_1 position is what increase the binding of the compound to the bone surface (Nancollas *et al.,* 2006). Moreover, these high affinity drugs present lower desorption to the surrounding environment and lower diffusion to regions deep within the bone. This allowed doctors to prescribe decreased dosages of medication while boosting its effectiveness (Chavassieux *et al.,* 2019; Fleisch *et al.,* 1970; Hassler *et al.,* 2015; Iba *et al.,* 2020; Nancollas *et al.,* 2006; Russell, 2007). After binding to the surface of bones, the bisphosphonates radicals, especially the R_2 sites, become a preferential spot for OCs to approach; OCs "consume" the medication causing their apoptosis (Russell, 2007).

Bisphosphonates are recommended to the treatment of bone diseases, including OP, Paget's disease and many genetically inherited by infants, such as OI (Cremers *et al.,* 2019; Papapoulos and Cremers, 2007; Siris *et al.,* 1996). In general, their main benefits to diseased bones involve the inhibition of bone resorption, decreasing fracture risk and pain management (Cremers *et al.,* 2019). In severe OI, specifically in children and adolescents, bisphosphonates have shown to increase BMD of lumbar spine, to reduce fracture rate and improve mobility with increased quality of life (Astrom, 2002).

2.6. Animal models for bone diseases

Animal research is typically thought of as involving rodents and monkeys (Kan, 2013; Mirzoyan *et al.,* 2019). More recently, due to a necessity to find alternatives to mammals testing (replace), to enhance the amount of information obtained using fewer individuals (reduce), and to decrease distress caused to the animals (refine), alternative models like the zebrafish and the drosophila melanogaster (also known as common fruit fly) were proposed (Embry *et al.,* 2010; Lieschke and Currie, 2007; Mirzoyan *et al.,* 2019). The adoption of the "*replace, reduce and*

refine" principles in research is known as 3Rs and, despite not substituting higher vertebrates models completely, have been shown dependable for diverse fields of study (e.g., genomics and metabolism) (eBioMedicine, 2022). **Table 3** shows a summary of two common animal models used in research with their respective strengths and weaknesses for the purpose of pre-clinical research.

Table 3 Attributes of key animals used to model human disease. Data extracted from Lieschke (2017).

Attributes of disease model	Model organism	
	Zebrafish	Mouse
Husbandry infrastructure	$	$$$
Cost per animal per year	$	$$$
Characterized inbred strains	-	+ + + +
Outbred laboratory strains	+ + +	+ +
Anatomical similarity	+	+ +
Molecular or genetic similarity	+ +	+ + +
Pathological similarity	+ +	+ + +
Storage; for example, freezing sperm	Yes	Yes

$ Relative cost. More symbols mean higher price.

- Not a strength or not relevant.

+ Strength or relevant. ++++ Mean outstanding strength of the model.

2.6.1. Zebrafish

Zebrafish (*Danio rerio*) are 2~5 cm long freshwater fish originated from Southeast Asia. Zebrafish emerged as an important substitute to mammals due to its remarkable characteristics, such as small size, genetic traceability and optical transparency while infants (Busse *et al.*, 2020). In addition, they show strong biological similarities to humans, with ~70% of genetic correspondence (Lieschke and Currie, 2007; Mackay *et al.*, 2013), and in some parts, these fish can be more complex than humans (e.g., number of bones in the skull) (Bird and Mabee, 2003).

Zebrafish produce a high number of externally developing embryos supporting large scale research (Busse *et al.*, 2020). They achieve their maturity in about three months of development, while humans achieve at 15 years of age, if both genders are included (Lieschke and Currie, 2007); then, by using zebrafish model, researchers may reduce the time spent on the exacerbation of clinical conditions and medicament effects, improving animal welfare by, for example, reducing pain (Bailone *et al.*, 2020). Zebrafish husbandry is cheaper, not requiring extensive apparatus (Dubińska-Magiera *et al.*, 2016; Lieschke and Currie, 2007) and demands a relatively low stocking cost, as it is possible to raise a higher number of individuals in the same room (Fleming *et al.*, 2005; Lieschke and Currie, 2007; Pasqualetti *et al.*, 2015). Thus, zebrafish model contributes strongly to the 3Rs of animal experiment once that, for example, the number of rodents is reduced.

Since the studies involving zebrafish started, in the 1990s, researchers have been exploring the potential of the *Danio rerio* as a model to bone maturation (Chang *et al.*, 2018), bone-related diseases and defects (Bergen *et al.*, 2019; Carnovali *et al.*, 2016; Carson *et al.*, 2018; Chen *et al.*, 2017; Fisher *et al.*, 2003; Fleming *et al.*, 2005; Yan *et al.*, 2019), heart-related diseases (Genge *et al.*, 2016), organs regeneration (Azevedo *et al.*, 2011; Cardeira *et al.*, 2016; Lin *et al.*, 2020; Wan and Goldman, 2016), among others (Marques *et al.*, 2019). Specifically, for GIOP, zebrafish raised in popularity after Barret and colleagues (2006) first proposed a methodology to exacerbate the disease by adding glucocorticoid in the fish's water. They took advantage of the transparent characteristic of young zebrafish and observed their stained bones with fluorescence microscope; with this they were able to highlight bone features that are characteristic of osteoporotic bones.

Zebrafish are more versatile in comparison to mammals due to mammal's limited ability to regenerate their tissues (Marques *et al.*, 2019). Zebrafish are vertebrates capable of

regenerating their fins, scales, retina, spinal cord and heart among other structures (Cardeira *et al.,* 2016; Iovine, 2007). This is a process not limited by the fish's age, and happen throughout their lifetime, independently of repeated amputations or injuries (Azevedo *et al.,* 2011). For bone diseases research, this feature allows the tracking of the bone evolution throughout the initial stages of development (embryos) and permits the assessment of drugs' effects during the regenerative stages.

Zebrafish have two distinct types of bone formation (Bird and Mabee, 2003; Breeland *et al.,* 2021). The fish's fins and scales are dermal bones, while the backbone and skull are endochondral. This opens a diverse range of possibilities in assessing the unique features of bone diseases. The options for zebrafish skeleton visualisation are diverse; among the most common techniques are the μ-CT and observation under fluorescent light (Barrett *et al.,* 2006; Silvent *et al.,* 2017). μ-CT is a powerful, high cost and time-consuming technique. With it is possible to observe bones in 3-D models as well as to calculate bone metrics such as BMD (gold standard parameter for bone diseases) (Charles *et al.,* 2017; Monma *et al.,* 2019).

A less costly and less time-consuming option is the direct observation of bones under fluorescent light. This method requires a dark room and can be used in anaesthetised fish, enabling the follow-up of same individuals (Cardeira *et al.,* 2016). Moreover, 3D visualisation of bones and calculation of bone metrics is restricted. The most commonly used staining dye for bone observation in zebrafish is Alizarin Red-S (AR-S) (Fleming *et al.,* 2005; Knopf *et al.,* 2011). AR-S is a compound able to attach spontaneously to calcium-containing tissues and be used to observe the various aspects of bone mineralisation (Bensimon-Brito *et al.,* 2016a). These set of methodologies have been performed in many studies to evaluate the mineral quality (Bergen *et al.,* 2019) and to assess anabolic or catabolic effects of different medicine commonly used in the treatment of OP and other bone-related diseases (Carson *et al.,* 2018;

Chen *et al.*, 2017; Fleming *et al.*, 2005; Geurtzen *et al.*, 2017). Examples of the utilization of AR-S staining and fluorescence observation can be seen in **Fig. 15**.

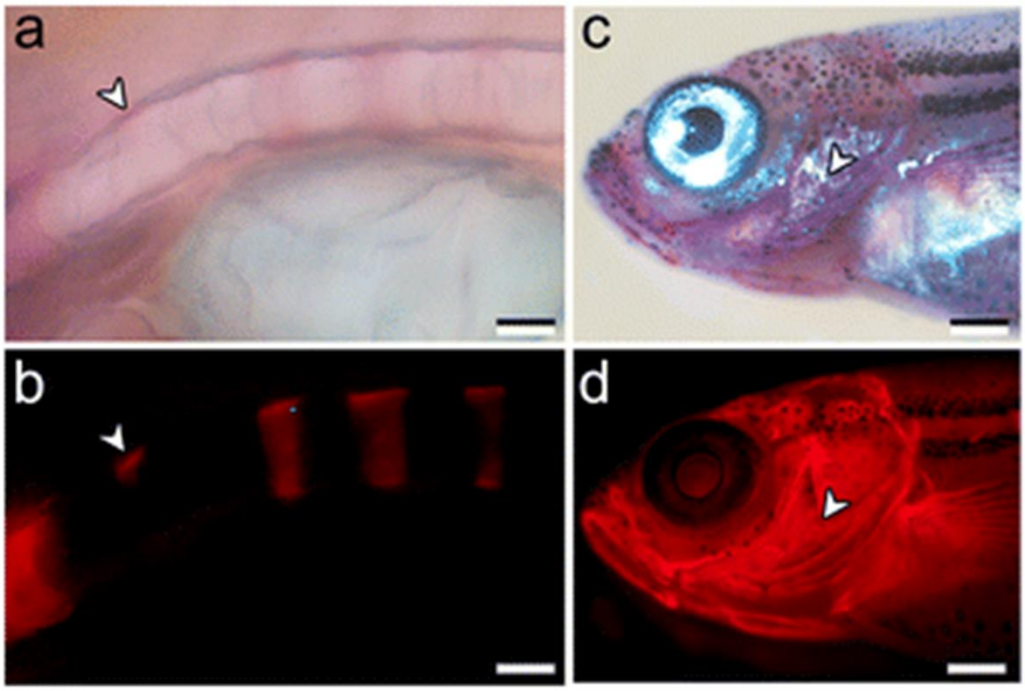

Fig. 15 AR-S staining of young (10 dpf) zebrafish, showing features in (a-b) the vertebrae and (c-d) the skull. The bright field images (a and c) show less details than the observation of the stained tissue observed in the images below (white arrowheads). Image obtained from Bensimon-Brito et al., (2016).

2.6.1.1. Caudal Fin

Zebrafish caudal fin allow the experimentation to be performed in living anesthetized animals, since no euthanasia is needed for resection/regeneration protocols (Azevedo *et al.*, 2011; Cardeira *et al.*, 2016). The follow up of the same animal throughout the duration of the experimentation, potentially, minimize the effects of intrinsic variations that may be present in

big populations. In other words, the same fish can be compared in two or more endpoints. **Fig. 16** shows the morphology of a zebrafish caudal fin.

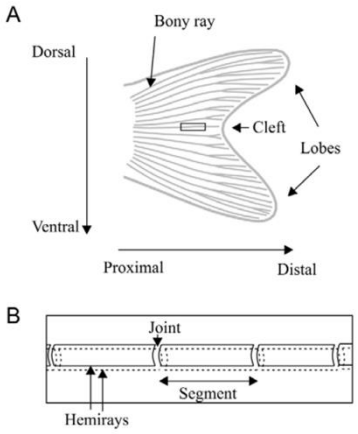

Fig. 16 Morphology of zebrafish caudal fin (a-b). (a) The fin has a bi-lobed shape with tiny bony rays (also known as lepidotrichia) within it; as the bony rays approach the cleft, they display a bifurcation. (b) Details of a single bony ray; these rays are formed by two hemi rays that do not connect to each other. Image obtained from Rolland-Lagan et al., (2012).

The zebrafish caudal fin displays a fast and robust regenerative process; it is of easy access and has simple architecture, causing little to no stress to the animal to be resected or analysed (Azevedo *et al.*, 2011; de Vrieze *et al.*, 2014). The anatomy of the fin consists of segmented bony rays connected by mesenchymal tissue, all placed within an epidermis (Azevedo *et al.*, 2011). The tail fin presents a bi-lobed shape, common in most fish, indicating that the bony rays localized near to the dorsal and ventral sides, grow faster and longer than the ones presented in the cleft (Cardeira *et al.*, 2016). The fins of young fish are translucent, which enables readily images of its cells or stained calcified matrix to be visualized with fluorescence spectroscopy and µ-CT (Silvent *et al.*, 2017); as the fish grow older, the caudal fin's dermis lose its transparency but can still be observed under fluorescent light (Azevedo *et al.*, 2011).

2.6.1.2. Vertebrae

Zebrafish vertebrae is composed of 31 bone segments, on average, and possess four distinct parts, each one with its own anatomical differences and utilities: The Weberian Apparatus (WA1 to WA4), the pre-caudal vertebrae (PC1 to PC10), the caudal vertebrae (CV1 to CV14) and the caudal fin vertebrae (CFV1 to CFV3) (Bird and Mabee, 2003). The minerals located in the zebrafish backbone have higher BMD than the fish fin bony rays. The increased BMD may be attributed to the endochondral bone formation, rather than dermal (Bird and Mabee, 2003; Breeland *et al.,* 2021). Because of this, the preferred method to assess bone morphology and morphometrics in this location is by using μ-CT technology (Bird and Mabee, 2003; Charles *et al.,* 2017; Monma *et al.,* 2019). μ-CT enables small features/defects detection if high resolution is used (small voxel size); the current literature using μ-CT for skeletal assessment in zebrafish uses a broad range of resolutions (μm / voxel size), ranging from 5~7 μm (Charles *et al.,* 2017; Monma *et al.,* 2019), to more than 20 μm (Hur *et al.,* 2017). Despite preferred, μ-CT is not the only option. AR-S have shown effectiveness in the observation zebrafish backbone, although the fish must have their scales removed prior observation (Bensimon-Brito *et al.,* 2016b); young fish are desirable in this technique. **Fig. 17** shows a side view of a zebrafish skeleton (excluding the skull), highlighting in distinct colours the anatomy of the vertebrae.

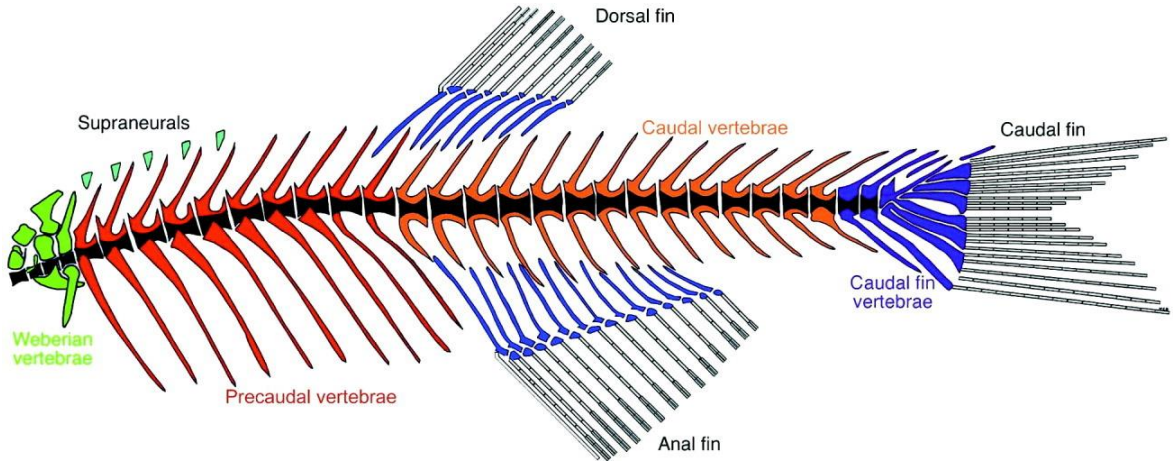

Fig. 17 Representation of the skeleton of a zebrafish with the WA (in green), the PC (in red), the CV (in orange), and the CFV (in blue). Image obtained from Bird & Mabee (2003).

In comparison to the caudal fin, the zebrafish vertebrae represent a more robust model for preclinical studies. Its similarities with mammal's bones go beyond bone formation; the changes in the mechanical properties while ageing is, at some degree, comparable to those of mammals (Chang *et al.,* 2018). In addition, their vertebrae have a layered structure, with each segment of the vertebrae starting its mineralisation from the centre and terminates by increasing its thickness through the axial direction (Bird and Mabee, 2003). The layered configuration generates heterogeneity in the mechanical properties of vertebrae segments. It has been demonstrated that the elastic modulus (*E*) and hardness (*H*) decrease from the centre of the bone outward (Ge *et al.,* 2006; Zhang *et al.,* 2002). Despite its bulky volume in comparison to fish's lepidotrichia, characterising the mechanical properties of these bones can be tricky. Thus, mechanical analysis on macrolevel (e.g., bending or compression) is not feasible (Ge *et al.,* 2006). AFM and NI have been used for this purpose and displayed to be sensitive enough to detect small mechanical alterations with high significance (Chang *et al.,* 2018; Ge *et al.,* 2006; Zhang *et al.,* 2002).

2.6.2. Rodents

As example of OI and OP, bone diseases can be overwhelmingly heterogenous (Mäkitie *et al.*, 2019; Sillence *et al.,* 1979; Van Dijk and Sillence, 2014). It is safe to state that mapping the different phenotypes of these diseases in human subjects, can be challenging. Rodents are considered excellent pre-clinical subjects for bone diseases due to their versatility. Mice display high degree of genetic conservation, process and interact with medicines in similar fashion as humans and other mammals do (Kan, 2013). Moreover, their cell biology and physiology are also homologous to humans (Lieschke and Currie, 2007). **Fig. 18** shows a representation of the skeleton of a mouse. Similarly, to what is observed in other mammals, the bone of mice originates from embryonic mesoderm, a reason why their bones (e.g., femur) are very similar to the one of humans (Carretero *et al.,* 2017). The drawbacks of rodents in research involve their size, infrastructure needs for husbandry, and high cost for maintenance (Kan, 2013; Lieschke and Currie, 2007).

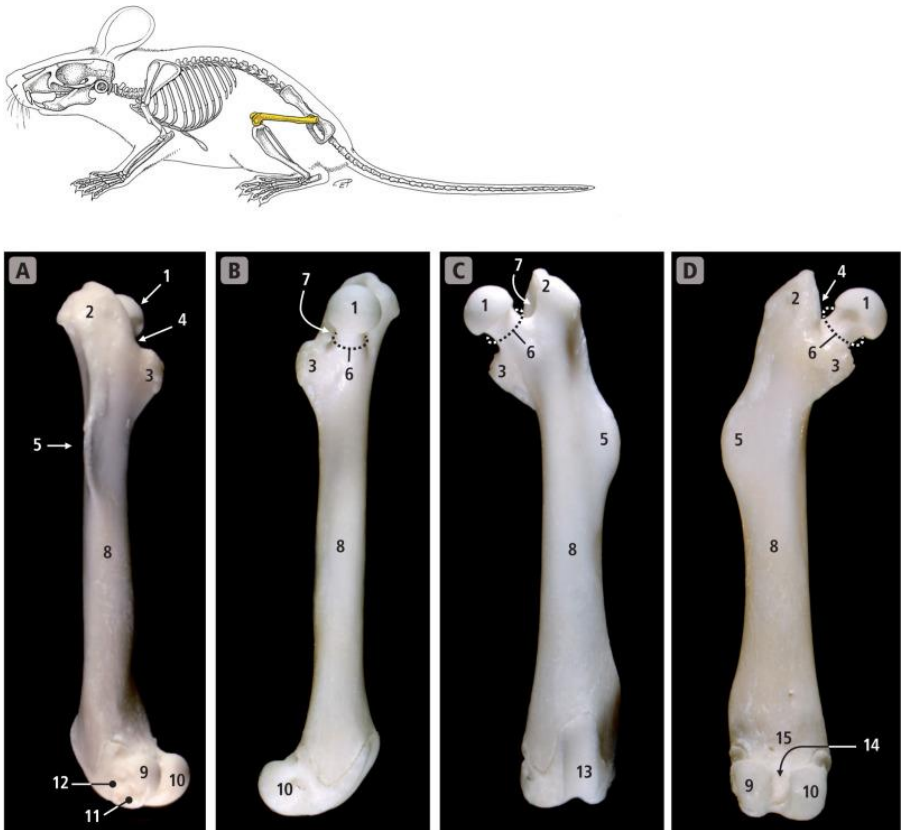

Fig. 18 Schematic highlighting the femoral bone in mouse (top). (A) shows the lateral view, (B) the medial view, (C) the cranial view and (D) the caudal view. The numbers in the figures represent: (1) head of femur, (2) greater trochanter, (3) lesser trochanter, (4) intertrochanteric crest, (5) third trochanter, (6) neck of femur, (7) trochanteric fossa, (8) body of femur, (9) lateral condyle, (10) medial condyle, (11) extensor fossa, (12) fossa for m. popliteus, (13) femoral trochlea, (14) intercondylar fossa and (15) popliteal surface.

With the advances in genetic modification of mice, the production of a wide range of OI phenotypes was possible, with more than twenty genetic variations been reported to the moment of this writing (Carriero *et al.,* 2016). Although the number of genetic possibilities increased in the last decade, from the point of view of developing safer treatment strategies for specific OI variations, the number is still insufficient (Alcorta-Sevillano *et al.,* 2022). Among the available mice models, the *oim*, the Amish mice (*Het G610C*) and the brittle mice (*Brtl*)

are extensively used (Alcorta-Sevillano *et al.,* 2022; Lee *et al.,* 2022). In addition, other mice mutations may have similar genetic features as *oim* but do not show OI brittle phenotype (Lee *et al.,* 2022). This is the case of the C*ol1a2*-null, also known as *tm1b* (Skarnes *et al.,* 2011).

2.6.2.1. Osteogenesis imperfecta murine (*oim*)

Oim is the most commonly used model for severe OI III (Carriero *et al.,* 2016; Fratzl, 2008). This mutation gained popularity due to its spontaneous generation from the breed between mice *C3H/HeJ* and *C57BL/6JLe* (Chipman *et al.,* 1993). This means that the *oim* mice are not "genetically engineered" as it occurs in other mutations (Lee *et al.,* 2022; Skarnes *et al.,* 2011). The *oim* mutants display abnormal folding of the pro-α2(I) due to a guanidine deletion at nucleotide 3983 of the *Col1a2* gene. The consequence of this misfolding prevents its association with pro-α1(I) chains, which results in excessive quantities of abnormal homotrimeric $(\alpha1)_3$ in the ECM (Alcorta-Sevillano *et al.,* 2022). The mice affected by this mutation displayed severe osteopenia, reduced body size, fragile bone fractures, and skeletal deformation (as observed in the **Fig. 19**).

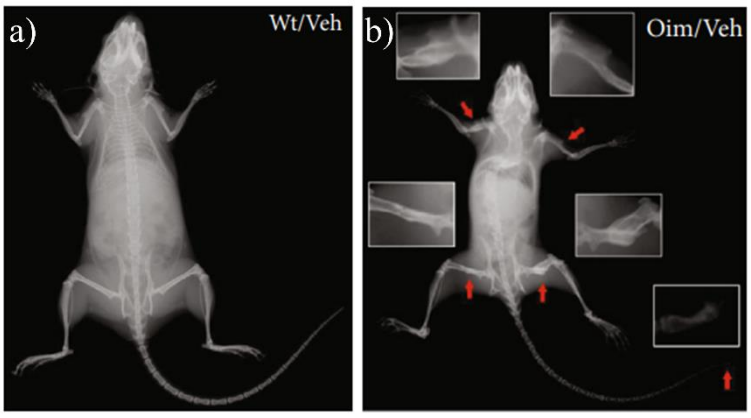

Fig. 19 Ray micrographs of (a) WT and (b) oim mice. While WT present normal bones, oim shows curvatures and signs of low mineral density, as highlighted by the red arrows. Image adapted from Shi et al., (2021).

Lee *et al.*, (2022) evaluated the mechanical properties of *oim* femurs at the macrolevel. They used three-point bending test to verify the ultimate strength and *E* among other mechanical properties. At 8 weeks (8w) of age, *oim*/Hom mice have shown ultimate strength for both male and female mice, compared to WT; oim/Het had intermediate properties to WT and Hom. For Hom animals with 18w of age, the ultimate strength decreased, while the *E* increased in comparison to Hom 8w mice. With this they demonstrated that Hom individuals have more severe phenotype than any other group of comparison.

2.6.2.2. Tm1b

Tm1b mice have similar genetics to *oim* mice. The *tm1b* mutation is C*ol1a2*-null, which also promotes collagen molecules with homotrimeric configuration $(\alpha 1)_3$ (Lee *et al.*, 2022). Differently from *oim* animals, *tm1b* do not show brittle bone phenotype classic of OI condition. Thus, they cannot be considered an OI model in their essence. However, C*ol1a2*-null mutation, in humans, is related to increased pressure in the arteries due to arterial stiffening (Brull *et al.*, 2001). *Tm1b* mice are genetically engineered from a knockout-first allele (*tm1a*) by *Cre*-mediated recombination (Skarnes *et al.*, 2011), as shown in the **Fig. 20**.

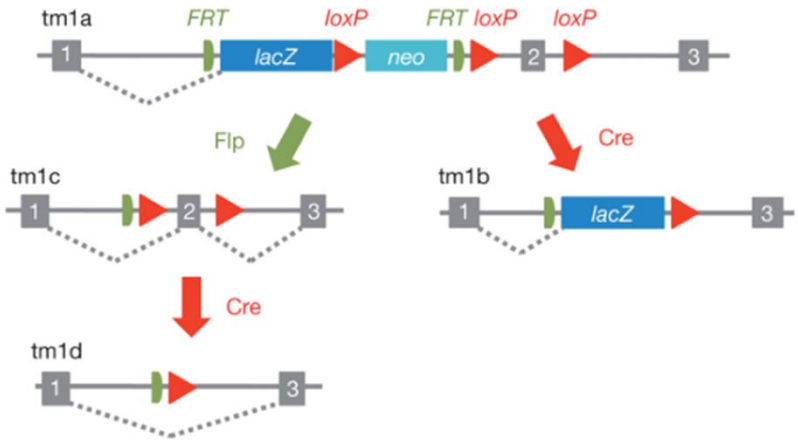

Fig. 20 Genetic engineering of tm1b mutation from the knockout-first allele (tm1a). Image obtained from Skarnes et al., (2011).

2.7. Summary

In summary, this literature review presented valuable information regarding diseased mineralised tissues, more specifically, about OP and OI. The information contained in this second chapter is relevant to this thesis. The author highlighted the importance of bone diseases to the quality of life of people of young ages and to the elderly. Bone diseases are a hot topic and will cause burden in the future. In this chapter, the author mentioned important parameters of bone quality, such as bone density and biomechanics. Further on this thesis, the author will deepen the analysis on important characterisation methods for bone quality assessment and will make use of equipment like fluorescence microscope, SEM, μ-CT, and NI, among others, to measure bones affected by OP and OI. Both zebrafish and *oim* mice will be used as subjects.

References

Ackermann, M., Chao, L., Bergstrom, C.T., Doebeli, M., 2007. On the evolutionary origin of aging. Aging Cell 6, 235–244.

Adami, G., Saag, K.G., 2019. Glucocorticoid-induced osteoporosis update. Current Opinion in Rheumatology 31, 388–393.

Alcorta-Sevillano, N., Infante, A., Macías, I., Rodríguez, C.I., 2022. Murine Animal Models in Osteogenesis Imperfecta: The Quest for Improving the Quality of Life. IJMS 24, 184.

Andersen, T.L., Abdelgawad, M.E., Kristensen, H.B., Hauge, E.M., Rolighed, L., Bollerslev, J., Kjærsgaard-Andersen, P., Delaisse, J.-M., 2013. Understanding Coupling between Bone Resorption and Formation. The American Journal of Pathology 183, 235–246.

Ashournia, H., Johansen, F.T., Folkestad, L., Diederichsen, A.C.P., Brixen, K., 2015. Heart disease in patients with osteogenesis imperfecta — A systematic review. International Journal of Cardiology 196, 149–157.

Astrom, E., 2002. Beneficial effect of long-term intravenous bisphosphonate treatment of osteogenesis imperfecta. Archives of Disease in Childhood 86, 356–364.

Azevedo, A.S., Grotek, B., Jacinto, A., Weidinger, G., Saúde, L., 2011. The Regenerative Capacity of the Zebrafish Caudal Fin Is Not Affected by Repeated Amputations. PLoS ONE 6, e22820.

Bailone, R.L., Fukushima, H.C.S., Ventura Fernandes, B.H., De Aguiar, L.K., Corrêa, T., Janke, H., Grejo Setti, P., Roça, R.D.O., Borra, R.C., 2020. Zebrafish as an alternative animal model in human and animal vaccination research. Lab Anim Res 36, 13.

Barrett, R., Chappell, C., Quick, M., Fleming, A., 2006. A rapid, high content, in vivo model of glucocorticoid-induced osteoporosis. Biotechnology Journal 1, 651–655.

Becker, D.E., 2013. Basic and Clinical Pharmacology of Glucocorticosteroids. Anesthesia Progress 60, 25–32.

Bembey, A.K., Oyen, M.L., Bushby, A.J., Boyde, A., 2006. Viscoelastic properties of bone as a function of hydration state determined by nanoindentation. Philosophical Magazine 86, 5691–5703.

Bensimon-Brito, A., Cardeira, J., Dionísio, G., Huysseune, A., Cancela, M.L., Witten, P.E., 2016a. Revisiting in vivo staining with alizarin red S - a valuable approach to analyse zebrafish skeletal mineralisation during development and regeneration. BMC Dev Biol 16, 2.

Bergen, D.J.M., Kague, E., Hammond, C.L., 2019. Zebrafish as an Emerging Model for Osteoporosis: A Primary Testing Platform for Screening New Osteo-Active Compounds. Frontiers in Endocrinology 10.

Bird, N.C., Mabee, P.M., 2003. Developmental morphology of the axial skeleton of the zebrafish, Danio rerio (Ostariophysi: Cyprinidae). Developmental Dynamics 228, 337–357.

Bonicelli, A., Kranioti, E.F., Xhemali, B., Arnold, E., Zioupos, P., 2022. Assessing bone maturity: Compositional and mechanical properties of rib cortical bone at different ages. Bone 155, 116265.

Bowman, S.M., Keaveny, T.M., Gibson, L.J., Hayes, W.C., McMahon, T.A., 1994. Compressive creep behavior of bovine trabecular bone. Journal of Biomechanics 27, 301–310.

Breeland, G., Sinkler, M.A., Menezes, R.G., 2021. Embryology, Bone Ossification, in: StatPearls. StatPearls Publishing, Treasure Island (FL).

Brull, D.J., Murray, L.J., Boreham, C.A., Ralston, S.H., Montgomery, H.E., Gallagher, A.M., McGuigan, F.E.A., Davey Smith, G., Savage, M., Humphries, S.E., Young, I.S., 2001. Effect of a *COL1A1* Sp1 Binding Site Polymorphism on Arterial Pulse Wave Velocity: An Index of Compliance. Hypertension 38, 444–448.

Buck, D.W., Dumanian, G.A., 2012. Bone Biology and Physiology: Part I. The Fundamentals. Plastic and Reconstructive Surgery 129, 1314–1320.

Burley, M., Campbell, J.E., Dean, J., Clyne, T.W., 2020. A methodology for obtaining primary and secondary creep characteristics from indentation experiments, using a recess. International Journal of Mechanical Sciences 176, 105577.

Bushby, A.J., Ferguson, V.L., Boyde, A., 2004. Nanoindentation of bone: Comparison of specimens tested in liquid and embedded in polymethylmethacrylate. Journal of Materials Research 19, 249–259.

Busse, B., Galloway, J.L., Gray, R.S., Harris, M.P., Kwon, R.Y., 2020. Zebrafish: An Emerging Model for Orthopedic Research. J. Orthop. Res. 38, 925–936.

Cardeira, J., Gavaia, P.J., Fernández, I., Cengiz, I.F., Moreira-Silva, J., Oliveira, J.M., Reis, R.L., Cancela, M.L., Laizé, V., 2016. Quantitative assessment of the regenerative and mineralogenic performances of the zebrafish caudal fin. Scientific Reports 6.

Carretero, A., Ruberte, J., Navarro, M., Nacher, V., Mendes-Jorge, L., 2017. Osteology, in: Morphological Mouse Phenotyping. Elsevier, pp. 7–53.

Carnovali, M., Ottria, R., Pasqualetti, S., Banfi, G., Ciuffreda, P., Mariotti, M., 2016. Effects of bioactive fatty acid amide derivatives in zebrafish scale model of bone metabolism and disease. Pharmacological Research 104, 1–8.

Carriero, A., Enderli, T., Burtch, S., Templet, J., 2016. Animal models of osteogenesis imperfecta: applications in clinical research. ORR Volume 8, 41–55.

Carson, M.A., Nelson, J., Cancela, M.L., Laizé, V., Gavaia, P.J., Rae, M., Heesch, S., Verzin, E., Gilmore, B.F., Clarke, S.A., 2018. Screening for osteogenic activity in extracts from Irish marine organisms: The potential of Ceramium pallidum. PLOS ONE 13, e0207303.

Chandra, A., Rajawat, J., 2021. Skeletal Aging and Osteoporosis: Mechanisms and Therapeutics. IJMS 22, 3553.

Chang, A.Y., Skirbekk, V.F., Tyrovolas, S., Kassebaum, N.J., Dieleman, J.L., 2019. Measuring population ageing: an analysis of the Global Burden of Disease Study 2017. The Lancet Public Health 4, e159–e167.

Chang, Z., Chen, P.-Y., Chuang, Y.-J., Akhtar, R., 2018. Zebrafish as a model to study bone maturation: Nanoscale structural and mechanical characterization of age-related changes in the zebrafish vertebral column. Journal of the Mechanical Behavior of Biomedical Materials 84, 54–63.

Charles, J.F., Sury, M., Tsang, K., Urso, K., Henke, K., Huang, Y., Russell, R., Duryea, J., Harris, M.P., 2017. Utility of quantitative micro-computed tomographic analysis in zebrafish to define gene function during skeletogenesis. Bone 101, 162–171.

Chavassieux, P., Chapurlat, R., Portero-Muzy, N., Roux, J., Garcia, P., Brown, J.P., Libanati, C., Boyce, R.W., Wang, A., Grauer, A., 2019. Bone-Forming and Antiresorptive Effects of Romosozumab in Postmenopausal Women with Osteoporosis: Bone Histomorphometry and Microcomputed Tomography Analysis After 2 and 12 Months of Treatment. Journal of Bone and Mineral Research 34, 1597–1608.

Chen, J.-R., Lai, Y.-H., Tsai, J.-J., Hsiao, C.-D., 2017. Live Fluorescent Staining Platform for Drug-Screening and Mechanism-Analysis in Zebrafish for Bone Mineralisation. Molecules 22, 2068.

Chen, P.-Y., McKittrick, J., 2011. Compressive mechanical properties of demineralized and deproteinized cancellous bone. Journal of the Mechanical Behavior of Biomedical Materials 4, 961–973.

Cheng, T.-T., Lai, H.-M., Yu, S.-F., Chiu, W.-C., Hsu, C.-Y., Chen, J.-F., Chen, Y.-C., 2018. The impact of low-dose glucocorticoids on disease activity, bone mineral density, fragility fractures, and 10-year probability of fractures in patients with rheumatoid arthritis. Journal of Investigative Medicine 66, 1004–1007.

Cheung, C.-L., Ang, S.B., Chadha, M., Chow, E.S.-L., Chung, Y.-S., Hew, F.L., Jaisamrarn, U., Ng, H., Takeuchi, Y., Wu, C.-H., Xia, W., Yu, J., Fujiwara, S., 2018. An updated hip fracture projection in Asia: The Asian Federation of Osteoporosis Societies study. Osteoporosis and Sarcopenia 4, 16–21.

Chipman, S.D., Sweet, H.O., McBride, D.J., Davisson, M.T., Marks, S.C., Shuldiner, A.R., Wenstrup, R.J., Rowe, D.W., Shapiro, J.R., 1993. Defective pro alpha 2(I) collagen synthesis in a recessive mutation in mice: a model of human osteogenesis imperfecta. Proc. Natl. Acad. Sci. U.S.A. 90, 1701–1705.

Cho, T.-J., Choi, I.H., Chung, C.Y., Yoo, W.J., Lee, K.S., Lee, D.Y., 2007. Interlocking Telescopic Rod for Patients with Osteogenesis Imperfecta: The Journal of Bone & Joint Surgery 89, 1028–1035.

Clarke, B., 2008. Normal Bone Anatomy and Physiology. Clinical Journal of the American Society of Nephrology 3, S131–S139.

Colloca, G., Di Capua, B., Bellieni, A., Fusco, D., Ciciarello, F., Tagliaferri, L., Valentini, V., Balducci, L., 2020. Biological and Functional Biomarkers of Aging: Definition, Characteristics, and How They Can Impact Everyday Cancer Treatment. Curr Oncol Rep 22, 115.

Compston, J., 2018. Glucocorticoid-induced osteoporosis: an update. Endocrine 61, 7–16.

Consensus development conference: Diagnosis, prophylaxis, and treatment of osteoporosis, 1993. The American Journal of Medicine 94, 646–650.

Cooper, C., Campion, G., Melton, L.J., 1992. Hip fractures in the elderly: A world-wide projection. Osteoporosis Int 2, 285–289.

Cooper, M.S., 2010. Glucocorticoid-induced osteoporosis: how best to avoid fractures. Therapeutic Advances in Chronic Disease 1, 17–23.

Cremers, S., Drake, M.T., Ebetino, F.H., Bilezikian, J.P., Russell, R.G.G., 2019. Pharmacology of bisphosphonates. Br J Clin Pharmacol 85, 1052–1062.

Cutcliffe, H.C., DeFrate, L.E., 2021. Four-Point Bending Testing for Mechanical Assessment of Mouse Bone Structural Properties, in: Hilton, M.J. (Ed.), Skeletal Development and Repair, Methods in Molecular Biology. Springer US, New York, NY, pp. 199–215.

Dall'Ara, E., Cheong, V.S., 2022. Bone biomechanics, in: Human Orthopaedic Biomechanics. Elsevier, pp. 97–120.

de Vrieze, E., van Kessel, M.A.H.J., Peters, H.M., Spanings, F.A.T., Flik, G., Metz, J.R., 2014. Prednisolone induces osteoporosis-like phenotype in regenerating zebrafish scales. Osteoporosis International 25, 567–578.

Deckard, C., Walker, A., Hill, B.J.F., 2017. Using three-point bending to evaluate tibia bone strength in ovariectomized young mice. J Biol Phys 43, 139–148.

Devogelaer, J.-P., Goemaere, S., Boonen, S., Body, J.-J., Kaufman, J.-M., Reginster, J.-Y., Rozenberg, S., Boutsen, Y., 2006. Evidence-based guidelines for the prevention and treatment of glucocorticoid-induced osteoporosis: a consensus document of the Belgian Bone Club. Osteoporos Int 17, 8–19.

Diab, T., Condon, K.W., Burr, D.B., Vashishth, D., 2006. Age-related change in the damage morphology of human cortical bone and its role in bone fragility. Bone 38, 427–431.

Drake, M.T., Clarke, B.L., Khosla, S., 2008. Bisphosphonates: Mechanism of Action and Role in Clinical Practice. Mayo Clinic Proceedings 83, 1032–1045.

Dubińska-Magiera, M., Daczewska, M., Lewicka, A., Migocka-Patrzałek, M., Niedbalska-Tarnowska, J., Jagla, K., 2016. Zebrafish: A Model for the Study of Toxicants Affecting Muscle Development and Function. International Journal of Molecular Sciences 17, 1941.

Ebenstein, D.M., Pruitt, L.A., 2006. Nanoindentation of biological materials. Nano Today 1, 26–33.

Ebert, T., Tran, N., Schurgers, L., Stenvinkel, P., Shiels, P.G., 2022. Ageing – Oxidative stress, PTMs and disease. Molecular Aspects of Medicine 86, 101099.

eBioMedicine, 2022. The 3Rs of Animal Research. eBioMedicine 76, 103900.

El-Gazzar, A., Högler, W., 2021. Mechanisms of Bone Fragility: From Osteogenesis Imperfecta to Secondary Osteoporosis. IJMS 22, 625.

Embry, M.R., Belanger, S.E., Braunbeck, T.A., Galay-Burgos, M., Halder, M., Hinton, D.E., Léonard, M.A., Lillicrap, A., Norberg-King, T., Whale, G., 2010. The fish embryo toxicity test as an animal alternative method in hazard and risk assessment and scientific research. Aquatic Toxicology 97, 79–87.

Etich, J., Leßmeier, L., Rehberg, M., Sill, H., Zaucke, F., Netzer, C., Semler, O., 2020. Osteogenesis imperfecta—pathophysiology and therapeutic options. Mol Cell Pediatr 7, 9.

Everts, V., Delaissé, J.M., Korper, W., Jansen, D.C., Tigchelaar-Gutter, W., Saftig, P., Beertsen, W., 2002. The Bone Lining Cell: Its Role in Cleaning Howship's Lacunae and Initiating Bone Formation. J Bone Miner Res 17, 77–90.

Fan, J., Abedi-Dorcheh, K., Sadat Vaziri, A., Kazemi-Aghdam, F., Rafieyan, S., Sohrabinejad, M., Ghorbani, M., Rastegar Adib, F., Ghasemi, Z., Klavins, K., Jahed, V., 2022. A Review of Recent Advances in Natural Polymer-Based Scaffolds for Musculoskeletal Tissue Engineering. Polymers 14, 2097.

Fassier, A., 2021. Telescopic rodding in children: Technical progression from Dubow–Bailey to Fassier–Duval™. Orthopaedics & Traumatology: Surgery & Research 107, 102759.

Fisher, S., Jagadeeswaran, P., Halpern, M.E., 2003. Radiographic analysis of zebrafish skeletal defects. Developmental Biology 264, 64–76.

Fleisch, H.A., Russell, R.G.G., Bisaz, S., Mühlbauer, R.C., Williams, D.A., 1970. The Inhibitory Effect of Phosphonates on the Formation of Calcium Phosphate Crystals in vitro and on Aortic and Kidney Calcification in vivo. Eur J Clin Invest 1, 12–18.

Fleming, A., Sato, M., Goldsmith, P., 2005. High-Throughput In Vivo Screening for Bone Anabolic Compounds with Zebrafish. Journal of Biomolecular Screening 10, 823–831.

Florencio-Silva, R., Sasso, G.R.D.S., Sasso-Cerri, E., Simões, M.J., Cerri, P.S., 2015. Biology of Bone Tissue: Structure, Function, and Factors That Influence Bone Cells. BioMed Research International 2015, 1–17.

Folkestad, L., Hald, J.D., Canudas-Romo, V., Gram, J., Hermann, A.P., Langdahl, B., Abrahamsen, B., Brixen, K., 2016. Mortality and Causes of Death in Patients with Osteogenesis Imperfecta: A Register-Based Nationwide Cohort Study. J Bone Miner Res 31, 2159–2166.

Forlino, A., Marini, J.C., 2016. Osteogenesis imperfecta. The Lancet 387, 1657–1671.

Fratzl, P., 2008. Collagen: Structure and Mechanics, an Introduction, in: Fratzl, Peter (Ed.), Collagen. Springer US, Boston, MA, pp. 1–13.

Ge, J., Wang, X., Cui, F., 2006. Microstructural characteristics and nanomechanical properties across the thickness of the wild-type zebrafish skeletal bone. Materials Science and Engineering: C 26, 710–715.

Gehlbach, S., Saag, K.G., Adachi, J.D., Hooven, F.H., Flahive, J., Boonen, S., Chapurlat, R.D., Compston, J.E., Cooper, C., Díez-Perez, A., Greenspan, S.L., LaCroix, A.Z., Netelenbos, J.C., Pfeilschifter, J., Rossini, M., Roux, C., Sambrook, P.N., Silverman, S., Siris, E.S., Watts, N.B., Lindsay, R., 2012. Previous fractures at multiple sites increase the risk for subsequent fractures: The global longitudinal study of osteoporosis in women. J Bone Miner Res 27, 645–653.

Genge, C.E., Lin, E., Lee, L., Sheng, X., Rayani, K., Gunawan, M., Stevens, C.M., Li, A.Y., Talab, S.S., Claydon, T.W., Hove-Madsen, L., Tibbits, G.F., 2016. The Zebrafish Heart as a Model of Mammalian Cardiac Function, in: Nilius, B., de Tombe, P., Gudermann, T., Jahn, R., Lill, R., Petersen, O.H. (Eds.), Reviews of Physiology, Biochemistry and Pharmacology, Vol. 171. Springer International Publishing, Cham, pp. 99–136.

Geurtzen, K., Vernet, A., Freidin, A., Rauner, M., Hofbauer, L.C., Schneider, J.E., Brand, M., Knopf, F., 2017. Immune Suppressive and Bone Inhibitory Effects of Prednisolone in Growing and Regenerating Zebrafish Tissues. Journal of Bone and Mineral Research 32, 2476–2488.

Gibson, L.J., 2003. Cellular Solids. MRS Bull. 28, 270–274.

Gochuico, B.R., Hossain, M., Talvacchio, S.K., Zuo, M.X.G., Barton, M., Dang Do, A.N., Marini, J.C., 2023. Pulmonary function and structure abnormalities in children and young adults with osteogenesis imperfecta point to intrinsic and extrinsic lung abnormalities. J Med Genet jmg-2022-109009.

Gullberg, B., Johnell, O., Kanis, J.A., 1997. World-wide Projections for Hip Fracture: Osteoporos Int 7, 407–413.

Hadjidakis, D.J., Androulakis, I.I., 2006. Bone Remodelling. Annals of the New York Academy of Sciences 1092, 385–396.

Hajat, C., Stein, E., 2018. The global burden of multiple chronic conditions: A narrative review. Preventive Medicine Reports 12, 284–293.

Harada, S., Rodan, G.A., 2003. Control of osteoblast function and regulation of bone mass. Nature 423, 349–355.

Hassler, N., Gamsjaeger, S., Hofstetter, B., Brozek, W., Klaushofer, K., Paschalis, E.P., 2015. Effects of long-term alendronate treatment on postmenopausal osteoporosis bone material properties. Osteoporosis International 26, 339–352.

Holmes, D.F., Lu, Y., Starborg, T., Kadler, K.E., 2018. Collagen Fibril Assembly and Function, in: Current Topics in Developmental Biology. Elsevier, pp. 107–142.

Homik, J., Suarez-Almazor, M.E., Shea, B., Cranney, A., Wells, G.A., Tugwell, P., 1998. Calcium and vitamin D for corticosteroid-induced osteoporosis. Cochrane Database of Systematic Reviews.

Hughes, M.L., Touron, D.R., 2021. Aging in Context: Incorporating Everyday Experiences into the Study of Subjective Age. Front. Psychiatry. 9;12:633234.

Hur, M., Gistelinck, C.A., Huber, P., Lee, J., Thompson, M.H., Monstad-Rios, A.T., Watson, C.J., McMenamin, S.K., Willaert, A., Parichy, D.M., Coucke, P., Kwon, R.Y., 2017. MicroCT-based phenomics in the zebrafish skeleton reveals virtues of deep phenotyping in a distributed organ system. eLife 6, e26014.

Iba, K., Takada, J., Sonoda, T., Yamashita, T., 2020. Effect of continuous long-term treatment for 10 years with bisphosphonate on Japanese osteoporosis patients. Journal of Bone and Mineral Metabolism 38, 240–247.

Ibrahim, A., Magliulo, N., Groben, J., Padilla, A., Akbik, F., Abdel Hamid, Z., 2020. Hardness, an Important Indicator of Bone Quality, and the Role of Collagen in Bone Hardness. JFB 11, 85.

Iovine, M.K., 2007. Conserved mechanisms regulate outgrowth in zebrafish fins. Nat. Chem. Biol. 3, 613–618.

Jensen, P.R., Andersen, T.L., Chavassieux, P., Roux, J.-P., Delaisse, J.-M., 2021. Bisphosphonates impair the onset of bone formation at remodelling sites. Bone 145, 115850.

Kan, L., 2013. Animal Models of Bone Diseases-A, in: Animal Models for the Study of Human Disease. Elsevier, pp. 353–390.

Kanis, J.A., Johnell, O., De Laet, C., Johansson, H., Oden, A., Delmas, P., Eisman, J., Fujiwara, S., Garnero, P., Kroger, H., McCloskey, E.V., Mellstrom, D., Melton, L.J., Pols, H., Reeve, J., Silman, A., Tenenhouse, A., 2004. A meta-analysis of previous fracture and subsequent fracture risk. Bone 35, 375–382.

Kelley, G.A., Kelley, K.S., Kohrt, W.M., 2013. Exercise and Bone Mineral Density in Premenopausal Women: A Meta-Analysis of Randomized Controlled Trials. International Journal of Endocrinology 2013, 1–16.

Knopf, F., Hammond, C., Chekuru, A., Kurth, T., Hans, S., Weber, C.W., Mahatma, G., Fisher, S., Brand, M., Schulte-Merker, S., Weidinger, G., 2011. Bone Regenerates via Dedifferentiation of Osteoblasts in the Zebrafish Fin. Developmental Cell 20, 713–724.

Laan, R.F.J.M., 1993. Low-Dose Prednisone Induces Rapid Reversible Axial Bone Loss in Patients with Rheumatoid Arthritis: A Randomized, Controlled Study. Ann Intern Med 119, 963.

Lacroix, D., 2009. Biomechanical Aspects of Bone Repair. Bone Repair Biomat (4). 106-118.

Langdahl, B., Ferrari, S., Dempster, D.W., 2016. Bone modelling and remodelling: potential as therapeutic targets for the treatment of osteoporosis. Therapeutic Advances in Musculoskeletal 8, 225–235.

Laurent, M.R., Goemaere, S., Verroken, C., Bergmann, P., Body, J.-J., Bruyère, O., Cavalier, E., Rozenberg, S., Lapauw, B., Gielen, E., 2022. Prevention and Treatment of Glucocorticoid-Induced Osteoporosis in Adults: Consensus Recommendations from the Belgian Bone Club. Front. Endocrinol. 13, 908727.

Lee K. J., Lisa Rambault, George Bou-Gharios, Peter D. Clegg, Riaz Akhtar, Gabriela Czanner, Rob van‘t Hof, Elizabeth G. Canty-Laird; 2022 Collagen (I) homotrimer potentiates the osteogenesis imperfecta (oim) mutant allele and reduces survival in male mice. Dis Model Mech 1 September; 15 (9): dmm049428.

Lieschke, G.J., Currie, P.D., 2007. Animal models of human disease: zebrafish swim into view. Nat Rev Genet 8, 353–367.

Lin, X., Patil, S., Gao, Y.-G., Qian, A., 2020. The Bone Extracellular Matrix in Bone Formation and Regeneration. Front. Pharmacol. 11, 757.

Linde, F., Hvid, I., and Pongsoipetch, B., 1989. Energy absorptive properties of human trabecular bone specimens during axial compression. J. Orthop. Res. 7: 432-439.

Liu, Y., Luo, D., Wang, T., 2016. Hierarchical Structures of Bone and Bioinspired Bone Tissue Engineering. Small 12, 4611–4632.

Loundagin, L.L., Haider, I.T., Cooper, D.M.L., Edwards, W.B., 2020. Association between intracortical microarchitecture and the compressive fatigue life of human bone: A pilot study. Bone Reports 12, 100254.

Ma, C., Du, T., Niu, X., Fan, Y., 2022. Biomechanics and mechanobiology of the bone matrix. Bone Res 10, 59.

Mackay, E.W., Apschner, A., Schulte-Merker, S., 2013. A bone to pick with zebrafish. BoneKEy Reports 2.

Mäkitie, R.E., Costantini, A., Kämpe, A., Alm, J.J., Mäkitie, O., 2019. New Insights into Monogenic Causes of Osteoporosis. Front. Endocrinol. 10, 70.

Marcu, F., Bogdan, F., Muţiu, G., Lazăr, L., 2011. The histopathological study of osteoporosis. Rom J Morphol Embryol 52, 321–325.

Marengoni, A., Angleman, S., Melis, R., Mangialasche, F., Karp, A., Garmen, A., Meinow, B., Fratiglioni, L., 2011. Aging with multimorbidity: A systematic review of the literature. Ageing Research Reviews 10, 430–439.

Marques, I.J., Lupi, E., Mercader, N., 2019. Model systems for regeneration: zebrafish. Development 146, dev167692.

Mc Donald, D., Mc Donnell, T., Martin-Grace, J., Mc Manus, G., Crowley, R.K., 2023. Systematic review of health related-quality of life in adults with osteogenesis imperfecta. Orphanet J Rare Dis 18, 36.

Mercer, C., He, M.Y., Wang, R., Evans, A.G., 2006. Mechanisms governing the inelastic deformation of cortical bone and application to trabecular bone. Acta Biomaterialia 2, 59–68.

Meyers, M.A., Chen, P.-Y., 2014. Biological Materials Science: Biological Materials, Bioinspired Materials, and Biomaterials. Cambridge University Press, Cambridge.

Mirzoyan, Z., Sollazzo, M., Allocca, M., Valenza, A.M., Grifoni, D., Bellosta, P., 2019. Drosophila melanogaster: A Model Organism to Study Cancer. Front. Genet. 10, 51.

Mohamed, A.M., 2008. An overview of bone cells and their regulating factors of differentiation. Malays J Med Sci 15, 4–12.

Monma, Y., Shimada, Y., Nakayama, H., Zang, L., Nishimura, N., Tanaka, T., 2019. Aging-associated microstructural deterioration of vertebra in zebrafish. Bone Reports 11, 100215.

Morgan, E.F., Unnikrisnan, G.U., Hussein, A.I., 2018. Bone Mechanical Properties in Healthy and Diseased States. Annu. Rev. Biomed. Eng. 20, 119–143.

Nancollas, G.H., Tang, R., Phipps, R.J., Henneman, Z., Gulde, S., Wu, W., Mangood, A., Russell, R.G.G., Ebetino, F.H., 2006. Novel insights into actions of bisphosphonates on bone: Differences in interactions with hydroxyapatite. Bone 38, 617–627.

Natali, A.N., Carniel, E.L., Pavan, P.G., 2008. Constitutive modelling of inelastic behaviour of cortical bone. Medical Engineering & Physics 30, 905–912.

NHS, 2022. Osteoporosis: An Overview [website]. URL https://www.nhs.uk/conditions/osteoporosis/ (accessed 3.26.19).

Novitskaya, E., Zin, C., Chang, N., Cory, E., Chen, P., D'Lima, D., Sah, R.L., McKittrick, J., 2014. Creep of trabecular bone from the human proximal tibia. Materials Science and Engineering: C 40, 219–227.

Oftadeh, R., Perez-Viloria, M., Villa-Camacho, J.C., Vaziri, A., Nazarian, A., 2015. Biomechanics and Mechanobiology of Trabecular Bone: A Review. Journal of Biomechanical Engineering 137, 010802.

Pahr, D.H., Reisinger, A.G., 2020. A Review on Recent Advances in the Constitutive Modeling of Bone Tissue. Curr Osteoporos Rep 18, 696–704.

Papapoulos, S.E., Cremers, S.C.L.M., 2007. Prolonged Bisphosphonate Release after Treatment in Children. N Engl J Med 356, 1075–1076.

Parambi, D.G.T., Unnikrishnan, M.K., Marathakam, A., Mathew, B., 2020. Demographic and Epidemiological Aspects of Aging, in: Nabavi, S.M., D'Onofrio, G., Nabavi, S.F. (Eds.), Nutrients and Nutraceuticals for Active & Healthy Ageing. Springer Singapore, Singapore, pp. 1–14.

Pasqualetti, S., Congiu, T., Banfi, G., Mariotti, M., 2015. Alendronate rescued osteoporotic phenotype in a model of glucocorticoid-induced osteoporosis in adult zebrafish scale. International Journal of Experimental Pathology 96, 11–20.

Pienkowski, D., Wood, C.L., Malluche, H.H., 2019. Young's modulus and hardness of human trabecular bone with bisphosphonate treatment durations up to 20 years. Osteoporos Int 30, 277–285.

Pollintine, P., Luo, J., Offa-Jones, B., Dolan, P., Adams, M.A., 2009. Bone creep can cause progressive vertebral deformity. Bone 45, 466–472.

Rachner, T.D., Khosla, S., Hofbauer, L.C., 2011. Osteoporosis: now and the future. The Lancet 377, 1276–1287.

Rashmi, R., Mohanty, S.K., 2023. Examining chronic disease onset across varying age groups of Indian adults using competing risk analysis. Sci Rep 13, 5848.

Rho, J.-Y., Tsui, T.Y., Pharr, G.M., 1997. Elastic properties of human cortical and trabecular lamellar bone measured by nanoindentation. Biomaterials 18, 1325–1330.

Robinson, N.B., Krieger, Katherine, Khan, F.M., Huffman, W., Chang, M., Naik, A., Yongle, R., Hameed, I., Krieger, Karl, Girardi, L.N., Gaudino, M., 2019. The current state of animal models in research: A review. International Journal of Surgery 72, 9–13.

Rodriguez-Florez, N., Oyen, M.L., Shefelbine, S.J., 2013. Insight into differences in nanoindentation properties of bone. Journal of the Mechanical Behavior of Biomedical Materials 18, 90–99.

Rizzoli, R., Biver, E., 2015. Glucocorticoid-induced osteoporosis: who to treat with what agent? Nat Rev Rheumatol 11, 98–109.

Rose, M.R., 1991. Evolutionary biology of aging. Oxford University Press, New York.

Russell, R.G.G., 2007. Bisphosphonates: Mode of Action and Pharmacology. Pediatrics 119, S150–S162.

Russell, R.G.G., Mühlbauer, R.C., Bisaz, S., Williams, D.A., Fleisch, H., 1970. The influence of pyrophosphate, condensed phosphates, phosphonates and other phosphate

compounds on the dissolution of hydroxyapatite in vitro and on bone resorption induced by parathyroid hormone in tissue culture and in thyroparathyroidectomised rats. Calc. Tis Res. 6, 183–196.

Screen, H.R.C., Berk, D.E., Kadler, K.E., Ramirez, F., Young, M.F., 2015. Tendon Functional Extracellular Matrix: TENDON FUNCTIONAL EXTRACELLULAR MATRIX. J. Orthop. Res. 33, 793–799.

Sharir, A., Barak, M.M., Shahar, R., 2008. Whole bone mechanics and mechanical testing. The Veterinary Journal 177, 8–17.

Sillence, D.O., Senn, A., Danks, D.M., 1979. Genetic heterogeneity in osteogenesis imperfecta. Journal of Medical Genetics 16, 101–116.

Silvent, J., Akiva, A., Brumfeld, V., Reznikov, N., Rechav, K., Yaniv, K., Addadi, L., Weiner, S., 2017. Zebrafish skeleton development: High resolution micro-CT and FIB-SEM block surface serial imaging for phenotype identification. PLoS ONE 12, e0177731.

Silverman, S., Curtis, J., Saag, K., Flahive, J., Adachi, J., Anderson, F., Chapurlat, R., Cooper, C., Diez-Perez, A., Greenspan, S., Hooven, F., Le Croix, A., March, L., Netelenbos, J.C., Nieves, J., Pfeilschifter, J., Rossini, M., Roux, C., Siris, E., Watts, N., Compston, J., 2015. International management of bone health in glucocorticoid-exposed individuals in the observational GLOW study. Osteoporos Int 26, 419–420.

Siris, E., Weinstein, R.S., Altman, R., Conte, J.M., Favus, M., Lombardi, A., Lyles, K., McIlwain, H., Murphy, W.A., Reda, C., Rude, R., Seton, M., Tiegs, R., Thompson, D., Tucci, J.R., Yates, A.J., Zimering, M., 1996. Comparative study of alendronate versus etidronate for the treatment of Paget's disease of bone. The Journal of Clinical Endocrinology & Metabolism 81, 961–967.

Skarnes, W.C., Rosen, B., West, A.P., Koutsourakis, M., Bushell, W., Iyer, V., Mujica, A.O., Thomas, M., Harrow, J., Cox, T., Jackson, D., Severin, J., Biggs, P., Fu, J., Nefedov, M., de Jong, P.J., Stewart, A.F., Bradley, A., 2011. A conditional knockout resource for the genome-wide study of mouse gene function. Nature 474, 337–342.

Szabo, E., Rimnac, C., 2022. Biomechanics of immature human cortical bone: A systematic review. Journal of the Mechanical Behavior of Biomedical Materials 125, 104889.

Szulc, P., 2020. Impact of Bone Fracture on Muscle Strength and Physical Performance - Narrative Review. Curr Osteoporos Rep 18, 633–645.

Tadano, S., Giri, B., 2011. X-ray diffraction as a promising tool to characterize bone nanocomposites. Science and Technology of Advanced Materials 12, 064708.

Taylor, M., Cotton, J., Zioupos, P., 2002. Finite Element Simulation of the Fatigue Behaviour of Cancellous Bone. Meccanica 37, 419–429.

United Nations, 2017a. World population ageing, 2017 highlights. United Nations., New York.

United Nations, 2017b. World population prospects, The 2017 revision. United Nations., New York.

Van Dijk, F.S., Sillence, D.O., 2014. Osteogenesis imperfecta: Clinical diagnosis, nomenclature and severity assessment. Am. J. Med. Genet. 164, 1470–1481.

Xie, S., Manda, K., Wallace, R.J., Levrero-Florencio, F., Simpson, A.H.R.W., Pankaj, P., 2017. Time Dependent Behaviour of Trabecular Bone at Multiple Load Levels. Ann Biomed Eng 45, 1219–1226.

Wan, J., Goldman, D., 2016. Retina regeneration in zebrafish. Current Opinion in Genetics & Development 40, 41–47.

Wang, J., Yang, C., Liu, Y., Li, Y., Xiong, Y., 2022. Using Nanoindentation to Characterize the Mechanical and Creep Properties of Shale: Load and Loading Strain Rate Effects. ACS Omega 7, 14317–14331.

Wang, H., Dwyer-Lindgren, L., Lofgren, K.T., Rajaratnam, J.K., Marcus, J.R., Levin-Rector, A., Levitz, C.E., Lopez, A.D., Murray, C.J., 2012. Age-specific and sex-specific mortality in 187 countries, 1970–2010: a systematic analysis for the Global Burden of Disease Study 2010. The Lancet 380, 2071–2094.

Wang, X., Bank, R.A., Tekoppele, J.M., Agrawal, C.M., 2001. The role of collagen in determining bone mechanical properties. Journal of Orthopaedic Research 19, 1021–1026.

Weigele, J., Franz-Odendaal, T.A., 2016. Functional bone histology of zebrafish reveals two types of endochondral ossification, different types of osteoblast clusters and a new bone type. J. Anat. 229, 92–103.

Whyte, M.P., 2023. Osteopetrosis: Discovery and early history of "marble bone disease." Bone 171, 116737.

Wirth, T., 2019. The orthopaedic management of long bone deformities in genetically and acquired generalized bone weakening conditions. Journal of Children's Orthopaedics 13, 12–21.

World Health Organization, 2020. Global Burden of Disease Collaborative Network, Global Burden of Disease Study 2019 (GBD 2019) Results. Institute for Health Metrics and Evaluation – IHME.

Wu, A.-M., Bisignano, C., James, S.L., Abady, G.G., Abedi, A., Abu-Gharbieh, E., Alhassan, R.K., Alipour, V., Arabloo, J., Asaad, M., Asmare, W.N., Awedew, A.F., Banach, M., Banerjee, S.K., Bijani, A., Birhanu, T.T.M., Bolla, S.R., Cámera, L.A., Chang, J.-C., Cho, D.Y., Chung, M.T., Couto, R.A.S., Dai, X., Dandona, L., Dandona, R., Farzadfar, F., Filip, I., Fischer, F., Fomenkov, A.A., Gill, T.K., Gupta, B., Haagsma, J.A., Haj-Mirzaian, A., Hamidi, S., Hay, S.I., Ilic, I.M., Ilic, M.D., Ivers, R.Q., Jürisson, M., Kalhor, R., Kanchan, T., Kavetskyy, T., Khalilov, R., Khan, E.A., Khan, M., Kneib, C.J., Krishnamoorthy, V., Kumar, G.A., Kumar, N., Lalloo, R., Lasrado, S., Lim, S.S., Liu, Z., Manafi, A., Manafi, N., Menezes, R.G., Meretoja, T.J., Miazgowski, B., Miller, T.R., Mohammad, Y., Mohammadian-Hafshejani, A., Mokdad, A.H., Murray, C.J.L., Naderi, M., Naimzada, M.D., Nayak, V.C., Nguyen, C.T., Nikbakhsh, R., Olagunju, A.T., Otstavnov, N., Otstavnov, S.S., Padubidri, J.R., Pereira, J., Pham, H.Q., Pinheiro, M., Polinder, S., Pourchamani, H., Rabiee, N., Radfar, A., Rahman, M.H.U., Rawaf, D.L., Rawaf, S., Saeb, M.R., Samy, A.M., Sanchez Riera, L., Schwebel, D.C., Shahabi, S., Shaikh, M.A., Soheili, A., Tabarés-Seisdedos, R., Tovani-Palone, M.R., Tran, B.X., Travillian, R.S., Valdez, P.R., Vasankari, T.J., Velazquez, D.Z., Venketasubramanian, N., Vu, G.T., Zhang, Z.-J., Vos, T., 2021. Global, regional, and national burden of bone fractures in 204 countries and territories, 1990–2019: a systematic analysis from the Global Burden of Disease Study 2019. The Lancet Healthy Longevity 2, e580–e592.

Wu, Z., Baker, T.A., Ovaert, T.C., Niebur, G.L., 2011. The effect of holding time on nanoindentation measurements of creep in bone. Journal of Biomechanics 44, 1066–1072.

Yan, C., Zhang, S., Wang, C., Zhang, Q., 2019. A fructooligosaccharide from Achyranthes bidentata inhibits osteoporosis by stimulating bone formation. Carbohydrate Polymers 210, 110–118.

Yuan, X., Chen, S., Sun, C., Yuwen, L., 2022. A novel early diagnostic framework for chronic diseases with class imbalance. Sci Rep 12, 8614.

Zhang, Y., Cui, F.Z., Wang, X.M., Feng, Q.L., Zhu, X.D., 2002. Mechanical properties of skeletal bone in gene-mutated stöpseldtl28d and wild-type zebrafish (Danio rerio) measured by atomic force microscopy-based nanoindentation. Bone 30, 541–546.

Zhu, B., Hu, S., Guo, J., Dong, Z., Dong, Y., Li, F., 2023. Differences in the global exposure, mortality and disability of low bone mineral density between men and women: the underestimated burden in men. BMC Public Health 23, 991.

Zimmermann, E.A., Busse, B., Ritchie, R.O., 2015. The fracture mechanics of human bone: influence of disease and treatment. Bonekey Rep 4, 743.

Zinganell, A., Hegen, H., Walde, J., Bauer, A., Berek, K., Barket, R., Auer, M., Bsteh, G., Donnemiller, E., Egger, A., Grams, A., Griesmacher, A., Kroiss, A.S., Rettenwander, F., Tschallener, M., Tschoner, A., Berger, T., Deisenhammer, F., Di Pauli, F., 2023. Screening for osteoporosis in people with MS: A new risk score. Multiple Sclerosis and Related Disorders 74, 104726.

Zysset, P.K., Edward Guo, X., Edward Hoffler, C., Moore, K.E., Goldstein, S.A., 1999. Elastic modulus and hardness of cortical and trabecular bone lamellae measured by nanoindentation in the human femur. Journal of Biomechanics 32, 1005–1012.

3. Chapter 3: Methods

This chapter provides information on the main characterisation methods used in the building of this thesis. The first section of this chapter (3.1) will focus on animal maintenance and then in fluorescence microscopy (3.2), which was used to observe the mineralogenic performance of zebrafish lepidotrichia during its regenerative process. Section 3.3 will outline SEM and its ability in observing the morphology of mineralised tissues. Section 3.4 and 3.5 will briefly talk about Raman spectroscopy and AFM, respectively. Section 3.6 elaborates how computed tomography scans are used traditionally to assess BMD (and other bone morphometrics) in OP and OI and how they can be used in zebrafish for the study of GIOP. Finally, section 3.7 emphasises NI and its application in measuring the biomechanics of bones in zebrafish and mice models.

This methods chapter is organised in a way that first will be given a background about the characterisation method, then the methodology used in this thesis is described.

3.1. Animal maintenance

3.1.1. Pilot studies

Prior to the development of the work involving zebrafish, pilot studies were performed so the parameters used had their suitability trialled (e.g., container volume and medicine concentration) and to develop methodological consistency. This was necessary since the circulating water system in the zebrafish facility could not support this study, as medicine would circulate to other tanks, affecting other researcher's fish. The pilot studies were divided into two stages:

1) A set of twelve retired fish were split into two groups and put into separate containers (supporting 500 mL of liquid each) with either fish tank water (five fish) or PN (seven fish). Both tanks had 1/3 of their content with or without medicine changed daily, maintaining (theoretically) the same concentration of medicine in the experimental tank. In the first 7 days of the pilot study, only two of the seven fish receiving PN survived. At the time, it was raised the possibility that fish were competing with each other for food, causing fish potentially less affected by PN to thrive in comparison to other fish. The fish that did not survived were found with visible injuries in their caudal fin, probably caused by fighting, as reported elsewhere (Oliveira *et al.*, 2011). All the fish in the container with only fish tank water survived.
2) In a second pilot studies, twelve fish were separated (isolated), each in their own container containing PN (seven fish) or not (five fish), similar to what is shown in **Fig. 21**. Each container had 120 mL of fish tank water and, again, had 1/3 of their content renewed daily. By the end of seven days of this trial, only one of the fish receiving PN was found dead, and the trial was continued for another 21 days, simulating the full

procedures carried on in this thesis. By the end of the full trial period, only three fish died (two from PN group and one from only fish tank water).

Fig. 21 Set up in which the experiments involving zebrafish in this thesis were carried out. Each container was numbered for randomisation and had only one fish inside each of them. Eppendorf with water was used as weight to hold the lids in place, not allowing fish to jump out of the reservoir. Figure by the author.

The second protocol was discussed in the group and deemed appropriate to use in the experiments carried on in this thesis.

3.1.2. Zebrafish maintenance in caudal fin study

Adult three-month-old WT AB strain zebrafish (n = 46), with average length of 30.73 ± 4.32 mm, were obtained from the Taiwan Zebrafish Core Facility at Academia Sinica (TZCAS). The fish were maintained inside tanks in recirculating water system under a 14/10-hour light/dark cycle at 28 °C and were fed twice a day, as described in the Zebrafish Book (Westerfield, 1995), until they were sorted to experimentation. After the fish were assigned to their experimental group, the light/dark and feeding cycles were not changed; a fraction of the

water was renewed daily, mimicking the recirculating system to an extent and to ensure the medication concentration (exposure) remained constant during the experiments. The experimental use of zebrafish was approved by the Experimental Animal Care and Use Committee of NTHU (IACUC approval number: 10048).

3.1.3. Zebrafish maintenance vertebrae study

Twenty-six (n = 26) seven-month-old WT AB strain zebrafish of both sexes, measuring 26.09 ± 2.16 mm in length, were obtained from the TZCAS. In accordance with the UN (2022), the life expectancy, for combined genders, in the World is around 72 years old; the fish used in this research would then be comparable to human adolescents with 14 years old, representing 19.4 % of human average lifespan.

Until the experimentation, the fish were maintained in an environment with recirculating water system, with daily light/dark cycles at 28°C, and fed twice a day (Westerfield, 2000). The experimental use of zebrafish was backed by the Experimental Animal Care and Use Committee of NTHU (IACUC approval number: 10048). This research was conducted in accordance with the Animal Research: Reporting of *in vivo* Experiments (ARRIVE) guidelines (Percie du Sert *et al.,* 2020). The *n* used in each experiment was decided based on previous experience with pilot studies and anticipating loss of individuals during medication management. No animals were excluded from the research. The experiments were not blinded (e.g., the person administering the medicine to the experimental groups of fish had full knowledge which treatment was given to each of the fish in the tanks).

3.1.3.1. Experimental group allocation

The fish were randomly assigned to numbered containers with 120 mL of water. Each fish was kept in a separated tank throughout the experimentation. The containers were then randomly allocated into four groups depending on the treatment proposed using the function "*rand()*" in Microsoft Excel.

Two different concentrated stock solutions containing Prednisolone or Alendronate were prepared and stored under refrigeration during the experimentation: The stock solution (A) had PN dissolved in DMSO, while the stock solution (B) had ALN dissolved in tank water.

In seven of the tanks (n = 7), the stock solution A was diluted in fish tank water to a final concentration of 50 µM (Geurtzen and Knopf, 2018). The fish remained inside the tanks for 21 days and one-third of the water with the relative proportion of medicine was changed daily; the individuals that received this treatment were labelled as "PN". A second group composed of seven fish (n = 7) received the stock solution B diluted into the fish tank water to a final concentration of 30 µM each, for 21 days. One-third of water with the relative proportion of medicine was switched daily and the individuals were labelled as "ALN." In a third group of seven fish (n = 7), firstly, the fish received the stock solution A diluted to 50 µM for 21 days and, sequentially, received the solution B diluted to 30 µM for another 21 days (42 days, in total, under treatment). For the total duration of the drugs administration, one-third of the water with the respective medicine was changed daily. The individuals that received A + B intervention were labelled as "PN + ALN." The remaining five fish (n = 5) were raised for 21 days in fish tank water only and had their water changed in the same conditions as the other groups; they were labelled as "CTRL". During the whole experimentation, the diet and light/dark cycles remained unchanged. The fish were then euthanized by an overdose of Tricaine and isoflurane cocktail (Huang *et al.,* 2010). They were properly labelled and kept at

-21 °C until further use. Seven (n = 7) fish died naturally during the administration of the medicine: two (n = 2) from the PN group, three from ALN (n = 3) and two (n = 2) from PN + ALN. A flow-chart describing the experimental setup is shown in **Fig. 22**.

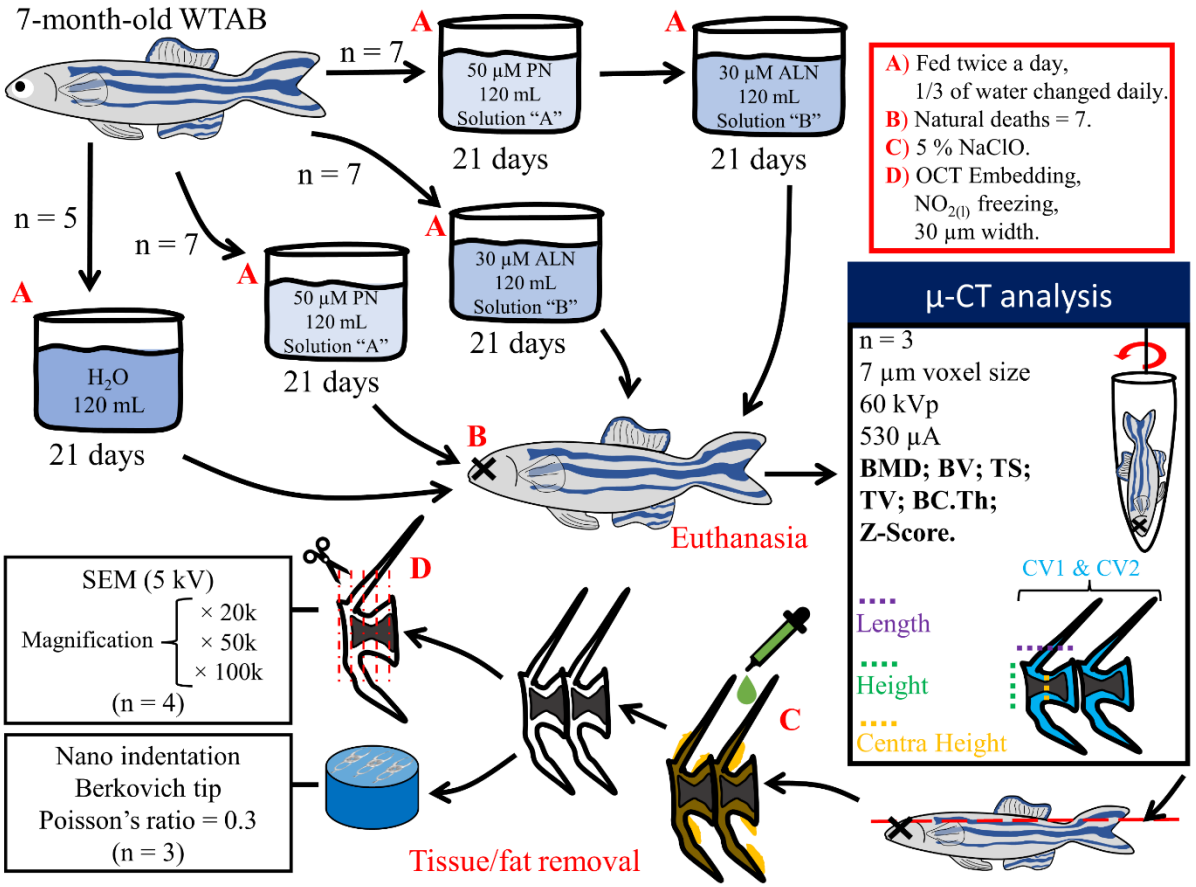

Fig. 22 Flowchart showing the steps performed in this study. Fish were first treated with the corresponding medication, euthanised and scanned with µ-CT prior their vertebrae was removed for further morphological and biomechanical assessment.

3.1.4. Murine model maintenance

All breeding and maintenance of animals was performed under project licences PP4874760 and P92F55CB2, in compliance with the Animals (Scientific Procedures) Act 1986 and UK

Home Office guidelines, as found elsewhere (Lee *et al.*, 2022). This study had approval from the AWERB (Animal Welfare and Ethical Review Body) of the University of Liverpool.

The misfolding and absence of α2(I) polypeptide chain was assessed using *oim* (*col1a2*^{oim}, C57BL/6J) and *tm1b* (*col1a2*$^{tm1b(EUCOMM)Wtsi}$, C57BL/6N) mouse lines, respectively. The *tm1b* line was generated from *Cre* deletion of a "knockout-first" allele *tm1a* (*col1a2*$^{tm1a(EUCOMM)Wtsi}$, C57BL/6N) (Skarnes *et al.*, 2011). *Oim*, and *tm1b* groups were presented as either Het or Hom mutants. As controls, WT mice were assessed.

3.1.4.1. Mouse dissection

WT, *oim* and *tm1b* mice were euthanised for a previous work (Lee *et al.*, 2022) at 8 and 18 weeks of age; WT and *tm1b* mice were also euthanised at 52 weeks of age. *Oim* mice were not maintained up to 52w due to welfare considerations for Hom that showed spontaneous fractures. In total 145 mouse femurs were received to be used in this study. There are two distinct WT groups; each of them was paired either with *oim* or *tm1b*. Since *oim* and *col1a2*-null were raised separately, in order to avoid potential extrinsic effects influence (e.g., mice from different batch) it was decided to evaluate WT separately with *oim* and *tm1b*. The distribution of gender and number of mice used per group are described in **Table 4**.

Table 4 Number of mouse femurs assessed in each of the mutations. In total, 145 femurs (one per mouse) were analysed in this study. Table by the author.

Mutation	Gender	*oim*			*tm1b*		
		Age			Age		
		8w	18w	52w	8w	18w	52w
WT	F	4	4	-	6	5	4
	M	4	5	-	6	5	5
Het	F	4	4	-	6	5	5
	M	4	4	-	6	5	6
Hom	F	5	5	-	6	5	4
	M	4	4	-	6	5	4

3.2. Fluorescence microscopy

Fluorescence microscopy is a technique used to observe cells, tissues and objects through the lens of a microscope. Fluorescence microscopy is one of the most used equipment to assess biological tissues due to its simple operation (compared to other microscopy techniques), sensitivity, specificity (e.g., visualise specific proteins or tissues) and versatility (Budinger and Brahme, 2014). Fluorescence phenomena was first described in 1852 in minerals that could re-emit red light when stimulated by an ultraviolet source (Stokes, 1852). Many years later, fluorescence was applied to biological materials (Sanderson *et al.,* 2014). Since then, it has become a powerful tool for the assessment of materials due to applications that are not available in common bright field microscopes.

The fluorescence process involves absorption and re-emission of energy. A material, cell or object will absorb energy (photons) and will emit, partially, that energy (photon) back to the microscope. Since part of the energy is lost in this process, the photons received back in the microscope have longer wavelengths (λ), resulting in the contrast we observe in the microscope screen (Sanderson *et al.,* 2014). Thus, fluorescence microscopes have the task of separating the re-emitted light from the excitation light (bright field) with enough resolution or, in other words,

to separate what is valuable in the sample (signal) from what is background. To perform its function properly, fluorescence microscopes have many key components within them. **Fig. 23** shows a schematic of an inverted fluorescence microscope, highlighting some of these parts.

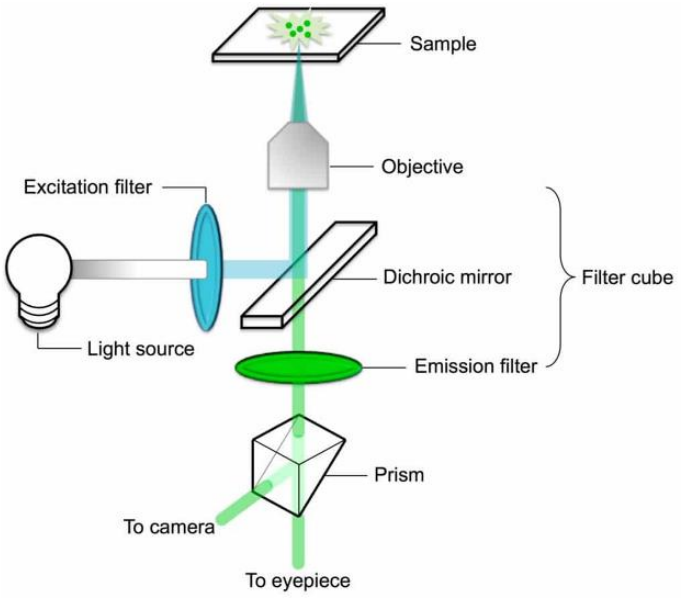

Fig. 23 Representation of the light path through an inverted microscope. The process of generating the image response in the computer screen starts on the light source, represented by the lamp in the left side of the image. The light is refracted and reach the sample, showed in the top. Finally, only the light corresponding the desired λ should reach the eye piece in the bottom. Image obtained from Abd-Alameer (2020).

To obtain fluorescence images, a light source is required. This light source emits energy and the excitation filter selectively "clean" the emitted energy to a specific peak excitation λ. In the filter cube, a mirror positioned 45° will separate the excitatory light from the source, from the light re-emitted by the material analysed. The objective lens will magnify and focus the light onto the surface of the sample that will emit fluorescence. The now less energetic light passes through the objective lens and the mirror, reaching the emission filter that, again, separates the λ that are not desired from the important ones. The light then reaches the eyepiece where the fluorescent image is created (Abd-Alameer *et al.,* 2020).

If bone visualisation is the main target of the characterisation via fluorescence microscopy, then a compound is used to stain it, as this material do not show spontaneous fluorescence with bright light. In zebrafish mineral evaluation, AR-S and Alcian blue are the most common dyes for fluorescence observations (Pfefferli and Jaźwińska, 2015). Zebrafish can absorb the staining compound with their operculum, digestive tract and osmosis through their skin (Cardeira *et al.*, 2016). These dyes have a selective attachment to calcium salts that exists in bone; this selective attachment creates the necessary difference between what is background (not useful) and what is mineralised tissue (site of interest). To obtain high resolution images from bone staining protocols, the fish should be in contact with the dye for enough time, creating a strong bond between the staining compound and the bone. Moreover, it is important to wash the sample by immersing it in a water media without the dye for enough time. An AR-S-stained lobe of zebrafish is shown in **Fig. 24**. With the correct application of the technique to stain zebrafish's lepidotrichia, even the details on the actinotrichia could be highlighted. This demonstrates the power and importance of the technique for mineralised tissues assessment.

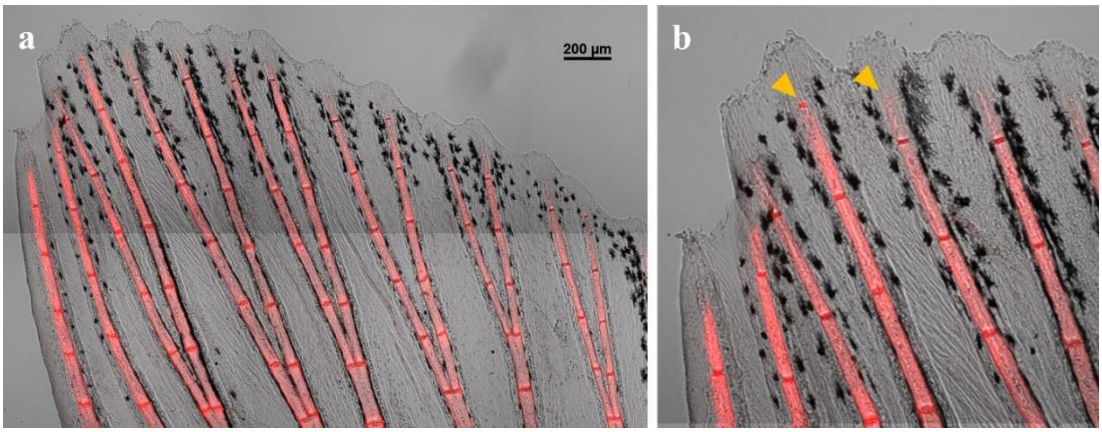

Fig. 24 AR-S-stained zebrafish lepidotrichia (in red). (a) Dorsal lobe of a zebrafish showing the segments in distal part of the fin. (b) Zoom-in from (a), showing the tiny brush-like actinotrichia (yellow arrowheads). Image by the author.

3.2.1. GIOP protocol zebrafish lepidotrichia

A workflow related to the experimentation involving zebrafish is in **Fig 25**. Fish were selected from the initial forty-six (**refer to section 3.1.2**) and were immersed for 15 minutes in a 0.01% AR-S (Sigma Aldrich; Missouri, MO, US) with its pH adjusted to ~7.4 with potassium hydroxide solution. A pH of 7.4 mimics the pH of Phosphate Buffered Solution (PBS), inhibiting that tissue is damaged in the process of staining (Chazotte, 2012; Bensimon-Brito *et al.*, 2016). The fish were rinsed in fish tank water for three times every 5 minutes to remove the excess of AR-S staining (Bensimon-Brito *et al.*, 2016), Then, the fish were anaesthetized individually in a 200 mL solution containing 70 ppm of Tricaine (Sigma Aldrich; Missouri, MO, USA), adjusted to pH ~7.2 (± 0.1) with sodium hydroxide, 130 µL of isoflurane (Alfa Aesar; Loughborough, Leicestershire, UK) and ethanol (isoflurane:ethanol = 1:9), as described elsewhere (Huang *et al.*, 2010). The anaesthetized fish were placed carefully onto a cell and tissue culture disk (Biofil; Kaohsiung, TW) and the tiles images of the bright field (T-PMT-T3) and fluorescent light (Cy3-T3) of the lepidotrichia were taken with an inverted confocal microscope (LSM 800; Carl Zeiss, Oberkochen, Germany). The pinhole size was set to 4.49 A.U., with a bit depth of 8-bits and the detection gain were set to 170 V and 680 V (T-PMT-T3 and Cy3-T3, respectively). The pictures obtained were labelled as zero days (0 d). The other fifteen fish were raised separately, in fish tank water only, for later use.

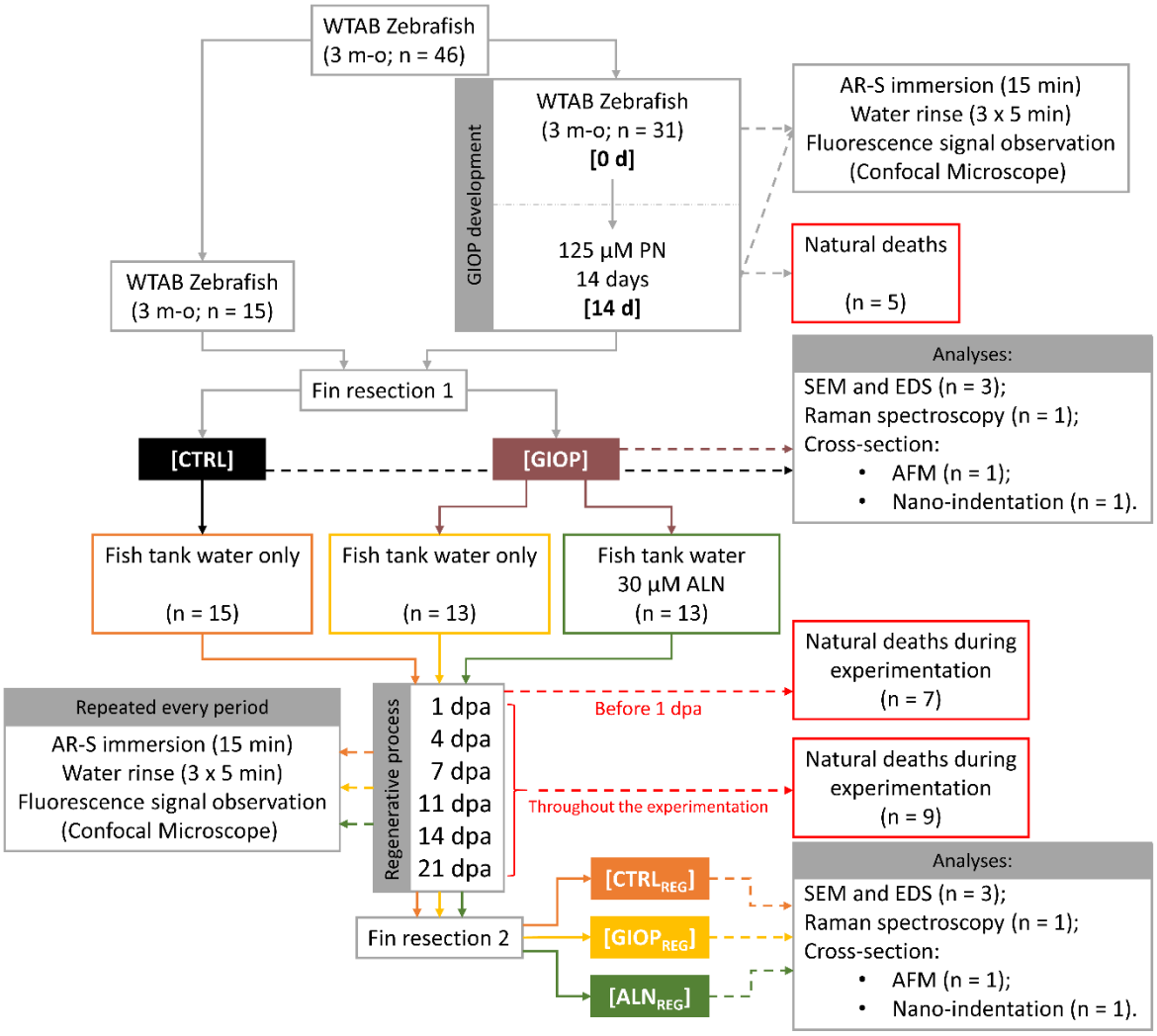

Fig. 25 Workflow of the study with zebrafish lepidotrichia.

After being imaged, the zebrafish were put individually into 120 mL of fish tank water containing PN (Sigma Aldrich; Missouri, MO, USA) previously dissolved in 0.1% of dimethyl sulfoxide (DMSO; J.T. Baker; Pennsylvania, PA), in a final concentration of 125 µM. For 14 days, 1/3 of water with the medicine was changed daily. After 14 d, the fish were AR-S stained, anaesthetized and analysed again by an inverted microscope using the same parameters as described previously. The caudal fins images had the pixel intensity of the ventral lobe bony rays measured with ImageJ 1.52a (Wayne Rasband, NIH, Bethesda, MD). The pixel intensities

were then transformed into percentage and both groups of images were compared. Five fish died naturally during the treatment (e.g., showed no apparent body injuries).

3.1.1.1. Fish fin resection

The fish not previously exposed to any medicines (n = 15) were sorted and put individually into containers with fish tank water only. Individually, both the untreated and fish with osteoporotic phenotype (n = 26) were anaesthetized and the caudal fin resection were performed ~3 segments proximal to the first lepidotrichia bifurcation. The fins amputated from the group of untreated fish were labelled as CTRL; the fins from the group with OP were labelled as GIOP. The fish were put into a recovery basin containing fish tank water only before the treatment started.

3.1.1.2. Medicine administration and *de novo* mineralisation

The amputated living fish were put into numbered containers and were assigned into three groups according to the treatment proposed. The fish with GIOP were divided into two treatment groups: thirteen fish (n = 13) were assigned to tanks filled with 120 mL of fish tank water only, while the other half (n = 13) were added to tanks with 120 mL water containing ALN (Alfa Aesar; Loughborough, Leicestershire, UK) in a concentration of 30 µM. The untreated fish (n = 15) were put to regenerate in tanks containing 120 mL of fish tank water only. The zebrafish remained in numbered containers for 21 d, and one-third of the water with and without medicine were refreshed daily. The regeneration process for each fish was followed up, and images were recorded at 1-, 4-, 7-, 11-, 14- and 21-days post amputation (dpa). In each of the timepoints, AR-S staining, water rinsing, and anaesthetic procedure were performed individually in each fish; the images were obtained with an inverted confocal microscope, as described previously. Before 1 dpa analysis was performed, seven fish (n = 7)

with osteoporotic phenotype died naturally (three from the group assigned to fish tank water only and four fish from the ALN intervention group). The lepidotrichia *de novo* mineralisation was quantified in accordance with the parameters suggested by Cardeira *et al.,* (2016). A summary of these parameters is shown in **Table 5**. Using ImageJ, the values extracted from the images analysed were transformed into distance or area (mm or mm^2, respectively) by calibrating the pixel values with the scalebar showed in the images, prior the calculations were performed.

Table 5 Summary of the mineralisation/regeneration parameters proposed by Cardeira et al., (2016) to explore the mineralogenic performance in zebrafish caudal fin models.

***De novo* mineralisation quantification parameters.**
RMA: the real mineralised area was determined by the area inside the full contour of the mineralised rays, from the resection plane to the most distal bony rays' tips.
RAY: the mean ray width was defined as de mean value extracted from the length of each fin ray, measured using the first segment below the resection extension.
REG: total regenerated area obtained from the full contour of the caudal fin tissue.
STU: the stump width corresponded to the length of the amputation plane.
RMA / RAY: Mineral deposition within the regenerated lepidotrichia.
REG / STU: Regenerated tissue within the resection plane length.

These parameters represent the not mineralised tissue with the fish caudal fin (REG and STU) and the mineralised tissue (lepidotrichia) that is contained in the caudal fin (RMA and RAY). The **Fig. 26** represent how these parameters were obtained from the fish fins. The values obtained were used to quantify the ratio of bone per area of fin tissue.

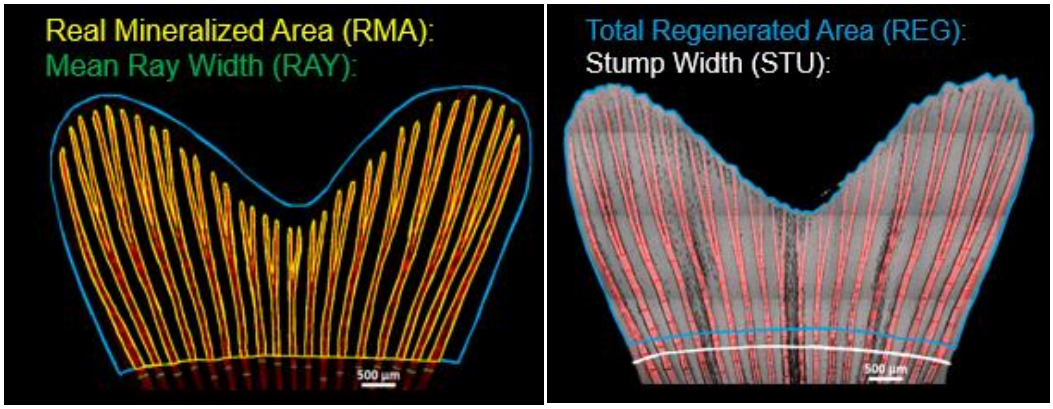

Fig. 26 Colour representing each of the mineralised tissue (RMA and RAY) and non-mineralised tissue (REG and STU) used to determine the lepidotrichia growth after zebrafish fin resection. Image by the author based on parameters proposed by Cardeira et al., 2016.

3.1.1.3. Second fin resection

After 21 dpa, the regenerated fins were resected using procedures as described previously. The fins extracted from the fish immersed in fish tank water only (no previous disease condition) were labelled as $CTRL_{REG}$; the caudal fins amputated from the group of fish that previously developed osteoporotic-like bones and were let to regenerate in fish tank water only, were called $GIOP_{REG}$ and, finally, the fish with OP condition treated with ALN were labelled as ALN_{REG}. A summary of the treatment groups proposed are shown in **Table 6**.

Table 6 Summary of the experimental conditions used in this study

B. Zebrafish treatment condition		
Group	**Resection**	**Condition**
CTRL	1st	Untreated zebrafish
GIOP	1st	Zebrafish treated with 125 µM PN for 14 days
$CTRL_{REGEN}$	2nd	CTRL condition + fish tank water only for 21 days
$GIOP_{REGEN}$	2nd	GIOP condition + fish tank water only for 21 days
ALN_{REGEN}	2nd	GIOP condition + fish tank water + 30 µM ALN for 21 days

3.3. Scanning electron microscopy

SEM is one of the most widely used technique to characterise the morphology of materials on micro- and nano-level with high resolution. Differently from bright field microscopes that use a light source to produce images, SEM uses the two forms of electron interactions with samples: elastic and inelastic interactions (Zhou *et al.,* 2006). When an electron (or electron beam) is aimed to the surface of a specific material, distinct types of electrons will be scattered back to the microscope's reading device. In elastic interactions, the incident electron is deflected back, with minimal energy loss, by outer shell electrons (situation of most conserved energy). If electrons are scattered more than 90° from the incident beam, they are called backscattered electrons and are useful for composition analysis and imaging (Goldstein *et al.,* 2003). Inelastic interactions occur by the numerous collisions occurring between the incident electrons with electrons and atoms of the sample. Inelastic interactions lead to increased energy exchange in comparison to elastic interactions. Secondary electrons are a consequence of this highly energetic exchange and are also used to image and analyse the surface of samples. All these signals are generated not just by the bouncing of electrons in samples surfaces, but by their penetration and interaction with the available specimen atoms. This penetration creates an affected zone within the specimen. The area and depth of this zone is dependent on the beam energy and sample density (atomic number) (Goldstein *et al.,* 2003). **Fig. 27** shows the possible signals generated by electron beam-sample inelastic and elastic interactions.

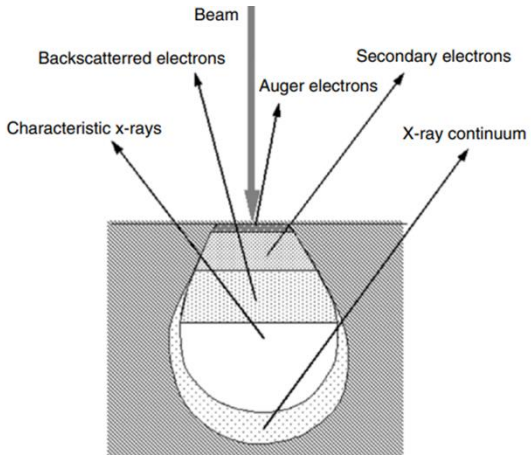

Fig. 27 Possible signals occurring from electron beam-sample surface collisions. Each of these signals have specific uses in sample imaging and composition profiling. Image from Goldstein et al., (2003).

In addition to backscattered and secondary electrons, elastic and inelastic interactions also generate Auger electrons and x-rays. X-rays, in particular, have an interesting application with SEM, as they can be used with backscattered electrons to produce qualitative data on samples, which means that the composition can be assessed. For qualitative data analysis, energy dispersive spectroscopy (EDS) is used (Dorozhkin, 2012). SEM are normally equipped with EDS, so the composition can be monitored in the SEM screen. SEM/EDS can be also used for quantitative analysis of the composition; however, they are considered less dependable than qualitative ones. SED/EDS combined have shown strong benefits for the study of biological materials like bone. Mahamid *et al.,* (2008) used SEM/EDS to characterise both the morphology and composition of zebrafish caudal fin bones. In this study they found that in the beginning of zebrafish lepidotrichia mineralisation, an amorphous phase of apatite-like mineral is formed. **Fig. 28** shows a schematic with SEM and EDS results obtained from zebrafish caudal fin analysis.

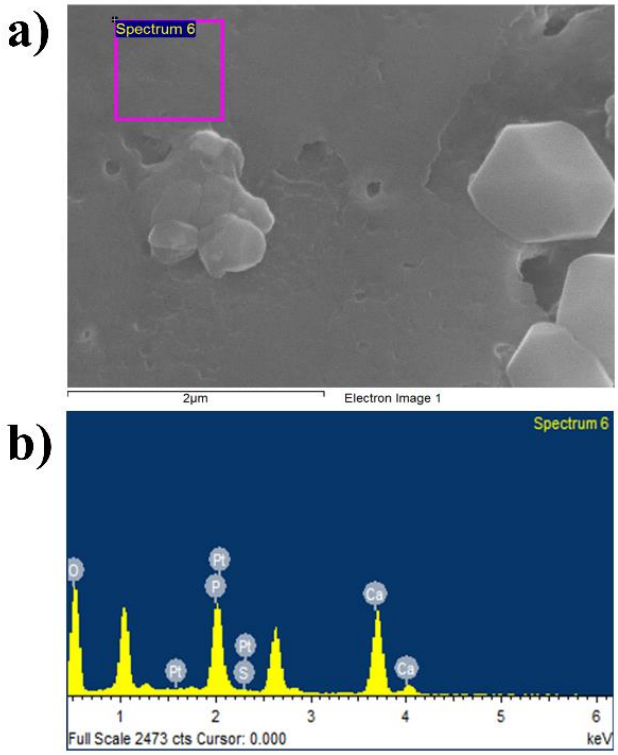

Fig. 28 (a) SEM image and (b) EDS composition spectra obtained from zebrafish lepidotrichia. Oxygen (O), platinum (Pt), sulphur (S), phosphorus (P) and calcium (Ca) were found in the composition. Image by the author.

3.3.1. SEM of zebrafish lepidotrichia

The amputated zebrafish caudal fins (n = 3; each group) were put onto microscope glass slides and were bleached with 5% sodium hypochlorite solution (J.T. Baker; Pennsylvania, PA) in order to remove external tissue and fatty components (Mahamid *et al.*, 2008). The bleaching solution was washed out with deionized water and the fins were dehydrated in ethanol series (50-, 75-, and 100%) for 15 minutes sequentially. The exposed bones were then separated into proximal and distal regions by performing a section ~2 segments proximal to the cleft. The proximal and distal parts were rapidly frozen under liquid nitrogen and crushed into small particles with mortar and pestle. The still frozen particles were critical-point-dried in a Samdri-795 critical point dryer (Tousimis®; Maryland, MD) and evaluated. The morphology of

proximal and distal regions of the fins were observed using a SEM SU8010 (Hitachi; Chiyoda, Japan) equipped with an EDS. Calcium (Ca) and phosphorus (P) atomic percentages, were recorded in five different sites using EDS. The areas of analysis were fixed to 7 × 7 μm^2 and the equipment voltage was set to 15 kV for both characterization methods.

3.3.2. SEM of zebrafish vertebrae

3.3.2.1. Vertebrae segment separation

Zebrafish were positioned individually onto microscope glass slides, and, with a scalpel, an incision was performed below the first dorsal stripe. Using n° 5 tweezers, the cavity was maintained opened, and the tissues adjacent to the backbone were carefully removed. Gently, the fish had their vertebral column extracted and put onto a petri dish; the excess of tissue was removed with 5% NaClO solution, and by further mechanical removal with a scalpel. The vertebra segments belonging to the PC1 to PC10 and CV1 to CV14 were disconnected from each other, numbered relative to their position, and stored at -21 °C in 24-well plates. The vertebrae segments from the WA and the endpoint of the CFV were not used in this research but were stored for training purposes.

3.3.2.2. SEM procedure

PC vertebra segments of different zebrafish (n = 4) were positioned with their axial or sagittal surface facing the bottom of cryomolds. The cryomolds were filled with OCT and indirectly frozen with liquid nitrogen until they became opaque-white. The then solid moulds were wrapped in aluminium foil and stored at -21 °C until use. The OCT blocks were cut into slices of 30 µm of thickness with a microtome CM3050 S (Leica Microsystems GmbH; Wetzlar, Germany), and the generated axial and sagittal pieces were fixed onto microscope glass slides.

The slides were further cleaned from the excess of OCT with PBS, formulated with NaCl, KH_2PO_4, Na_2HPO_4 and KCl (Chazotte, 2012), with its pH adjusted to ~7.4. Then, the slices were dried and were transferred to aluminium stubs properly covered with conductive copper tape; the samples had their surface sputtered with a thin layer of platinum for 90 seconds and the bone morphologies were observed with a SEM SU8010 (Hitachi, Chiyoda, Japan) at 5 kV.

3.4. Raman spectroscopy

Raman spectroscopy is a technique that involves the vibration of the molecules and ions within biological or engineering materials. The light that is scattered due to vibrational effects, loses energy, elongating its λ, the difference between the λ of the incident light to the λ of the scattered light correspond to specific shift in the Raman spectrum (Morris and Mandair, 2011). Thus, with this technique it is possible to analyse peak of calcium phosphates in bone (Bennet *et al.,* 2014; Morris and Mandair, 2011).

3.4.1. Raman spectroscopy of zebrafish caudal fin

Raman spectra were obtained with a Raman spectrometer iHR550 (Horiba Scientific Ltd.; Kyoto, Japan) equipped with a laser confocal microscope IX71 (Olympus; Tokyo, Japan). A 10x magnification lens and a laser source with wavelength of 632.81 nm were used and the equipment acquisition time was set to 20 s with three co-additions. One amputated caudal fin (n = 1), with comparable size and with eighteen lepidotrichia each were selected and transferred to opaque 3D printed polymer substrates. The bones were exposed with sodium hypochlorite and subsequently dehydrated in ethanol series. A total of 96 equidistant points (~700 μm distant) had the spectrum recorded and the area under the phosphate peak (~960 cm^{-1}) were calculated using LabSpec 6 software (Horiba Scientific Ltd.; Kyoto, Japan). The integrated values were plot as a heat colour map to the position analysed.

3.5. Atomic force microscopy

AFM is a scanning probe microscopy that is used to interact with the surface of samples. The mode which AFM interact with samples relies on a cantilever with a tip in its end. When this tip approaches the surface of a material, the interaction forces between sample/probe deflects the cantilever. With this, the cantilever is able to record the average roughness (Ra) of a surface as well as its morphology (Zhou and Du, 2022).

3.5.1. Surface profile and roughness of zebrafish lepidotrichia

3.5.1.1. Sample preparation

Two amputated fins of each group (n = 2) were gently placed into a cryomold (TissueTek®; Sakura Finetek Europe B.V., Netherlands) and were totally covered with Optimal Cutting Temperature (OCT) compound (TissueTek®; Sakura Finetek Europe B.V., Netherlands). The compounds were indirectly frozen using liquid nitrogen, covered with aluminium foil and stored at -21 °C until used. The blocks were cut into 30 µm thick slices, perpendicularly to the bony rays' direction growth direction, at -21 °C, with a microtome CM3050 S (Leica Microsystems GmbH; Wetzlar, Germany), as described elsewhere (Chang *et al.,* 2018). The used thickness is over the minimum standard accepted to sub-micron analyses (Fischer-Cripps, 2000). The sliced samples were fixed in properly labelled microscope glass slides and the excess of OCT was washed using PBS with pH of ~7.4, formulated as described by Chazotte (2012). One of the cross-sectioned samples was used in the surface roughness analysis, while the other was used for mechanical evaluation.

3.5.1.2. Surface roughness measurements

The surface profiles of sliced samples were observed using an Icon® AFM (Bruker, Massachusetts, MA). The AFM was operated in tapping mode in air using a non-conductive silicon nitride tip with a nominal radius of 4 µm (Nanosensors™; Neuchâtel, Switzerland). The spring constant was 42 N/m with resonant frequency of 330 kHz. The equipment was set to a scan rate of 0.99 Hz and the images were captured with a resolution of 256 pixels/line. The third lepidotrichia from dorsal part was used in this technique. One slice between the 2nd and 3rd segments proximal to resection plane, and other between the 2nd and 3rd segment near to the distal tips, had the surface profile and roughness recorded. Five areas of 2 μm^2 were measured and the average value of Ra was calculated with the software NanoScope Analysis v1.4 (Bruker, Massachusetts, MA), similarly as found elsewhere (Ihnatouski *et al.*, 2020).

3.6. Micro-Computed tomography

Differently from fluorescence microscopy, µ-CT uses x-ray to photograph thin layers of samples to build their whole image. µ-CT is a laboratory adaptation from the computed tomography equipment that is often used for skeletal assessment in humans. This reduced version is an interesting platform to analyse small animals and tiny samples with high resolution (Ritman, 2004). µ-CT scanners need three parts to generate a 3D model: x-ray source, samples holder and an x-ray detector, as it is shown in the **Fig. 29**.

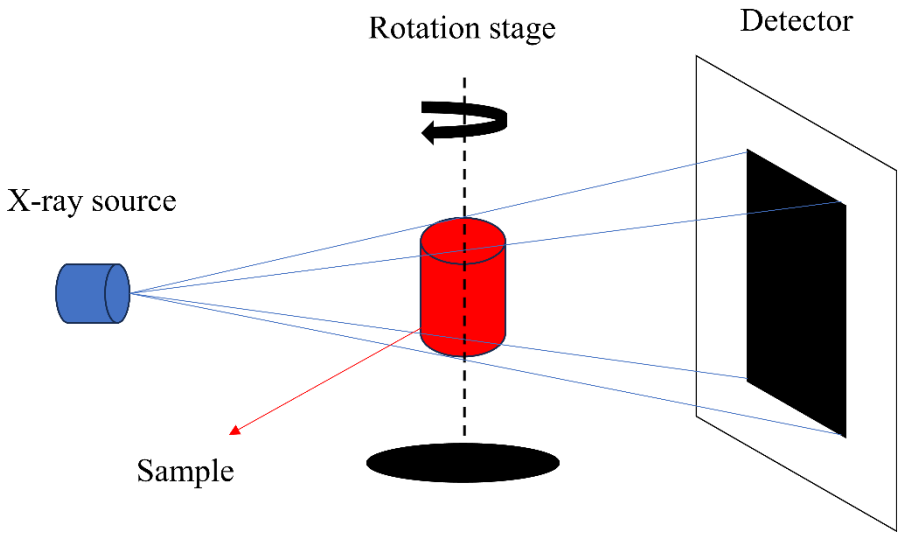

Fig. 29 µ-CT apparatus showing the x-ray source, rotation stage where the sample is loaded and the detector. It is possible to move samples closer and further away from the x-ray source; this would generate different resolutions of scans. Figure by the author.

To generate scans, electrons are accelerated to high speeds by an electric field created in the source. By using software, it is possible to adjust the current desired in the analysis; this allow the control of the number of electrons emitted by the source, similarly to what is done in SEM analysis (Ritman, 2004). Once the x-rays hit the sample, 2D images are produced and, layer by layer, each of the 2D scans can be added together, forming a 3D projection of the sample. µ-CT differs from the computed tomography scanners used in medical care by the fact that, in the latter, the sample (patient) remain laid down in a bed while the source move around it; in µ-CT, the sample rotates 360°. Intuitively, the slower the rotation, the higher the resolution of the scan and the time used in the analysis (Ritman, 2004). After the scan is completed, a software is used to fully investigate the sample. An example of reconstructed image obtained with µ-CT can be seen in **Fig. 30**.

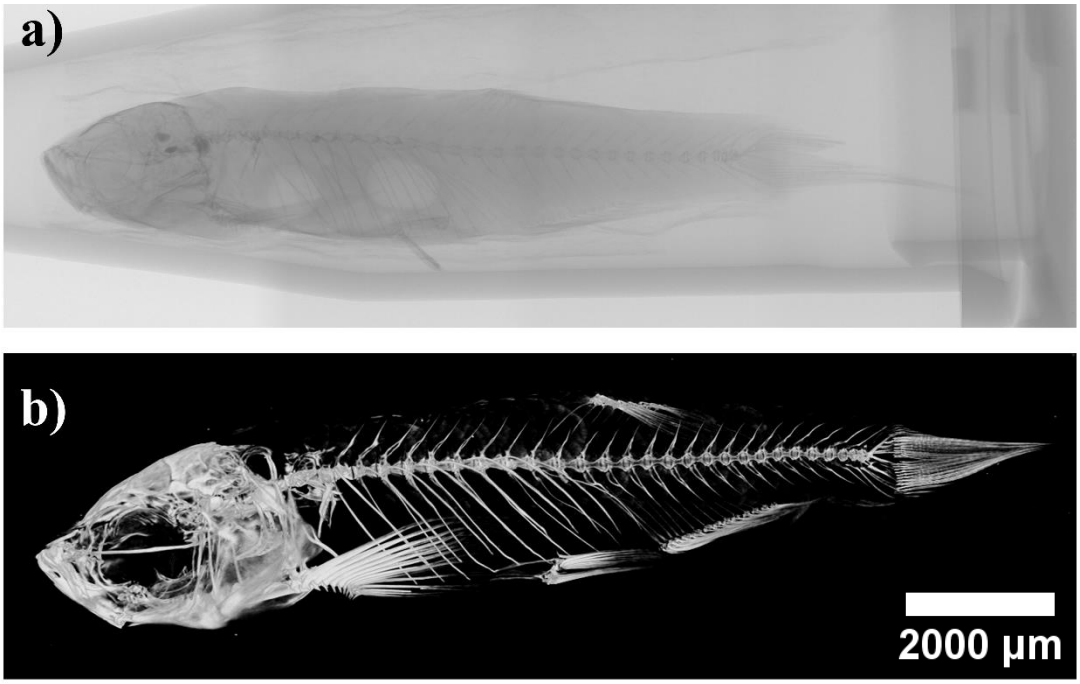

Fig. 30 µ-CT scan of a whole zebrafish. (a) The projection image of a zebrafish (dark grey) inside a sample testing tube. (b) Reconstructed image showing the full skeleton of a zebrafish. The contrast obtained in the images is possible due to the difference in density between the fish bones, their skin, organs and the testing tube. Image by the author.

In the biomedical field, both quantitative and qualitative analyses of bone are paramount for the full understanding of diseases. Qualitative evaluation allows the discovery of abnormalities within the skeleton, such as pathological or ectopic bone formations, fractures or micro-cracks, regions with malformation of mineralised tissue and locations with low BMD (Charles *et al.,* 2017; Eriksen, 1986). In animal models, µ-CT is considered the standard analysis for the diagnosis and detection of bone diseases such as OP and OI (Charles *et al.,* 2017; Lee *et al.,* 2022). In a recent study, µ-CT was used to investigate the morphometrics of *oim*/Hom mice femurs (Lee *et al.,* 2022). They found that the tissue-mineral density decreased in both male and female mice in comparison to the control group. When Lee *et al.,* analysed the mice femurs qualitatively, they found deteriorated trabecular bone. In another study, µ-CT was used to

assess gene function during skeletogenesis in zebrafish (Charles *et al.*, 2017). They found that, if fish of the same age are compared, their BMD is conserved between males and females.

3.6.1. BMD of zebrafish vertebrae (CV1 and CV2)

Three euthanized fish of each group (n = 3) were put into 11 mm diameter sample tubes and immobilised with wrapping tissue. The samples were scanned with a SkyScan 2211 Multiscale X-Ray Nanotomograph (Bruker; Massachusetts, MA, US) in air. After analysis, each fish was put into the freezer at -21 °C until they were further used. The detailed images were obtained with a resolution of 7 µm/voxel size with micro-focus scanning. The equipment voltage was set to 60 kVp, the current used was 530 µA, with 6-Watt output. The image reconstruction was performed and corrected by reconstruction software (Instarecon; Illinois, IL, US). Reconstructed cross-sections were reoriented, and the ROI was chosen. Scans of the vertebral columns were performed at 700 µm diameter / 100 pixels, and the bone volume (BV), tissue volume (TV) (Monma *et al.*, 2019), and cortical bone thickness (B.Th) (Hildebrand and Rüegsegger, 1997) for both CV1 and CV2 were calculated. Similarly, the BV / TV was deduced based in the data obtained. The BMD of CV1 and CV2 were also assessed using a software supplied by the instrument manufacturer (CTAn v.1.18; Bruker, Illinois, IL, US). BMD measurements were calibrated using phantoms of known HAp density. Z-Scores were calculated based on the BMD values of CTRL zebrafish (Genest *et al.*, 2021). For further morphometric analyses, we have used CTVox (Bruker, Illinois, IL, US) and DataViewer (Bruker, Illinois, IL, US) software, also supplemented by the manufacturer. Further morphometric analyses of the ROI were performed using ImageJ 1.52a (Wayne Rasband, National Institutes of Health, Bethesda, MD). The greyscale threshold/data range was set between 1 and 230 to avoid null-data and remove small noise generated by fish scales (e.g., floating pixels). Moreover, the images were not post processed for beautification purposes.

3.7. Nanoindentation

There is a growing interest in analysing the mechanical properties of engineering and biological materials at sub tissue level. Among the methods used for this purpose, NI with nanoindenter is recognised as one of the leading techniques (Ebenstein and Pruitt, 2006; Pei *et al.*, 2022). NI is able to assess diverse types of samples, such as thin films, and biomimetic and biological materials (Ebenstein and Pruitt, 2006). Traditional mechanical tests (e.g., three-point bending) are limited to the size of the instrument, not being suitable for samples of reduced sizes such as zebrafish and mice bones. Samples as big as mice femurs, however, can be evaluated by the traditional machines if these are adapted or re-scaled to bones sizes (Lee *et al.*, 2022). In addition, macro-scale mechanical tests measure properties over the whole extension of the sample, being destructive for this reason. NI allows the user to interrogate samples in small areas. Thus, it is of particular interest the use of NI in materials with heterogenous composition, such as the bones (Ge *et al.*, 2006) and many other biomaterials.

Nanoindenter are simple machines in their building, calibration procedure and operation, if compared to other instruments able to carry NI tests (e.g., AFM). However, they are overly sensitive to external forces (e.g., wind and temperature variations). To maintain the desired precision while the equipment is indenting the samples, the room/environment accommodating the apparatus must remain under controlled conditions. **Fig. 31** shows the main components of a nanoindenter.

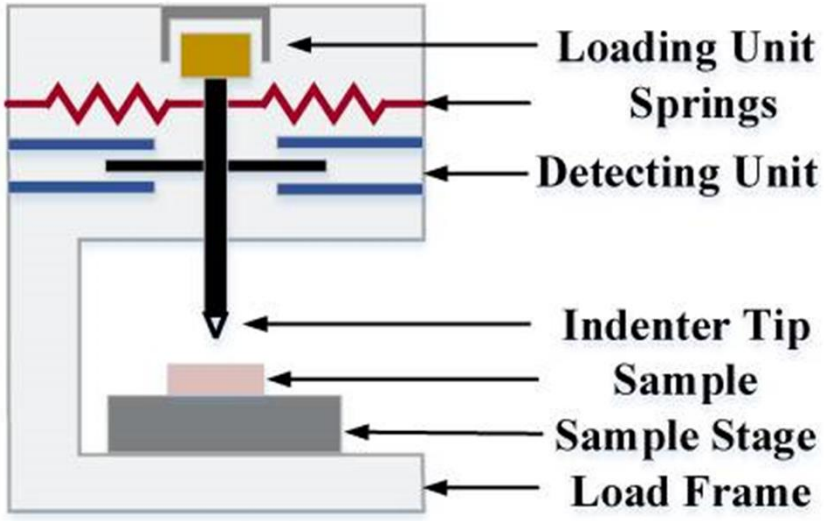

Fig. 31 Sketch of the main parts of a nanoindenter. Image from Qian & Zhao (2018).

The loading unit has a piezoelectric element that expands/shrink to control its mechanical motion. The springs and detecting unit operate together; while the detecting unit measure the displacement occurring on the surface of the sample, the spring work as a coupling mechanism to ensure that every "unit" of raw force will generate a relative depth of penetration. The indenter's tip is one of the variables that makes nanoindenter versatile; by changing the shape of the tip (e.g., pyramidal to spherical or flat-ended), dissimilar materials can be analysed. It is conventional to use pyramidal tips for biological hard tissues (Ebenstein and Pruitt, 2006). Finally, the sample stage is what allow the user to control the coordinates of each indent, by moving *x*, *y* and *z* directions (Qian and Zhao, 2018).

In NI, the indenter tip is normally made out of a material with known *E* and Poisson's ratio (υ), like diamond. Diamond is a naturally stiff material; this characteristic allows the indenter's probe tip to penetrate the surface of materials with high mechanical properties. It is conventional for the operator of the nanoindenter to either limit the maximum load (*P*) or displacement (*h*) that should be used in the experiment. This means that, for example, if the

user choses to limit the maximum *P*, then the equipment will apply force onto the sample surface until the maximum *P* is reached. The consequential *h* from this value will be then recorded as a variable, and the software will give an output in the form of a *P vs. h* curve (Oliver and Pharr, 1992, 2004). Generally speaking, the mechanical properties of most engineering and biological materials are time (*t*) dependent. Thus, it is logical to think that NI is also a time-sensitive technique (Ebenstein and Pruitt, 2006). **Fig. 32** shows a *P vs. h* graph generated with a specific loading regime.

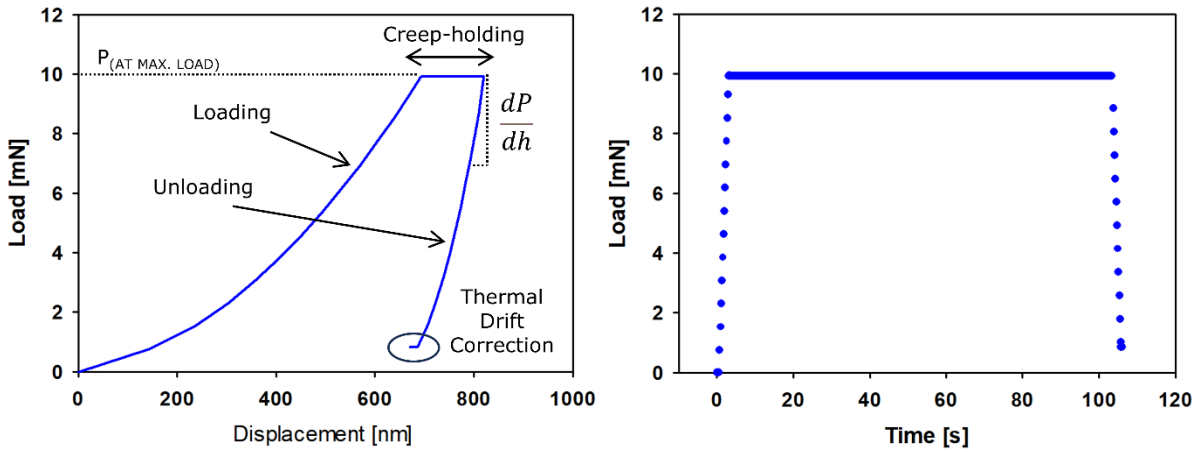

Fig. 32 Classic P-h curve of bone, showing the key features of the curve (left) and the load regime (right) obtained from creep studies. The trapezoidal shapes in both graphs are related to hold times of 100 s. Figure by the author.

The curves seeing above are different from the curves obtained from tensile tests (stress-strain), in which the mechanical qualities of the material can be derived from. In NI, analytical approaches are required in order to calculate *E* and *H* from the unloading part of the *P-h* curves (Qian and Zhao, 2018). Two of the most commonly used analytical methods are Oliver and Pharr (O-P) and Hertz (Fischer-Cripps, 2000; Oliver and Pharr, 1992). O-P method is used in materials indented by pyramidal shaped indenters (i.e., Berkovich), while the Hertz method focusses on soft tissues indented by dull tips (i.e., sphere) (Fischer-Cripps, 2000). The O-P

method assumes that the loading portion of *P-h* curves have an elastic-plastic contact mode, and, at the start of the unloading part, only elastic recovery occurs. Thus, the relationship *P-h* during unloading follows the power law, described in the equation 4.

$$P = \alpha(h - h_f)^{\beta} \quad (4)$$

Where h_f is the final residual indentation depth and α and β are fitting constants related to the shape of the indenter's tip. Due to the fact that O-P method assumes elastic-only behaviour in the beginning of the unloading curve, it is possible to deduce that the stiffness (S_T) at the end of the holding time can be described using the equation 5.

$$P = \frac{dP}{dh} \quad (5)$$

Once the S_T and the unloading contact area (A_U) are known, it is possible to proceed to the calculation of the reduced elastic modulus (E_R), by the equation 6.

$$E_R = \frac{\sqrt{\pi}}{2}\frac{S_T}{\sqrt{A_U}} \quad (6)$$

If we decouple the E_R (combined modulus of the tip and the sample), we will have the *E*, as described in the equation 7.

$$\frac{1}{E_R} = \frac{(1-\nu_s^2)}{E_s} + \frac{(1-\nu_i^2)}{E_i} \quad (7)$$

Where the subscripts, s and i, indicate *E* related to the sample and indented, respectively.

In other words, to measure the *E* and *H* of a material using NI based on O-P method and a pyramidal Berkovich tip, a series of steps are needed, as mentioned elsewhere (Oliver and Pharr, 1992, 2004). This method assumes that the material in the boundary indenter tip/sample surface, behaves in a way that it can be described by models of simple geometry, without taking in consideration the pile-up of material around the tip (Oliver and Pharr, 2004). **Fig. 33** shows the contact geometries created by a NI tip when in contact with the surface of a material, where h_s is the amount of sink-in, h_c is the contact area and ϕ is the indenter's half-included angle.

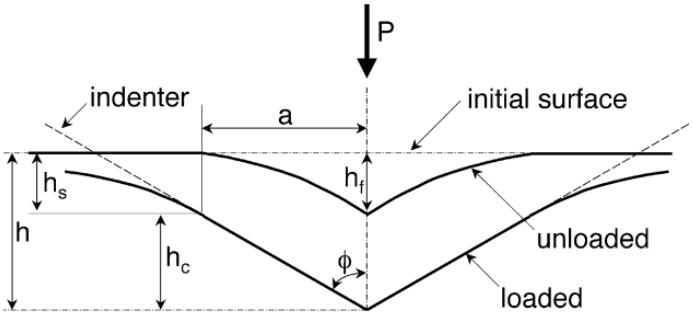

Fig. 33 Contact geometries of the unloading process in NI. Image by Oliver and Pharr, 2004.

The h_c can be found using equation 8 and, afterwards, the *H* of the material can be calculated using the area relative to h_c, as in the equation 9.

$$h_c = h_{MAX} - \epsilon \frac{P_{MAX}}{S} \quad (8)$$

$$\mathrm{H} = \frac{P_{MAX}}{A(h_c)} \quad (9)$$

As mentioned previously in this chapter, the O-P method works well with hard biomaterials such as bone (Pei *et al.,* 2022; Sun *et al.,* 2016). One example of its use is for creep-holding curves, where indentation depth is plotted against increased holding times (Bonicelli *et al.,* 2022; Khalili *et al.,* 2023; Wu *et al.,* 2011). The creep index (C_{IT}) of a material can be calculated with the equation 10.

$$C_{IT}(\%) = \frac{h_{max} - h_b}{h_{max}} \times 100 \quad (10)$$

Where h_b and h_{max} are the displacements at the beginning and end of the hold period, respectively.

3.7.1. Nanoindentation of zebrafish lepidotrichia

Three consecutive slices from each proximal and distal region had their mechanical properties evaluated. A Tribo-Indenter (TI 980; Bruker, Minnesota, MN) equipped with a Berkovich tip was used in order to measure the E_R and H of the samples. The depth of each indentation was controlled to 100 nm and the loading, holding and unloading times were set to 5 s each. A series of ~26 and ~20 indentations, for proximal and distal sites, respectively, distributed in 3 lines, were performed at the midway point of the hemi rays of the third dorsal lepidotrichia. The distance between each measurement was set 100 nm in order to minimize the effects of neighbour indentations. In addition, both E_R and H were calculated in relation to their mineral ratios obtained from the proximal regions.

3.7.2. Nanoindentation of zebrafish vertebrae

For the procedures on the separation of the segments of zebrafish vertebrae that were used in this analysis, head to **section 3.3.2.1**.

CV bones were positioned and fixed in the bottom of plastic metallography moulds with their axial surface facing down. The moulds were poured gently with epoxy resin, let to set overnight and were ground with silicon-carbide papers and polished with 0.2 μm alumina slurry. A nanoindenter G200 system with a DCM-II head (KLA-Tencor, California, CA, US) and equipped with a Berkovich (three-sided pyramidal) tip with 20 nm radius was used. *E* and *H* of the samples were calculated via O-P method (Oliver and Pharr, 2004, 1992). A Poisson's ratio of 0.3 was assumed for the bone samples. Bones of three different zebrafish (n = 3) per group were measured. The indentations had their load controlled to 0.5 mN and the holding times were set to 0 s each. All the biomechanical testing was conducted in temperature-controlled laboratory at 22 °C. Multiple indentations were conducted distant to each other to alleviate interaction effects between two measurements.

3.7.3. Nanoindentation murine model

3.7.3.1. Sample preparation for NI

Mice femurs were separated from adjacent bones, cleaned from blood and remaining tissues, and were stored in laboratory tubes with 70% ethanol (EtOH) before the experiments in this study were performed (Lee *et al.*, 2022). When the bones were received, they were dehydrated in ethanol series (50-, 70-, 95- and ~99% EtOH), for 30 minutes each step, under ultrasonic bath. A final dehydration step was performed overnight, without agitation, using absolute EtOH.

Any humidity had to be removed from the samples to allow a better filling by the acrylic resin and avoid bubbles in the interface bone/polymer.

The then dehydrated bones were positioned into the bottom of pre-greased, 25 mm wide, plastic moulds and were mounted horizontally in low viscosity epoxy resin (Epo-Flo; Metprep, UK). The resin blocks were kept shallow as it facilitates the next process of clamping and sectioning. The resin mounts were let to cure overnight. The blocks were de-moulded and had their sides trimmed parallel to each other. They were fixed, one at a time, into a metal sectioning vice and sections of 2.5mm thickness were cut transversely to the mice femurs, using precision diamond saw (Accutom; Struers, Copenhagen, Denmark). The resultant slices were then cleaned in EtOH under ultrasound agitation, dried and positioned with their axial surface facing the bottom of pre-greased plastic moulds one more time. The specimens were re-mounted with low viscosity resin, labelled and let to cure overnight. Once fully cured, the solid blocks were removed from the moulds, cleaned in 70% EtOH in bath ultrasound, dried and had their surface refined by mechanical grinding. The mesh (#) of silicon carbide sandpapers was increased gradually, starting from #300, up to #2500, for better results. The ground surface was inspected after every griding step with optical microscope. The samples were then polished in a semi-automatic polishing machine (Autopol; Metaserv, Buehler, US). **Fig. 34** shows a workflow from mice dissection to the final steps of embedding.

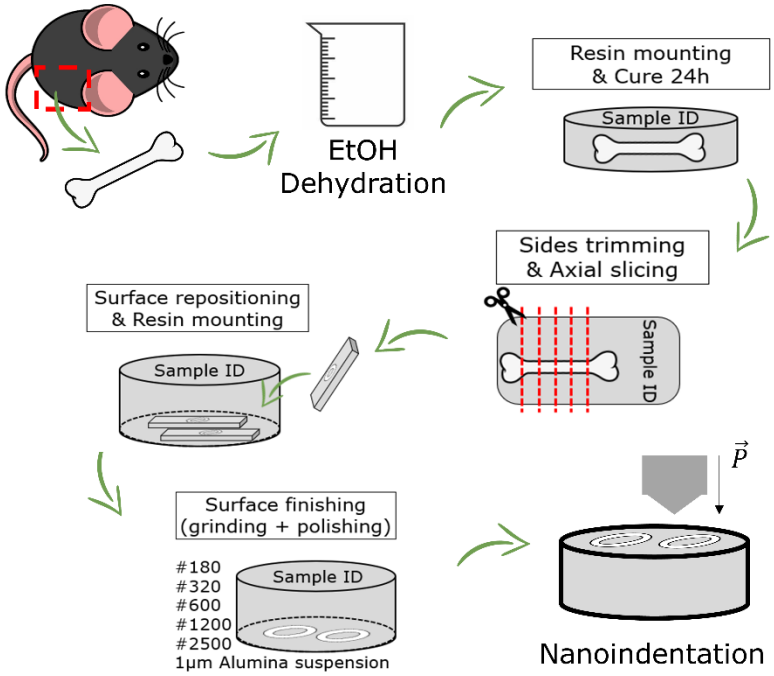

Fig. 34 Mouse femurs were received, dehydrated and prepared to NI through a series of embedding into acrylic resin and surface finishing. Image by the author.

3.7.3.2. *E* and *H* measurements

Mechanical analysis was performed with a nanoindenter G200 system with a DCM-II head (KLA-Tencor, CA, USA), equipped with a Berkovich (three-sided pyramidal) diamond tip with 20nm of radius. A load of 10 mN was used with a loading time of 2.5s, and an assumed Poisson's ratio of 0.3 (Oliver and Pharr, 2004). The mounted samples were fixed with super glue onto a metal stage and had their height levelled to the same plane as a central silica standard platform. The nanoindenter was calibrated using an aluminium standard ring prior each batch of four samples were analysed.

Before and after the bones were indented, a fused silica standard with known *E*, was indented eight times to verify if the calibration was maintained across the experimentation. Using the

built-in equipment microscope, the cortical region of mice femurs was localised, and the focus was adjusted. The samples were indented ~15 times across their surface in locations chosen manually, but distant from each other so neighbouring indents did not influence each other. The *E* and *H* were determined using the O-P method (Oliver and Pharr, 2004, 1992). Defective indents (e.g., indenter head failing contact with samples' surface) were removed from the results. The linearity between *E* and *H* was verified by scatterplots for all groups and the Pearson correlation (r^2) was calculated.

3.7.3.3. Creep behaviour

Two different peak holding times of 10s and 100s were measured to further explore viscoelastic behaviour of sound and diseased mice femurs. In order to question the samples on their creep behaviour, subsets of the *load vs. displacement* data were used. Thus, the regions before and after the peak-hold plateau were not considered for creep analysis, as described elsewhere (Wu *et al.*, 2011). The change in depth occurring during creep-hold times was calculated by subtracting h_{max} from h_b. The C_{IT} of femurs were calculated using the equation (10) in **section 3.7**, as suggested by Bonicelli *et al.*, (2022).

3.8. Statistical analyses

3.8.1. Zebrafish caudal fin study

Descriptive analysis was performed on SEM, Raman-mapping and AFM images. All the statistical analyses were performed with SigmaPlot 12.0 (Systat Software; San Jose, CA). The normality of the samples was verified using Shapiro-Wilk Test ($p < 0.01$). The t-test was used to verify the statistical significance of GIOP treatment ($p < 0.01$). Two-way ANOVA was used

for the remaining pixel-related measurements, elemental analyses, surface roughness, E_R and H ($p < 0.01$).

3.8.2. Zebrafish vertebrae study

The data was tested for normality using the Shapiro-Wilk test. Parametric or non-parametric statistical methods were chosen depending on if results passed or failed the normality test. The numerical values obtained with µ-CT passed the normal distribution test ($p > 0.01$) and were analysed with One-Way ANOVA followed by Dunn's post-hoc test for comparisons against the control ($p < 0.01$); the nano-hardness and elastic modulus passed normality test ($p < 0.01$) and were thus analysed with One-Way ANOVA and Dunn's post-hoc test for pairwise comparisons ($p < 0.01$). All statistical analysis was conducted with Sigma Plot 14.5 (Systat Software; San Jose, CA). In addition, descriptive analyses were performed on skeleton features obtained with µ-CT scans and in the morphology of mineralised tissue visualised with SEM.

3.8.3. Murine models study

The normality of data was verified using Shapiro-Wilk test. The *E* of 18-weeks-old *oim* mice did not pass the normality test; in *tm1b* mice femurs, the *H* of 8- and 18-weeks-old and the *E* of 8-weeks-old mice failed to pass the normality test ($p < 0.05$). The data that did not displayed normal distribution were transformed to normal with Johnson's method using Minitab (Minitab, Inc.; Pennsylvania, US) prior further statistical analysis. *E* and *H* interactions within each mouse mutation (*oim* and *tm1b*) were tested with One-Way ANOVA with Dunn's method ($p < 0.05$). C_{IT} data passed the normality test ($p > 0.05$) and had their significance tested with One-way ANOVA ($p < 0.05$). SigmaPlot 14.5 (Systat Software Inc.; Chicago, US) was used for statistical evaluation and plotting of data.

3.9. Summary

This chapter, in summary, showed critical methodologies applied in the development of this thesis. Fluorescence microscopy was used in zebrafish caudal fin model to observe fish's lepidotrichia regenerative processes after amputation. SEM was used to visualise bones in zebrafish caudal fin and vertebrae; μ-CT, conversely, was used in zebrafish vertebrae to calculate important parameters such as BMD. NI was used to assess the biomechanics in all animal models in this thesis. Given the importance of biomechanics of diseased bones in this thesis, a series of equations related to O-P model were highlighted.

References

Abd-Alameer, S.A., Daway, H.G., Rashid, H.G., 2020. Quality of medical microscope Image at different lighting condition. IOP Conf. Ser.: Mater. Sci. Eng. 871, 012072.

Bennet, M., Akiva, A., Faivre, D., Malkinson, G., Yaniv, K., Abdelilah-Seyfried, S., Fratzl, P., Masic, A., 2014. Simultaneous Raman Microspectroscopy and Fluorescence Imaging of Bone Mineralization in Living Zebrafish Larvae. Biophysical Journal 106, L17–L19.

Bensimon-Brito, A., Cardeira, J., Dionísio, G., Huysseune, A., Cancela, M.L., Witten, P.E., 2016. Revisiting in vivo staining with alizarin red S - a valuable approach to analyse zebrafish skeletal mineralization during development and regeneration. BMC Developmental Biology 16.

Bonicelli, A., Kranioti, E.F., Xhemali, B., Arnold, E., Zioupos, P., 2022. Assessing bone maturity: Compositional and mechanical properties of rib cortical bone at different ages. Bone 155, 116265.

Budinger, T.F., Brahme, A. (Eds.), 2014. Comprehensive biomedical physics. Volume 1, Nuclear medicine and molecular imaging. Elsevier, Amsterdam.

Cardeira, J., Gavaia, P.J., Fernández, I., Cengiz, I.F., Moreira-Silva, J., Oliveira, J.M., Reis, R.L., Cancela, M.L., Laizé, V., 2016. Quantitative assessment of the regenerative and mineralogenic performances of the zebrafish caudal fin. Sci Rep 6, 39191.

Charles, J.F., Sury, M., Tsang, K., Urso, K., Henke, K., Huang, Y., Russell, R., Duryea, J., Harris, M.P., 2017. Utility of quantitative micro-computed tomographic analysis in zebrafish to define gene function during skeletogenesis. Bone 101, 162–171.

Dorozhkin, S.V., 2012. Calcium orthophosphates and human beings: A historical perspective from the 1770s until 1940. Biomatter 2, 53–70.

Ebenstein, D.M., Pruitt, L.A., 2006. Nanoindentation of biological materials. Nano Today 1, 26–33.

Eriksen, E.F., 1986. Normal and Pathological Remodelling of Human Trabecular Bone: Three-Dimensional Reconstruction of the Remodelling Sequence in Normal and in Metabolic Bone Disease*. Endocrine Reviews 7, 379–408.

Fischer-Cripps, A.C., 2000. A review of analysis methods for sub-micron indentation testing. Vacuum 58, 569–585.

Ge, J., Wang, X., Cui, F., 2006. Microstructural characteristics and nanomechanical properties across the thickness of the wild-type zebrafish skeletal bone. Materials Science and Engineering: C 26, 710–715.

Goldstein, J.I., Newbury, D.E., Echlin, P., Joy, D.C., Lyman, C.E., Lifshin, E., Sawyer, L., Michael, J.R., 2003. Scanning Electron Microscopy and X-ray Microanalysis: Third Edition. Springer US, Boston, MA.

Huang, W.-C., Hsieh, Y.-S., Chen, I.-H., Wang, C.-H., Chang, H.-W., Yang, C.-C., Ku, T.-H., Yeh, S.-R., Chuang, Y.-J., 2010. Combined Use of MS-222 (Tricaine) and Isoflurane Extends Anesthesia Time and Minimizes Cardiac Rhythm Side Effects in Adult Zebrafish. Zebrafish 7, 297–304.

Ihnatouski, M., Pauk, J., Karev, D., Karev, B., 2020. AFM-Based Method for Measurement of Normal and Osteoarthritic Human Articular Cartilage Surface Roughness. Materials 13, 2302.

Khalili, M.H., Williams, C.J., Micallef, C., Duarte-Martinez, F., Afsar, A., Zhang, R., Wilson, S., Dossi, E., Impey, S.A., Goel, S., Aria, A.I., 2023. Nanoindentation Response of 3D Printed PEGDA Hydrogels in a Hydrated Environment. ACS Appl. Polym. Mater. 5, 1180–1190.

Lee K. J., Lisa Rambault, George Bou-Gharios, Peter D. Clegg, Riaz Akhtar, Gabriela Czanner, Rob van't Hof, Elizabeth G. Canty-Laird; 2022 Collagen (I) homotrimer potentiates the osteogenesis imperfecta (oim) mutant allele and reduces survival in male mice. Dis Model Mech 1 September; 15 (9): dmm049428.

Mahamid, J., Sharir, A., Addadi, L., Weiner, S., 2008. Amorphous calcium phosphate is a major component of the forming fin bones of zebrafish: Indications for an amorphous precursor phase. Proc. Natl. Acad. Sci. U.S.A. 105, 12748–12753.

Morris, M.D., Mandair, G.S., 2011. Raman Assessment of Bone Quality. Clinical Orthopaedics & Related Research 469, 2160–2169.

Oliver, W.C., Pharr, G.M., 2004. Measurement of hardness and elastic modulus by instrumented indentation: Advances in understanding and refinements to methodology. J. Mater. Res. 19, 3–20.

Oliver, W.C., Pharr, G.M., 1992. An improved technique for determining hardness and elastic modulus using load and displacement sensing indentation experiments. J. Mater. Res. 7, 1564–1583.

Oliveira, R.F., Silva, J.F., Simões, J.M., 2011. Fighting Zebrafish: Characterization of Aggressive Behavior and Winner–Loser Effects. Zebrafish 8, 73–81.

Pei, S., Zhou, Y., Li, Y., Azar, T., Wang, W., Kim, D.-G., Liu, X.S., 2022. Instrumented nanoindentation in musculoskeletal research. Progress in Biophysics and Molecular Biology 176, 38–51.

Pfefferli, C., Jaźwińska, A., 2015. The art of fin regeneration in zebrafish: The Art of Fin Regeneration. Regeneration 2, 72–83.

Qian, L., Zhao, H., 2018. Nanoindentation of Soft Biological Materials. Micromachines 9, 654.

Ritman, E.L., 2004. Micro-Computed Tomography—Current Status and Developments. Annu. Rev. Biomed. Eng. 6, 185–208.

Sanderson, M.J., Smith, I., Parker, I., Bootman, M.D., 2014. Fluorescence Microscopy. Cold Spring Harb Protoc 2014, pdb.top071795.

Stokes, G., 1852. XXX. On the change of refrangibility of light. Phil. Trans. R. Soc. 142, 463–562.

Sun, X., Zhao, H., Yu, Y., Zhang, S., Ma, Z., Li, N., Yu, M., Hou, P., 2016. Variations of mechanical property of out circumferential lamellae in cortical bone along the radial by nanoindentation. AIP Advances 6, 115116.

Wu, Z., Baker, T.A., Ovaert, T.C., Niebur, G.L., 2011. The effect of holding time on nanoindentation measurements of creep in bone. Journal of Biomechanics 44, 1066–1072.

Zhou, W., Apkarian, R., Wang, Z.L., Joy, D., 2006. Fundamentals of Scanning Electron Microscopy (SEM), in: Zhou, W., Wang, Z.L. (Eds.), Scanning Microscopy for Nanotechnology. Springer New York, New York, NY, pp. 1–40.

Zhou, Y., Du, J., 2022. Atomic force microscopy (AFM) and its applications to bone-related research. Progress in Biophysics and Molecular Biology 176, 52–66.

4. Chapter 4: Zebrafish caudal fin as a model for GIOP

This chapter is composed of the first study done in this thesis. This chapter is already fully published in *JBMR Plus* with the title "***Influence of Prednisolone and Alendronate on the de novo Mineralization of Zebrafish Caudal Fin***" and was adapted for the purpose of this thesis.

A brief introduction will be given on zebrafish caudal fin (section 4.2.1) and then the reasoning for targeting zebra fish caudal fin as the first model in this thesis (section 4.2.2). This chapter follow with the results (section 4.3), discussion on the findings (section 4.4) and conclusions (section 4.5).

Contribution of authors

FRB, Y-JC, RA and P-YC designed the study and draft the manuscript. FRB was responsible for data acquisition and made figures/tables and data analysis. Y-JC, RA, Y-RS and P-YC were responsible for critical comments. P-YC and RA supervised the research.

4.1. Abstract

Dysregulated balance between bone resorption and formation mediates the onset and progression of OP. The administration of PN is known to induce OP while ALN is commonly used to reverse the process. The aim of this study was to apply various analytical approaches to evaluate the compositional, morphological and mechanical properties of regenerative zebrafish lepidotrichia affected by PN and ALN. Adult 3-month-old zebrafish were used. The fin bony rays were assessed with confocal microscope to examine the mineral regeneration within the fin tissue, SEM/EDS, Raman spectroscopy, AFM and nanoindenter. PN hampered the mineral formation in the lepidotrichia while the fin was regenerating; sequential treatment with ALN boosted the mineral formation. In all treatments proposed, the layered structure of bones was preserved. High heterogeneity was observed in the Ca/P ratio of fish that intake PN only. PN attenuated the reduced E and H levels (5.60 ± 5.04 GPa and 0.12 ± 0.17 GPa, respectively), while ALN recovered them to the pre-amputation condition (8.68 ± 8.74 GPa and 0.34 ± 0.47 GPa, respectively). This study suggest zebrafish as a reliable assay system to investigate the various effects of medicines in the *de novo* mineralisation process.

4.2. Introduction

4.2.1. Zebrafish caudal fin model in bone diseases

Zebrafish are small teleost fish and have emerged as a suitable model to study bone diseases (Bergen *et al.,* 2019; Lin *et al.*, 2019) due to their feasibility for *in vivo* imaging, easy follow up potential, and their conserved bone physiology with humans (Bensimon-Brito *et al.,* 2016; Bruneel and Witten, 2015; Cardeira *et al.*, 2016). One of the most notorious characteristics of zebrafish is their ability to regenerate fins after resection (Uemoto *et al.,* 2020). Once amputation is performed, their caudal fins trigger a spontaneous process of repair, attaining similar shape and function as the inborn appendage (Cardeira *et al.,* 2016; Pfefferli and Jaźwińska, 2015; Uemoto *et al.,* 2020). It has been previously demonstrated that dedifferentiated OBs play a key role in the lepidotrichia's regenerative process (Geurtzen *et al.,* 2014). Conversely, the role of OCs in the fin's regeneration process is still not clear (Geurtzen *et al.,* 2017). However, when PN is administered simultaneously to a regenerative process, the recruitment of OCs to the injured site is irregular (Geurtzen *et al.,* 2017, 2014; Geurtzen and Knopf, 2018), which may impair the regrowth and properties of the newly formed fin. Thus, the mineral depletion caused by GIOP, may decrease the area of mineralised tissue in fish caudal fin (Barrett *et al.,* 2006). ALN, on the other hand, may increase the mineralised area (Pasqualetti *et al.*, 2015).

4.2.2. Rationale for targeting zebrafish caudal fin as our first study in bone diseases

The application of resection/regeneration processes are simple, it enables the longitudinal evaluation of the same individual, minimizing any potential effects caused by each individual

characteristic and also complies with the 3Rs in ethical Guidelines for animals' research (Bruneel and Witten, 2015; Embry *et al.*, 2010). Understanding how medicines influence the lepidotrichia' properties in zebrafish, could enhance the understanding on the pathophysiology of diseased mineralised tissues. The aim of this study was to evaluate, the appearance, the composition and mechanical properties of zebrafish caudal fin bones after the onset of GIOP; the properties of ALN treated fish were also assessed. We evaluated fish after five distinct treatments:

1) First resection:
    a. fish in fish-tank water only (CTRL).
    b. fish that intake PN (GIOP).
2) Second resection
    a. Fish in fish tank water only ($CTRL_{REGEN}$).
    b. PN fish in fish-tank water only (PN_{REGEN}).
    c. PN fish treated with ALN (ALN_{REGEN}).

4.3. Results

4.3.1. Drug effects on mineralisation

The pixel intensity (i.e., mineralisation level) of the images captured with fluorescence confocal microscopy (**Fig. 35A-B**) were obtained and transformed quantitatively. The values prior to and after treatment with PN were plotted (**Fig. 35C**). Notably, the zebrafish treated with PN presented a significant drop on their lepidotrichia' fluorescence intensity ($p < 0.01$). The decreased signal intensity indicates lower mineralisation within the tissue, which is a characteristic of the bones with GIOP phenotype. The effect of medicine on the *de novo* mineralisation of zebrafish's caudal fins are shown in the various scatter plots of **Fig. 35D-G**.

It is apparent that the behaviour of the regenerative process is dictated by the different conditions used (**Fig. 35D-F**). Also, two different cluster regions were clearly noticed in all plots: in a first phase (P1), the values were all grouped at the y-axis' origin (RMA / RAY = 0), and in a second phase (P2), a linear increase were observed (RMA / RAY > 0).

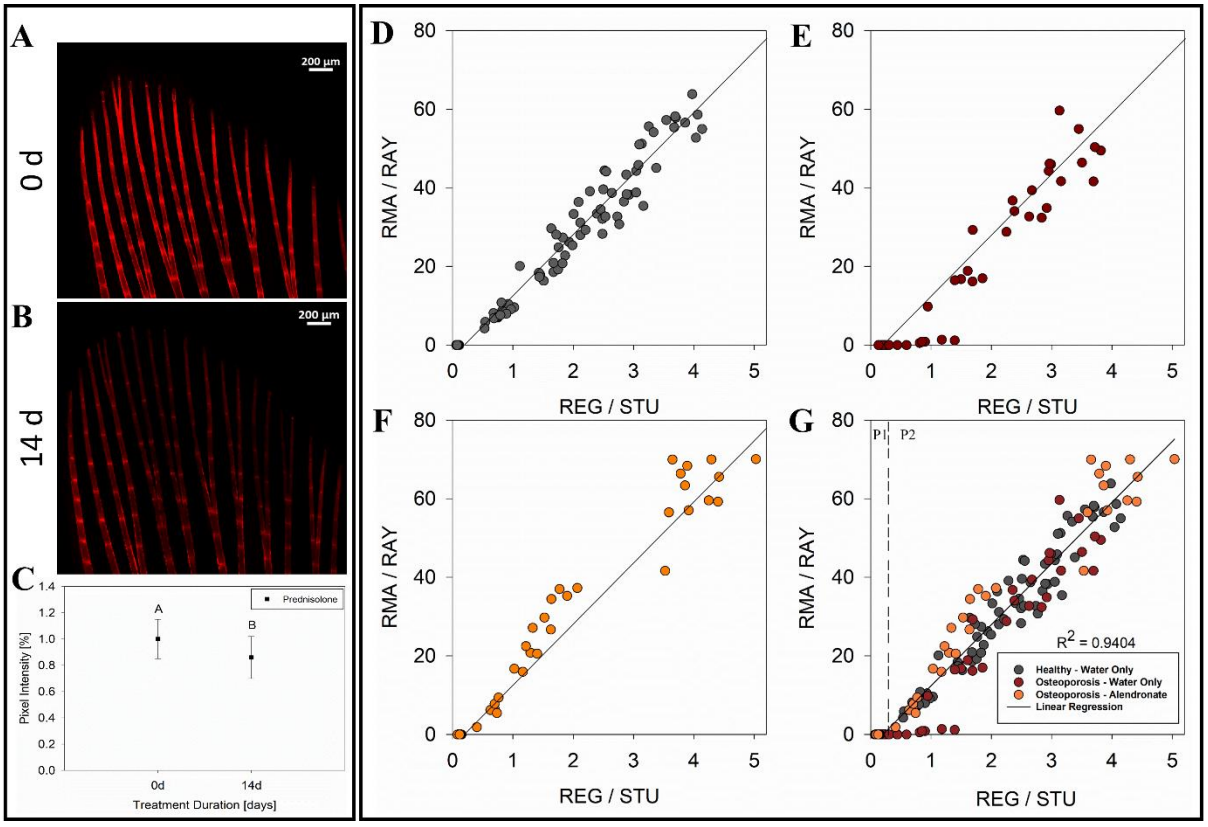

Fig. 35 GIOP development and scatter plots showing the de novo mineralisation vs. the overall regeneration. Lepidotrichia fluorescence signal before (A) and after (B) the treatment with PN. Representation of fluorescence intensities for all the fish analysed (C). Healthy fish regenerating in fish tank water only (D); fish with GIOP phenotype regenerating in fish tank water only (E); fish with GIOP phenotype regenerating in fish tank water containing ALN (F); all treatments plotted in the same graphic with linear regression analysis showing the strong relationship between the variables (G). P1 and P2 (linear increase) regions are displayed (D) separated by the dashed line. R^2 showed the strong and positive interaction between variables. Different capital letters indicate statistically significant difference ($p < 0.01$).

The time-lapsed tracking of the caudal fin regeneration on non-treated subjects are displayed in **Fig. 36**. The bright field, fluorescence and merged columns represent the caudal fin regeneration, the *de novo* mineralisation and the overall regenerative process, respectively. The first mineral deposits within the regenerating tissue were stained by AR-S at 4 dpa. Fish subjects from the CTRL group displayed their first lepidotrichia bifurcation at 4 dpa.

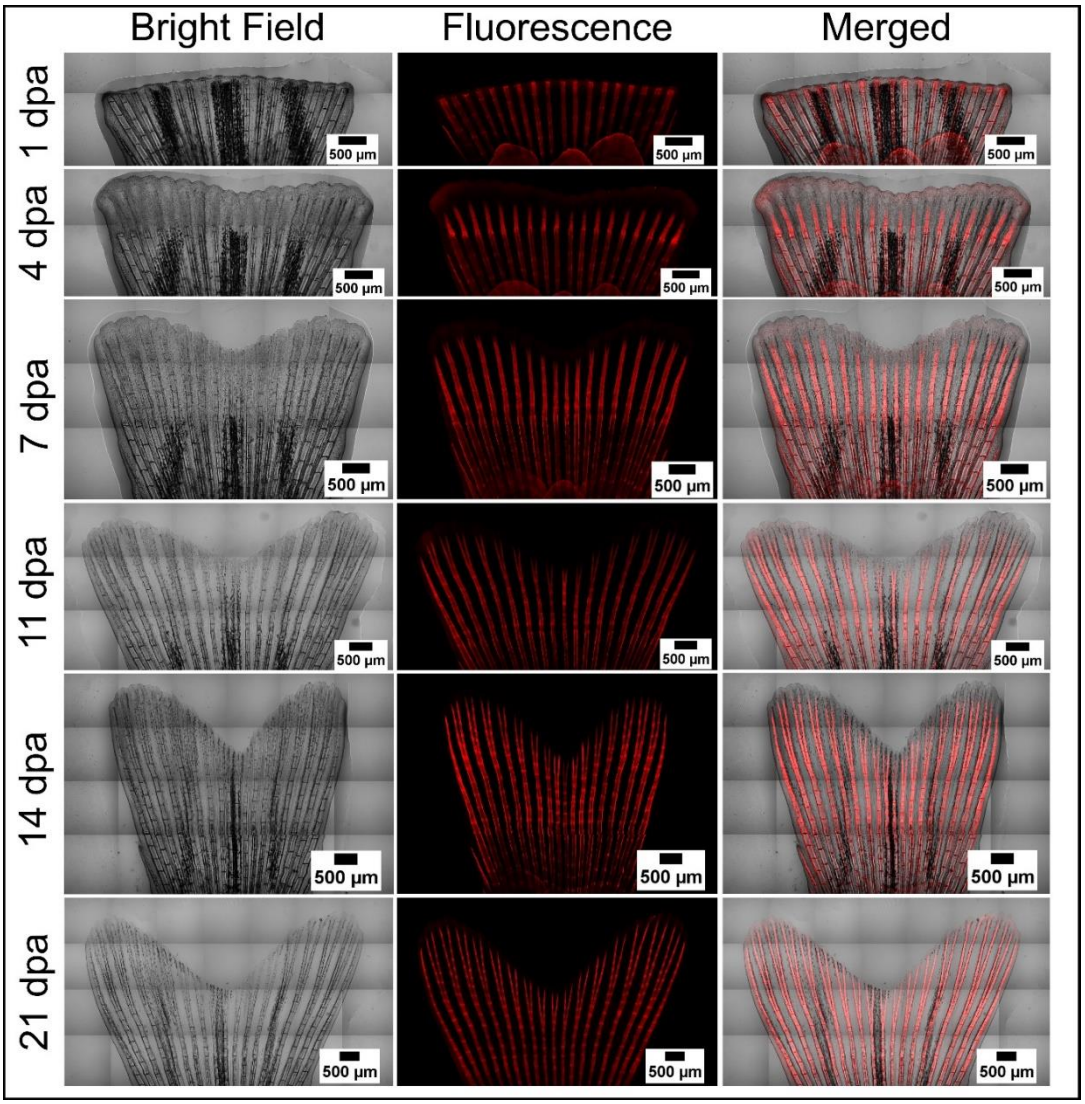

Fig. 36 Bone and tissue regeneration process of zebrafish caudal fin. The bright field column represents the tissue growth; the fluorescence column represents the de novo mineralisation process; the merged column images represent the overall process (tissue + mineral) regeneration. The scale bar sizes are 500 µm.

4.3.2. Ultrastructural and compositional analysis of zebrafish bone

A scheme of the procedures prior SEM imaging are displayed in **Fig. 37A**. The ultrastructural features of crushed bony fin rays are shown in the **Fig. 37B**. Arrangements with well-defined edges and organized in layered structures of minerals, were predominant on the proximal regions of CTRL, $CTRL_{REGEN}$ and ALN_{REGEN}. The average diameter of the structures calculated for CTRL, $CTRL_{REGEN}$ and ALN_{REGEN} were 102.49 (±14.64) nm, 118.63 (± 8.43) nm and 125.60 (± 10.38) nm, respectively. On distal zones, for all groups with the exception of ALN_{REGEN}, it was observed that there was a prevalence of structures with grooves on the surface. On the other hand, for ALN_{REGEN} distal region, structures were organised in coexistent small spherical-like and plate-like shapes. The elemental content of the SEM images was verified by EDS, and the results are shown in **Table 7**. The Ca content of samples in the proximal region varied from 5.77 ± 1.64 (GIOP) to 27.23 ± 3.59 (CTRL) and the P, for the same region, varied from 3.96 ± 0.50 (GIOP) to 15.68 ± 1.42 (CTRL). In all groups but GIOP, a higher percentage of Ca was found in the proximal part of the amputated fin. Similar phenomenon was observed for the Ca/P ratio; statistically significant differences was observed for CTRL, GIOP, $CTRL_{REG}$ and $GIOP_{REGEN}$ when comparing proximal to distal parts ($p < 0.01$). The difference in the distinct parts of ALN_{REGEN}, however, was not significant ($p > 0.01$). The highest significant value was obtained for CTRL (1.74 ± 0.10) and $CTRL_{REGEN}$ (1.56 ± 0.06) in the proximal region ($p < 0.01$).

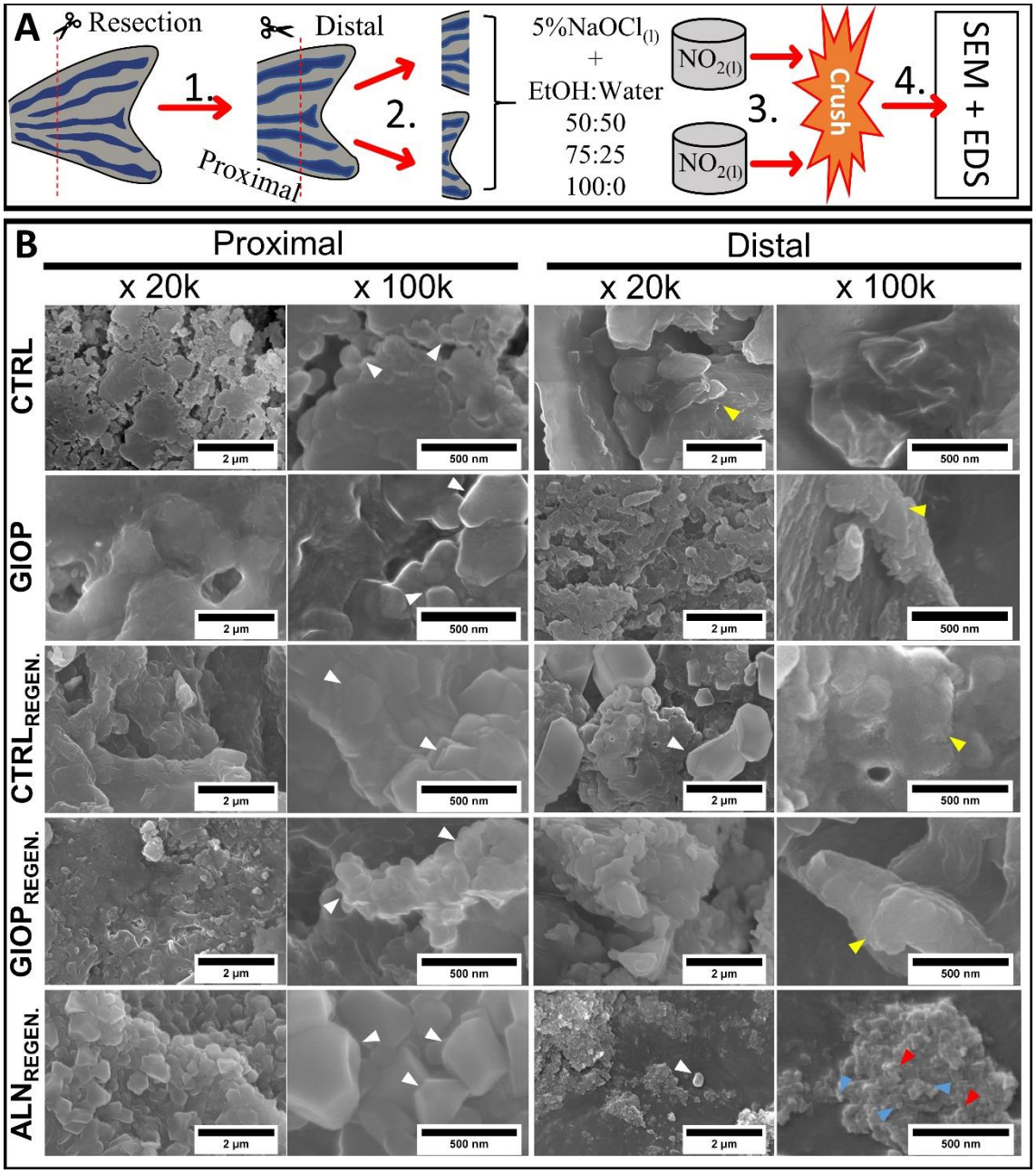

Fig. 37 Scheme and SEM images of proximal and distal crushed bones extracted from zebrafish caudal fins before and after the proposed treatments, in ×20k and ×100k magnifications. (A) Processes performed prior SEM analysis. (B) Proximal crushed parts showed minerals with bigger size and well-defined shapes, which was not commonly found in distal counterparts (white arrowheads), while the distal sites showed minerals resembling amorphous phases (yellow arrowheads). The distal region of ALN_{REGEN} showed grouped small spherical-like (light blue arrowheads) and plate-like morphologies (red arrowheads).

Table 7 EDS results (mean ± SD) for proximal and distal bones of zebrafish caudal fin.

Group	Elements [atomic%]				Ca/P [atomic%]	
	Proximal		Distal		Proximal	Distal
	Ca	P	Ca	P		
CTRL	27.23 ± 3.59	15.68 ± 1.42	7.78 ± 1.22	5.35 ± 0.79	1.74 ± 0.10 ^{Aa}	1.45 ± 0.05 ^{Ab}
GIOP	5.77 ± 1.64	3.96 ± 0.50	6.25 ± 1.19	4.96 ± 0.92	1.46 ± 0.04 ^{Ba}	1.26 ± 0.01 ^{Bb}
CTRL$_{REGEN}$	11.85 ± 0.76	7.60 ± 0.31	8.28 ± 0.40	6.34 ± 0.27	1.56 ± 0.06 ^{ABa}	1.31 ± 0.03 ^{ABb}
GIOP$_{REGEN}$	10.11 ± 2.19	7.39 ± 1.51	5.28 ± 2.26	4.22 ± 1.31	1.37 ± 0.02 ^{Ba}	1.25 ± 0.21 ^{Bb}
ALN$_{REGEN}$	11.57 ± 1.41	7.78 ± 0.83	4.46 ± 0.81	3.24 ± 0.67	1.49 ± 0.03 ^{Ba}	1.38 ± 0.04 ^{ABa}

Capital letters mean significant statistical difference in the same column ($p < 0.01$).
Small letters mean significant difference in the same row ($p < 0.01$).

4.3.3. Calcium-phosphate profile

Raman spectroscopy was used to analyse the intensity of the $\nu_1 PO_4^{3-}$ peak (~960 cm^{-1}) in each of the zebrafish lepidotrichia, from proximal region to the distal tips (**Fig. 38A**). Three phosphate and one carbonate peaks showed to be characteristic of zebrafish appendage bones: $\nu_1 PO_4^{3-}$, $\nu_2 PO_4^{3-}$, $\nu_4 PO_4^{3-}$ and CO_3^{2-}. The area below the $\nu_1 PO_4^{3-}$ peak was calculated for each of the 96 sites measured, and a heatmap from a representative sample was produced (**Fig. 38B**). From proximal (A1) to distal (A5), it is clear that the $\nu_1 PO_4^{3-}$ intensity decreases as the distance from the resection plane increases. However, the decreased gradient of intensity was not observed in all bony rays. Moreover, CRTL$_{REGEN}$ and GIOP$_{REGEN}$ presented lower intensities at the distal parts in comparison to other groups, indicating that the newly formed bones display lower $\nu_1 PO_4^{3-}$ intensities. ALN$_{REGEN}$ presented the highest area below the curve from all samples in their proximal region.

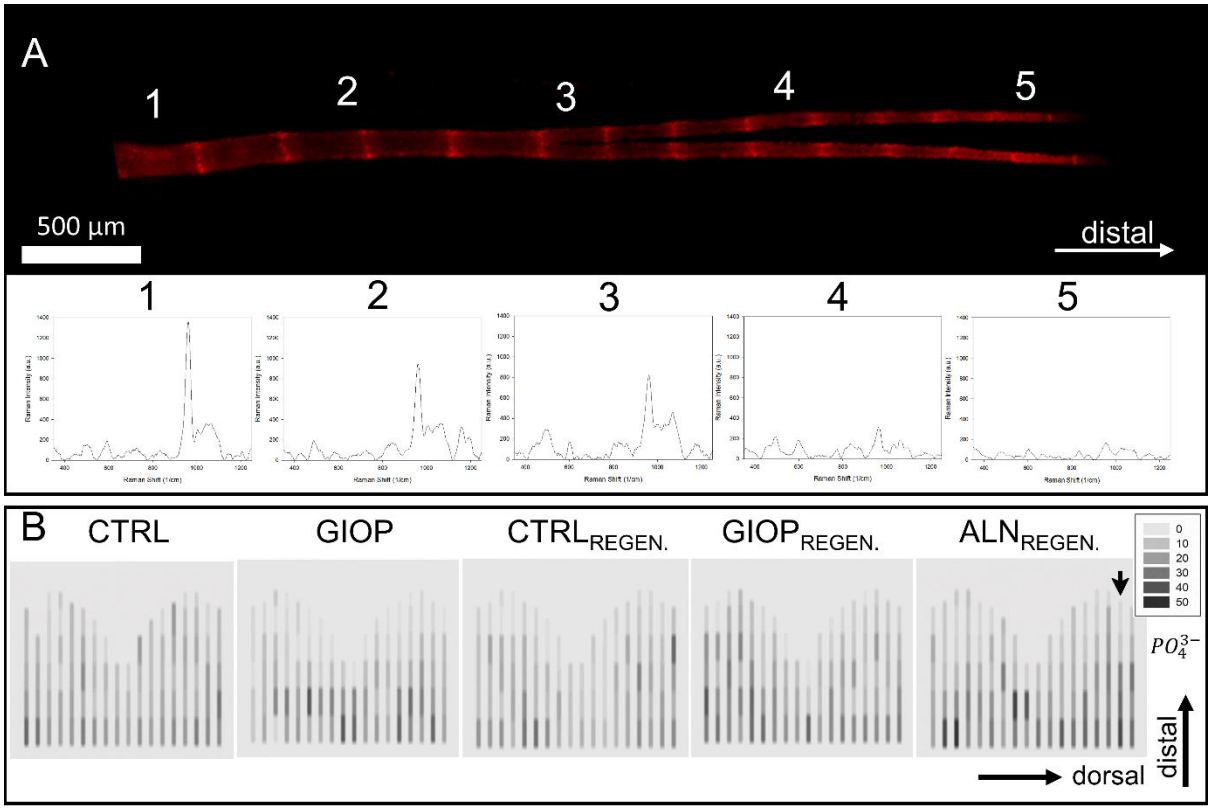

Fig. 38 Montage containing a representative zebrafish caudal fin bony ray and the Raman spectra obtained. (A) Representation of the 17th lepidotrichia (dorsal region of the fin) of the ALN$_{REGEN}$ group isolated from the fluorescence images obtained in confocal microscope; (A1-5) five different spots of interest along the growth direction were measured and the respective Raman peaks were obtained for each region. Heat colour plots representing the total area below the curve for the phosphate peak of ~962 cm^{-1}; the black arrow indicates the bony ray represented in the Raman spectra shifts above (B). The legend box shows the total values of the areas divided by 10^3. The darker the spots, the higher the mineral intensity of the signal.

4.3.4. Surface topography and roughness

The **Fig. 39A** shows the methodology used to obtain the slices from zebrafish fins. The 3D surface profiles recorded for the proximal and distal caudal fin cross-sections are represented in **Fig. 39B**. In general, the proximal regions of all groups have displayed densely-packed structures on their surfaces, with small and abrupt bumps (grooves). On the other hand, at distal locations, the previously mentioned irregular profile, was substituted by comparatively less frequent irregularities. On distal sites collagen fibrils were found emerging on the surface of a less mineralised area (**Fig. 39C**). The collagen fibres were found to exhibit a periodicity range from 57 nm to 94 nm (**Fig. 39D**). From the acquired images, the mean value of surface roughness was then calculated based on the Ra parameter; the results are described in the Supplemental **Fig. 39E**. No statistically significant difference was observed among groups for proximal region ($p > 0.01$). However, the distal region of GIOP group presented significant higher roughness compared both with their proximal part and to all other distal regions evaluated ($p < 0.01$).

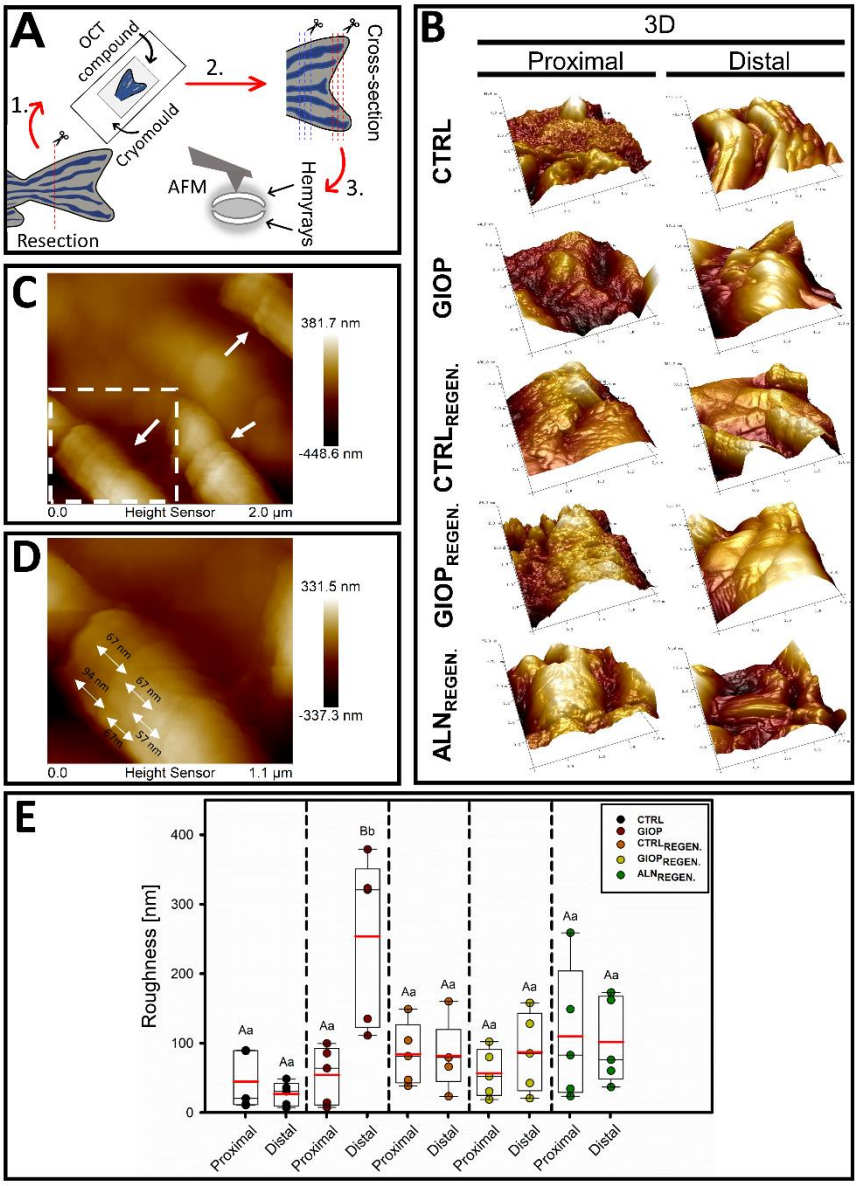

Fig. 39 (A) Procedure steps from resection of the zebrafish caudal fins to the analysis with AFM. (B) 3D representation of the cross-section slices analysed by AFM. (C) The distal part of $CTRL_{REGEN}$ group showing collagen fibres bundles (white single arrows). (D) Region of interest (ROI) of the collagen fibre bundle from the white square in "B"; double arrows show the periodic unit from a fibril (d ~ 75 nm). (E) Box-plots with means (red horizontal line) of the roughness obtained from proximal and distal parts of fins by AFM. Capital letters indicate significant statistically difference between the different regions (proximal and distal) within the same treatment ($p < 0.01$). Lowercase letters indicate significant statistically difference between the same region (proximal or distal) among different treatments ($p < 0.01$).

4.3.5. Mechanical properties

The effects of PN and ALN on zebrafish lepidotrichia were also assessed regarding the mechanical properties. **Fig. 40A** summarizes the procedure of cross-section. The values of the E_r (**Fig. 40B**) and H (**Fig. 40C**) obtained at proximal and distal bones of the fins. By means of E_r values, the proximal part of CTRL, GIOP and ALN_{REGEN} were significantly higher than $CTRL_{REGEN}$ and $GIOP_{REGEN}$ ($p < 0.01$). If the values obtained at the proximal locations are compared within each other, the highest statistically significant value obtained was 8.68 ± 8.74 GPa (ALN_{REGEN}) and the lowest was 4.57 ± 2.62 GPa ($CTRL_{REGEN}$) ($p < 0.01$). By means of H, however, the proximal sites of both CTRL and ALN_{REGEN} (0.29 ± 0.23 GPa and 0.34 ± 0.47 GPa, respectively), were significantly higher than the distal parts (0.06 ± 0.05 GPa and 0.02 ± 0.01 GPa, respectively) ($p < 0.01$). The high standard deviations found (e.g., ALN_{REGEN}) may be related to the impossibility to perform finishing procedures on sectioned samples. Even though, statistically significant values were found. Also, both mechanical testing values were plotted in relation to the mineral ratio (**Fig. 40D-E**). The two (E_r and H), despite showing a weak dependence to Ca/P (R^2 equal to 0.1757 and 0.3262, respectively), showed a positive correlation.

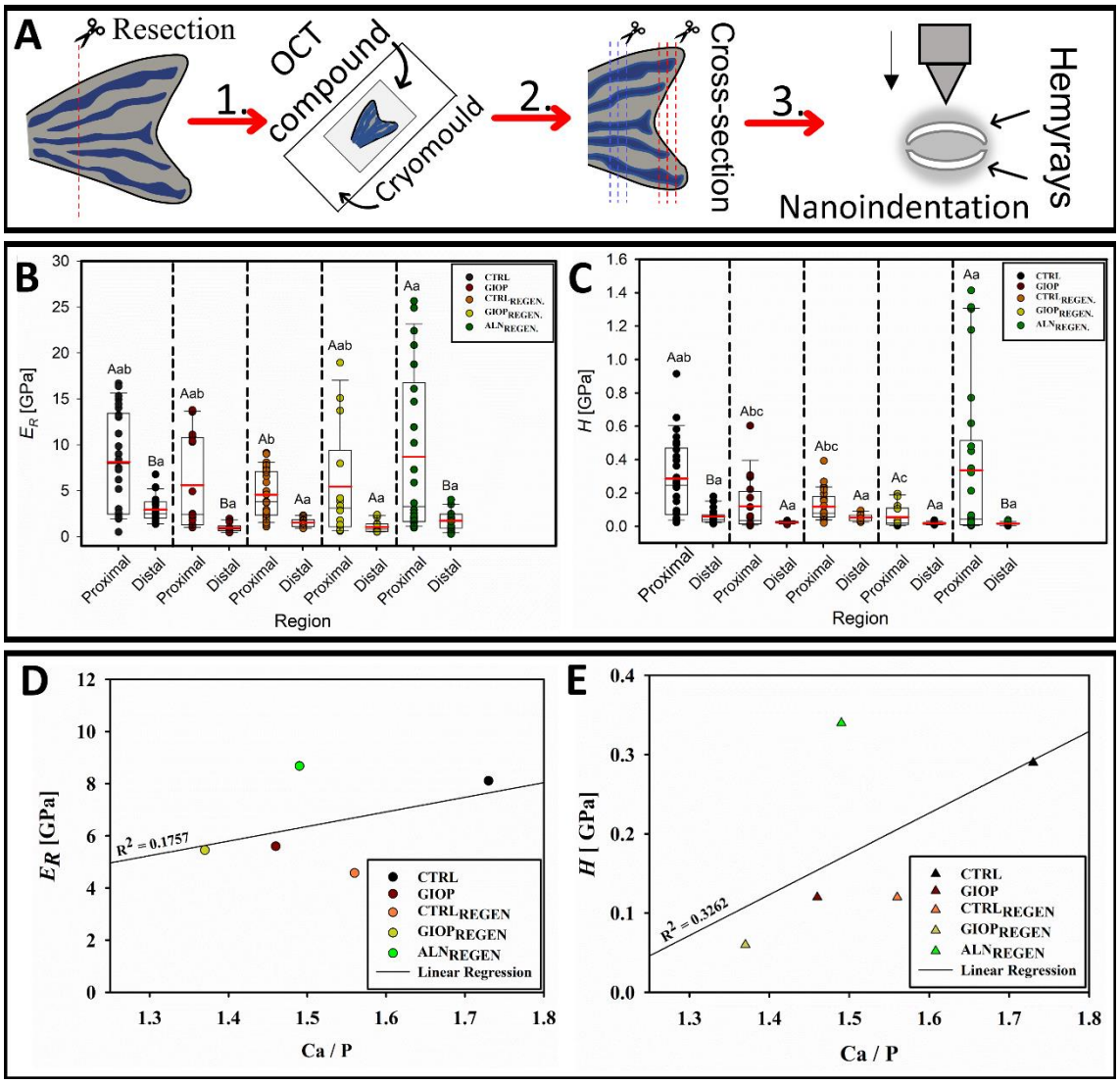

Fig. 40 Mechanical performance of zebrafish lepidotrichia. Procedure steps to obtain the caudal fin's slices for mechanical evaluation (A). Box-plots with means (red horizontal line) and median (black horizontal line) of the E_r (B) and H (C) obtained from proximal and distal parts of fins with a tribo-indenter. The average values of the proximal parts of both E_r and H plotted against the Ca/P ratio (D). The regression lines show a weak but positive correlation between the variables. Capital letters indicate significant statistically difference between the different regions (proximal and distal) within the same treatment ($p < 0.01$). Lowercase letters indicate significant statistically difference between the same region (proximal or distal) among different treatments ($p < 0.01$).

4.4. Discussion

In this work, materials science principles were implemented to assess the properties of healthy, GIOP and ALN treated zebrafish bones at the multi-scale level. The fish were anaesthetized with a cocktail of Tricaine and isoflurane in order to minimize the side effects of the dopant (Collymore *et al.,* 2014; Huang *et al.,* 2010). The fish had their fins resected and were left to regenerate during 21 days in water tanks with or without ALN. A second resection was performed, and the effects of the various treatments were evaluated with a series of structural, elemental and mechanical analysis. In agreement to previous research findings on higher vertebrate animal models, our study verified the reproducibility and reliability of the zebrafish model on the study of mineralised tissues. PN and ALN significantly affected the fin bones properties in comparison to the controls. Our data showed that ALN was able to restore the overall properties of zebrafish caudal fin osteoporotic bones to the levels of untreated fish. Interestingly, the appearance of bone is more affected by the region that the minerals were extracted (proximal or distal) than by the treatment proposed, while the Ca/P ratio showed difference in both situations. This reinforces the benefits of materials science approach to evaluate diseased mineralised structures in a multi-scale level. These findings provide insights in new strategies to evaluate diseased bones, especially on those with GIOP phenotypes and drug action analysis.

The lepidotrichia of zebrafish is considered a powerful model to evaluate the various aspects of bone remodelling. The caudal fin is divided into proximal and distal regions, being the proximal part closer to the fish body (Bird and Mabee, 2003). The proximal part is more mineralised than the distal part, which has a lower mineral-to-collagen ratio, to allow higher mobility when swimming (Bird and Mabee, 2003; Cardeira *et al.,* 2016). Their ability to re-mineralise after resection is widely known (Cardeira *et al.,* 2016; Pfefferli and Jaźwińska,

2015). We have thus used resection/regeneration protocols to exacerbate the drug effect before collecting the samples for analysis. By using the GIOP protocol proposed in this work, the fluorescence intensity of caudal fin bones displayed a ~15% reduction within two weeks, which configures the development of GIOP-like phenotype. In rodents, however, the development of OP may need increased time, depending on the bone analysed (Yousefzadeh *et al.,* 2020). Hence, our evaluation protocol was rapid and sensitive enough to obtain significant results. Our data reconfirm the reliability of adult zebrafish caudal fin to be used as a dependable model to verify GIOP (Lin *et al.,* 2019).

Cardeira *et al.,* (2016) suggested analysing the caudal fin *de novo* mineralisation by calculating RMA, RAY, REG and STU of many zebrafish during caudal fin regeneration. Here, the drugs' after-effects in the lepidotrichia could be clearly observed with the methodology proposed. The scatter behaviour plotted for each treatment was strongly related to the type of medicine given to the fish. The group with no intervention during the regenerative process, had the values calculated distributed above and below the linear regression line. This may represent the natural variation of each fish when no external elements interfere in the regenerative process. Any deviation from the regression line, should indicate effects of stimulation (points above) or halt (points below) of the mineral deposition (Cardeira *et al.,* 2016). Corroborating with studies that demonstrate PN as an anti-mineralogenic compound (Barrett *et al.,* 2006; Bergen *et al.,* 2019; De Vrieze *et al.,* 2014; He *et al.,* 2018), we found lower values for the group that received no further intervention after developing osteoporotic-like phenotype (values below regression line). In contrast, most of values for fish that received the pro-mineralogenic compound (ALN), were shown above the same line (over-mineralisation). Our after-effect plots suggest that this methodology may be useful for the testing different anti- and pro-mineralogenic compounds, and reconfirm PN and ALN to decrease and increase, respectively, the mineral deposition within zebrafish bones. The *in vivo* approach of time-lapsed analysis on the same subject, may

have also contributed to enhance the evidence strength of our results. Considering the potential of zebrafish models, we have reconfirmed zebrafish as a suitable organism for the evaluation of bone mineralisation, which could enable reduced use of rodents in future research (Bruneel and Witten, 2015).

The *de novo* mineralisation of zebrafish caudal fins involves a series of complex events (Azevedo *et al.,* 2011; Pfefferli and Jaźwińska, 2015; Uemoto *et al.,* 2020). From the initial bone formation to the development of the actinotrichia, the mineralised tissue is known to be composed of different structures, depending on the availability of Ca and P resources (Mahamid *et al.,* 2008). The intake of mineralogenic compounds could then affect the zebrafish bones at a multi-scale level (Russell *et al.,* 2008). We have analysed the appearance and mineral content of two distinct regions of the bony-rays affected by PN or ALN, before and after the regrowth. The mineralised structures found in the proximal region are clearly different from the distal minerals; they presented well-defined edges and contours. Similar morphologies were almost inexistent in the bones obtained from distal sites. The underlying mineralisation process in the zebrafish caudal fins occurs from the proximal to the distal region by the addition of newly-formed minerals at the furthermost edge of each fin (Mahamid *et al.,* 2008). The administration of medicines did not seem to have visibly affected the appearance of the minerals observed at the proximal regions. Interestingly, the fish that received ALN displayed coexistent small rounded and plate-like shapes in the distal sites; similar structures could not be observed in high magnification SEM images in other treatment conditions. Coexisting round and plate-like minerals were found in amorphous forms of calcium-phosphates (Mahamid *et al.,* 2010, 2008), which are related to the first stages of mineralisation (Mahamid *et al.,* 2011). The mineralisation course of events starts with the saturation of an amorphous calcium phosphate (ACP) phase, followed by the mineral deposition within the collagen fibres and subsequent crystal growth (Ge *et al.,* 2006; Mahamid *et al.,* 2010). Moreover, the natural

layered structures of bone were preserved (Chang *et al.,* 2018). Similar structures have been reported in previous studies (Mahamid *et al.,* 2008). Hence, our results suggest that the treatment with bisphosphonate do not reconfigure the natural morphology of bones during the 21 days of zebrafish appendage regeneration but may have accelerated the transition between mineral development stages.

The mineral balance and bone remodelling potentials are intimately related to the Ca and P content in the site (Chang *et al.,* 2018). In the conditions proposed in this work, a broad range of Ca, P and mineral ratios were found in the fin's bones. This finding corroborates with the concepts that several types of minerals coexist in zebrafish caudal fin bones (Mahamid *et al.,* 2010, 2008). The Ca/P proportion was found to significantly decrease in proximal-distal direction. This behaviour was observed for all but ALN_{REGEN} group. Higher mineral ratios, reason with the less pronounced effects of mineralogenic compounds in the proximal regions. On the other hand, lower mineral availability, represented by decreased Ca/P ratios, could be more influenced by both PN and ALN (de Vrieze *et al.,* 2012). This is shown by the significant lower mineral ratios found in the bones of fish after the intake of PN and the narrow difference between the proximal and distal parts of bones affected by ALN. Our multi-scale analysis suggests that ALN increase the mineral ratio of ACP in vulnerable areas first. In the same manner, PN may affect the distal areas first, which enhances the vulnerability and may favour the binding of ALN to the bone (Geurtzen *et al.,* 2017).

To completely understand the effects of medicines and diseases in mineralised tissues, the evaluation of characteristics in molecular level is essential (Hassler *et al.,* 2015; Toledano *et al.,* 2018). The intensity of the peaks observed in Raman analysis was strongly related to the vibration of the molecules excited while the test was performed (Bennet *et al.,* 2014; Morris and Mandair, 2011; Toledano *et al.,* 2018). Overall, the proximal regions displayed increased

areas below the ~960 cm^{-1} peak. Our compositional analysis of Ca/P ratio has shown a vast range of mineral ratios depending on the treatment and the mineral profile suggests a similar outcome. However, any difficulties related to the use of bulk characterisation methods (e.g., Raman Spectroscopy) in mineralised tissues with strongly mixed crystalline and amorphous phases should not be ignored and may also explain the results obtained (Mahamid *et al.*, 2008).

Osteoporotic-like bones are characterised by the mineral resorption caused by increased OCs activity that often reconfigure the microarchitecture of bones (Chavassieux *et al.*, 2019; Kim *et al.*, 2018; Rolvien *et al.*, 2020). Following the overall trend in this research, the proximal areas verified by AFM revealed a different appearance from those obtained from distal sites. The frequent and low amplitude peaks images found in the bones extracted from the proximal regions are characteristic from highly mineralised tissues (Dorozhkin, 2012; Ge *et al.*, 2006). As we analysed spots distant to the resection plane, a less mineralised characteristic was observed, and collagen fibres were exposed ($CTRL_{REGEN}$). The collagen fibres were presented with variable periodicity. The type I collagen commonly found in zebrafish bones is well known to have periodicity of 67 nm (Wang *et al.*, 2012). Lower periodicity lengths are related to the initial stages of minerals in zebrafish, and, in favourable conditions, the periodicity increases its length (Ge *et al.*, 2006). This reconfirm that the zebrafish bones are composed by distinct phases and development stages of Ca and P (Mahamid *et al.*, 2010, 2008).

The osteoporotic phenotype is related to poor mechanical properties due to its mineral deficiency and higher porosity in comparison to sound bones (Bernhard *et al.*, 2013; Loundagin *et al.*, 2020). The mechanical attributes of zebrafish bones should be intimately related to the microstructure and to the composition of the mineralised tissue (Chang *et al.*, 2018; Ge *et al.*, 2006; Wang *et al.*, 2012). The highly mineralised structures found in the proximal bones showed, in general, increased E_r and H. At the distal regions, where the ratio of non-mineralised

tissues raises, the surfaces were found to be softer, but not significantly lower for all the conditions proposed. In proximal bones, the reduction in *H* caused by the administration of PN was countered by the intake of ALN. The efficacy of bisphosphonates is strongly related to their affinity to bind to the bones and ability to suppress the Farnesyl pyrophosphate synthase, essential to the natural pathways of OCs (Russell *et al.,* 2008). The regulation of the balance between ossification and bone resorption led to increased mineral levels, as we demonstrated with EDS. The pro-mineralogenic compound was not only able to recover the E_r and *H* to the original values of healthy bones, but it also showed adequate increase, not significantly surpassing the natural value of non-treated individuals (Hassler *et al.,* 2015). In order to verify the relationship between the mechanical analysis and composition of bone, we have calculated the Pearson's correlation value. The E_r and *H* have showed a low, but positive, interaction with the Ca/P ratios of the proximal regions affected by the medicine. This outcome reaffirms the feasibility of a multi-scale approach to study sound and diseased bones, affected or not, by mineralogenic compounds.

This study fills a gap on the topic of diseased mineralised tissues using a time-lapsed approach of following the same individual throughout the experimentation. To the best of our knowledge, this is the first study to use a series of materials science approaches and correlate with zebrafish bones under the effect of PN and reconfirm ALN was able to rescue the osteoporotic phenotype of the fish, which was achieved by the restoration of the E_r and *H* to the normal range. However, although zebrafish is considered a powerful model to study bone-related disease and mineralisation, there are some limitations in their use that were already summarised (Chang *et al.,* 2018; Geurtzen *et al.,* 2017, 2014): (1) The bone remodelling process differs from the mammals especially due to the presence of mono- and multinucleated OCs; (2) The nature of the lepidotrichia is dermal ossification, which also mechanistically differs them from the mammals; (3) Despite a complete mapping of properties alongside the caudal fin bony-rays

were performed and comparisons between different single pieces of bones could be done, the variability in different individuals was not tested (e.g. Raman mapping); (4) Moreover, zebrafish bones are under the effect of a different loading environment than non-aquatic mammals. Thus, the results here proposed should be taken carefully. Despite that, the mechanical evaluation, in the conditions proposed, showed to be precise enough to assess zebrafish bones with different mineral levels. Our research could help to develop new strategies to evaluate overall quality of diseased mineralised tissues, especially on those with osteoporotic phenotypes and drug action analysis.

4.5. Conclusions

Zebrafish lepidotrichia were shown to be a feasible and fast model to study the elemental, structural and mechanical characteristics of bones affected by anti- and pro-mineralogenic medicines. The administration of PN during the time proposed reduced in about 15% the fluorescence intensity of the zebrafish caudal fin bones. The anti-mineralogenic medicine also showed to reduce the Ca/P of the distal bones to 1.26, while ALN was able to partially recover it to the untreated levels (Ca/P = 1.38) and increase the mineral organisation. The mechanical behaviour of the bones was also restored to the initial range by the pro-mineralogenic compound. The presented approach may be used to assess different compounds and have the potential to be used in newly developed drugs related to bone remodelling. Further research should be done regarding the long-termed intake of medicines or their dose dependence on the properties of bones.

References

Azevedo AS, Grotek B, Jacinto A, Weidinger G, Saúde L. 2011. The Regenerative Capacity of the Zebrafish Caudal Fin Is Not Affected by Repeated Amputations. Karl MO, editor. PLoS ONE. 28;6(7).

Barrett R, Chappell C, Quick M, Fleming A. 2006. A rapid, high content, in vivo model of glucocorticoid-induced osteoporosis. Biotechnol. J. 1(6):651–5.

Bennet M, Akiva A, Faivre D, Malkinson G, Yaniv K, Abdelilah-Seyfried S, Fratzl P, Masic A. 2014. Simultaneous Raman Microspectroscopy and Fluorescence Imaging of Bone Mineralization in Living Zebrafish Larvae. Biophys. J.;106(4):L17–9.

Bensimon-Brito A, Cardeira J, Dionísio G, Huysseune A, Cancela ML, Witten PE. 2016. Revisiting in vivo staining with alizarin red S - a valuable approach to analyse zebrafish skeletal mineralization during development and regeneration. BMC Dev. Biol. 16(1).

Bergen DJM, Kague E, Hammond CL. 2019. Zebrafish as an Emerging Model for Osteoporosis: A Primary Testing Platform for Screening New Osteo-Active Compounds. Front. Endocrinol. 29;10.

Bernhard A, Milovanovic P, Zimmermann EA, Hahn M, Djonic D, Krause M, Breer S, Püschel K, Djuric M, Amling M, Busse B. 2013. Micro-morphological properties of osteons reveal changes in cortical bone stability during aging, osteoporosis, and bisphosphonate treatment in women. Osteoporos. Int. 24(10):2671–80.

Bruneel B, Witten PE. 2015. Power and challenges of using zebrafish as a model for skeletal tissue imaging. Connect. Tissue Res. 56(2):161–73.

Cardeira J, Gavaia PJ, Fernández I, Cengiz IF, Moreira-Silva J, Oliveira JM, Reis RL, Cancela ML, Laizé V. 2016. Quantitative assessment of the regenerative and mineralogenic performances of the zebrafish caudal fin. Sci. Rep.;6(1).

Chang Z, Chen P-Y, Chuang Y-J, Akhtar R. 2018. Zebrafish as a model to study bone maturation: Nanoscale structural and mechanical characterization of age-related changes in the zebrafish vertebral column. J. Mech. Behav. Biomed. Mater. 84:54–63.

Chavassieux P, Chapurlat R, Portero‐Muzy N, Roux J, Garcia P, Brown JP, Libanati C, Boyce RW, Wang A, Grauer A. 2019. Bone ‐ Forming and Antiresorptive Effects of Romosozumab in Postmenopausal Women with Osteoporosis: Bone Histomorphometry and Microcomputed Tomography Analysis After 2 and 12 Months of Treatment. J. Bone Miner. Res. 34(9):1597–608.

Chazotte B. 2012. Labelling Golgi with Fluorescent Ceramides. Cold Spring Harb. Protoc. 2012(8).

Cheng T-T, Lai H-M, Yu S-F, Chiu W-C, Hsu C-Y, Chen J-F, Chen Y-C. 2018. The impact of low-dose glucocorticoids on disease activity, bone mineral density, fragility fractures, and 10-year probability of fractures in patients with rheumatoid arthritis. J. Investig. Med. 66(6):1004–7.

Dorozhkin SV, Epple M. 2002. Biological and Medical Significance of Calcium Phosphates. Angew. Chem. Int. Ed. 41(17):3130–46.

Dreinhöfer KE, Mitchell PJ, Bégué T, Cooper C, Costa ML, Falaschi P, Hertz K, Marsh D, Maggi S, Nana A, Palm H, Speerin R, Magaziner J. 2018. A global call to action to improve the care of people with fragility fractures. Injury. 49(8):1393–7.

Embry MR, Belanger SE, Braunbeck TA, Galay-Burgos M, Halder M, Hinton DE, Léonard MA, Lillicrap A, Norberg-King T, Whale G. 2010. The fish embryo toxicity test as an animal alternative method in hazard and risk assessment and scientific research. Aquat. Toxicol. 97(2):79–87.

Fischer-Cripps AC. 2000. A review of analysis methods for sub-micron indentation testing. Vacuum.58(4):569–85.

Ge J, Wang X, Cui F. 2006. Microstructural characteristics and nanomechanical properties across the thickness of the wild-type zebrafish skeletal bone. Mater. Sci. Eng. C. 26(4):710–5.

Geurtzen K, Knopf F, Wehner D, Huitema LFA, Schulte-Merker S, Weidinger G. 2014. Mature osteoblasts dedifferentiate in response to traumatic bone injury in the zebrafish fin and skull. Development. 1;141(11):2225–34.

Geurtzen K, Knopf F. 2018. Adult Zebrafish Injury Models to Study the Effects of Prednisolone in Regenerating Bone Tissue. J. Vis. Exp. 18;(140).

Geurtzen K, Vernet A, Freidin A, Rauner M, Hofbauer LC, Schneider JE, Brand M, Knopf F. 2017. Immune Suppressive and Bone Inhibitory Effects of Prednisolone in Growing and Regenerating Zebrafish Tissues. J. Bone Miner. Res. 32(12):2476–88.

Hassler N, Gamsjaeger S, Hofstetter B, Brozek W, Klaushofer K, Paschalis EP. 2015. Effects of long-term alendronate treatment on postmenopausal osteoporosis bone material properties. Osteoporos. Int. 26(1):339–52.

He H, Wang C, Tang Q, Yang F, Xu Y. 2018. Possible mechanisms of prednisolone-induced osteoporosis in zebrafish larva. Biomed. Pharmacother. 101:981–7.

Huang W-C, Hsieh Y-S, Chen I-H, Wang C-H, Chang H-W, Yang C-C, Ku T-H, Yeh S-R, Chuang Y-J. 2010. Combined Use of MS-222 (Tricaine) and Isoflurane Extends Anesthesia Time and Minimizes Cardiac Rhythm Side Effects in Adult Zebrafish. Zebrafish. 7(3):297–304.

Iba K, Takada J, Sonoda T, Yamashita T. 2020. Effect of continuous long-term treatment for 10 years with bisphosphonate on Japanese osteoporosis patients. J. Bone Miner. Metab. 38(2):240–7.

Kim G-J, Yoo HS, Lee KJ, Choi JW, Hee An J. 2018. Image of the Micro-Computed Tomography and Atomic-Force Microscopy of Bone in Osteoporosis Animal Model. J. Nanosci. Nanotechnol. 18(10):6726–31.

Knopf F, Hammond C, Chekuru A, Kurth T, Hans S, Weber CW, Mahatma G, Fisher S, Brand M, Schulte-Merker S, Weidinger G. 2011. Bone Regenerates via Dedifferentiation of Osteoblasts in the Zebrafish Fin. Dev. Cell. 20(5):713–24.

Lin Y, Xiang X, Chen T, Gao C, Fu H, Wang L, Deng L, Zeng L, Zhang J. 2019. In vivo monitoring and high-resolution characterizing of the prednisolone-induced osteoporotic process on adult zebrafish by optical coherence tomography. Biomed. Opt. Express. 10(3):1184.

Loundagin LL, Haider IT, Cooper DML, Edwards WB. 2020. Association between intracortical microarchitecture and the compressive fatigue life of human bone: A pilot study. Bone Rep. 12:100254.

Ma X, Xu Z, Ding S, Yi G, Wang Q. 2017. Alendronate promotes osteoblast differentiation and bone formation in ovariectomy-induced osteoporosis through interferon-β/signal transducer and activator of transcription 1 pathway. Exp. Ther. Med. 27.

Mahamid J, Addadi L, Weiner S. 2011. Crystallization Pathways in Bone. Cells Tissues Organs.;194(2–4):92–7.

Mahamid J, Aichmayer B, Shimoni E, Ziblat R, Li C, Siegel S, Paris O, Fratzl P, Weiner S, Addadi L. 2010. Mapping amorphous calcium phosphate transformation into crystalline mineral from the cell to the bone in zebrafish fin rays. Proc. Natl. Acad. Sci. 107(14):6316–21.

Mahamid J, Sharir A, Addadi L, Weiner S. 2008. Amorphous calcium phosphate is a major component of the forming fin bones of zebrafish: Indications for an amorphous precursor phase. Proc. Natl. Acad. Sci. 105(35):12748–53.

Morris MD, Mandair GS. 2011. Raman Assessment of Bone Quality. Clin. Orthop. Relat. Res. 469(8):2160–9.

Odén A, McCloskey EV, Kanis JA, Harvey NC, Johansson H. 2015. Burden of high fracture probability worldwide: secular increases 2010–2040. Osteoporos. Int. 26(9):2243–8.

Pasqualetti S, Congiu T, Banfi G, Mariotti M. 2015. Alendronate rescued osteoporotic phenotype in a model of glucocorticoid-induced osteoporosis in adult zebrafish scale. Int. J. Exp. Pathol. 96(1):11–20.

Pfefferli C, Jaźwińska A. 2015. The art of fin regeneration in zebrafish: The Art of Fin Regeneration. Regeneration. 2(2):72–83.

Rachner TD, Khosla S, Hofbauer LC. 2011. Osteoporosis: now and the future. The Lancet. 377(9773):1276–87.

Rolvien T, Milovanovic P, Schmidt FN, Kroge S, Wölfel EM, Krause M, Wulff B, Püschel K, Ritchie RO, Amling M, Busse B. 2020. Long-Term Immobilization in Elderly Females Causes a Specific Pattern of Cortical Bone and Osteocyte Deterioration Different from Postmenopausal Osteoporosis. J. Bone Miner. Res.

Russell RGG. 2007. Bisphosphonates: Mode of Action and Pharmacology. Pediatrics. Mar;119(Supplement 2):S150–62.

Schönbörner AA, Boivin G, Baud CA. 1979. The mineralization processes in Teleost fish scales. Cell Tissue Res. 202(2).

Toledano M, Toledano-Osorio M, Guerado E, Caso E, Aguilera FS, Osorio R. 2018. Biochemical assessment of nanostructures in human trabecular bone: Proposal of a Raman micro spectroscopy-based measurements protocol. Injury. 49:S11–21.

Uemoto T, Abe G, Tamura K. 2020. Regrowth of zebrafish caudal fin regeneration is determined by the amputated length. Sci. Rep. 10(1).

Wang L, Liu B, Li H, Yang W, Ding Y, Sinogeikin SV, Meng Y, Liu Z, Zeng XC, Mao WL. 2012. Long-Range Ordered Carbon Clusters: A Crystalline Material with Amorphous Building Blocks. Science. 337(6096):825–8.

Westerfield M. 1995. The Zebrafish Book. A Guide for the Laboratory Use of Zebrafish (Danio rerio). 3rd ed. Eugene, OR: University of Oregon Press.

Yousefzadeh N, Kashfi K, Jeddi S, Ghasemi A. 2020. Ovariectomized rat model of osteoporosis: a practical guide. EXCLI J.;19:89–107.

5. Chapter 5: Nanoindentation as an alternative method to assess diseased bones in zebrafish

---

The second study in this thesis is currently submitted to The Journal of the Mechanical Behaviour of Biological Materials with the title "**Alendronate Improves Osteoporotic Vertebral Bone Quality in Zebrafish Model**;" the text was adapted for the purpose of this thesis.

A brief introduction will be given on zebrafish caudal fin (section 5.2) and then the reasoning for targeting zebra fish caudal fin as the first model in this thesis (section 5.2.1). This chapter follow with the results (section 5.3), discussion on the findings (section 5.4) and limitations (5.5), and conclusions (section 5.6).

Contribution of authors

FRB, Y-JC, RA and P-YC designed the study and draft the manuscript. FRB was responsible for data acquisition and made figures/tables and data analysis. Y-JC, RA, and P-YC were responsible for critical comments. P-YC and RA supervised the research.

5.1. Abstract

Glucocorticoid-induced osteoporosis changes the microarchitecture of bones, increasing bone susceptibility to fragile fractures. Zebrafish vertebrae have been used as an alternative model for GIOP, but assessing structural and mechanical alterations caused by medications remains a challenge in this model. Thus, this study aimed to evaluate the after-effects of PN and ALN on the microarchitecture, morphology, and mechanical attributes of zebrafish vertebrae. Adult 7-month-old zebrafish were distributed into four groups: CTRL, PN, ALN, and PN + ALN. After the treatments were completed, fish vertebrae were analysed with μ-CT, SEM and NI. Fish that received ALN showed pathological mineralisation within their vertebrae segments. BMD decreased in PN and ALN compared to CTRL; however, PN + ALN recovered the values to healthy levels. The *E* of fish that received ALN and PN + ALN were significantly higher than CTRL. ALN increased the hardness of zebrafish's vertebrae to the highest value among the treatments. Conversely, PN + ALN showed unaltered values compared to CTRL, but significantly higher than the PN group. This study concludes that if ALN is administered after GIOP development, it has potential to rescue GIOP by recovering BMD, Z-Scores and bone nanohardness in zebrafish vertebrae model.

5.2. Introduction

5.2.1. Potential of zebrafish vertebrae to model bone diseases

Zebrafish (*danio rerio*) are small teleost fish with strong genetic similarities to humans and relative rapid bone maturation (Lin *et al.,* 2022). Zebrafish are considered a powerful model to diverse diseases, including GIOP (Lin *et al.,* 2022, 2019). The endochondral nature of their vertebrae may favour its use over zebrafish's fin in bone disease models (Weigele and Franz-Odendaal, 2016). The most common method to assess the interaction between zebrafish skeleton and mineralogenic medication is by staining their skeleton and observing its features with fluorescence microscopes (Rosa *et al.,* 2021). AR-S staining studies in zebrafish have shown reduced mineralisation of the vertebrae caused by PN (Barrett *et al.,* 2006; Lin *et al.,* 2019), indicating that their backbone is susceptible to GIOP. More robust techniques, such as μ-CT, have been proposed to investigate BMD in zebrafish using phantoms of HAp (Charles *et al.,* 2017; Geurtzen *et al.,* 2017). To date, mechanical studies involving zebrafish vertebrae were used to assess bone maturation (Chang *et al.,* 2018) and genetic mutations (Zhang *et al.,* 2002), but not medicine-vertebrae interaction.

Bone fragility is known to be a major issue in GIOP. Despite the advances in our understanding of GIOP model and its treatments, we still lack information on the correlation between the BMD and the biomechanical behaviour of zebrafish affected by the disease (Axelsson *et al.,* 2017). Hence, this study aimed to further clarify the interaction between anti- and pro-mineralogenic compounds, administered alone or in sequence, and zebrafish backbone. We approached the subject by assessing the BMD, and other morphometric parameters, with μ-CT, as well as the biomechanical values (with NI) of zebrafish vertebrae after the onset of GIOP and the treatment with ALN. In this work it was evaluated fish in four different conditions:

A. Fish only in fish-tank water (no addition of medication; CTRL).
B. Fish that received PN, simulating GIOP condition (PN).
C. Fish that received ALN, simulating a situation of treatment of "healthy" fish (ALN).
D. Fish that received first PN and then were treated with ALN (PN + ALN).

5.3. Results

5.3.1. Bone morphometry and mineral density

Three fish of each group were randomly selected and scanned with µ-CT. Their skeletal characteristics are shown in **Fig. 41**. When set to the same pixel range, PN and ALN had lower intensity signals if compared to CTRL (**Fig. 41a**). Lower signals obtained with µ-CT are related to GIOP. On the contrary, we observed higher pixel intensities within the vertebrae of PN + ALN group. The length of CV1 and CV2 vertebrae were normalized with their respective radius; this minimized the effects of comparing different individuals. The results were plotted in the **Fig. 41b**. Significant decreased length/radius ratio was found in PN + ALN group in comparison to the CTRL ($p < 0.05$), which demonstrates an alteration in the proportion of the vertebrae. Bone details inside the vertebral cavity can be seen with sagittal and axial cuts (**Fig. 41c**). Pathological mineralisation sites were found within the vertebra segments of ALN and PN + ALN fish; CTRL and PN groups did not displayed any sign of pathological ossification. The calcifications were found connecting two different vertebrae bones (e.g., PC5 to PC6 and PC6 to PC7 in ALN group) and had either a hollow or a filled core. Moreover, they have at least one point of connection to the vertebral body. The internal ossifications found in PN + ALN group had higher pixel intensity than ALN alone (**Fig. 41d**).

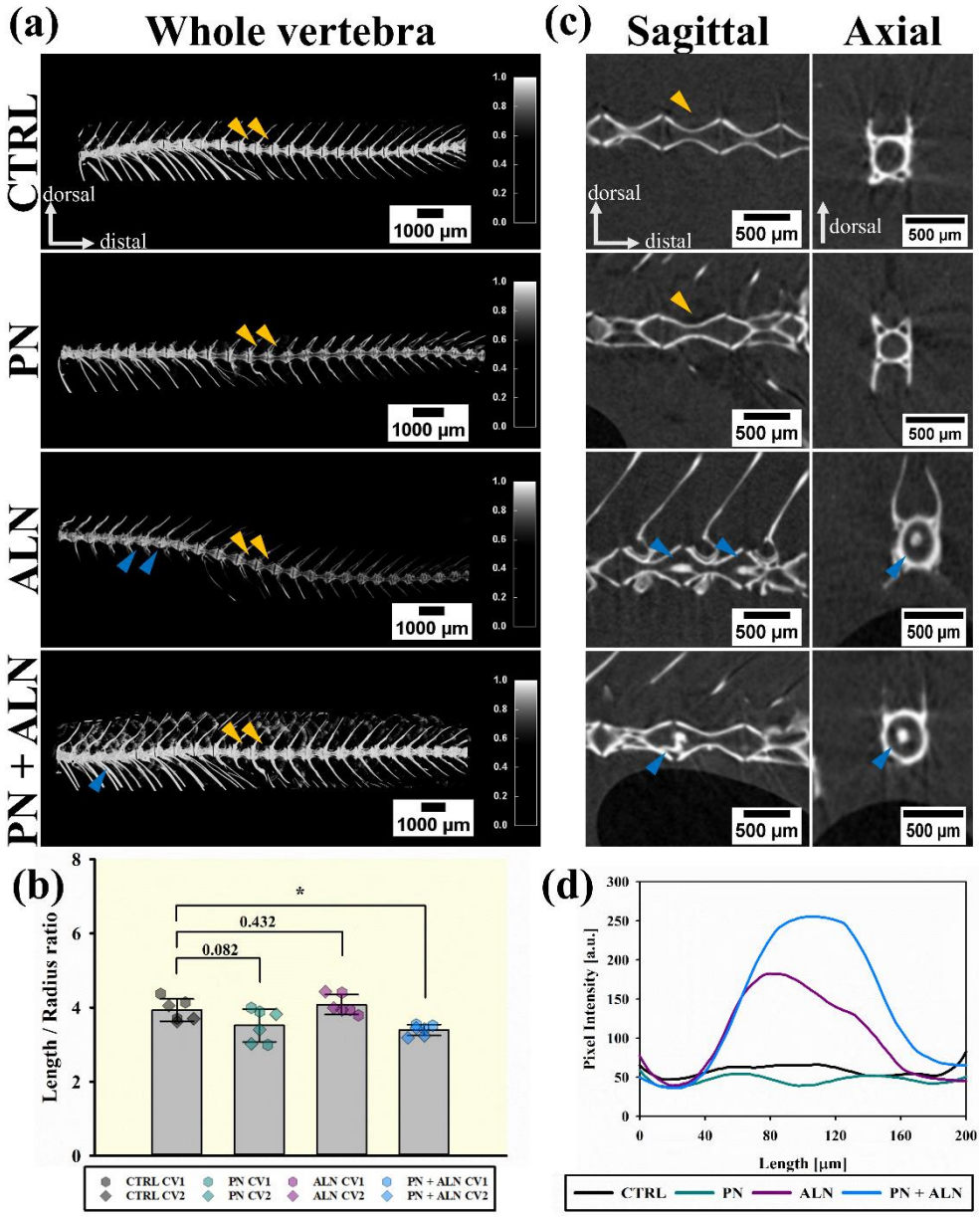

Fig. 41 Montage with the various features of zebrafish skeleton obtained with µ-CT scan. (a) Isolated whole vertebrae of CTRL, PN, ALN and PN + ALN representative samples; (b) Ratio between the length and radius; (c) Sagittal and axial views showing pathological mineralisation in the centra of ALN and PN + ALN groups; (d) pixel intensity measured from side-to-side of the axial surface of single vertebra. High pixel intensities show the pathological mineral signals found in ALN and PN + ALN groups. The blue arrowheads show the position in which the abnormal minerals were found. The yellow arrowheads show the CV1 and CV2 vertebrae; they were used for the purposes of calculations in this research. Significance: * < 0.05, ** < 0.01 and * < 0.001.***

The various volumetric and surface measurements performed with the reconstruction software are displayed in the **Fig. 42a-c**. The BV was assessed; PN + ALN group have shown significantly higher values in comparison to CTRL ($p < 0.001$); conversely, TV values showed a low range variation from $2.77 \times 10^{-6} \pm 8.59 \times 10^{-7}$ cm^3 (ALN) to $3.11 \times 10^{-6} \pm 7.48 \times 10^{-7}$ cm^3 (PN + ALN), with no significant effect of the medicines ($p > 0.05$). The B.Th of PN and PN + ALN groups showed increased values than CTRL group ($p < 0.05$ and $p < 0.01$, in this order). BV was then divided by the TV (**Fig. 42d**). BV / TV is an important parameter for bone diseases diagnosis, however, has shown no significant difference among the groups ($p > 0.05$). BMD measurements are shown in the **Fig. 42e**. Differently from BV / TV, the BMD of PN and ALN displayed lower values than CTRL ($p < 0.001$); this not simply reaffirm the potential of PN in decreasing the BMD in zebrafish vertebrae, but also showed that ALN, if administered alone, may decrease the BMD. PN + ALN displayed similar range of BMD values to CTRL ($p > 0.05$). The Z-Scores are represented in the **Fig. 42f**; corroborating with mineral density results, the Z-Scores of both groups (PN and ALN) were found on the bottom part of the graph, within the range of osteopenia/osteoporosis (from -1 to -3), while PN + ALN values were in the range of CTRL bones (from -1 to 1).

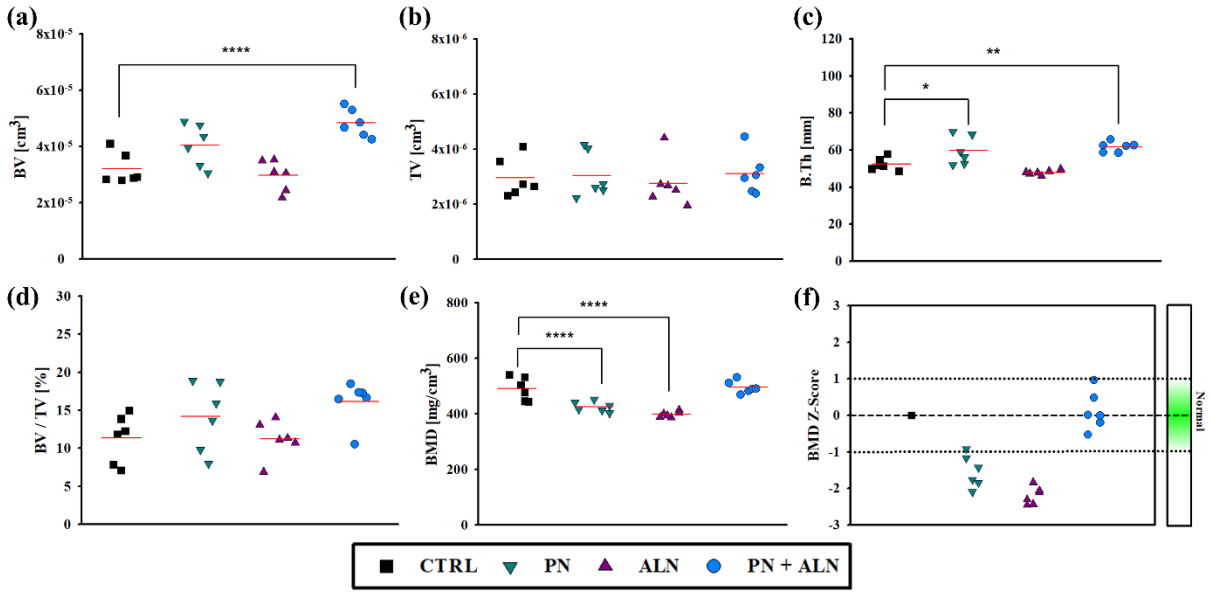

Fig. 42 Morphometric data obtained with µ-CT: (a) BV; (b) TV; (c) B.Th; (d) BV / TV; (e) BMD. Z-Scores calculated based on the BMD levels of CTRL group fish. Significance: * < 0.05, ** < 0.01 and * < 0.001.***

5.3.2. Bone morphology

The bone morphologies are displayed in the **Fig. 43a-l**. We have highlighted ROI containing mineralised tissues features and magnified up to ×100k; it is possible to observe that, in general, the various treatments had no effect on the natural layered structure of bones, neither on the typical carbonated HAp surface appearance (red arrowheads in **43c, 43f, 41i,** and **43l**). In the CTRL group, the densely packed, greater in size, plate-like structures (yellow arrowheads in **43b-c**) are predominant. Among the other groups, these structures were replaced by small-sized, highly mixed (forming an interconnected lattice), round- and plate-like structures (blue arrowheads in **43e-f, 43h-i** and **43-l**). The later structures may be correlated with the use of the different treatments and the active bone remodelling on the surface of these bones.

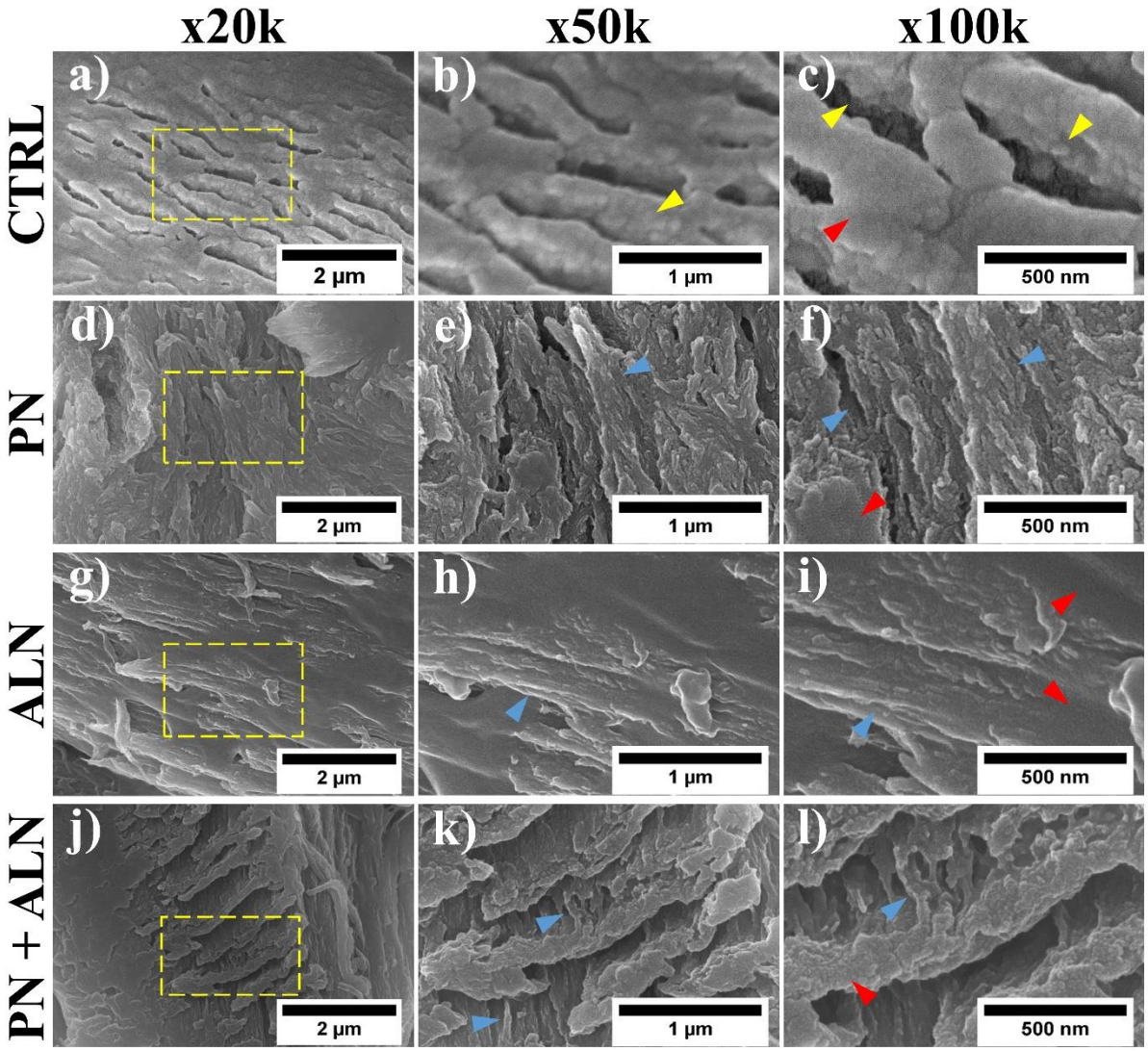

Fig. 43 SEM images of 30 µm slices of zebrafish vertebrae. (4b-c) Yellow arrowheads show the deeply entangled minerals within the tissue. (4e-f, 4h-i and 4k-l) Blue arrowheads represent the small and abundant mineralised structures present in all groups that received medicine intervention. (4f, 4i and 4l) Red arrowheads highlight the carbonated HAp-like structures found in the surface of all bones, indicating the medicines do not change this natural feature.

5.3.3. Nano-mechanical evaluation

A series of indentations were conducted on various locations of the axial surface of zebrafish vertebrae (**Fig. 44a**). Representative *load vs. displacement* curves is shown in **Fig. 44b**; a lower displacement in the surface of bone indicate increased mechanical properties. The plots including the results of *H* and the *E* are displayed in the **Fig. 44c-d**. PN group showed higher *E* heterogeneity (20.76 ± 3.46 GPa) than CTRL group (22.74 ± 1.60 GPa). However, ALN and PN + ALN reduced this heterogeneity to CTRL standard (27.27 ± 1.59 GPa and 25.68 ± 2.07 GPa, respectively). *H* of all groups displayed homogenous distribution. Fish that had ALN displayed bones with higher *E* than CTRL and PN groups ($p < 0.001$). In terms of *H*, ALN alone presented the highest values overall, being significantly higher than CTRL and PN ($p < 0.001$). When ALN was used in sequence to PN (PN + ALN), the *H* increased if compared to PN ($p < 0.001$) but remained in the same range as of the CTRL fish ($p > 0.05$). Thus, ALN was able to recover the once depleted hardness of GIOP bones, to CTRL levels; this might indicate a mechanism of osteoporosis phenotype rehabilitation.

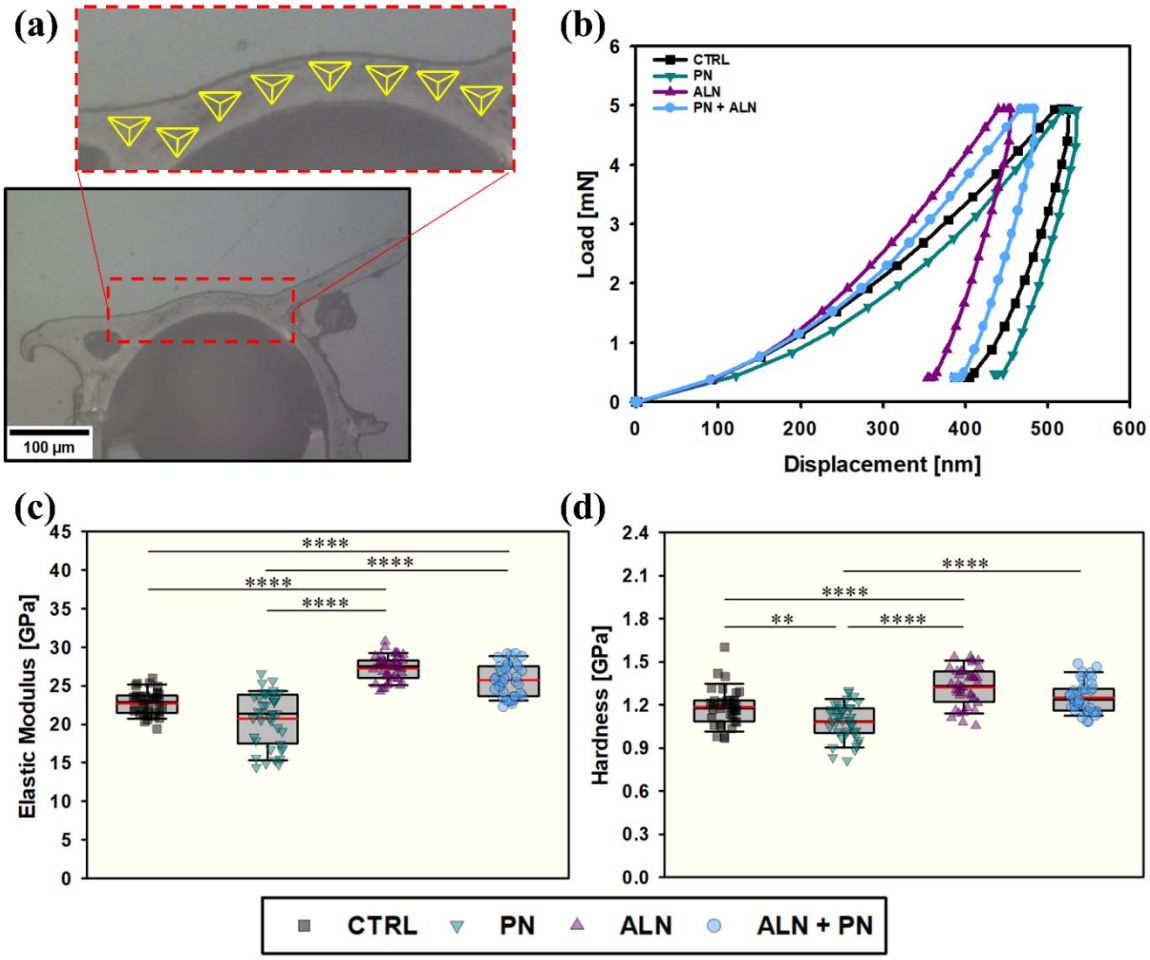

Fig. 44 Scheme and results of nanoindentation (a-d). (a) Microscope view of zebrafish vertebrae axial surface, with region of interest and sketch of nanoindentation sites (as yellow pyramids). (b) Representative plot curves of nanoindentation, load vs. displacement; the load was fixed to 5 mN. (c-d) E and H results for each of the treatments proposed. Significance: * < 0.05, ** < 0.01 and * < 0.001.***

5.4. Discussion

In this study, we explored the effects of the intake of PN and ALN, either administered alone or in succession, on the various characteristics of zebrafish vertebrae, and compare them with unmedicated fish (CTRL). Zebrafish medication was performed by adding the drugs into the fish's water. It has been reported that zebrafish consume compounds put into water by body

osmosis and by their gastrointestinal tract (Pasqualetti *et al.,* 2015); they also metabolise these drugs similarly to other mammals (i.e., rodents and humans) (Vliegenthart *et al.,* 2014). In a second moment, we mapped critical bone elements, such as the BMD, *E*, and *H*. We used a robust model to analyse the medicines aftermath, by the application of a well-established spatial tomography technique (Charles *et al.,* 2017; Cotti *et al.,* 2020; Hayes *et al.,* 2013; Hur *et al.,* 2017; Khajuria and Karasik, 2020; Monma *et al.,* 2019; Silvent *et al.,* 2017) and measured the BMD of the CV1 and CV2 of zebrafish vertebrae (Bird and Mabee, 2003; Weigele and Franz-Odendaal, 2016). Our results, in the conditions proposed, restate PN as a compound effective to induce GIOP, and ALN, if managed as a treatment to a previous condition, as a pro-mineralogenic agent. The affirmation of these statements occurs by the means of the reduced BMD, Z-Scores and *H* found in PN group, in opposition to the natural BMD, Z-Scores and *H* levels in PN + ALN fish (assuming natural as the values observed in the CTRL group). When ALN was consumed alone, we found lower BMD and Z-Scores, but increased mechanical properties compared to CTRL group. In addition, ALN reduced modulus' heterogeneity in zebrafish vertebrae. Our findings add to the current knowledge on bone diseases as it shows different approaches to GIOP modelled in zebrafish, with sub-tissue biomechanical analysis employed together with traditional techniques (computed tomography).

If fish of the same age and strain are compared, zebrafish has been demonstrated to have consistent skeleton metrics and BMD independently of their gender (Charles *et al.,* 2017). We have used wild-type zebrafish to model GIOP due to their conserved bone physiology to humans (Barrett *et al.,* 2006; Bruneel and Witten, 2015). The high-resolution imaging technique here applied, despite not novel for zebrafish backbone characterisation (Charles *et al.,* 2017; Khajuria and Karasik, 2020), demonstrated refined enough to detect pathological mineralisation in the tissue. Additionally, small morphometric variations caused by the compounds were obtained with high significance. Pathological ossifications were previously

reported for 45-month-old zebrafish, which also presented spine curvature (Monma *et al.,* 2019); healthy seven-month-old individuals are not expected to show signs of pathological mineralisation, neither abnormal curved spine. Since none of the treatment regimen here used led to curved spines, we believe that bisphosphonate intake played a key role in the development of pathological mineralisation within the vertebrae. We have focused in analysing quantitatively the volumetric and bone density specifically for the CV1 and CV2 vertebrae (Bird and Mabee, 2003). Hence, the measurements performed in this study were not jeopardized by any abnormal minerals, as they were all found in the PC vertebrae. With the setup proposed in this study, PN showed no effect on BV / TV of treated fish. Geurtzen and colleagues (2017) also used the medicine to exacerbate OP in zebrafish and, corroborating with the findings in this thesis, the values of BV / TV obtained in their study showed no significant difference from those of fish used in their control group. Thus, BV / TV might not be an ideal parameter to identify GIOP in zebrafish

Bone densitometry is considered a gold-standard analysis for osteopenia and OP classification (Iba *et al.,* 2020; Khajuria and Karasik, 2020). Surprisingly, using our setup, despite BV / TV remaining unaltered, BMD decreased in PN and ALN groups, agreeing with the lower signal intensities recorded using μ-CT technique. Fish that received PN were expected to develop GIOP and, consequently, reduced BMD. Geurtzen and collaborators (2017) found no significance in BMD for whole body skeletal assessment in zebrafish. It is widely known PN's potential to induce GIOP in zebrafish lepidotrichia (Barrett *et al.,* 2006; Lin *et al.,* 2019). But the glucocorticoid mode of action in zebrafish vertebrae is still not fully clear. It has been previously shown that, in dermal bones, it impairs OBs function and decrease OCs recruitment in injury sites (Geurtzen *et al.,* 2017). Pasqualetti *et al.,* (2015) demonstrated, using zebrafish scales, that PN treatment activates OCs massively, recruiting them from blood circulation. The impairment of OBs function, alongside with the high activation of OCs in PN sites, may have

significantly decreased the BMD of fish in PN group. ALN otherwise, targets OCs, reducing bone removal (Russell, 2007) and stabilizing the BMD in humans diagnosed with OP (Iba *et al.*, 2020) and in ovariectomized Wistar rats (Ma *et al.*, 2017). We medicated healthy zebrafish with ALN only and observed decreased BMD. Bone resorption and formation are believed to be coupled phenomena (Eriksen, 1986), and thus ALN has been associated to decreased bone formation (Jensen *et al.*, 2021). As consequence, in ALN only group, no therapeutic effect related to BMD was achieved. Conversely, when ALN was administered to counteract GIOP (PN + ALN), its potential to boost previously depleted BMD, and consequently reverse the Z-Scores to healthy levels, is visible.

Since the BMD of diseased zebrafish bones seems to contribute more to osteoporosis determination than BV / TV, it is reasonable to believe the stacking of minerals was affected. We thus proposed to verify the morphology of the forming minerals with imaging technique (Georgiadis *et al.*, 2016). Zebrafish bones are composed by a different range of minerals, with different Ca/P ratios and morphologies depending on their location (Mahamid *et al.*, 2008). After treatment, it was not a surprise that the natural layered structures of bones were preserved. However, the disposal of the minerals into the mineralised collagen matrix was visually different. The minerals found in CTRL, seems to be strongly entangled into the bone matrix, while the mineralised structures observed in every other group seems less entrapped within it. We assume this as the contours in CTRL group are more distinguishable and larger comparing with PN, ALN, or PN + ALN. The intake of medicines influenced the overall process of bone deposition and, thus, might be related to the minerals' entanglement and appearance, but not to their inherent layered hierarchical structure (Georgiadis *et al.*, 2016; Mahamid *et al.*, 2008). This outcome is especially important since the treatment with ALN, in an ideal situation, is not expected to affect the natural characteristics of bones (Hassler *et al.*, 2015).

This study was complemented by assessing the biomechanics of zebrafish vertebrae at sub-tissue level. NI is a powerful tool to assess small samples (Zhang *et al.*, 2002; Zimmermann *et al.*, 2019) and was used to evaluate the axial surface of zebrafish vertebral segments. Both *E* and *H* are important properties of bone. They both contribute to the overall mechanical strength of the tissue, being *E* strongly related to the organic content, while *H* is to the mineral phase (Ibrahim *et al.*, 2020). The mechanical properties obtained with this method showed a decreasing trend starting from ALN > PN + ALN > CTRL > PN. The displacement generated in the surfaces of the bones were around 100 nm lower in the groups with increased mechanical properties (~400 nm) at the peak force. Our measured *E* and *H*, for PN group, showed both a decrease of ~9% compared to the CTRL. Conversely, the *E* and *H* levels of ALN and ALN + PN groups increased by ~20% and ~13% their *E* and by ~12% and ~6% their *H*, respectively. In addition, the *E* data obtained from PN was more scattered than other groups, implying that GIOP increased mechanical heterogeneity in zebrafish vertebrae, reducing *E* values locally. It has been well documented that increased OCs activity generates shallow cavities on the surface of resorbed bone (Mohamed, 2008), which affects mechanical strength. Despite the *E* in PN remained in CTRL level, the major difference between its lowest and highest value might indicate a mechanism of bone fragility, as the regions within the lower range of *E* might serve as crack initiation or propagation spots (Ibrahim *et al.*, 2020). Yet again, with the methodology proposed, NI have shown effectiveness to distinguish small biomechanical alterations in zebrafish backbone affected by different treatment conditions. Due to technical difficulties in the shipping of the samples from NTHU to UoL, the analysis of creep was not performed in zebrafish vertebrae.

5.5. Limitations

With the use of materials science approaches, zebrafish vertebrae have demonstrated potential to be used as a drug screening tool for bone-related diseases. However, a few limitations related to this work must be stated: (1) we did not evaluate before/after properties of the same individuals, as the euthanasia is necessary to extract the fish's vertebrae; (2) the loading environment in which zebrafish lives (water), directly affect their remodelling ability and, consequently, bone formation (Khajuria and Karasik, 2020); (3) even though zebrafish vertebra is relatively bigger in size compared with its lepidotrichia, their axial surface is still very small (~50 μm) and difficult to standardize after embedded; and (4) this study did not evaluated the alterations in the properties on the sagittal direction nor in the collagen configuration. Based on previous literature, collagen arrangement within the mineralised matrix is important for bones to maintain their biomechanics. Thus, other studies should be carried to further the knowledge in bone diseases modelled in zebrafish. Additionally, studies involving cells were not the scope of this research and should be conducted in the future.

5.6. Conclusions

Zebrafish delivers a readily available model to study medicines interactions with mineralised tissues. Within the limitations, we have highlighted morphometric structures affected by PN and/or ALN and paralleled our findings with the biomechanical properties of zebrafish vertebrae. Despite GIOP and its treatment with ALN not showing high sensitivity with *E*, the BMD and *H* both changed with the treatments. Our approach adds to the current knowledge that ALN can rescue diseased mineralised tissues properties when administered after the onset of GIOP. This happens by the means of the restored BMD, Z-Scores and *H*.

References

Axelsson, K.F., Nilsson, A.G., Wedel, H., Lundh, D., Lorentzon, M., 2017. Association Between Alendronate Use and Hip Fracture Risk in Older Patients Using Oral Prednisolone. JAMA 318, 146.

Barrett, R., Chappell, C., Quick, M., Fleming, A., 2006. A rapid, high content, in vivo model of glucocorticoid-induced osteoporosis. Biotechnol. J. 1, 651–655.

Bird, N.C., Mabee, P.M., 2003. Developmental morphology of the axial skeleton of the zebrafish, Danio rerio (Ostariophysi: Cyprinidae). Dev. Dyn. 228, 337–357.

Bruneel, B., Witten, P.E., 2015. Power and challenges of using zebrafish as a model for skeletal tissue imaging. Connect. Tissue Res. 56, 161–173.

Cardeira, J., Gavaia, P.J., Fernández, I., Cengiz, I.F., Moreira-Silva, J., Oliveira, J.M., Reis, R.L., Cancela, M.L., Laizé, V., 2016. Quantitative assessment of the regenerative and mineralogenic performances of the zebrafish caudal fin. Sci. Rep. 6.

Chandra, A., Rajawat, J., 2021. Skeletal Aging and Osteoporosis: Mechanisms and Therapeutics. Int. J. Mol. Sci. 22, 3553.

Charles, J.F., Sury, M., Tsang, K., Urso, K., Henke, K., Huang, Y., Russell, R., Duryea, J., Harris, M.P., 2017. Utility of quantitative micro-computed tomographic analysis in zebrafish to define gene function during skeletogenesis. Bone 101, 162–171.

Chazotte, B., 2012. Labelling Golgi with Fluorescent Ceramides. Cold Spring Harb. Protoc. 2012, pdb.prot070599.

Chotiyarnwong, P., McCloskey, E.V., 2020. Pathogenesis of glucocorticoid-induced osteoporosis and options for treatment. Nat. Rev. Endocrinol. 16, 437–447.

Cotti, S., Huysseune, A., Koppe, W., Rücklin, M., Marone, F., Wölfel, E.M., Fiedler, I.A.K., Busse, B., Forlino, A., Witten, P.E., 2020. More Bone with Less Minerals? The Effects of Dietary Phosphorus on the Post-Cranial Skeleton in Zebrafish. Int. J. Mol. Sci. 21, 5429.

Delaisse, J.-M., Andersen, T.L., Kristensen, H.B., Jensen, P.R., Andreasen, C.M., Søe, K., 2020. Re-thinking the bone remodelling cycle mechanism and the origin of bone loss. Bone 141, 115628.

Embry, M.R., Belanger, S.E., Braunbeck, T.A., Galay-Burgos, M., Halder, M., Hinton, D.E., Léonard, M.A., Lillicrap, A., Norberg-King, T., Whale, G., 2010. The fish embryo toxicity test as an animal alternative method in hazard and risk assessment and scientific research. Aquat. Toxicol. 97, 79–87.

Eriksen, E.F., 1986. Normal and Pathological Remodelling of Human Trabecular Bone: Three-Dimensional Reconstruction of the Remodelling Sequence in Normal and in Metabolic Bone Disease*. Endocr. Rev. 7, 379–408.

Genest, F., Claußen, L., Rak, D., Seefried, L., 2021. Bone mineral density and fracture risk in adult patients with hypophosphatasia. Osteoporos. Int. 32, 377–385.

Georgiadis, M., Müller, R., Schneider, P., 2016. Techniques to assess bone ultrastructure organization: orientation and arrangement of mineralized collagen fibrils. J. R. Soc. Interface 13, 20160088.

Geurtzen, K., Knopf, F., 2018. Adult Zebrafish Injury Models to Study the Effects of Prednisolone in Regenerating Bone Tissue. J. Vis. Exp.

Geurtzen, K., Vernet, A., Freidin, A., Rauner, M., Hofbauer, L.C., Schneider, J.E., Brand, M., Knopf, F., 2017. Immune Suppressive and Bone Inhibitory Effects of Prednisolone in Growing and Regenerating Zebrafish Tissues. J. Bone Miner. Res. 32, 2476–2488.

Hassler, N., Gamsjaeger, S., Hofstetter, B., Brozek, W., Klaushofer, K., Paschalis, E.P., 2015. Effects of long-term alendronate treatment on postmenopausal osteoporosis bone material properties. Osteoporos. Int. 26, 339–352.

Hayes, A.J., Reynolds, S., Nowell, M.A., Meakin, L.B., Habicher, J., Ledin, J., Bashford, A., Caterson, B., Hammond, C.L., 2013. Spinal Deformity in Aged Zebrafish Is Accompanied by Degenerative Changes to Their Vertebrae that Resemble Osteoarthritis. PLoS ONE 8, e75787.

Hildebrand, T., Rüegsegger, P., 1997. A new method for the model-independent assessment of thickness in three-dimensional images. J. Microsc. 185, 67–75.

Huang, W.-C., Hsieh, Y.-S., Chen, I.-H., Wang, C.-H., Chang, H.-W., Yang, C.-C., Ku, T.-H., Yeh, S.-R., Chuang, Y.-J., 2010. Combined Use of MS-222 (Tricaine) and Isoflurane Extends Anesthesia Time and Minimizes Cardiac Rhythm Side Effects in Adult Zebrafish. Zebrafish 7, 297–304.

Hur, M., Gistelinck, C.A., Huber, P., Lee, J., Thompson, M.H., Monstad-Rios, A.T., Watson, C.J., McMenamin, S.K., Willaert, A., Parichy, D.M., Coucke, P., Kwon, R.Y., 2017. MicroCT-based phenomics in the zebrafish skeleton reveals virtues of deep phenotyping in a distributed organ system. eLife 6, e26014.

Iba, K., Takada, J., Sonoda, T., Yamashita, T., 2020. Effect of continuous long-term treatment for 10 years with bisphosphonate on Japanese osteoporosis patients. J. Bone Miner. Metab. 38, 240–247.

Ibrahim, A., Magliulo, N., Groben, J., Padilla, A., Akbik, F., Abdel Hamid, Z., 2020. Hardness, an Important Indicator of Bone Quality, and the Role of Collagen in Bone Hardness. J. Funct. Biomater. 11, 85.

Jensen, P.R., Andersen, T.L., Chavassieux, P., Roux, J.-P., Delaisse, J.-M., 2021. Bisphosphonates impair the onset of bone formation at remodelling sites. Bone 145, 115850.

Khajuria, D.K., Karasik, D., 2020. Novel model of restricted mobility induced osteopenia in zebrafish. J. Fish Biol. jfb.14369.

Lin, W.-Y., Dharini, K., Peng, C.-H., Lin, C.-Y., Yeh, K.-T., Lee, W.-C., Lin, M.-D., 2022. Zebrafish models for glucocorticoid-induced osteoporosis. Tzu Chi Med. J. 34, 373.

Lin, Y., Xiang, X., Chen, T., Gao, C., Fu, H., Wang, L., Deng, L., Zeng, L., Zhang, J., 2019. In vivo monitoring and high-resolution characterizing of the prednisolone-induced osteoporotic process on adult zebrafish by optical coherence tomography. Biomed. Opt. Express 10, 1184.

Ma, X., Xu, Z., Ding, S., Yi, G., Wang, Q., 2017. Alendronate promotes osteoblast differentiation and bone formation in ovariectomy-induced osteoporosis through interferon-β/signal transducer and activator of transcription 1 pathway. Exp. Ther. Med.

Mahamid, J., Sharir, A., Addadi, L., Weiner, S., 2008. Amorphous calcium phosphate is a major component of the forming fin bones of zebrafish: Indications for an amorphous precursor phase. Proc. Natl. Acad. Sci. 105, 12748–12753.

Meyers, M.A., McKittrick, J., Chen, P.-Y., 2013. Structural Biological Materials: Critical Mechanics-Materials Connections. Science 339, 773–779.

Mohamed, A.M., 2008. An overview of bone cells and their regulating factors of differentiation. Malays. J. Med. Sci. MJMS 15, 4–12.

Monma, Y., Shimada, Y., Nakayama, H., Zang, L., Nishimura, N., Tanaka, T., 2019. Aging-associated microstructural deterioration of vertebra in zebrafish. Bone Rep. 11, 100215.

Oliver, W.C., Pharr, G.M., 2004. Measurement of hardness and elastic modulus by instrumented indentation: Advances in understanding and refinements to methodology. J. Mater. Res. 19, 3–20.

Oliver, W.C., Pharr, G.M., 1992. An improved technique for determining hardness and elastic modulus using load and displacement sensing indentation experiments. J. Mater. Res. 7, 1564–1583.

Pasqualetti, S., Congiu, T., Banfi, G., Mariotti, M., 2015. Alendronate rescued osteoporotic phenotype in a model of glucocorticoid-induced osteoporosis in adult zebrafish scale. Int. J. Exp. Pathol. 96, 11–20.

Percie du Sert, N., Ahluwalia, A., Alam, S., Avey, M.T., Baker, M., Browne, W.J., Clark, A., Cuthill, I.C., Dirnagl, U., Emerson, M., Garner, P., Holgate, S.T., Howells, D.W., Hurst, V., Karp, N.A., Lazic, S.E., Lidster, K., MacCallum, C.J., Macleod, M., Pearl, E.J., Petersen, O.H., Rawle, F., Reynolds, P., Rooney, K., Sena, E.S., Silberberg, S.D.,

Steckler, T., Würbel, H., 2020. Reporting animal research: Explanation and elaboration for the ARRIVE guidelines 2.0. PLOS Biol. 18, e3000411.

Russell, R.G.G., 2007. Bisphosphonates: Mode of Action and Pharmacology. Pediatrics 119, S150–S162.

Silvent, J., Akiva, A., Brumfeld, V., Reznikov, N., Rechav, K., Yaniv, K., Addadi, L., Weiner, S., 2017. Zebrafish skeleton development: High resolution micro-CT and FIB-SEM block surface serial imaging for phenotype identification. PLOS ONE 12, e0177731.

United Nations Department of Economic and Social Affairs, Population Division., 2022. World Population Prospects 2022: Summary of Results. UN DESA/POP/2022/TR/NO. 3.

Vandewalle, J., Luypaert, A., De Bosscher, K., Libert, C., 2018. Therapeutic Mechanisms of Glucocorticoids. Trends Endocrinol. Metab. 29, 42–54.

Vliegenthart, A.D.B., Tucker, C.S., Del Pozo, J., Dear, J.W., 2014. Zebrafish as model organisms for studying drug-induced liver injury: Zebrafish and drug-induced liver injury. Br. J. Clin. Pharmacol. 78, 1217–1227.

Weigele, J., Franz-Odendaal, T.A., 2016. Functional bone histology of zebrafish reveals two types of endochondral ossification, different types of osteoblast clusters and a new bone type. J. Anat. 229, 92–103.

Westerfield, M., 2000. The Zebrafish Book: A Guide for the Laboratory Use of Zebrafish (Danio Rerio). University of Oregon Press.

Yeh, E.J., Gitlin, M., Sorio, F., McCloskey, E., 2023. Estimating the future clinical and economic benefits of improving osteoporosis diagnosis and treatment among postmenopausal women across eight European countries. Arch. Osteoporos. 18, 68.

Zhang, Y., Cui, F.Z., Wang, X.M., Feng, Q.L., Zhu, X.D., 2002. Mechanical properties of skeletal bone in gene-mutated stöpseldtl28d and wild-type zebrafish (Danio rerio) measured by atomic force microscopy-based nanoindentation. Bone 30, 541–546.

Zimmermann, E.A., Riedel, C., Schmidt, F.N., Stockhausen, K.E., Chushkin, Y., Schaible, E., Gludovatz, B., Vettorazzi, E., Zontone, F., Püschel, K., Amling, M., Ritchie, R.O., Busse, B., 2019. Mechanical Competence and Bone Quality Develop During Skeletal Growth. J. Bone Miner. Res. 34, 1461–1472.

6. Chapter 6: Osteogenesis imperfecta murine model for severe osteogenesis imperfecta

---

In this chapter, a brief introduction to *oim* and *tm1b* murine models is given (section 6.2.1). The rationale for using murine model in OI (section 6.2.2) and the gap in the literature (section 6.2.3) are covered. The biomechanics of *oim* and *tm1b* mice femurs are discussed (section 6.4).

6.1. Abstract

Type I collagen is a fundamental protein found in vertebrate bones serving as a site for mineral nucleation and growth. It is commonly arranged in heterotrimers containing $(\alpha1)_2(\alpha2)_1$ chains. Connective tissue diseases may arise with abnormal trimers setups (i.e., *col1a2*-null $(\alpha1)_3$). OI is an inherited disease that originates from dysfunctional α2 chains and may cause bone brittleness. NI has the potential to complement traditional tomography methods in evaluating the mechanical behaviour of OI bones. This study aimed to assess the biomechanics of femurs of *oim* mice and compared to *col1a2*-null (*tm1b*) and WT mice. Femurs of 8-, 18- and 52-weeks-old female (F) and male (M) mice were included in the study. The biomechanics of bones were evaluated with NI using O-P method. The viscoelastic behaviour was explored by variation of holding times (10 s and 100 s). *E*, *H* and C_{IT} were determined. Increasing the holding times from 10 s to 100 s reduced *H* values by ~15 %, while *E* remained unaltered. *E* of 8 w *oim*/Hom females showed lower mechanical values than WT and Het. In general, as mice aged, the mechanical properties of their bones increased. C_{IT} of 8 w *oim*/Hom mice was the highest among the genotypes assessed. A higher C_{IT} in younger *oim*/Hom mice might explain the prevalence of bone fractures at later stages of life.

6.2. Introduction

6.2.1. Murine models for bone diseases

Oim mutation is the most common pre-clinical murine model of OI(III) (Alcorta-Sevillano *et al.*, 2022; Fratzl, 2008). *Oim*/Hom bones are formed solely of homotrimeric $(\alpha1)_3$ collagen due to a dysfunction in the encoding of α2(I) chains (Skarnes *et al.*, 2011). *Oim* mice show severe osteopenia, reduced body size, fragile bone fractures, and skeletal deformation (Carriero *et al.*, 2016; Lee *et al.*, 2022). A potential reason for poor bone biomechanics in *oim* mice is the abnormal orientation and stacking of homotrimeric collagen in the ECM (Mcbride, Jr. *et al.*, 1992; Raghunath *et al.*, 1994). Although, it has been demonstrated recently that another homotrimeric mutation (*col1a2*-null) do not display bones with impaired mechanical properties (Lee *et al.*, 2022). This suggests that reduced bone biomechanics arise from *oim* mutant alleles and its protein byproducts (Lee *et al.*, 2022). At the macrolevel, it has been shown that the ultimate stress of *oim* bone is lower than WT mice; however, in the same study, no significant difference was found for the *E* of *oim*/Hom femurs compared to WT (Lee *et al.*, 2022). Vanleene *et al.*, (2012) used both three-point bending tests and NI to assess the biomechanics of *oim* and WT tibias. They found no difference in *E* measured at macrolevel, but NI revealed significant decrease in the *E* of *oim* mutants.

6.2.2. Rationale for using a murine model for bone diseases

Among the numerous pre-clinical human substitutes (e.g., zebrafish) for the study of bone diseases, murine models, more specifically, the *oim* mutant, have been shown of great relevance for heterogenous conditions such as OI (Alcorta-Sevillano *et al.*, 2022). *Oim* mutation is spontaneous (breed between *C3H/HeJ* and *C57BL/6JLe* mice) (Chipman *et al.*, 1993), so there is no need for drug treatment to exacerbate OI phenotype. Mice have stronger

genetic, anatomical and pathological similarities with humans than other minor vertebrates (Lieschke and Currie, 2007). Murine models have both trabecular and cortical bones, which is not the case in other vertebrate models (Geurtzen *et al.,* 2017). In bone diseases pre-clinical studies, the analysis of analogous structures might strengthen the evidence of the results. In addition, mammalian bone is composed exclusively of multinucleated OCs, which play a key role in bone diseases (Laizé *et al.,* 2014). Thus, the robustness and genetic conservation of *oim* model has the potential to shed light on the relationship between collagen defects and bone mechanical properties.

6.2.3. Defining the gap in the literature

OI is a condition known to cause bone fragility and, depending on the severity of phenotype, skeletal deformation (Sillence, 1981; Sillence *et al.,* 1979; Van Dijk and Sillence, 2014). In some cases, prescribing bisphosphonates to regulate BMD, encouraging healthy lifestyle and managing bone pain is not sufficient to promote better quality of life to OI patients (Astrom, 2002). The management of severe bone curvatures sometimes requires surgical interventions, with the insertion of metallic prostheses to guide the process of bone ossification (Fassier, 2021). Trabecular bone creep is one of the main reasons why diseased bones fracture (Pollintine *et al.,* 2009) and is a loosening mechanism in bone implants (Novitskaya *et al.,* 2014). Although the mechanical properties of OI bone have been evaluated at the macro (Lee *et al.,* 2022; Vanleene *et al.,* 2012) and sub-tissue level (Vanleene *et al.,* 2012) in *oim* model, low attention has been given to the effects of bone creep in OI. Here, NI was used to evaluate the *E*, *H* and creep behaviour of *oim* femurs. The femurs of *oim* mice were indented with different hold-time periods to assess the viscoelastic response of the diseased bones. The results were compared to WT bones and to *col1a2*-null. Mice of both sexes and ages ranging from early adulthood (8 w)

to late adulthood (52 w) were included. In this work it was evaluated mice femurs in diverse conditions. In all cases, M and F individuals were used:

A. Two main mutations were analysed *oim* (simulating misfolding of *col1a2* chains) and *tm1b* (simulating *col1a2*-null).
    a. Wild-type mice were incorporated into both *oim* and *tm1b* groups since they were raised in different months of the year.
    b. Het mice were tested to understand the effects of mixed genetics.
    c. Hom mice were tested to verify the effects of genotype mutation.
B. Hold times of 10 s and 100 s were used in all samples.

6.3. Results

Nanoindentation was performed in ~145 mice femurs and the mechanical properties were accesses in terms of *E*, *H* and C_{IT}. Box plots with the *E* and *H* for 10- and 100 s holding times is shown in **Fig. 45a-j**. As the hold times were increased from 10 s to 100 s, the *H* recorded for *oim* and *tm1b* mice decreased ~15 %, while the *E* remained constant. This indicates that *H* was more sensitive to prolonged creep-holding than *E*. For both 8- and 18 w, *oim*/Hom showed lower *E* than WT ($p < 0.001$). Conversely, the *H* of *oim*/Hom despite showing no significant difference at 8w, increased in comparison to WT ($p < 0.01$). *Oim*/Hom female mice show lower mechanical properties if compared to males of the same mutation/age (**Fig. 45a-b**). The difference between the genders in *oim*/Hom disappeared at 18-weeks of age (**Fig. 45c-d**); observing the data, the mechanical properties of *oim*/Hom male seem to have decreased from ~25 GPa to ~21 GPa, while females increased from ~15 GPa to 21 GPa between 8- and 18 w. In addition, the *E* and *H* of *oim*/Hom increased in homogeneity as the mice aged. *Oim*/Het demonstrated intermediate *E* in comparison to WT and Hom. The scattering of data points across the genotypes at all ages in *tm1b* mice is less pronounced than the scatter observed in

oim mice. Female mice in compound Het of *tm1b* mutation, showed higher mechanical properties than male mice of compound Het. Compound *oim*/Het did not show similar behaviour. *Tm1b*/Hom has an additive effect in reducing the mechanical properties of female and male mice at young ages (8 w), however, the *E* and *H* of *tm1b* mice with Hom genotype gradually increased at 18- and 52 w of age (**Fig. 45e-j**). Despite WT and *tm1b*/H*et al*so showed to increase mechanical properties with age, the femurs of Hom mice of this mutation showed the highest modulus and resistance to plastic deformation.

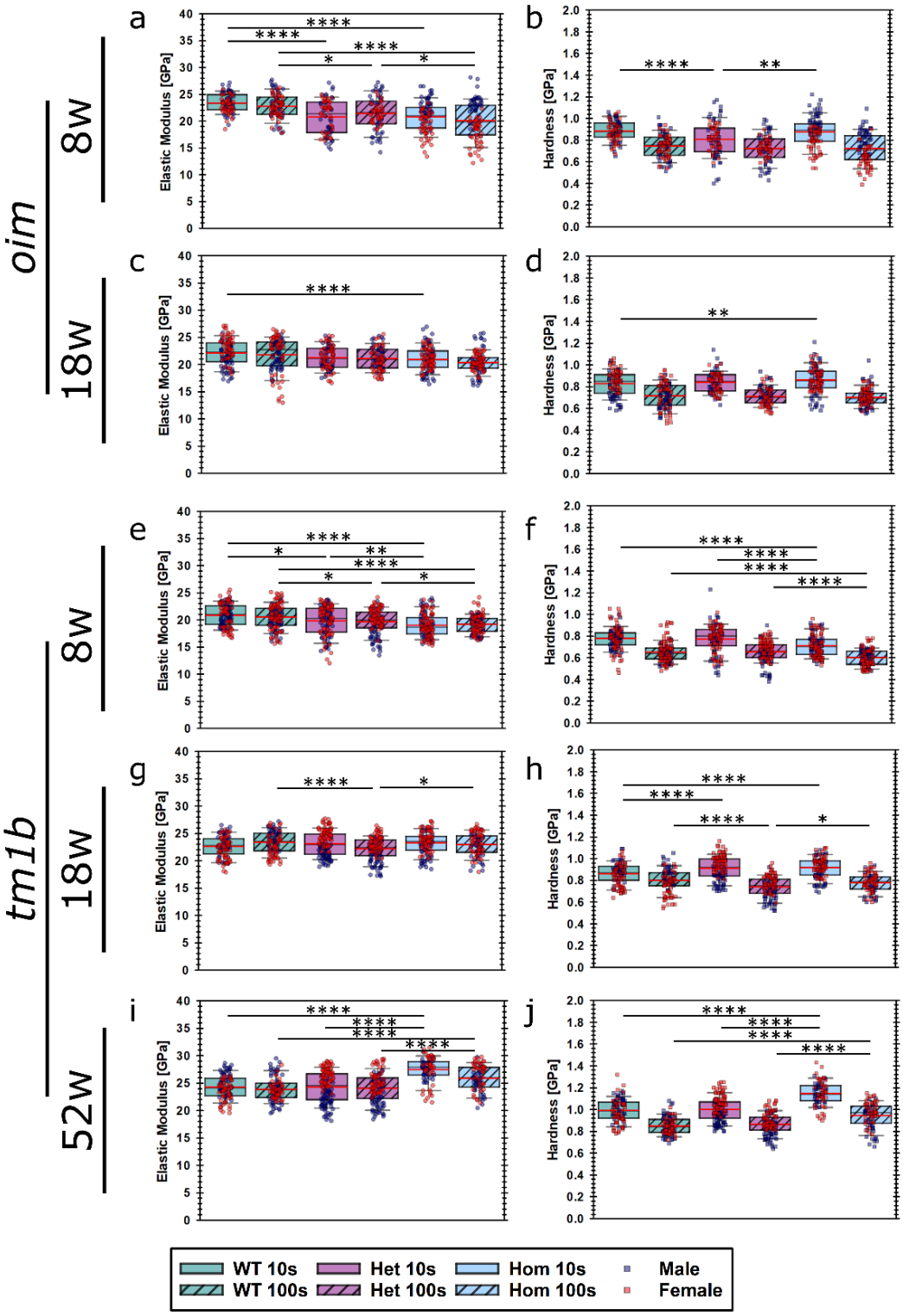

Fig. 45 Mechanical properties of mice femurs. (a-j) NI was used to obtain the E and H of oim (a-d) and tm1b (e-j) mice. Statistical comparisons were performed only between equivalent hold times. Each point in the box plots is a single indentation. * < 0.05; ** < 0.01; * < 0.001.***

Given the high heterogeneity of mechanical properties found in mutations critical for this study (e.g., *oim*/Hom), regression lines were plotted. The scatterplots resulting from this analysis are shown in **Fig. 46**; the values for the Pearson correlation (r^2) are displayed in **Table 8**.

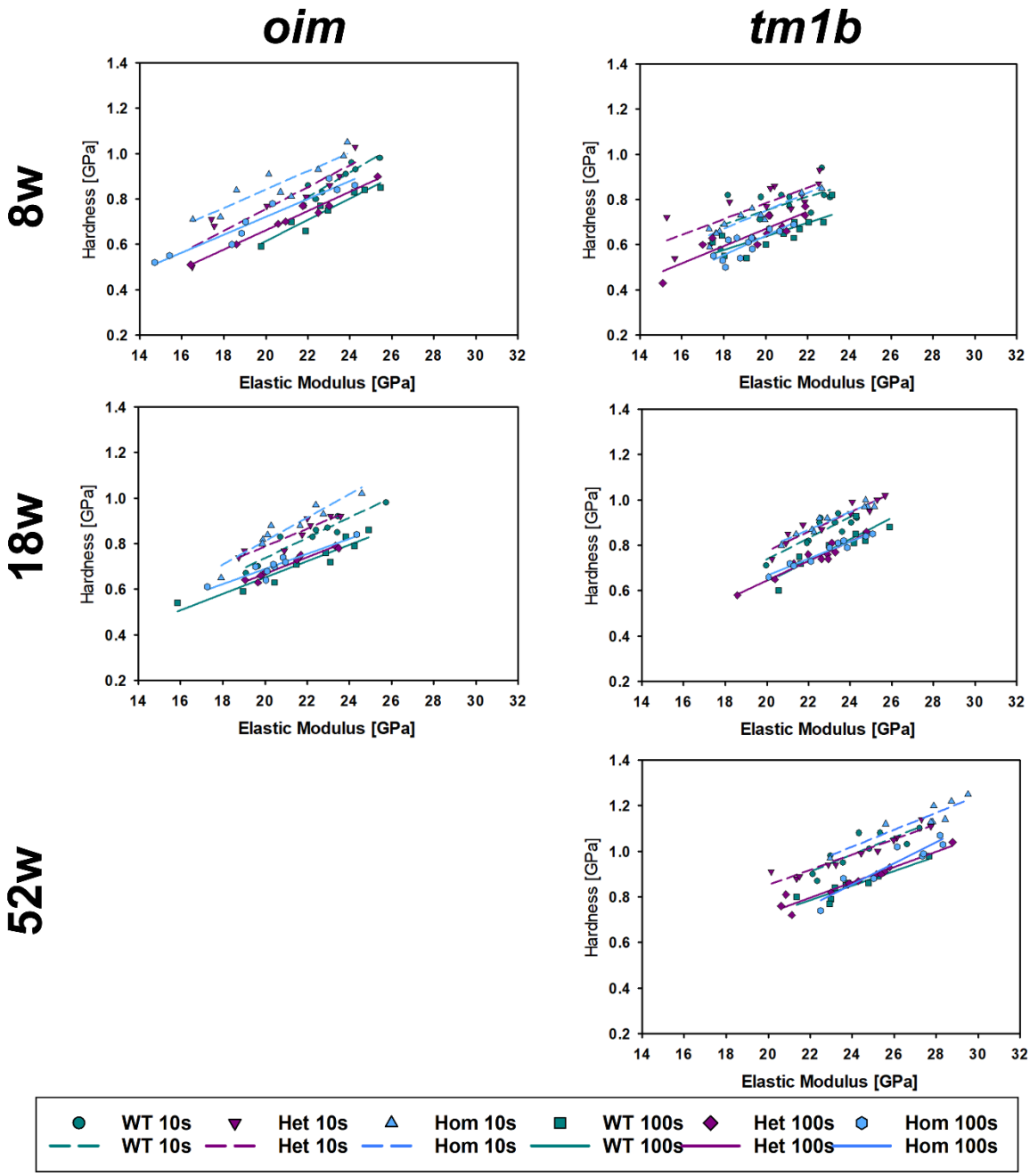

Fig. 46 Linear correlation between E and H. Each of the points in the scatter plots are the averaged value for each femur tested. The longer the regression lines, the higher is the heterogeneity of measurements.

Table 8 Pearson correlation (r2) of mice femurs.

Mutations	Genotype	Hold times and age					
		10s			100s		
		8w	18w	52w	8w	18w	52w
	WT	0.8258	0.8836	-	0.9089	0.9025	-
oim	**Het**	0.8402	0.8278	-	0.9704	0.9414	-
	Hom	0.7951	0.8850	-	0.9249	0.8601	-
	WT	0.2653	0.6973	0.6544	0.5678	0.7375	0.8163
tm1b	**Het**	0.5957	0.8775	0.9096	0.7376	0.9158	0.9186
	Hom	0.8632	0.9081	0.8154	0.6191	0.9522	0.8373

- Not evaluated

The linear correlation between *E* and *H* was found to be positive for all mutations and genotypes. In general, the linear correlation *E-H* was stronger for hold times of 100 s. Long lines can be observed in 8w *oim* (full blue lines), which demonstrate the heterogeneity of the mechanical properties in this group of mice. From 8- to 18 w, the scatter plots for *oim* data remained positioned in a similar quadrant in the plot; this shows no significant increase of mechanical properties with age. Exception is the approximation of 18 w *oim*/Hom values, with 10 s hold-times (dashed yellow), that inclined to the y-axis, displaying higher resistance to plastic deformation with time. On the other hand, *tm1b* scatterplots show a clear tendency to move to the upper right corner of the graphs. Thus, the mechanical properties of mice femurs in this group have shown to increase with time. The shorter lines in *tm1b* also demonstrate higher homogeneity if compared to *oim*.

The results for the calculated depth of penetration are displayed in **Fig. 47**. During the first 10 s of holding the indenter's tip in contact with the surface of bones, a rapid increase in depth was observed. This initial 10 s accounted for ~50 % of the total displacement occurring during creep-holding. The remaining ~50 % occurred in the course of 90 s, as its possible to infer from the plots. The highest change in depth was observed in young *oim*/Hom mice (157.03 nm, on average), indicating that the samples obtained from mice of this age and genotype have lower

mechanical properties and are more prone to time-dependent deformation (creep deformation). *Tm1b*/Hom mice, at 8 weeks of age, also showed bones prone to creep deformation. However, as this group aged up to 52 w, the lowest depth of penetration overall, for 100 s hold times, was recorded (101.99 nm, on average). The variability of the penetration depths decreased in all groups as the mice grew older, indicating high heterogeneity in younger mice.

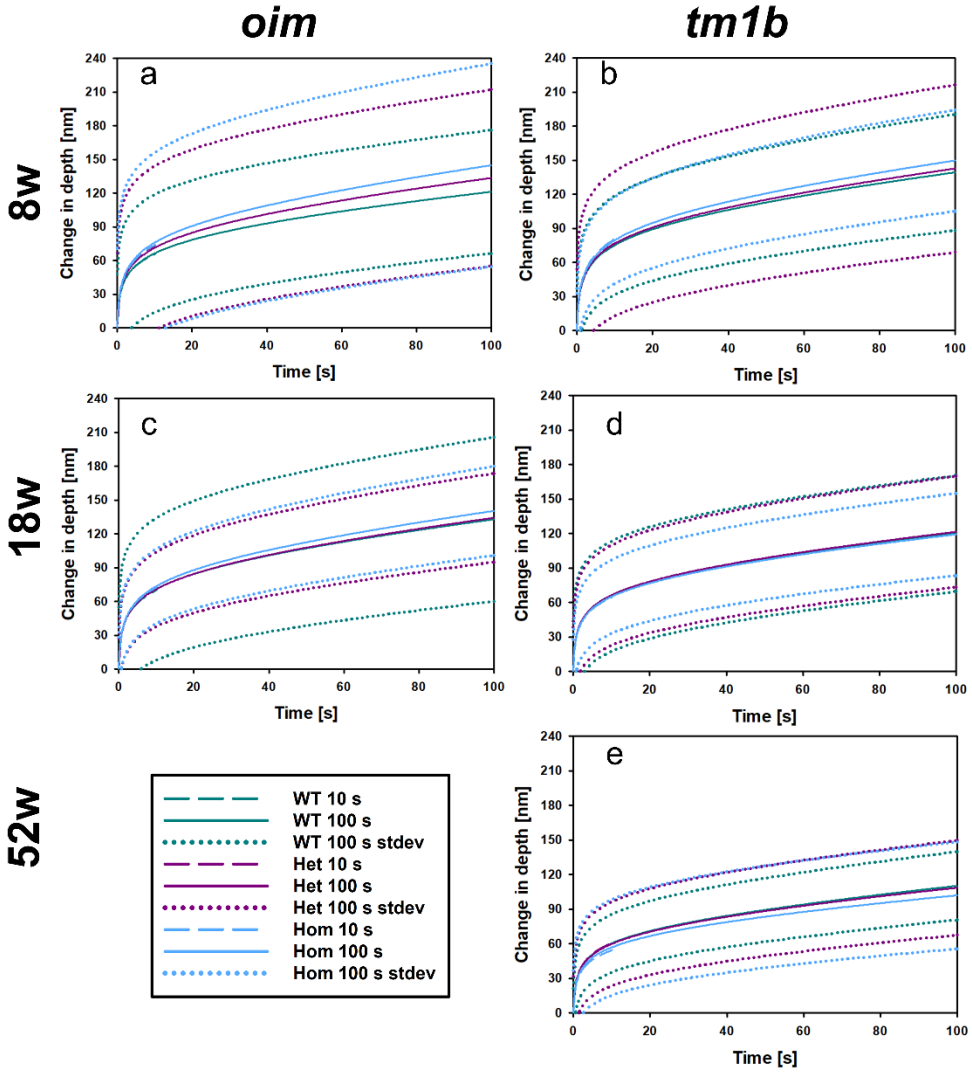

Fig. 47 Change in depth, in nm, of mice femurs under a constant load. The values displayed in this image were generated through the averaging of each samples load vs. displacement curves.

The C_{IT} for each mutation was calculated and the values obtained are displayed in **Fig. 48a-e.** Creep measures the amount of displacement occurring in the materials' surface when loads are held for prolonged times. In this work, two distinct creep-loading regimens were proposed.

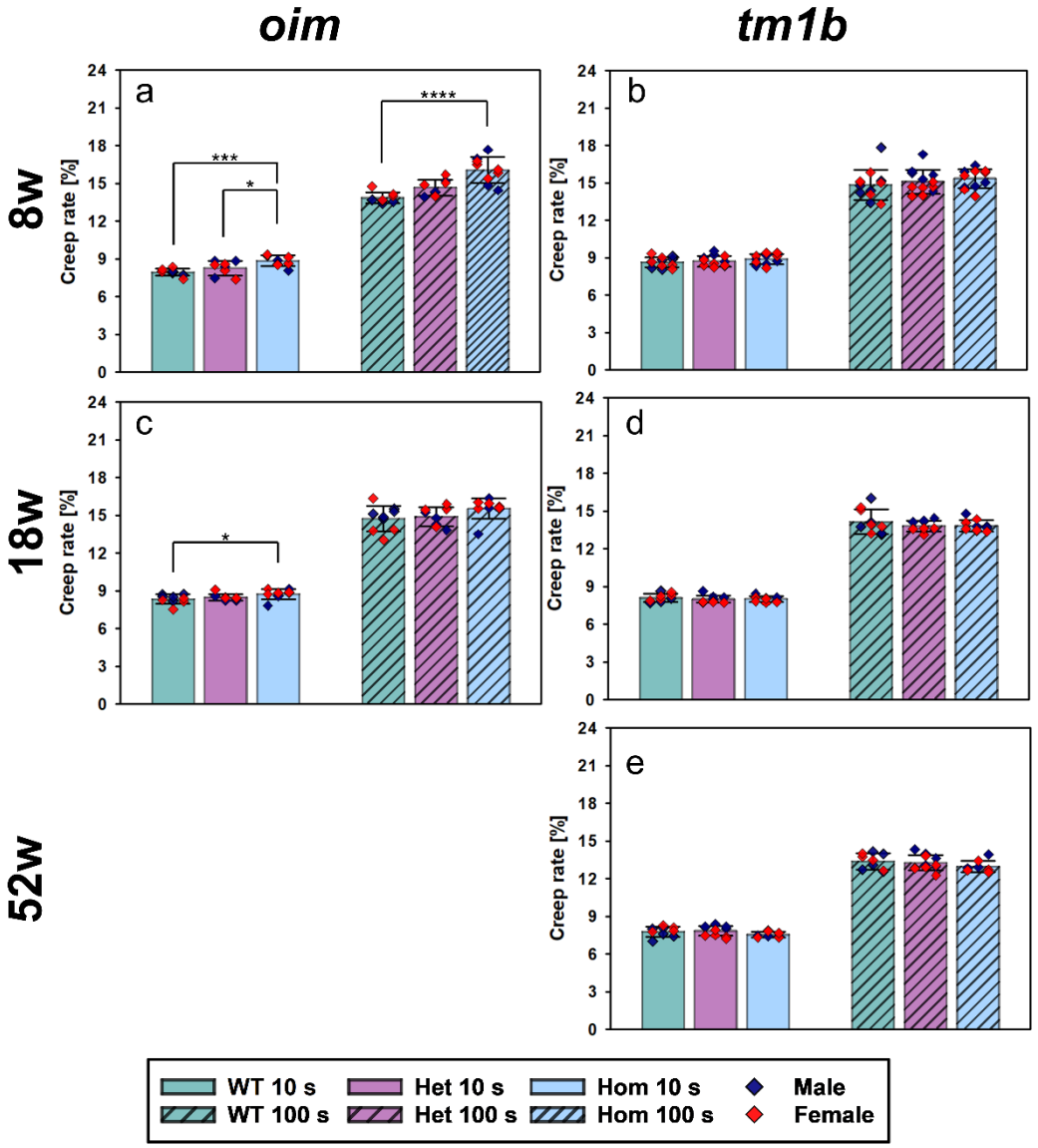

Fig. 48 Creep rates calculated with the displacements in the beginning and end of creep-hold periods. (a, c) Oim mutants displayed increased C_{IT} in comparison with oim/Het and WT. (b, d, e) The absence of α2(I) chains seem to have no effect on bone creep rate. * < 0.05; ** < 0.01; * < 0.001.***

For holding times of 100 s, bone samples undergo higher C_{IT} than samples being indented with lower hold times (10 s). Increasing the hold-times by 90 s led to a two-fold increase in C_{IT}. Comparing mice of same age but different genotype, *col1a2* misfolding produce bones

significantly more susceptible to creep ($p < 0.001$). In *col1a2*-null, conversely, C_{IT} remained unchanged for both large and small holding times ($p > 0.05$). Femurs obtained from 8w *oim*/Hom also showed similar behaviour even for low hold times. At 18 w, due to bone maturation, the C_{IT} of *oim*/Hom reduced to similar levels of WT; *oim*/Het bones showed intermediate mechanical properties to both *oim*/Hom and WT. High C_{IT} found in mouse mutations that resemble/model severe cases of OI, are in accordance with the findings suggesting OI has brittle bone phenotype or poor biomechanics.

6.4. Discussion

Mechanical properties of bone are fundamental for the understanding of the underlying mechanism behind bone quality. Diseases that target bones, such as OI, deplete the mechanical properties of the tissue, by changing its microstructure, which may lead to bone fractures (Pollintine *et al.,* 2009). OI is a heterogenous disease in its nature (Sillence *et al.,* 1979) and, despite efforts have been made to further our understanding on this rare genetic disease, the relationship between collagen misfolding and brittle bones phenotype is still not clear (Lee *et al.,* 2022). With the difficulties in obtaining human samples to address OI, murine models were proposed (Lee *et al.,* 2022; Shapiro *et al.,* 1995). *Oim* is considered the most important pre-clinical subject for the research of OI(III); *oim* mice produce dysfunctional α2(I) chains that cannot be incorporated properly into collagen fibrils, causing the formation of $(\alpha1)_3$ fibres (Chipman *et al.,* 1993). A different mouse mutation, called *tm1b* (*col1a2*-null), also produce homotrimeric $(\alpha1)_3$, however, these mice do not display brittle bone phenotype at macroscale level (Lee *et al.,* 2022). In this study, the cortical region of femurs of both *oim* and *tm1b* was assessed with NI and compared to controls (WT). The biomechanical quality of the murine bones was verified by the means of *E, H,* depth of penetration, and C_{IT}. Ultimately, the reduced

bone biomechanics at initial stages of life of *oim* mice seem to play a key role for bone fragility in later stages of adulthood.

The *E* of a material has intricate relationship with its elastic (reversible) deformation, while *H* is normally understood as the resistance to plastic (irreversible) deformation. In biological materials, *H* and *E* display a linear relationship across multiple orders of magnitude; such linearity may be used as a proxy for material quality (Labonte *et al.*, 2017). *Oim*/Hom mutation showed reduced *E* as compared to WT mice of the same age (8- and 18 w) independently of the hold time used. This result agrees with a previous study that used NI to assess the mechanical response of murine models (Vanleene *et al.*, 2012). Conversely, the *H* was on the same levels of the WT group, and, with ageing, it showed to increase in comparison to the bones of healthy mice. In addition, both *H* and *E* measurements showed high variability within *oim*/Hom. This finding suggests that the genetic heterogeneity of OI phenotypes (Sillence *et al.*, 1979) might also be extended to localised mechanical properties. Female *oim*/Hom mice bones exhibited lower biomechanics than males at 8 w. Lee *et al.*, (2022) found that females *oim*/Hom have decreased body size in comparison to female WT. It has been demonstrated that the low mechanical properties observed specifically in young female *oim* mice might be an additive effect of subproducts of homotrimeric collagen and reduced bone morphometrics (Lee *et al.*, 2022; Yao *et al.*, 2013). Interestingly, although *tm1b* do not display fragile bones at the macrolevel, their nanomechanical properties at 8 w of age decreased in comparison to WT and *tm1b*/Het. Among the mice genotypes assessed *tm1b*/Hom showed the most pronounced increase with age. Unfortunately, due to concerns with *oim*/Hom mice showing spontaneous fractures as they advanced in age, their mechanical properties at 52 w of age still remains unaddressed. However, the *H* in this group of mice increased from 8- to 18w, suggesting an increasing trend with age, similarly to what was observed in *tm1b*/Hom.

Creep is a mechanical behaviour known to cause negative effects in diseased bones (Pollintine *et al.,* 2009). Creep has been related to the shortening of human stature due to vertebral compression and as a major player in the loosening of bone correcting surgical implants (Cho *et al.,* 2007; Novitskaya *et al.,* 2014). Collagen mutations have significant effects in bone microarchitecture (Van Dijk and Sillence, 2014) and, depending on the severity of the phenotype, microarchitectural decrease can resemble of those in secondary OP (El-Gazzar and Högler, 2021), potentially increasing the susceptibility of bones to creep deformation. As expected, by promoting increased hold times between indenter's Berkovich tip and the surface of a viscoelastic material such as bone, led to increase in the depth of penetration and C_{IT}. Overall, C_{IT} values were nearly two-fold for 100 s measurements in comparison to 10 s. *Col1a2*-null showed decreased *E* and *H*, however, these two properties seem to have had no effects in the C_{IT} at any point in their life (8-, 18- or 52 w). On the contrary, *oim*/Hom bones presented high susceptibility to creep deformation at 8 w, but with difference due to gender. Most of OI-related fractures occur in the initial stages of people (Folkestad *et al.,* 2017; Strevel *et al.,* 2005). Middle aged individuals tend to suffer less from fractures since bone morphometrics (i.e., BMD) are on their peak (Forlino and Marini, 2016). For menopausal women with OI, fracture rates tend to increase again (Folkestad *et al.,* 2017). For 18 w *oim*/Hom mice, C_{IT} returned to WT levels. This might suggest that one of the mechanisms for fractures in the early life in murine models is the high susceptibility of their bones to creep deformation. In addition, especially in *oim*/Hom females, the additive effects of low bone *E* and *H*, with increased C_{IT} might serve as a proper environment to the development of bone cracks that, if not healed properly, can influence fracture risk in an elderly body (Gehlbach *et al.,* 2012; Kanis *et al.,* 2004).

6.5. Limitations

A clear limitation in this study is the impossibility to evaluate *oim*/Hom mice at later stages in their lives. *Oim*/Hom is a model for severe cases of OI(III), showing spontaneous fractures that affected their ambulation and ability to perform routine activities. To minimise the suffering of these animals, complying with the guidelines for the use of animals in research, they were euthanised before reaching 52 w of age (Lee *et al.*, 2022). Despite being considered an optimal pre-clinical model for OI, *oim* mice are quadrupedal; thus, the loads being applied to their bones is different from the loads human bones are used. A final limitation in this study is the lack of morphometric measurements (e.g., BMD and cortical/trabecular thickness). Both properties are fundamental in diagnose and assessment of OI in clinic. Further studies should be conducted addressing the biomechanics of diseased bones at sub-tissue level and measurements of bone quality considered gold standard in medical environment.

6.6. Conclusion

Oim/Hom and *tm1b*/Hom mutations have synergistic effects in reducing *E* and *H* in young mice. Susceptibility to creep deformation showed to be exclusive of the *oim*/Hom pair. The combination of *oim*/H*et al*leviates the effects of *oim* in reducing the biomechanics in murine model. Ultimately, *col1a2* mutations increase the biomechanical properties of bone.

References

Alcorta-Sevillano, N., Infante, A., Macías, I., Rodríguez, C.I., 2022. Murine Animal Models in Osteogenesis Imperfecta: The Quest for Improving the Quality of Life. IJMS 24, 184.

Astrom, E., 2002. Beneficial effect of long-term intravenous bisphosphonate treatment of osteogenesis imperfecta. Archives of Disease in Childhood 86, 356–364.

Carriero, A., Enderli, T., Burtch, S., Templet, J., 2016. Animal models of osteogenesis imperfecta: applications in clinical research. ORR Volume 8, 41–55.

Chipman, S.D., Sweet, H.O., McBride, D.J., Davisson, M.T., Marks, S.C., Shuldiner, A.R., Wenstrup, R.J., Rowe, D.W., Shapiro, J.R., 1993. Defective pro alpha 2(I) collagen synthesis in a recessive mutation in mice: a model of human osteogenesis imperfecta. Proc. Natl. Acad. Sci. U.S.A. 90, 1701–1705.

Cho, T.-J., Choi, I.H., Chung, C.Y., Yoo, W.J., Lee, K.S., Lee, D.Y., 2007. Interlocking Telescopic Rod for Patients with Osteogenesis Imperfecta: The Journal of Bone & Joint Surgery 89, 1028–1035.

El-Gazzar, A., Högler, W., 2021. Mechanisms of Bone Fragility: From Osteogenesis Imperfecta to Secondary Osteoporosis. IJMS 22, 625.

Fassier, A., 2021. Telescopic rodding in children: Technical progression from Dubow–Bailey to Fassier–Duval™. Orthopaedics & Traumatology: Surgery & Research 107, 102759.

Folkestad, L., Hald, J.D., Ersbøll, A.K., Gram, J., Hermann, A.P., Langdahl, B., Abrahamsen, B., Brixen, K., 2017. Fracture Rates and Fracture Sites in Patients with Osteogenesis

Imperfecta: A Nationwide Register-Based Cohort Study: FRACTURE RATES IN OSTEOGENESIS IMPERFECTA. J Bone Miner Res 32, 125–134.

Forlino, A., Marini, J.C., 2016. Osteogenesis imperfecta. The Lancet 387, 1657–1671.

Fratzl, P., 2008. Collagen: Structure and Mechanics, an Introduction, in: Fratzl, Peter (Ed.), Collagen. Springer US, Boston, MA, pp. 1–13.

Gehlbach, S., Saag, K.G., Adachi, J.D., Hooven, F.H., Flahive, J., Boonen, S., Chapurlat, R.D., Compston, J.E., Cooper, C., Díez-Perez, A., Greenspan, S.L., LaCroix, A.Z., Netelenbos, J.C., Pfeilschifter, J., Rossini, M., Roux, C., Sambrook, P.N., Silverman, S., Siris, E.S., Watts, N.B., Lindsay, R., 2012. Previous fractures at multiple sites increase the risk for subsequent fractures: The global longitudinal study of osteoporosis in women. J Bone Miner Res 27, 645–653.

Geurtzen, K., Vernet, A., Freidin, A., Rauner, M., Hofbauer, L.C., Schneider, J.E., Brand, M., Knopf, F., 2017. Immune Suppressive and Bone Inhibitory Effects of Prednisolone in Growing and Regenerating Zebrafish Tissues. Journal of Bone and Mineral Research 32, 2476–2488.

Kanis, J.A., Johnell, O., De Laet, C., Johansson, H., Oden, A., Delmas, P., Eisman, J., Fujiwara, S., Garnero, P., Kroger, H., McCloskey, E.V., Mellstrom, D., Melton, L.J., Pols, H., Reeve, J., Silman, A., Tenenhouse, A., 2004. A meta-analysis of previous fracture and subsequent fracture risk. Bone 35, 375–382.

Labonte, D., Lenz, A.-K., Oyen, M.L., 2017. On the relationship between indentation hardness and modulus, and the damage resistance of biological materials. Acta Biomaterialia 57, 373–383.

Laizé, V., Gavaia, P.J., Cancela, M.L., 2014. Fish: a suitable system to model human bone disorders and discover drugs with osteogenic or osteotoxic activities. Drug Discovery Today: Disease Models 13, 29–37.

Lee K. J., Lisa Rambault, George Bou-Gharios, Peter D. Clegg, Riaz Akhtar, Gabriela Czanner, Rob van't Hof, Elizabeth G. Canty-Laird; 2022 Collagen (I) homotrimer potentiates the osteogenesis imperfecta (oim) mutant allele and reduces survival in male mice. Dis Model Mech 1 September; 15 (9): dmm049428.

Lieschke, G.J., Currie, P.D., 2007. Animal models of human disease: zebrafish swim into view. Nat Rev Genet 8, 353–367.

Mcbride, Jr., D.J., Kadler, K.E., Hojima, Y., Prockop, D.J., 1992. Self-Assembly into Fibrils of a Homotrimer of Type I Collagen. Matrix 12, 256–263.

Novitskaya, E., Zin, C., Chang, N., Cory, E., Chen, P., D'Lima, D., Sah, R.L., McKittrick, J., 2014. Creep of trabecular bone from the human proximal tibia. Materials Science and Engineering: C 40, 219–227.

Oliver, W.C., Pharr, G.M., 2004. Measurement of hardness and elastic modulus by instrumented indentation: Advances in understanding and refinements to methodology. J. Mater. Res. 19, 3–20.

Oliver, W.C., Pharr, G.M., 1992. An improved technique for determining hardness and elastic modulus using load and displacement sensing indentation experiments. J. Mater. Res. 7, 1564–1583.

Pollintine, P., Luo, J., Offa-Jones, B., Dolan, P., Adams, M.A., 2009. Bone creep can cause progressive vertebral deformity. Bone 45, 466–472.

Raghunath, M., Bruckner, P., Steinmann, B., 1994. Delayed Triple Helix Formation of Mutant Collagen from Patient with Osteogenesis Imperfecta. Journal of Molecular Biology 236, 940–949.

Shapiro, J.R., McBride, D.J., Fedarko, N.S., 1995. OIM and Related Animal Models of Osteogenesis Imperfecta. Connective Tissue Research 31, 265–268.

Sillence, D., 1981. Osteogenesis imperfecta: an expanding panorama of variants. Clin Orthop Relat Res 11–25.

Sillence, D.O., Senn, A., Danks, D.M., 1979. Genetic heterogeneity in osteogenesis imperfecta. Journal of Medical Genetics 16, 101–116.

Skarnes, W.C., Rosen, B., West, A.P., Koutsourakis, M., Bushell, W., Iyer, V., Mujica, A.O., Thomas, M., Harrow, J., Cox, T., Jackson, D., Severin, J., Biggs, P., Fu, J., Nefedov, M., de Jong, P.J., Stewart, A.F., Bradley, A., 2011. A conditional knockout resource for the genome-wide study of mouse gene function. Nature 474, 337–342.

Strevel, E.L., Papaioannou, A., Adachi, J.D., McNamara, M., 2005. Case report: osteogenesis imperfecta Elusive cause of fractures. Can Fam Physician 51, 1655–1657.

Van Dijk, F.S., Sillence, D.O., 2014. Osteogenesis imperfecta: Clinical diagnosis, nomenclature and severity assessment. Am. J. Med. Genet. 164, 1470–1481.

Vanleene, M., Porter, A., Guillot, P.-V., Boyde, A., Oyen, M., Shefelbine, S., 2012. Ultra-structural defects cause low bone matrix stiffness despite high mineralization in osteogenesis imperfecta mice. Bone 50, 1317–1323.

Wu, Z., Baker, T.A., Ovaert, T.C., Niebur, G.L., 2011. The effect of holding time on nanoindentation measurements of creep in bone. Journal of Biomechanics 44, 1066–1072.

Yao, X., Carleton, S.M., Kettle, A.D., Melander, J., Phillips, C.L., Wang, Y., 2013. Gender-Dependence of Bone Structure and Properties in Adult Osteogenesis Imperfecta Murine Model. Ann Biomed Eng 41, 1139–1149.

7. Chapter 7: Discussion

This chapter discusses sample hydration and its influence in biomechanics of bone (7.1), as well as the critical findings of this study (sections 7.2 and 7.3), correlating them with the existing literature in the subject. The final section of this chapter addresses the translation of animal models in research, to humans (7.4).

7.1. Effects of dehydration in nanoindentation

Bone is considered a hard biological tissue due to the amount of biomineral content (e.g., calcium phosphate) found in its structure (Oyen, 2015). Despite discussions involving the biomechanics of bone often neglect the effects of hydration on the *E* and *H* of the material for simplification (Bertassoni and Swain, 2012; Bushby *et al.,* 2004; Rho *et al.,* 1997), sample hydration still poses a significant amount of the bones mechanical properties (Oyen, 2015).

Water is one of the three components of bone (Meyers and Chen, 2014) and is responsible for its elasticity and ductility (Bushby *et al.,* 2004). Using NI to test bones often requires the samples to be embedded or included in some type of resin (Rho *et al.,* 1997); to achieve a proper result, the samples are often dehydrated, avoiding the formation of air pockets in the boundary bone/resin, but also ensuring a complete and uniform filling of the bones porosities with resin, holding the piece in place while a load is applied. The testing of hydrated samples require the state of hydration to be maintained for the whole process of testing, and various methods to maintain the necessary extended hydration have been proposed (Oyen, 2015). In general, when bone samples are tested in dehydrated condition, they appear to have higher stiffness than when hydrated (Bembey *et al.,* 2006; Rho *et al.,* 1997). A more pronounced effect is visible when the parameter analysed is the *H* of the dentin: in hydrated environment, the amount of displacement supported by the sample is around three times of those supported in dehydrated condition, indicating lower *H* (Rodriguez-Florez *et al.,* 2013).

For the purpose of this thesis, all the bone samples from zebrafish and mice were indented and had their biomechanics analysed in a state of dehydration. The values here obtained were compared within each other, where the methodology and conditions applied were strictly the same in for all samples in each study. Thus, comparison with other literature should be taken carefully.

7.2. Zebrafish models for human diseases

Zebrafish are small teleost fish that have been used in the biomedical field to model human-affecting bone diseases due to their physiological conservation with humans, low cost and potential to be imaged *in vivo* (Barrett *et al.*, 2006; Lin *et al.*, 2022). In this study the author found zebrafish to be a readily available model for GIOP, and a simple organism to perform the interventions required to achieve the objectives proposed (e.g., medicine administration and resection). Moreover, anaesthetizing the fish with a combination of MS-222 and Tricaine (Collymore *et al.*, 2014) caused no loss of fish during the experimentation. In order to perform finectomy, the author used the protocol developed by Cardeira *et al.*, (2016) which states that the cut should be performed at once and in the region just proximal to the first lepidotrichia bifurcation. Training on this procedure was conducted using retired fish. In relation to dissecting zebrafish vertebrae, the procedure was more complicated due to the size of the fish in comparison to the instrumentation and to the fragility of the vertebral segments. Prior training was performed using retired fish.

7.2.1. Zebrafish lepidotrichia

Because zebrafish caudal fin is able to regenerate spontaneously after being resected, the appeal to use this fish to observe the underlying mechanism of bone regeneration has increased in the recent years (Sehring *et al.*, 2022; Sehring and Weidinger, 2022). In the first work of this thesis, zebrafish were treated with PN to exacerbate GIOP phenotype. Fish fins were resected and, to some of the fish, ALN was given to counteract GIOP. The lepidotrichia regeneration chain of events was observed via fluorescent signal and described by the means of their RMA, RAY, REG and STU (Cardeira *et al.*, 2016). By calculating these parameters, it became clear that PN delayed and ALN boosted the regeneration of the bony rays. The data showed that the values

found for PN fish were scattered below the regression line. This means that the total mineralised area (y-axis) was reduced in proportion to the total regeneration of the fin tissue (x-axis). An opposite trend was observed in ALN group, where the points were mostly scattered above the regression line, meaning that the mineralised part increased faster than the outer tissue. These results corroborate with previous research involving zebrafish in showing that ALN is a compound able to increase mineralisation and that PN work as an anti-mineralogenic compound in zebrafish model (Chen *et al.,* 2017; Geurtzen *et al.,* 2017; He *et al.,* 2018; Lin *et al.,* 2019; Pasqualetti *et al.,* 2015).

Since there were clear effects of the medicine in bone formation, the author proposed to evaluate the appearance and composition of the mineralised tissue of the proximal and distal parts of the fish caudal fin with SEM/EDS. The mineralised structures found in the proximal region were clearly different from the distal minerals. Proximal bones were displayed in well-defined shapes, while the distal parts were either amorphous or in small granules of minerals, as example of ALN_{REGEN}. The underlying mineralisation process in the zebrafish caudal fins occurs from the proximal to the distal region by the addition of newly-formed minerals at the furthermost edge of each fin (Mahamid *et al.,* 2011, 2008). This means that the different appearance of minerals observed in proximal and distal regions are rather because of lepidotrichia anatomy and type of bone formation (Weigele and Franz-Odendaal, 2016) than due to an effect of PN or ALN. Similar mineral shapes were observed by Mahamid *et al.,* (2008) in their study. Ca/P ratio is an important parameter for bone quality (Chang *et al.,* 2018). A broad range of minerals Ca and P and Ca/P ratios were found in zebrafish lepidotrichia. This finding corroborates with the concepts that diverse types of minerals coexist in zebrafish lepidotrichia (Mahamid *et al.,* 2010, 2008). The Ca/P proportion was found to significantly decrease from proximal-to-distal direction. This trend was observed for all but ALN_{REGEN} group. In addition, the distal region of $GIOP_{REGEN}$ presented high heterogeneity. PN is a

compound known to influence the activity OCs (He *et al.*, 2018). High variability in $GIOP_{REGEN}$ reasons with local remove of mineral by OCs (Witten and Huysseune, 2009). The results here presented reconfirm the composition variability of the minerals that form zebrafish lepidotrichia (Mahamid *et al.*, 2010).

OP is often related to bones with poor mechanical properties due to reduced BMD and altered microarchitecture (Dickenson *et al.*, 1981; Loundagin *et al.*, 2020). With the analysis of proximal and distal sites of zebrafish caudal fin, the highly mineralised structures found in the proximal bones showed, in general, increased E_r and H. At the distal regions, where the amount of non-mineralised tissue increases in proportion to bone (as observed in fluorescence microscopy), the bones showed lower mechanical properties. The reduced H measured in proximal bones of GIOP and $GIOP_{REGEN}$ was reversed by the use of ALN, as can be observed in ALN_{REGEN}. E_R and H in ALN_{REGEN} group showed high variation. This heterogeneity can be attributes to local effects of mineralisation within the proximal region. NI is an important technique to detect small variations in biological materials (Ebenstein and Pruitt, 2006) and was able to assess the mechanical properties of samples as small as lepidotrichia hemi rays with high significance. To the best knowledge of the author, no studies have previously used NI to evaluate the mechanical properties of zebrafish vertebrae. Zebrafish caudal fin have been analysed mechanically at the macro level (Puri *et al.*, 2018) where a machine was used to immobilise the fish and evaluate the flexibility of their caudal fins; the authors concluded that the hydrodynamic performance of zebrafish was strongly related to the mechanical properties of the bony rays. Although the mobility of regenerating fins was not assessed in this thesis, it is possible to assume that by promoting the recovery of the mechanical properties to natural levels, ALN would improve the hydrodynamic performance of the fish, highlighting a potential therapeutic effect of the medicine. In order to verify the relationship between the measured mechanical properties and composition of bone, the Pearson's correlation of both E_r and H

versus Ca/P was calculated. The E_r and H showed low, but positive, interaction with the Ca/P ratios of the proximal regions affected by the medicine. This outcome reaffirms the feasibility of a multi-scale approach to study healthy and diseased bones, affected or not, by mineralogenic compounds.

7.2.2. Zebrafish vertebrae

Zebrafish have two distinct types of bone formation: dermal and endochondral (Weigele and Franz-Odendaal, 2016). Dermal bones are presented in the fish fins, while endochondral is in the skull and vertebrae (Bird and Mabee, 2003). The use of zebrafish vertebrae here shows a more robust model, with higher similarity with human long bones (Bruneel and Witten, 2015). Bone morphometry is the main characteristic analysed for the diagnosis of bone conditions like OP (Genest *et al.,* 2021; Kelley *et al.,* 2013). BV / TV and BMD were previously measured for zebrafish and have shown not to be affected by GIOP (Geurtzen *et al.,* 2017). The results in this thesis agreed partially with the findings of Geurtzen *et al.,* (2017); while BV / TV of PN zebrafish here did not show significant differences from CTRL, the BMD (and consequently the Z-Scores) decreased significantly ($p < 0.001$) from CTRL fish. Geurtzen *et al.*, (2017) used 50 μM of PN to exacerbate GIOP in zebrafish; this study used the same concentration. However, Geurtzen *et al.,* (2017) did not stated the volume of water that the fish were maintained and measured the BMD for the whole fish skeleton. It is possible that the low volume of water used in this thesis might restricted at some degree the movement of fish, causing the development of osteopenia (Khajuria and Karasik, 2020). Moreover, here the BMD was calculated based on the CV1 and CV2, as recommended elsewhere (Bird and Mabee, 2003). This might explain the significant differences in the BMD between the two studies. In addition, ALN as a treatment for GIOP also showed to increase B.Th and BV. ALN fish displayed pathological mineralisation within their vertebrae, phenomena that was not observed in other groups.

Pathological or ectopic mineralisation were observed in the later stages of life in zebrafish (Monma *et al.*, 2019). The fish evaluated in this study were seven-month-old; thus, the pathological mineral formations might be related to ALN mechanism of promoting bone formation.

The morphology of zebrafish vertebrae was analysed with SEM. The morphology of the minerals observed in this study differed from those observed for zebrafish caudal fin in (section 3.3.1). Differently from the previous study, the vertebrae were not crushed prior SEM observation, so the arrangement and alignment of the inorganic phase was preserved. A different explanation for this result is that the zebrafish caudal fin has dermal bone formation, while the vertebrae is endochondral (Weigele and Franz-Odendaal, 2016). However similar round- and plate-like structures were addressed by Mahamid *et al.*, (2008). The morphology of the minerals found in CTRL have shy contours, which might indicate they are strongly entangled within the bone matrix. Any other group that was treated with PN and/or ALN displayed smaller and more evident minerals. Mahamid *et al*. (2008) evidenced different mineral morphologies in the proximal and distal regions of the caudal fin. It was discussed that coexistence of plate-like spherical shaped carbonated apatite comprise a bone from transitional stages of mineralisation processes. So, the morphologies observed in the electron micrographs might indicate the effect of the medications in bone formation. Despite this, the layered structure was not affected (Georgiadis *et al.*, 2016; Mahamid *et al.*, 2010).

NI is a powerful technique to assess minimal alterations in the mechanical properties of biomaterials (Zhang *et al.*, 2002; Zimmermann *et al.*, 2019). The axial surface of zebrafish vertebrae was probed in locations near the middle layer of bone, so the indentations were not affected by regions of bone with different mechanical properties (e.g., endosteum and periosteum) (Zhang *et al.*, 2002). The mechanical properties obtained with NI showed a

decreasing trend from ALN > PN + ALN > CTRL > PN. PN presented high heterogeneity in their *E*. PN is known to promote osteoclastogenesis (Geurtzen *et al.*, 2017). With increased number of active OCs, the resorbed sites might have generated localised reduction of modulus. This large discrepancy between high and low mechanical values might also serve as a weak spot for the development of microcracks (Ibrahim *et al.*, 2020). Interestingly, ALN showed the highest mechanical properties overall despite its low BMD. Since the fish in this group were given ALN with no previous bone condition (e.g., GIOP), the mineralisation promoted by the bisphosphonate might have occurred in a disorganised way with. This abnormal situation might also indicate that medicating zebrafish with bone promoting drugs can jeopardize the balance between BMD and mechanical properties. On the contrary, PN + ALN group, despite also showing increased *E*, showed *H* in the same levels if compared to CTRL. Thus, ALN, when administered after the onset of GIOP, can elevate the *H* of diseased bones to healthy levels, indicating one of the many therapeutic effects of the medication in treating zebrafish with OP (Pasqualetti *et al.*, 2015).

7.3. Murine models for human diseases

Oim mice produce dysfunctional α2(I) chains that cannot be incorporated properly into collagen fibrils, causing the formation of $(\alpha1)_3$ fibres (Shapiro *et al.*, 1995). The production of dysfunctional α2(I) chains has been related to mechanisms that cause severe osteopenia, reduced body size, fragile bone fractures, and skeletal deformation (Carriero *et al.*, 2016; Lee *et al.*, 2022). *Tm1b* is a *col1a2*-null mutation that also produces $(\alpha1)_3$ (Skarnes *et al.*, 2011); however, *tm1b* mice do not display phenotype of bone fragility (Lee *et al.*, 2022). At macro scale, *oim* is weak (Lee *et al.*, 2022; Vanleene *et al.*, 2012) and *tm1b* is strong (Lee *et al.*, 2022) if compared to WT mice of similar age. In this work, NI was used to assess the properties of α2(I) collagen mutation at sub tissue level. For mice of young ages (8 w), *oim*/Hom and

tm1b/Hom displayed decrease in *E*. *H* of *oim*/Hom remained at the same level of WT but was reduced in *tm1b*/Hom. Female *oim*/Hom mice exhibited lower elasticity and resistance to plastic deformation in comparison to male *oim*/Hom. Due to this discrepancy between the properties of males and females, *oim*/Hom revealed high heterogeneity in their *E* and *H*. So, in addition to large genetic heterogeneity (Sillence *et al.,* 1979), OI also increases the heterogeneity within samples. The mechanical properties in *oim*/Het and *tm1b*/Het were located in the mid-point between WT and Hom. Thus, Het is a factor to alleviate the phenotype of OI in murine models.

Due to the impossibility to raise *oim* mice to 52 w (Lee *et al.,* 2022), the mechanical data for this mutation was restricted to up to 18 w; *tm1b* did not showed brittle bones phenotype, so mice were raised to 52 w. As *oim*/Hom mice reached 18 w, the biomechanics of their bones became less susceptible to plastic deformations, while the *E* was maintained lower compared to WT. Both the *E* and *H* of *tm1b* mice increased gradually from 8-, to 18- and to 52 w compared to WT. The mechanical properties of *tm1b* increased with age when measured with three-point bending (Lee *et al.,* 2022). Mineralised biological materials display strong linear relationship between *H* and *E*; such linearity may be considered as a parameter for bone quality (Labonte *et al.,* 2017). The linear correlation across all mice mutations and WT was positive. In general, *H-E* correlations were stronger for increased holding times (100 s). The trend of *tm1b* to increase its mechanical properties with age can be observed by the trend of the scatter plots to move to the up-right corner of the graphs.

Creep deformation has been related to vertebral shortening and bone implant failure to purpose due to loosening (Cho *et al.,* 2007; Pollintine *et al.,* 2009). Depending on the type of OI, the microarchitectural decrease of bones can resemble those in secondary OP (El-Gazzar and Högler, 2021), increasing the susceptibility to creep deformation due to trabecular disruption

(Novitskaya *et al.,* 2014; Pollintine *et al.,* 2009). Promoting a prolonged (100 s) contact between the Berkovich tip and the surface of cortical bone led C_{IT} to increase around 2-fold of the values obtained using restricted hold times (10 s). *Col1a2*-null showed decreased *E* and *H*, however, these two properties seem to have had no effects in the C_{IT} at any point in their life (8-, 18- or 52 w). Bone creep play a key role only when the local mechanical properties of the mineralised tissue are below a critical level, which increase the possibility of slipping mechanism between the interface osteons/bone matrix (Pollintine *et al.,* 2009). This might be the case for 8 w *oim*/Hom, which presented increased C_{IT} in comparison to WT and *oim*/Het. High creep susceptibility of *oim*/Hom reason with the high incidence of fractures in young individuals (Forlino and Marini, 2016). With increasing BMD during adulthood, the fracture risk decreases (Folkestad *et al.,* 2017). This statement has correlation with the data found for 18 w *oim*/Hom mice; the C_{IT} in this group returned to WT levels. The results here presented suggest that young (8 w) *oim*/Hom females could be at higher risk of bone fracture as *E* and *H* showed decreased values, and high susceptibility to creep deformation.

7.4. Translation to human research

Pre-clinical research in animals have provided many advancements to medical and pharmaceutical fields by, for example, development of new surgical techniques and vaccines. The use of animal models (especially mice) in research have provided important data and resources to alleviate human suffering (Robinson *et al.,* 2019). Despite this, it is of high importance to understand the limitations of translating results obtained in animal models to humans.

In the studies involving zebrafish in this thesis, first we used a regenerative protocol to understand how the mineralisation of bone occurs under the effects of 1) fish tank water, 2) PN and 3) ALN. With ALN treatment zebrafish were able to boost the regeneration of their

lepidotrichia compared to controls and PN. This evidenced that, with the setup we proposed, PN caused fish to develop OP and ALN could recover the osteoporotic state to natural levels; studies involving mice and humans have reported similar interaction among these medications and bone (Kashii *et al.,* 2008; Ma *et al.,* 2017). In relation to the BMD and mechanical properties of bone affected by OP and treated with ALN, yet again, our study with zebrafish showed conservation to human bone behaviour. The BMD and *H* measured in fish with OP showed lower values compared to the controls; the *E* was not changed. The use of bisphosphonate recover both properties to healthy levels. A study on the use of bisphosphonates and its relationship with BMD and mechanical properties in human bone was published (Burr, 2020); a linear relationship between BMD *vs.* ultimate load was proposed. This work does not access ultimate load of bones, however, a trend to increase zebrafish vertebrae mechanical properties with the increase in BMD can be inferred. A limitation of zebrafish bone in comparison to the human is the impossibility of testing it in macro-scale, thus, mathematical approaches could aid in the translation of zebrafish/human nanomechanical results.

Mice mutations are the most common animal model for human diseases (Mitchell *et al.*, 2015). In this thesis, an extensive characterisation of the biomechanics of genetically modified mice was performed. The available literature reports that the mechanical properties of human bone increases with age (Szabo and Rimnac, 2022) and the risk of fracture increases in people with history of fractures (Kanis and Kanis, 1994). The biomechanics of both *oim* and *tm1b* mice showed similar behaviour, being low at young individuals, but increasing as they aged, independently of OI phenotype, showing that both mammals have some degree of conservation in the biomechanics of their bones.

Advancing our understanding of human bone biomechanics and its relationship with bone diseases requires optimisation of the current characterisation methods. I believe that the instrumentation and approaches used in this thesis may, in the future, be applied to investigate human bone diseases. The direct translation of animal models to humans may not be feasible, but can potentially be fed into models, to better understand/predict the effects of a medical compounds in human bone, for example.

References

Barrett, R., Chappell, C., Quick, M., Fleming, A., 2006. A rapid, high content, in vivo model of glucocorticoid-induced osteoporosis. Biotechnol. J. 1, 651–655.

Bembey, A.K., Oyen, M.L., Bushby, A.J., Boyde, A., 2006. Viscoelastic properties of bone as a function of hydration state determined by nanoindentation. Philos Mag 86, 5691–5703.

Bertassoni, L.E., Swain, M.V., 2012. Influence of hydration on nanoindentation induced energy expenditure of dentin. J Biomech 45, 1679–1683.

Bird, N.C., Mabee, P.M., 2003. Developmental morphology of the axial skeleton of the zebrafish, Danio rerio (Ostariophysi: Cyprinidae). Develop Dyn 228, 337–357.

Bruneel, B., Witten, P.E., 2015. Power and challenges of using zebrafish as a model for skeletal tissue imaging. Connect Tissue Res 56, 161–173.

Burr, D.B., 2020. Fifty years of bisphosphonates: What are their mechanical effects on bone? Bone 138, 115518.

Bushby, A.J., Ferguson, V.L., Boyde, A., 2004. Nanoindentation of bone: Comparison of specimens tested in liquid and embedded in polymethylmethacrylate. J Mat Res 19, 249–259.

Cardeira, J., Gavaia, P.J., Fernández, I., Cengiz, I.F., Moreira-Silva, J., Oliveira, J.M., Reis, R.L., Cancela, M.L., Laizé, V., 2016. Quantitative assessment of the regenerative and mineralogenic performances of the zebrafish caudal fin. Sci Rep 6, 39191.

Chang, Z., Chen, P.-Y., Chuang, Y.-J., Akhtar, R., 2018. Zebrafish as a model to study bone maturation: Nanoscale structural and mechanical characterization of age-related changes

in the zebrafish vertebral column. Journal of the Mechanical Behavior of Biomedical Materials 84, 54–63.

Chen, J.-R., Lai, Y.-H., Tsai, J.-J., Hsiao, C.-D., 2017. Live Fluorescent Staining Platform for Drug-Screening and Mechanism-Analysis in Zebrafish for Bone Mineralization. Molecules 22, 2068.

Cho, T.-J., Choi, I.H., Chung, C.Y., Yoo, W.J., Lee, K.S., Lee, D.Y., 2007. Interlocking Telescopic Rod for Patients with Osteogenesis Imperfecta: The Journal of Bone & Joint Surgery 89, 1028–1035.

Collymore, C., Tolwani, A., Lieggi, C., Rasmussen, S., 2014. Efficacy and safety of 5 anesthetics in adult zebrafish (Danio rerio). J. Am. Assoc. Lab. Anim. Sci. 53, 198–203.

Dickenson, R.P., Hutton, W.C., Stott, J.R., 1981. The mechanical properties of bone in osteoporosis.

Ebenstein, D.M., Pruitt, L.A., 2006. Nanoindentation of biological materials. Nano Today 1, 26–33.

El-Gazzar, A., Högler, W., 2021. Mechanisms of Bone Fragility: From Osteogenesis Imperfecta to Secondary Osteoporosis. IJMS 22, 625.

Folkestad, L., Hald, J.D., Ersbøll, A.K., Gram, J., Hermann, A.P., Langdahl, B., Abrahamsen, B., Brixen, K., 2017. Fracture Rates and Fracture Sites in Patients with Osteogenesis Imperfecta: A Nationwide Register-Based Cohort Study: fracture rates in osteogenesis imperfecta. J Bone Miner Res 32, 125–134.

Forlino, A., Marini, J.C., 2016. Osteogenesis imperfecta. The Lancet 387, 1657–1671.

Genest, F., Claußen, L., Rak, D., Seefried, L., 2021. Bone mineral density and fracture risk in adult patients with hypophosphatasia. Osteoporos Int 32, 377–385.

Georgiadis, M., Müller, R., Schneider, P., 2016. Techniques to assess bone ultrastructure organization: orientation and arrangement of mineralized collagen fibrils. J. R. Soc. Interface. 13, 20160088.

Geurtzen, K., Vernet, A., Freidin, A., Rauner, M., Hofbauer, L.C., Schneider, J.E., Brand, M., Knopf, F., 2017. Immune Suppressive and Bone Inhibitory Effects of Prednisolone in Growing and Regenerating Zebrafish Tissues. Journal of Bone and Mineral Research 32, 2476–2488.

He, H., Wang, C., Tang, Q., Yang, F., Xu, Y., 2018. Possible mechanisms of prednisolone-induced osteoporosis in zebrafish larva. Biomedicine & Pharmacotherapy 101, 981–987.

Ibrahim, A., Magliulo, N., Groben, J., Padilla, A., Akbik, F., Abdel Hamid, Z., 2020. Hardness, an Important Indicator of Bone Quality, and the Role of Collagen in Bone Hardness. JFB 11, 85.

Kanis, J.A., Kanis, J.A., 1994. Assessment of fracture risk and its application to screening for postmenopausal osteoporosis: Synopsis of a WHO report. Osteoporosis Int 4, 368–381.

Kashii, M., Hashimoto, J., Nakano, T., Umakoshi, Y., Yoshikawa, H., 2008. Alendronate treatment promotes bone formation with a less anisotropic microstructure during intramembranous ossification in rats. J Bone Miner Metab 26, 24–33.

Kelley, G.A., Kelley, K.S., Kohrt, W.M., 2013. Exercise and Bone Mineral Density in Premenopausal Women: A Meta-Analysis of Randomized Controlled Trials. International Journal of Endocrinology 2013, 1–16.

Khajuria, D.K., Karasik, D., 2020. Novel model of restricted mobility induced osteopenia in zebrafish. J Fish Biol jfb.14369.

Labonte, D., Lenz, A.-K., Oyen, M.L., 2017. On the relationship between indentation hardness and modulus, and the damage resistance of biological materials. Acta Biomaterialia 57, 373–383.

Lee K. J., Lisa Rambault, George Bou-Gharios, Peter D. Clegg, Riaz Akhtar, Gabriela Czanner, Rob van‘t Hof, Elizabeth G. Canty-Laird; 2022 Collagen (I) homotrimer potentiates the osteogenesis imperfecta (oim) mutant allele and reduces survival in male mice. Dis Model Mech 1 September; 15 (9): dmm049428.

Lin, W.-Y., Dharini, K., Peng, C.-H., Lin, C.-Y., Yeh, K.-T., Lee, W.-C., Lin, M.-D., 2022. Zebrafish models for glucocorticoid-induced osteoporosis. Tzu Chi Med J 34, 373.

Lin, Y., Xiang, X., Chen, T., Gao, C., Fu, H., Wang, L., Deng, L., Zeng, L., Zhang, J., 2019. In vivo monitoring and high-resolution characterizing of the prednisolone-induced osteoporotic process on adult zebrafish by optical coherence tomography. Biomedical Optics Express 10, 1184.

Loundagin, L.L., Haider, I.T., Cooper, D.M.L., Edwards, W.B., 2020. Association between intracortical microarchitecture and the compressive fatigue life of human bone: A pilot study. Bone Reports 12, 100254.

Ma, X., Xu, Z., Ding, S., Yi, G., Wang, Q., 2017. Alendronate promotes osteoblast differentiation and bone formation in ovariectomy-induced osteoporosis through interferon-β/signal transducer and activator of transcription 1 pathway. Exp Ther Med.

Mahamid, J., Addadi, L., Weiner, S., 2011. Crystallization Pathways in Bone. Cells Tissues Organs 194, 92–97.

Mahamid, J., Aichmayer, B., Shimoni, E., Ziblat, R., Li, C., Siegel, S., Paris, O., Fratzl, P., Weiner, S., Addadi, L., 2010. Mapping amorphous calcium phosphate transformation into crystalline mineral from the cell to the bone in zebrafish fin rays. Proc. Natl. Acad. Sci. U.S.A. 107, 6316–6321.

Mahamid, J., Sharir, A., Addadi, L., Weiner, S., 2008. Amorphous calcium phosphate is a major component of the forming fin bones of zebrafish: Indications for an amorphous precursor phase. Proceedings of the National Academy of Sciences 105, 12748–12753.

Mitchell, S.J., Scheibye-Knudsen, M., Longo, D.L., De Cabo, R., 2015. Animal Models of Aging Research: Implications for Human Aging and Age-Related Diseases. Annu. Rev. Anim. Biosci. 3, 283–303.

Monma, Y., Shimada, Y., Nakayama, H., Zang, L., Nishimura, N., Tanaka, T., 2019. Aging-associated microstructural deterioration of vertebra in zebrafish. Bone Reports 11, 100215.

Novitskaya, E., Zin, C., Chang, N., Cory, E., Chen, P., D'Lima, D., Sah, R.L., McKittrick, J., 2014. Creep of trabecular bone from the human proximal tibia. Materials Science and Engineering: C 40, 219–227.

Oyen, M.L., 2015. Nanoindentation of hydrated materials and tissues. Curr Opi Solid State Mat Sci 19, 317–323.

Pasqualetti, S., Congiu, T., Banfi, G., Mariotti, M., 2015. Alendronate rescued osteoporotic phenotype in a model of glucocorticoid-induced osteoporosis in adult zebrafish scale. Int. J. Exp. Path. 96, 11–20.

Pollintine, P., Luo, J., Offa-Jones, B., Dolan, P., Adams, M.A., 2009. Bone creep can cause progressive vertebral deformity. Bone 45, 466–472.

Puri, S., Aegerter-Wilmsen, T., Jaźwińska, A., Aegerter, C.M., 2018. In vivo quantification of mechanical properties of caudal fins in adult zebrafish. The Journal of Experimental Biology 221, jeb171777.

Rho, J.-Y., Tsui, T.Y., Pharr, G.M., 1997. Elastic properties of human cortical and trabecular lamellar bone measured by nanoindentation. Biomaterials 18, 1325–1330.

Rodriguez-Florez, N., Oyen, M.L., Shefelbine, S.J., 2013. Insight into differences in nanoindentation properties of bone. Journal of the Mechanical Behavior of Biomedical Materials 18, 90–99.

Sehring, I., Mohammadi, H.F., Haffner-Luntzer, M., Ignatius, A., Huber-Lang, M., Weidinger, G., 2022. Zebrafish fin regeneration involves generic and regeneration-specific osteoblast injury responses. eLife 11, e77614.

Sehring, I., Weidinger, G., 2022. Zebrafish Fin: Complex Molecular Interactions and Cellular Mechanisms Guiding Regeneration. Cold Spring Harb Perspect Biol 14, a040758.

Shapiro, J.R., McBride, D.J., Fedarko, N.S., 1995. OIM and Related Animal Models of Osteogenesis Imperfecta. Connective Tissue Research 31, 265–268.

Sillence, D.O., Senn, A., Danks, D.M., 1979. Genetic heterogeneity in osteogenesis imperfecta. Journal of Medical Genetics 16, 101–116.

Skarnes, W.C., Rosen, B., West, A.P., Koutsourakis, M., Bushell, W., Iyer, V., Mujica, A.O., Thomas, M., Harrow, J., Cox, T., Jackson, D., Severin, J., Biggs, P., Fu, J., Nefedov, M., de Jong, P.J., Stewart, A.F., Bradley, A., 2011. A conditional knockout resource for the genome-wide study of mouse gene function. Nature 474, 337–342.

Szabo, E., Rimnac, C., 2022. Biomechanics of immature human cortical bone: A systematic review. Journal of the Mechanical Behavior of Biomedical Materials 125, 104889.

Vanleene, M., Porter, A., Guillot, P.-V., Boyde, A., Oyen, M., Shefelbine, S., 2012. Ultra-structural defects cause low bone matrix stiffness despite high mineralization in osteogenesis imperfecta mice. Bone 50, 1317–1323.

Weigele, J., Franz-Odendaal, T.A., 2016. Functional bone histology of zebrafish reveals two types of endochondral ossification, different types of osteoblast clusters and a new bone type. J. Anat. 229, 92–103.

Witten, P.E., Huysseune, A., 2009. A comparative view on mechanisms and functions of skeletal remodelling in teleost fish, with special emphasis on osteoclasts and their function. Biological Reviews 84, 315–346.

Zhang, Y., Cui, F.Z., Wang, X.M., Feng, Q.L., Zhu, X.D., 2002. Mechanical properties of skeletal bone in gene-mutated stöpseldtl28d and wild-type zebrafish (Danio rerio) measured by atomic force microscopy-based nanoindentation. Bone 30, 541–546.

Zimmermann, E.A., Riedel, C., Schmidt, F.N., Stockhausen, K.E., Chushkin, Y., Schaible, E., Gludovatz, B., Vettorazzi, E., Zontone, F., Püschel, K., Amling, M., Ritchie, R.O., Busse, B., 2019. Mechanical Competence and Bone Quality Develop During Skeletal Growth. J Bone Miner Res 34, 1461–1472.

8. Chapter 8: Conclusions and future work

This chapter summarises the key findings and contributions of this study. This chapter finishes with potential subjects for continuing the studies on diseased mineralised tissues.

8.1. Background

A protocol of zebrafish caudal fin resection/regeneration was used to understand the effects of anti- and pro-mineralogenic compounds in the resorption and formation of mineralised tissues, as well as their ability to affect the mechanical properties of fin bony rays. The limitation of the lepidotrichia in having dermal bone formation was addressed in a second moment by the use of zebrafish vertebrae. The gold standard equipment for the diagnosis of bone conditions was used. The data obtained with μ-CT were associated with nanoindentation to explain the relationship between bone quality (e.g., BMD) and poor mechanical properties of bones affected by OP. Bone diseases share an outcome of increased bone fragility. Throughout this study, the utility of nanoindenter to measure the localised biomechanics of diseased bones in animal models was verified. Oliver-Pharr method was used to question bones of a murine model for OI (*oim*) on their viscoelastic properties. A relationship between bone biomechanics and underlying mechanisms of fragility was proposed. Based on the objectives of this thesis, the key findings can be concluded in the next section.

8.2. Key findings and novelty of the research work

The first objective of this thesis was to investigate whether GIOP and the treatment with bisphosphonate, influence the morphology, biomechanics and mineralisation of zebrafish lepidotrichia. This study was the first to use standardised bone metrics (introduced by Cardeira *et al.*, (2016)) to demonstrate the ability of ALN to promote bone mineralisation and PN to halt the formation of new bone in zebrafish caudal fin. In addition, the susceptibility of zebrafish caudal fin bones to have their mechanical properties influenced negatively or positively in response to medication was verified.

The second objective was to assess the BMD (and other morphometric parameters), with μ-CT, and the biomechanical values of zebrafish vertebrae after the onset of GIOP and the treatment with bisphosphonate. To the best of the author's knowledge, the novelty of this work relies on analysing together, two of the most important properties of bones affected by OP, such as biomechanics and BMD, correlating them with the benefits of medicine intake. Zebrafish are a promising animal model for bone diseases. This thesis contributes to the current knowledge in this model by showing a series of characterisation methods that enable the use of zebrafish in biomechanical research and incorporating drug effects exacerbation.

The third and final objective in this thesis was to characterise the biomechanical properties of femurs of *oim* mice and compare to those of *col1a2*-null (*tm1b*) and wild type (WT). Murine models are no doubt better models for human diseases than zebrafish. Mice are terrestrial mammals; this means that the environment in which their skeleton is modelled (and remodelled) has higher similarity to humans natural habitat than underwater where zebrafish lives. To the best of my knowledge, this work adds to the current knowledge, not just insights onto potential mechanisms of bone fragility in OI, but a series of methodological processes that can be incorporated into medical practice to assess the overall quality of diseased bones. Creep deformation is steadily occurring in human and animal bones due to their constant dead weight. Creep deformation analysis can potentially be incorporated into the testing of human bone biopsies.

8.3. Overall summary

In conclusion, this study evaluates OP and OI, two bone diseases that are different in their nature, but that share phenotype of bone fragility and high prevalence of fractures. The studies involving zebrafish showed that osteoporotic phenotype is exacerbated by the means of reduced mineral formation (fin bony rays), reduced *H* (fin bony rays and vertebrae) and

reduction of BMD (vertebrae). One of the mechanisms by which ALN rescues osteoporotic bones is by restoring these properties to healthy levels. In murine models for collagen defects, the biomechanical properties increased with age, demonstrating that low *E* and *H*, and high C_{IT} at young ages play key role in the bone brittleness.

8.4. Future work

8.4.1. Nanomechanical mapping matching bone composition

This thesis has shown that the biomechanics of bone have relationship with bone morphometrics, such as BMD. With the use of an Electron Probe Microanalyzer, it is possible to map calcium and phosphate distribution across the thickness of cortical bone, for example. This method is non-destructive; thus, the same sample can be analysed with NI and the localised changes of biomechanics could be matched with calcium/phosphate ratios. An example of Electron Probe Microanalyzer evaluation is shown below in **Fig. 49**:

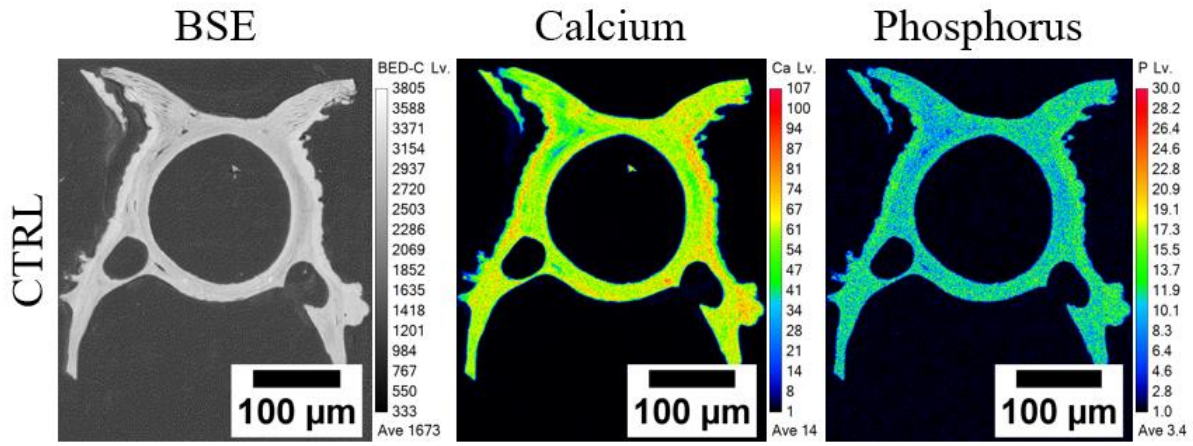

Fig. 49 Results for (left) backscattered electrons, (middle) calcium and (right) phosphorus distribution across the cortical region in zebrafish vertebrae bone. Figure by the author.

8.4.2. Creep analysis in zebrafish model

Oliver-Pharr method can be used to evaluate the creep behaviour of ageing zebrafish or zebrafish mutations that resemble human diseases, as the case of the *chihuahua* and the *sp7*. These fish can potentially cover the limitations of *oim* mice with advanced age that were shown in this thesis. This potential project would also benefit from the application of Miller-Norton exponential fitting to cover both primary and secondary creep regimes, as discussed previously in this thesis.

8.4.3. Nanomechanical mapping with high-speed NI

High speed nanoindentation uses the equipment processing capacity to perform multiple indentations, in matrix-like arrangements, with high speed. It does this by not recording *load vs. displacement* curves. This analysis could be useful for the observation of the full picture of the bone. This technique has the appeal of the visualisation, since heatmaps are generated after the sample is indented.

8.4.4. Effects of prolonged hold time periods in *oim* model

In this thesis it was shown that OI bones display elevated levels of C_{IT}. By increasing the plateau of hold times, the biomechanics of bone would be represented with higher degree of certainty and would resemble real life situations (e.g., constant creep happening in the long bones of our legs during standing position).

8.4.5. Murine model and medication

A similar approach that was done in fish in this thesis can potentially be applied in mouse mutants. Bone morphometrics and mechanical properties (both macro and sub tissue level) could be used to verify the therapeutic effect of drugs.

References

Cardeira, J., Gavaia, P.J., Fernández, I., Cengiz, I.F., Moreira-Silva, J., Oliveira, J.M., Reis, R.L., Cancela, M.L., Laizé, V., 2016. Quantitative assessment of the regenerative and mineralogenic performances of the zebrafish caudal fin. Sci Rep 6, 39191.

Carriero, A., Enderli, T., Burtch, S., Templet, J., 2016. Animal models of osteogenesis imperfecta: applications in clinical research. ORR Volume 8, 41–55.

Oliver, W.C., Pharr, G.M., 2004. Measurement of hardness and elastic modulus by instrumented indentation: Advances in understanding and refinements to methodology. J. Mater. Res. 19, 3–20.

Oliver, W.C., Pharr, G.M., 1992. An improved technique for determining hardness and elastic modulus using load and displacement sensing indentation experiments. J. Mater. Res. 7, 1564–1583.

Pollintine, P., Luo, J., Offa-Jones, B., Dolan, P., Adams, M.A., 2009. Bone creep can cause progressive vertebral deformity. Bone 45, 466–472.

Skarnes, W.C., Rosen, B., West, A.P., Koutsourakis, M., Bushell, W., Iyer, V., Mujica, A.O., Thomas, M., Harrow, J., Cox, T., Jackson, D., Severin, J., Biggs, P., Fu, J., Nefedov, M., de Jong, P.J., Stewart, A.F., Bradley, A., 2011. A conditional knockout resource for the genome-wide study of mouse gene function. Nature 474, 337–342.

Weigele, J., Franz-Odendaal, T.A., 2016. Functional bone histology of zebrafish reveals two types of endochondral ossification, different types of osteoblast clusters and a new bone type. J. Anat. 229, 92–103.